MODELLING OF VOLCANIC ASHFALL

A thesis presented in partial fulfilment of the

requirements for the degree of

Doctor of Philosophy

in

Mathematics

at

Massey University, Albany

New Zealand

Leng Leng Lim

2006

Abstract

Modelling of volcanic ashfall has been attempted by volcanologists but very little work has been done by mathematicians. In this thesis we show that mathematical models can accurately describe the distribution of particulate materials that fall to the ground following an eruption. We also report on the development and analysis of mathematical models to calculate the ash concentration in the atmosphere during ashfall after eruptions. Some of these models have analytical solutions.

The mathematical models reported on in this thesis not only describe the distribution of ashfall on the ground but are also able to take into account the effect of variation of wind direction with elevation. In order to model the complexity of the atmospheric flow, the atmosphere is divided into horizontal layers. Each layer moves steadily and parallel to the ground: the wind velocity components, particle settling speed and dispersion coefficients are assumed constant within each layer but may differ from layer to layer. This allows for elevation-dependent wind and turbulence profiles, as well as changing particle settling speeds, the last allowing the effects of the agglomeration of particles to be taken into account.

Acknowledgments

I would like to express my appreciation to my two supervisors, Prof. Robert McKibbin and Dr Winston L. Sweatman of the Institute of Information and Mathematical Sciences at Massey University, for giving me the opportunity to engage in this PhD study. I thank them for their teaching, patience, encouragement and the motivation given to me throughout the time of my study. In addition, I would like to thank Prof. Robert McKibbin for giving me the opportunity to attend conferences during this period. This has helped to build my confidence.

Next I would like to thank Massey University for giving me a three year PhD scholarship to fulfil my dream.

I would also like to express my special thanks to Dr Shehenaz Adam from the University of Alaska, Dr Mark Harmer from Massey University and Dr Mark Nelson from the University of Wollongong for patiently proofreading this thesis.

I would like to thank Mr Samir Bishay and Mr Stephen Ford, staff members of the Institute of Information and Mathematical Sciences at Massey University, for computer support during the time of my PhD study.

I would like to thank Prof. Chuck Connor of the Department of Geology at the University of South Florida for providing eruption data and contributing his ideas about volcanic modelling.

Last but not least I thank my family who are awaiting in Singapore for the completion of my PhD study and all my friends for constantly giving me moral support. Most importantly, I thank you God for keeping me safe, healthy and for the company throughout these three years in New Zealand.

Contents

Notation

c	particle mass concentration in the atmosphere	[kg m^{-3}]
C_s	drag constant	
D_c	cross-wind dispersion	[m^2 s^{-1}]
D_d	downwind dispersion	[m^2 s^{-1}]
D_h	horizontal dispersion in $x-y$ plane	[m^2 s^{-1}]
D_v	vertical dispersion	[m^2 s^{-1}]
D_x	horizontal dispersion in x direction	[m^2 s^{-1}]
D_y	horizontal dispersion in y direction	[m^2 s^{-1}]
D_z	vertical dispersion	[m^2 s^{-1}]
g	gravity	[m s^{-2}]
H	z-coordinate of the release point	[m]
L	turbulence length scale	[m]
M	source mass rate	[kg m^{-3} s^{-1}]
Q	mass release	[kg]
q	rate of mass release	[kg s^{-1}]
R	particle radius	[m]
Re	Reynolds number	
S	settling speed	[m s^{-1}]
U	mean horizontal wind speed in x direction	[m s^{-1}]
V	mean horizontal wind speed in y direction	[m s^{-1}]
t	time	[s]
X_0	x-coordinate of the release point	[m]
x	x-coordinate	[m]
Y_0	y-coordinate of the release point	[m]
y	y-coordinate	[m]
z	z-coordinate	[m]
Z_j	interface height	[m]
μ_a	dynamic viscosity of the air	[kg m^{-1} s^{-1}]
ν_a	kinematic viscosity of the air	[m^2 s^{-1}]
ρ_a	mass density of the air	[kg m^{-3}]
ρ_r	mass density of the particles	[kg m^{-3}]

Chapter 1

INTRODUCTION

modelling of volcanic ashfall is a process
so is life
the process of life
measures your sensitiveness and feelings

1.1 Volcanic activity in New Zealand

New Zealand is characterised by both a high density of active volcanoes and a high frequency of eruptions compared with the rest of the world. To date, most of the volcanic activity in New Zealand has occurred on the North Island. There are 48 volcanoes in the city of Auckland alone; luckily they are dormant. However, there are three volcanoes (Ruapehu, Ngauruhoe and White Island) that are currently active in New Zealand. Mount Tarawera, Tongariro, Mount Taranaki and Rangitoto are classed as dormant, although still considered to be eventual hazards. Volcanic activity in the Auckland area commenced around 150,000 years ago. Rangitoto was the last major eruption, taking place just 600 years ago [42].

In the past many lives have been lost in New Zealand due to volcanic eruptions (for example, in the 1886 eruption of Mount Tarawera, about 150 lives were lost). Besides the threat to life and property, the economic development of the country is also affected by volcanic eruptions. In the article "Under the volcanoes" [19] it is stated that the eruption of Mount Ruapehu, from 1995 to 1996, cost New Zealand at least $130 million.

There are 1500 potentially active volcanoes on Earth including New Zealand [45]. According to the report, "Space Volcano Observatory" [9], a third of them have been active in the last century, seventy are currently erupting, and about 30,000 people have died from volcanic eruptions in the past 50 years. It has been estimated that ten percent of the world population are living in areas close enough to volcanoes that

they may be affected by eruptions.

1.2 General Review

According to Sparks *et al.* [46], volcanic plumes are key features of explosive volcanism on Earth as they hold the potential for producing global environmental effects. Large-scale explosive eruptions can inject massive quantities of particles and gases into the atmosphere. The particles are basically fine-grained pyroclastic material composed of tiny particles of solidified molten rock [51].

1.2.1 Physical nature of volcanoes

There are basically two types of volcanoes: shield volcanoes (e.g. Iceland, Hawaii and Mount Etna) and strato (or composite) volcanoes (e.g. Mount St Helens, Mount Shasta, Stromboli, Vesuvio and Fujiyama) [32].

- Shield volcanoes are much wider than they are high and the slope angle is often less than 5°. The volcanoes are formed when the erupting lava has extremely low viscosity and typically for enduring effusive volcanism.

- Strato (or composite) volcanoes are typically only a few times wider than high and the slope angle is often much larger than 5°, sometimes reaching 35°. The volcanoes are typically composed of alternating layers of lava and tephra (ejecta) indicating alternating effusive and explosive activity.

1.2.2 Eruption styles

Eruption styles can be classified as Icelandic, Hawaiian, Strombolian, Vulcanian, Plinian, Caldera and Phreatic [32] [46].

- Icelandic has large amounts of very low-viscosity lava is non-explosive and forms plateaus.

- Hawaiian has low-viscosity lava is non-explosive and forms shield volcanoes.

- Strombolian has relatively small amounts of moderately high-viscosity lava and is usually peaceful. It forms scoria or cinder cones.

- Vulcanian has high-viscosity lava, moderately violent eruptions, moderately high-volatile content and moderately large eruption cloud.

- Plinian has very high-viscosity lava, violent eruptions, very high-volatile content shoots tephra high into atmosphere, and has pyroclastic flows. Tephra alternating with lava flows form strato-volcanoes.

- Calderas form after large amounts of magma have escaped from the magma chamber and there is roof collapse due to loss of support.

- Phreatic is phreatomagmatic and hydrovolcanic; from Greek "phrear" for well. Water interacts with lava to form vigorous eruptions.

In this thesis, eruptions which eject rock particles high into the atmosphere are modelled. These eruptions would typically be classified as Vulcanian and Plinian according to the list above. It is modelling the eventual deposition on the ground of these small particles (volcanic ash) which is the main interest of this study.

1.2.3 Ashfall

According to Cox [18], volcanic eruptions vary from gentle to violent, depending on the amount of gas in the magma. Ashfall is one of the main volcanic hazards to communities located in volcanic regions. During volcanic eruptions, ash is carried upward in volcanic plumes from heights of a few kilometers to a few tens of kilometers above the volcano vent, and this material settles through and is dispersed by the atmosphere. Within tens of kilometers of volcanic vents, accumulation can be sufficient to completely devastate property. Column heights of buoyant plume ash eruptions are typically in the range 1-30 km, with ash volumes of 0.5-500 km^3 and areas of ashfall of 0.0005-20,000 km^2, depending upon the scale of the eruption.

Many ash dispersion and deposit models rely on some modelling of the volcanic plume, or eruption column, to simplify forecasts of ashfall accumulation as a function of distance from the volcano. In this thesis, we develop solutions to model a variety of source shapes, including a point source, a horizontal line source, a vertical line source, a rectangle source and a circle source, and report the differences between the deposits produced by these different source shapes. Each of these source shapes may be related to some volcano plume structure, such as a strong plume (vertical line source), umbrella cloud (circle source), or co-ignimbrite plume (horizontal line source), or can be used to build a more complex plume structure (e.g. a series of circles to represent a buoyant weak plume). The details for modelling different shapes of source are presented in Chapter 4.

1.2.4 Why model volcanic ashfall?

An erupting volcano ejects rock fragments into the atmosphere and further fragmentation produces small ash particles. The falling ash is a hazard within the air as well as causing destruction and pollution when it settles on the ground. Besides aircraft, ash may also disrupt electricity and telephone networks [13]. Volcanic ash can travel hundreds to thousands of kilometres, the distance travelled depending on its size, the strength of the eruption and the physical condition of the atmosphere during the eruption.

Figure 1.1 illustrates the importance of modelling volcanic ashfall. It shows a helicopter struggling through ash while landing in a devastated area. Though the ash is microscopic it can be seen from Figure 1.1 that it poses a hazard to aircraft—the ash is fine enough to penetrate the engines of aircraft and cause damage. A mathematical model may produce hazard maps, which indicate areas which will be affected by ashfall.

Figure 1.1: A helicopter stirs up ash while trying to land in a devastated area. (Picture from http://vulcan.wr.usgs.gov/Glossary/Tephra/description_tephra.html.)

This thesis develops mathematical models of ashfall to help volcanologists produce better hazard maps more efficiently. It aims to develop models of the motion of the fine ash highlighted by the box in Figure 1.2. Because fine ash can be carried by wind over very long distances, it is important to know where it will be deposited in order to warn the public in the affected area. The models developed in this research can be used to determine the areas that would be covered by ash after an eruption.

1.3 Why mathematical models?

Suzuki [49] acknowledges that the mass of erupted material and thickness of tephra fallout are primary factors in understanding volcanic eruptions. Moreover, he claims

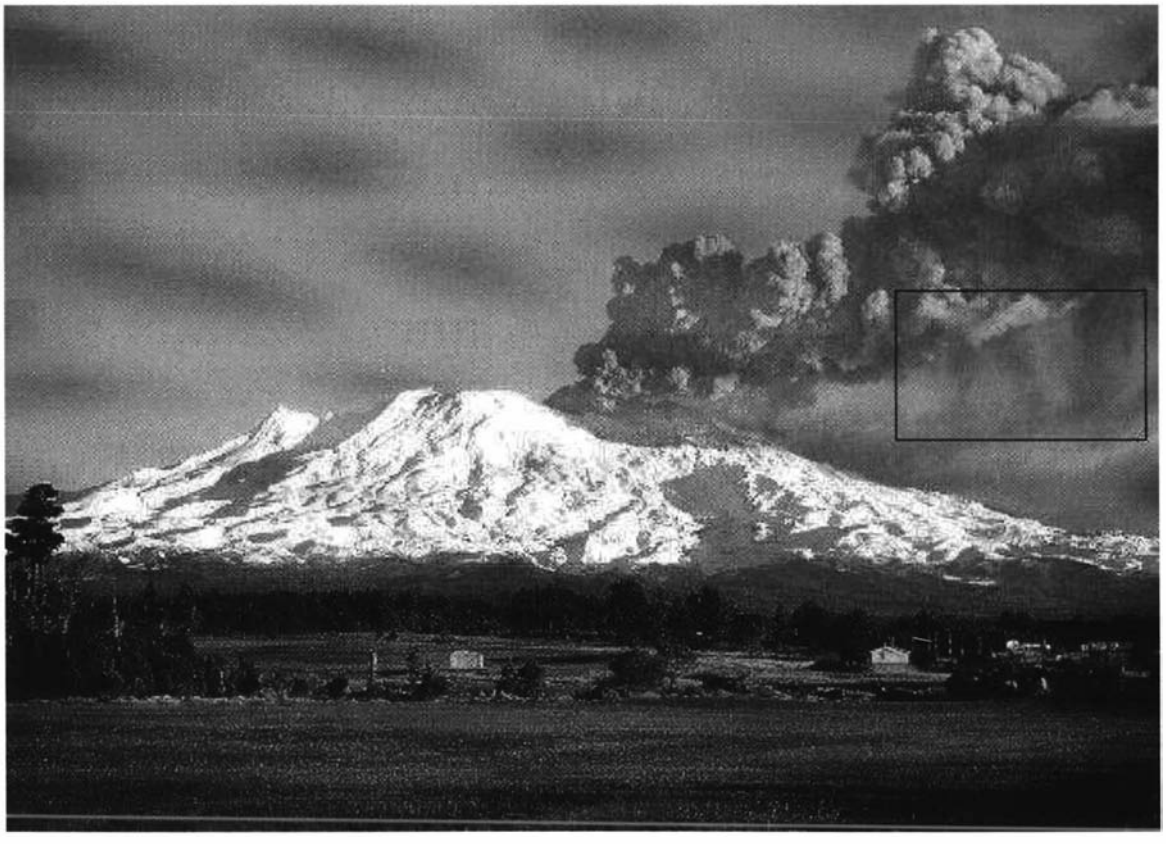

Figure 1.2: Mount Ruapehu erupting in 1996. (Picture taken from http://www.toursnz.com/nz/image/mtrua01.jpg.)

that there is no general theoretical basis for modelling fallout so his formulas for modelling eruptions were deduced from isopach/contour lines. Meteorological measurements were used, along with his model, to determine the characteristics of eruption patterns in order to predict the occurrence of the next eruption.

Although there are numerous approaches to modelling volcanic eruptions, Connor *et al.* [15] have pointed out that mathematical models have the advantage of describing the complex transport of particles explicitly. Consequently, mathematical models can help to produce better hazard maps. The advection-dispersion equation for modelling volcanic ashfall in this research is derived from the equation of conservation of mass. This equation is described in Chapter 2.

1.4 Some Existing Models

Currently there are no detailed models for describing volcanic ashfall that have analytic solutions. The existing models all require numerical solutions. Some existing models are ASHFALL [25] [26] [27], the Calpuff model [4], the Connor *et al.* model

[17] and HAZMAP [7]. They all model volcanic ashfall from an instantaneous point release. These models forecast ashfall accumulation on the ground for civil protection purposes, such as giving public warnings and planning mitigation measures.

- ASHFALL was developed by Hurst *et al.* [25] [26] [27] based on the study of the Pisa two-dimensional program by Armienti *et al.* [1] and Macedonio *et al.* [35] [36]. It was developed to assess the ashfall hazard from Mount Ruapehu in New Zealand, specifically to calculate the thickness of the ash. It uses wind speed and direction at different levels and times along with volcanological information such as the total volume of ashfall and distribution of fall velocities to calculate the distribution of ashfall. The model was developed numerically and considers particles smaller than a centimetre in diameter. The model does not allow for the settling speed to vary with elevation.

  Hurst *et al.* [26] claim that ASHFALL is a more realistic model than the Pisa two-dimensional program [1] [35] [36] as it can take into account wind speed at different heights and can quickly predict where and with what volume the ash would fall for a volcanic eruption. Hurst *et al.* also claim that ASHFALL was a better model than that of Glaze *et al.* [22] as Glaze *et al.* only modelled a single wind pattern. On the other hand, Hurst *et al.* conceded that their model has accuracy limitations. In the paper by Turner [27], the author highlights that the accuracy of the prevailing wind direction is important as it affects the distribution of ash predicted by ASHFALL.

- The Calpuff model [4] is a Lagrangian dispersion model that is used to simulate the release of particulate materials and their transport in the atmosphere. According to one of the team members in the Calpuff project, Augusto Neri (pers. comm.), the team are in the process of improving the model; the original code assumed that the mixture emitted is composed only of gases obeying the ideal gas law. The effectiveness of this model is still unknown at the time of writing this thesis.

- Connor *et al.* [17] used an advection-dispersion model which was based on Suzuki's model [49]. To address the limitation of the long computation time required for Suzuki's model, the model simplified the atmospheric conditions in several ways: the winds were assumed uniform with respect to height above the volcanic vent and particle motion in the column was treated probabilistically rather than deterministically. The resulting code was used to compile hazard curves and hazard maps for the Cerro Negro volcano, Nicaragua [15] [23].

- HAZMAP [7] was developed as part of the emergency response programme for the effects of volcanic ash. It was to test on the eruption of Soufriere Hills Volcano from 1995 to 1999. The model is numerical. It models the dispersion of the volcanic plume and the deposition of ash. The model was based on the theory of Armienti *et al.* [1] and Macedonio *et al.* [36]. It was reported that the predictions of HAZMAP are in good agreement with field data. However,

the model does not take into account the change in dispersion with respect to elevation.

There are some assumptions that are common to the models ASHFALL [26] and HAZMAP [7]. The vertical dispersion coefficient is assumed to be negligible, as the vertical dispersion is small above 500 metres, and the horizontal dispersion was considered isotropic and constant.

1.5 Purpose

Why our models?

The development of the advection-dispersion models discussed above required computation and extensive programming knowledge. The process of volcanology is undoubtly very complex, however, despite its complexity we believe that mathematical techniques and tools are able to capture and model these complicated processes.

The modelling of volcanic ashfall has been attempted by many volcanologists. All used geological processes to explain the cause of volcanic activity. Koyaguchi [30] observes that it is difficult to estimate the total amount of ejecta using geological methods because fine particles are likely to be dispersed in the atmosphere and cannot be accounted for in local deposits. Technically, the description of transport and dispersion of ash particles should be modelled using mechanics and fluid dynamics. Geologists have a good understanding of the deposition of large particles from an ash cloud, however, the behaviour of fine ash particles is less well understood. This is why Sparks [47] recognises that modelling of volcanic ashfall requires the collaboration of applied mathematicians and earth scientists. Modelling of ashfall requires understanding from many disciplines.

Similar to the existing models mentioned above, our models calculate the ash deposit on the ground. Two kinds of atmosphere models are considered in the development of our theory:

- *Uniform atmosphere* which assumes the parameters describing the atmosphere are uniform throughout the process of ashfall;
- *Layered atmosphere* which assumes the parameters describing the atmosphere are not uniform throughout the process of ashfall.

The rationale for this thesis is to extend the modelling of volcanic ashfall by using simple and efficient mathematical models. We aim to develop simple deterministic mathematical models which enable the effect of parameter variation to be explored more readily.

Our models allow for the settling speed to change during the process of ashfall (unlike the model ASHFALL [26]), take into account the expected changes in wind pattern (which Connor *et al.* [15] do not consider) and take into account the expected change in dispersion (assumed constant in HAZMAP [7]).

Figures 1.3 and 1.4 demonstrate the two kinds of atmosphere which are used in this thesis. In a uniform atmosphere (Figure 1.3), the parameters are assumed constant throughout the process of ashfall. A layered atmosphere model (Figure 1.4) is more realistic as it allows the parameters to change with elevation in atmospheric conditions, i.e. wind speed, settling speed and dispersion. In each horizontal layer there may be a different wind speed or direction. The pattern and distribution of the ash depends very much on the physical conditions of the atmosphere during the ashfall. Holasek *et al.* [24] point out that the ash distribution is controlled by wind dispersal and gravitational settling.

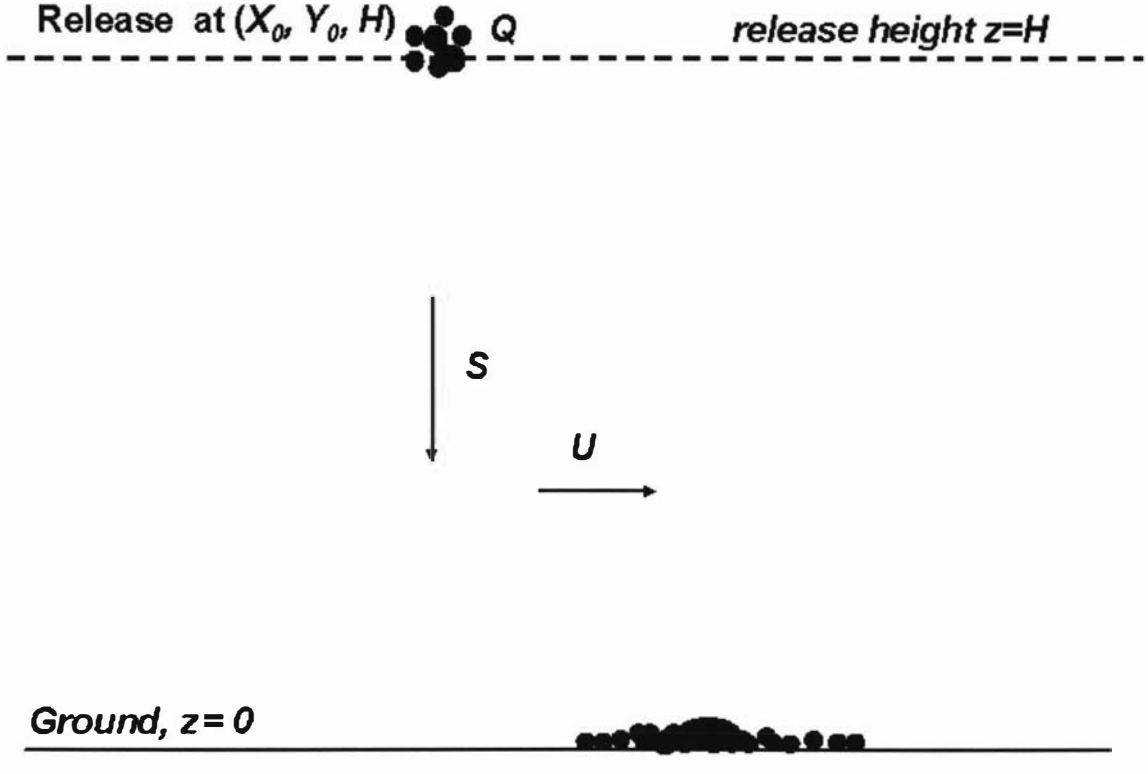

Figure 1.3: A schematic of a uniform atmosphere.

1.6 Problem

A difficulty encountered in this thesis was obtaining real eruption data. Most volcanologists are quite reluctant to share their data. Dr Augusto Neri of the National

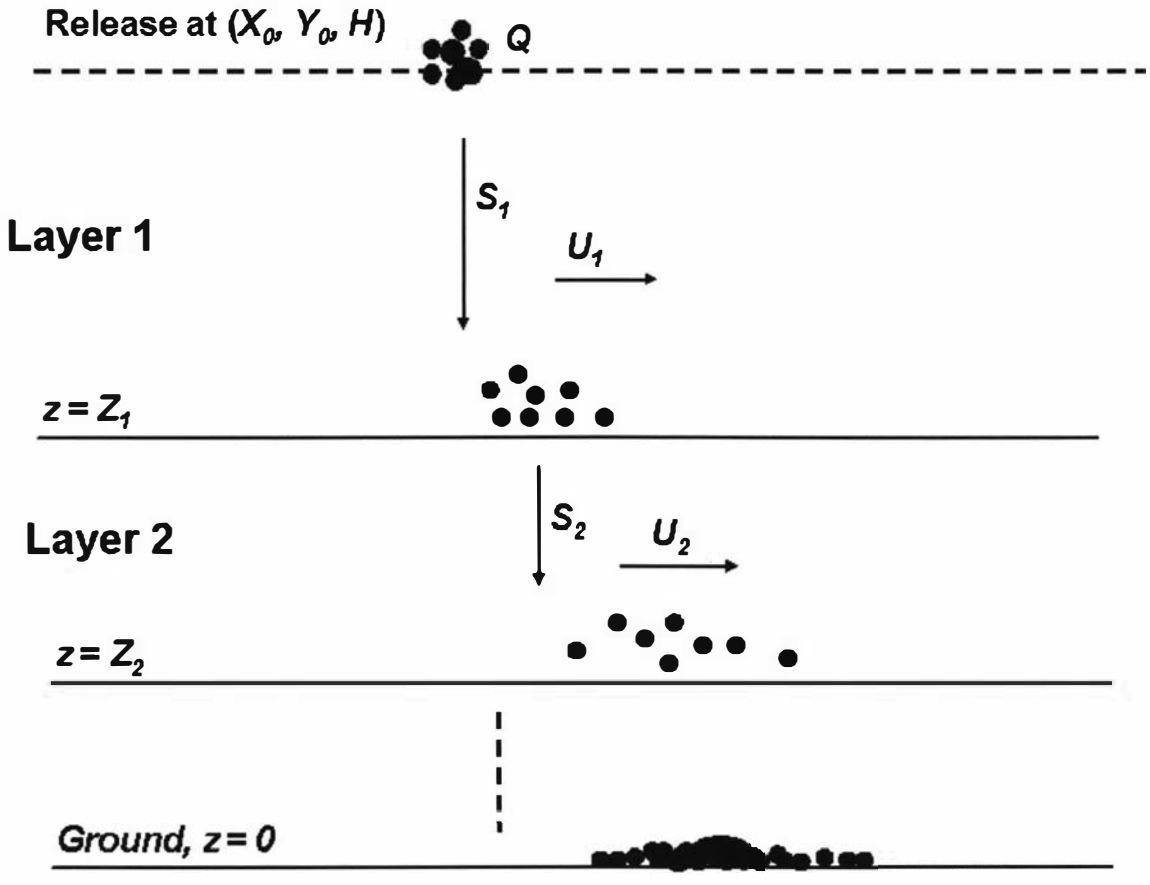

Figure 1.4: A schematic of a layered atmosphere.

Institute of Geophysics and Volcanology (Istituto Nazionale di Geofisica e Vulcanologia) in Italy and Dr Henry Gaudru of the United Nations (the International Strategy for Disasters Reduction (ISDR) adviser for volcanic risk mitigation) commented that people who compiled eruption data are usually unwilling to share their data (pers. comm.).

Due to the paucity of observational data from volcanologists, we found it very difficult to test the models developed in this thesis. Some assumptions had to be made in order to test our models. Fortunately, Prof. Chuck Connor of the Department of Geology at the University of South Florida provided some data (Table 1.1) (pers. comm.). Unfortunately, this data can only be used in our uniform atmosphere models. In order to apply it to our layered atmosphere models we used his data to estimate the required parameters (Table 1.2).

Table 1.1: Data of 1992 eruption of Cerro Negro Volcano, Nicaragua (from Prof. Chuck Connor of the Department of Geology at the University of South Florida).

Parameter	X_0	Y_0	H	Q	U	V	S	D_h	D_z
Value	0	0	7500	2.5×10^{10}	10	0	1	800	0

Table 1.2: Data used for some plots on layered atmosphere models.

Parameter		Layer 1	Layer 2	Layer 3	Layer 4
X_0	0				
Y_0	0				
H	7500				
Q	25×10^9				
U		10	-10	10	-10
V		0	0	0	0
S		1	1	1	1
D_h		800	800	800	800
D_z		0	0	0	0

1.7 Overview of the Thesis

Of the models discussed in Section 1.2, ASHFALL [25] [26] [27] is unable to take into account any change in settling speed during the process of ashfall; Connor *et al.* [17] do not consider any physical change in the atmosphere during the process of ashfall and HAZMAP [7] does not allow for change in dispersion during the process of ashfall. These are the areas which we address in this thesis.

The models developed in this thesis are based on ashfall from a point release, i.e. the release source is a single point. Our research is mainly on modelling the consequent distribution of ashfall on the ground and to obtain solutions that show the distribution pattern of ashfall. As mentioned, this thesis uses two approaches for the modelling of volcanic ashfall. One assumes a uniform atmosphere while the other assumes a layered atmosphere. The dispersion and wind speed are assumed constant throughout the ashfall in a uniform atmosphere whereas we allow for changes in dispersion, wind velocity or settling speed with respect to height during the process of ashfall in a layered atmosphere model.

The objective of this thesis is to develop three-dimensional models to calculate the concentration of ash in the atmosphere as a function of time and to calculate the deposit of ash on the ground for a three-dimensional atmosphere. We also make every possible effort to solve the models analytically.

This thesis reports on the development and analysis of our models. Chapters 2 and 3 describe the development of models using a uniform and a layered atmosphere, respectively. Chapters 4 and 5 report on the analyses of deposits and parameters in the advection-dispersion equation, respectively. Some work done on the estimation of parameters of ashfall is discussed in Chapter 6. Finally Chapter 7 summarises the thesis and gives conclusions and suggestions for future work. Some derivations and proofs required in the development of our models are presented in the Appendices.

Chapter 2

UNIFORM ATMOSPHERE MODELS

uniform pattern may be dull or simple
but it is a base to explore

What is a uniform atmosphere model?

In a uniform atmosphere model, the atmospheric parameters (wind speeds, settling speed, dispersion tensors) are assumed uniform throughout the process of ashfall. A schematic of a uniform atmosphere is shown in Figure 1.3.

Although the preliminary aim is to model volcanic ashfall in a three-dimensional atmosphere, some one- and two-dimensional models are investigated.

Four cases involving uniform atmosphere models are considered:

Case A - instantaneous release in the whole three-dimensional space;

Case B - instantaneous release in a three-dimensional half space bounded below by the ground;

Case C - steady release in the whole three-dimensional space;

Case D - steady release in half space.

Practically, it is more realistic to model volcanic ashfall in the half space for $0 \leq z < \infty$ (z is the vertical axis in a three-dimensional Cartesian coordinate system, where the $x - y$ plane is horizontal) because the ground is usually set at $z = 0$. However, it is not always possible to solve the advection-dispersion equation analytically on the domain $0 \leq z < \infty$. Zoppou *et al.* [57] pointed that very few analytical solutions have been found for the advection-dispersion equation and the analytical solutions found are subject to various boundary conditions.

2.1 Modelling

The deposit of ashfall from volcanic eruptions, pollen distribution by the wind, seabed contamination by dumping, and environmental pollution through airborne contaminants (solid or gaseous) can all be described by mathematical models which combine advection and dispersion. The description that follows is set in the context of volcanically-erupted ash (small rock particles), the analysis is the same for various other air-borne or water-transported particles [39].

This thesis deals with heavier-than-fluid releases. It includes discussion of sample results calculated from advection-dispersion models which take account of lateral drift caused by the wind, settling of the released particles and turbulence in the atmosphere.

At present, the accuracy of predictions are restricted by simplifying assumptions about the wind velocity and dispersion coefficients which represent the air turbulence. In practice, the precision will also be constrained by the inherent variability between similar releases due to turbulent dispersion. The models in this thesis aim to recreate a typical event (such aspects of variability have been explored in [50]).

The physical processes affecting the distribution of eruption materials are very complicated and some simplification within the models is necessary. Some of the main features captured by the models are [39]:

- At a given height, the wind is uniform in speed and direction, the settling speed for any given particle is constant and the turbulence length scales are uniform.
- The ground or bed surface is approximately horizontal - it is assumed that the fluid flow is parallel to the surface and that variation of topography is not severe enough to influence the average transport mechanisms.
- The material ejected by the volcano is released into the wind at a certain height. Each particle quickly takes up a velocity which corresponds to the wind speed laterally and the particle's terminal speed (the 'settling speed') vertically downwards.
- At a given height, turbulence within the air flow is modelled as having a certain characteristic length - since turbulence has a variety of scales, the length is a typical mean value for the flow.

2.2 Why Advection-Dispersion Equation?

The advection-dispersion equation can be used to describe transport of particles by wind and scattering by dispersion. It is widely applied to the study of solute transport

phenomena. The advection-dispersion equation used in this thesis can also be applied to the modelling of rainfall, pollution and water movement.

An early model developed by Suzuki [49] was a two-dimensional dispersion model. His model only considered horizontal dispersion as he found that, although small particles disperse in the atmosphere in both vertical and horizontal directions, the scale of horizontal turbulence is much greater than that of vertical turbulence. However, Connor *et al.* [15] considered Suzuki's model too simplified. Carey [12] observes that models using an advection-dispersion model describe ashfall better than the model of Suzuki [49], because the advection-dispersion model takes into account wind speed and direction along with altitude. Suzuki's model was modified by Glaze *et al.* [22] and has been tested against observation, with predicted mass distribution agreeing well with observed distributions. Armienti *et al.* [1] developed a three-dimensional advection-dispersion model, based on Suzuki's model, which was numerically solved.

In our study, a Cartesian coordinate system (x, y, z) is used, (x, y) measuring position with respect to a fixed origin on the ground and z measuring the height above the ground. As stated, it is assumed that the movement of the wind is horizontal, flowing parallel to the ground with mean velocity $\mathbf{u} = (U, V, 0)$, in the (x, y, z) coordinate system. In this chapter it is assumed that there is no variation in wind speed with height so that U and V are constant (variation in the parameters is incorporated into Chapter 3). The ash particles are assumed to be small and numerous, so that a locally-averaged mass concentration (mass per unit volume) can be defined which we denote $c = c(x, y, z, t)$.

The advection-dispersion equation is derived from conservation of mass:

$$\frac{\partial c}{\partial t} = -\nabla \cdot \mathbf{m} + M \tag{2.1}$$

where

M – source mass rate (mass per unit time per unit volume) and

$\mathbf{m}$ – mass flux of particles per unit area, defined by

$$\mathbf{m} \;=\; c\mathbf{u} - cS\mathbf{k} - \underline{\mathbf{D}} \otimes \nabla c \tag{2.2}$$

(where $\mathbf{k} = (0, 0, 1)$ is a unit vector).

There are three distinct components to the specific mass flux $\mathbf{m}$: the first is the mean advective flux $c\mathbf{u}$, caused by the movement of the wind; the second is the advective flux $-cS\mathbf{k}$, caused by the settling speed S; the third is the (mechanical) dispersive flux $-\underline{\mathbf{D}} \otimes \nabla c$, caused by the atmospheric turbulence, which is quantified by the dispersive tensor $\underline{\mathbf{D}}$ and the concentration gradient.

2.2.1 Advection due to the wind

Advection ($c\mathbf{u}$) describes the horizontal transport of particles by the wind. This thesis will consider only the movement of particles transported by the wind in x and y-directions. The wind speed in the z-direction is assumed zero by volcanologists [1] [6]. Because the wind does not flow through the ground, it is parallel to the ground at the ground surface, and is assumed to be so at higher elevations as well. Suzuki [49] assumed the horizontal wind speed to be a function of elevation z given in the form:

$$W(z) = W_0 \left(1 - \frac{z}{H}\right)^{\lambda}$$

where W_0 is the speed at $z = 0$, H is the maximum height of the eruption column and λ is a constant.

2.2.2 Dispersion

The dispersion term, $(-\underline{\mathbf{D}} \otimes \nabla c)$ in Equation (2.2), describes the spread of particles by the turbulence in the atmosphere.

In general, the dispersion tensor is of the form $\underline{\mathbf{D}} = \begin{bmatrix} D_{11} & D_{12} & 0 \\ D_{21} & D_{22} & 0 \\ 0 & 0 & D_{33} \end{bmatrix}$. (2.3)

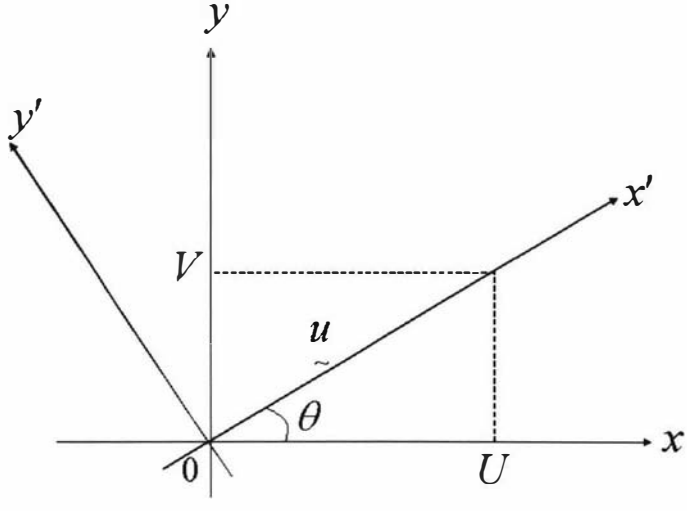

Figure 2.1: Horizontal plane of dispersion tensor coordinate system.

If we assume that the dispersion tensor has principal axes (x', y', z') (see Figure 2.1), x' and y' aligned parallel and perpendicular to the horizontal wind vector $\mathbf{u}$, with the parallel (downwind) component D_d, horizontal perpendicular (cross-wind) component D_c, and vertical component D_v, then

$$\underline{\mathbf{D}'} = \begin{bmatrix} D_d & 0 & 0 \\ 0 & D_c & 0 \\ 0 & 0 & D_v \end{bmatrix} \tag{2.4}$$

with respect to the (x', y', z') coordinate system.

In the (x', y', z') coordinate system, $\mathbf{u} = (W, 0, 0)$ is the wind vector, with wind speed W and $\mathbf{g} = (0, 0, -g)$. For the general coordinate system (x, y, z) we have $\mathbf{u} = (U, V, 0)$ with $U = W\cos\theta$ and $V = W\sin\theta$.

If the wind is blowing at an angle to both the x- and y-axes, $\underline{\mathbf{D}}$ can only be diagonal if $D_d = D_c$, i.e. the dispersion tensor is isotropic with $x - y$ plane. We write the coefficients as $(D_d, D_c, D_v) = (D_x, D_y, D_z)$. As volcanologists ([7], [15], [26]) assume the dispersion tensor is isotropic within the $x - y$ plane, i.e. $D_x = D_y$, we make the same assumption since there is little information about anisotropic dispersion.

The dispersion tensor is then written in the form $\underline{\mathbf{D}} = |\mathbf{u}|\underline{\mathbf{L}}$ where $|\mathbf{u}|$ is the mean horizontal wind speed $\sqrt{U^2 + V^2}$ and $\underline{\mathbf{L}}$ is a diagonal dispersion length tensor whose elements are the dominant atmospheric turbulence length scales so

$$D_x = L_x|\mathbf{u}|, \qquad D_y = L_y|\mathbf{u}|, \qquad D_z = L_z|\mathbf{u}|\,.$$

Because dispersion is proportional to the wind speed, if there is no wind then there is no dispersion, and the particles will therefore settle vertically to the ground.

2.2.3 Settling speed

The vertical falling speed of a particle depends on its mass and shape. In this study, the particles are assumed to be approximately spherical and therefore their size is defined by their radius. The speed v of a falling particle can be determined by resolving the gravitational and air drag forces:

$$m\frac{dv}{dt} = mg - \frac{1}{2}C_s\rho_a A v^2\,. \tag{2.5}$$

The drag coefficient C_s, depends on both the radius of particle R and the settling speed S. Perry [43] gives an expression for C_s as follows:

$$C_s = \frac{24}{Re}(1 + 0.14Re^{0.70}) \text{ for } Re \leq 1000 \text{ and} \tag{2.6}$$

$$C_s = 0.447 \text{ for } Re > 1000 \tag{2.7}$$

where

Re - Reynolds number, defined by $Re = \dfrac{\rho_a(2R)v}{\mu_a}$;

μ_a - dynamic viscosity of air ($= 1.461 \times 10^{-5}$ kg m^{-1} s^{-1});

R - radius of the particle (m);

ρ_r - mass density of the particles ($= 1000$ kg m^{-3});

m - mass of a particle $= volume \times density = \dfrac{4}{3}\pi R^3 \rho_r$ (kg);

A - cross-sectional area of the particle $= \pi R^2$ (m^2)

g - gravitational constant ($= 9.81$ m s^{-2});

ρ_a - mass density of the air ($= 1.225$ kg m^{-3});

$v(t)$ - falling speed of particles (m s^{-1});

S - settling speed of particles (m s^{-1}) = steady-state falling speed.

In general, for a particle which is moving vertically, the weight and air drag forces are not in balance and the particle either accelerates or decelerates. However, a steady-state is approached where $\dfrac{dv}{dt} = 0$. When this happens the particle is falling at its settling speed S. From Equation (2.5), S is given by

$$\frac{1}{2}C_s\rho_a A S^2 = mg\,. \tag{2.8}$$

In general, it is not possible to explicitly find the value of S from (2.8) unless $Re = \dfrac{2\rho_a RS}{\mu_a} > 1000$. For $Re < 1000$, the Equation (2.8) requires numerical solution.

A particle released from rest accelerates vertically downward according to Equation (2.5). Figure 2.2 shows two examples of the falling speed versus time for particles of radius $R = 0.2$ mm and $R = 0.4$ mm. Their settling speeds are calculated as 1.63 and 3.16 m/s respectively (indicated by * on the v-axis). Figure 2.3 shows the settling speed versus radius of particle. The two * indicate the settling speed of particles size $R = 0.2$ mm and $R = 0.4$ mm (as in Figure 2.2).

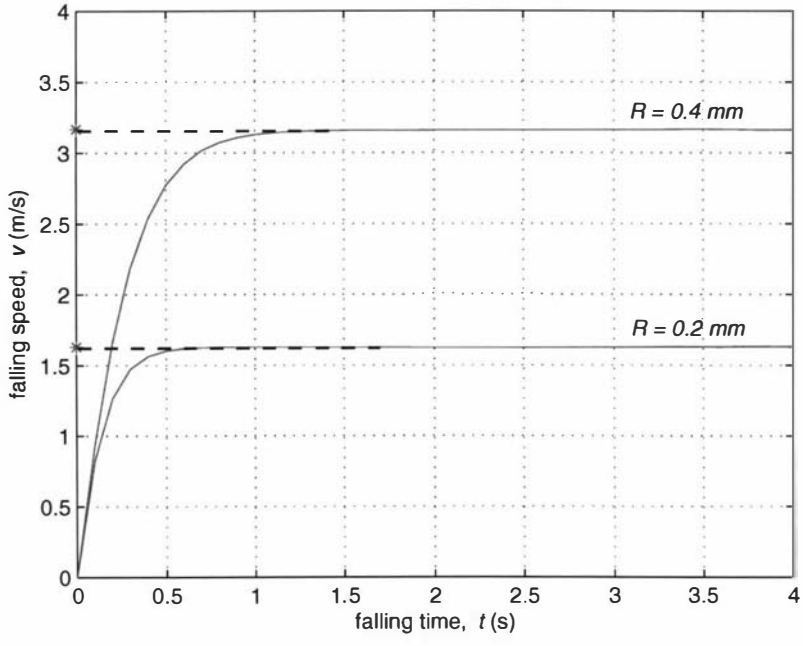

Figure 2.2: Falling speed versus time. Settling speeds indicated by * on v-axis.

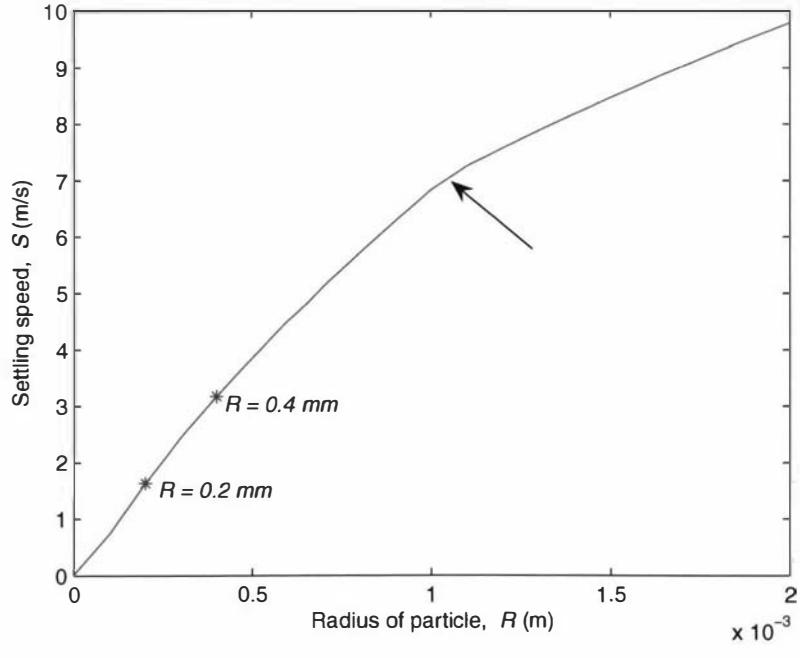

Figure 2.3: Settling speed versus radius of particle. The arrow marks the point where the Reynolds number is 1000. The larger the radius the larger the Reynolds number.

2.2.4 Advection-dispersion model

From Equations (2.1) and (2.2), we obtain

$$\frac{\partial c}{\partial t} + \nabla \cdot (c\mathbf{u} - cS\mathbf{k} - \underline{\mathbf{D}} \otimes \nabla c) = M\,. \tag{2.9}$$

Since we are only interested in circumstances in which atmospheric properties, and properties of the particle, vary in the z-direction, the dispersion $\underline{\mathbf{D}}$ and $\mathbf{u}$ are functions of z, S may be a function of z because of agglomeration. With the use of an isotropic dispersion tensor in the $x-y$ plane, the advection-dispersion Equation (2.9) becomes

$$\begin{aligned}&\frac{\partial c}{\partial t} + U(z)\frac{\partial c}{\partial x} + V(z)\frac{\partial c}{\partial y} - \frac{\partial}{\partial z}\left(S(z)c\right) - D_x(z)\frac{\partial^2 c}{\partial x^2} - D_y(z)\frac{\partial^2 c}{\partial y^2}\\ &-\frac{\partial}{\partial z}\left(D_z(z)\frac{\partial c}{\partial z}\right) = M(x,y,z,t).\end{aligned} \tag{2.10}$$

The Equation (2.10) is difficult to solve analytically for even simple z-dependence of the parameters. We therefore assume that all the parameters are constant. We assume a total mass Q (kg) of volcanic ash with uniform particle size is released at point (X_0, Y_0, H) in the atmosphere. Here H is the release height, X_0 and Y_0 are coordinates of x and y, respectively, at the release point ($t = 0$). Therefore, the source $M(x, y, z, t)$ in Equation (2.10) is $Q\delta(x - X_0)\delta(y - Y_0)\delta(z - H)\delta(t)$. The motion of ash is affected by the physical conditions in the atmosphere: the wind speed and direction and the turbulence which causes dispersion. U and V are wind speeds in the x and y directions, respectively, S is the settling speed in the z direction and D_x, D_y and D_z are the dispersion in the x, y and z directions, respectively, for the uniform atmosphere model. It is assumed that the wind speed, dispersion and settling speed are all constant. Since $D_x = D_y$, we will now write D_x and D_y as D_h (horizontal dispersion coefficient). The three-dimensional advection-dispersion Equation (2.10) becomes

$$\begin{aligned}&\frac{\partial c}{\partial t} + U\frac{\partial c}{\partial x} + V\frac{\partial c}{\partial y} - S\frac{\partial c}{\partial z} - D_h\frac{\partial^2 c}{\partial x^2} - D_h\frac{\partial^2 c}{\partial y^2} - D_z\frac{\partial^2 c}{\partial z^2}\\ =\;& Q\delta(x - X_0)\delta(y - Y_0)\delta(z - H)\delta(t)\,.\end{aligned} \tag{2.11}$$

We will use Equation (2.11) for the models in this thesis.

2.3 Case A: Instantaneous Release in Whole Space

In Case A, we define the downward flux as $Sc+D_z\frac{\partial c}{\partial z}$ with respect to time, $0 \leq t < \infty$, where the downward flux is assumed to pass through the "ground" $z = 0$. The total deposit f on the "ground" $(z = 0)$ is determined by integrating the downward flux with respect to time, $0 \leq t < \infty$,

$$f(x,y) = \int_0^\infty \left[Sc + D_z\frac{\partial c}{\partial z}\right]_{z=0} dt\,. \tag{2.12}$$

The unit of f is mass per unit area (kg m^{-2}) in the three-dimensional atmosphere.

The determination of the function $f(x,y)$, which is the deposit on the "ground" from eruption is important in order to warn the public of the area affected by the ashfall. The calculation of volumes of tephra deposits is difficult due to the nonlinear dependence of thickness on area. The review of some methods on calculating the deposit can be found in the paper [21].

The following sections describe the models for modelling the ashfall for instantaneous releases in one-, two- and three-dimensional atmospheres.

2.3.1 One-dimensional model

In this section, we assume there is no horizontal wind, i.e. $U = V = 0$ and $D_h = 0$. In this case, the three-dimensional model reduces to a one-dimensional model.

$$\frac{\partial c}{\partial t} - S\frac{\partial c}{\partial z} - D_z\frac{\partial^2 c}{\partial z^2} = Q\delta(z-H)\delta(t)\,.$$

In this model, the release source is located at the point $z = H$. Alternatively, in three-dimensions we may regard the release as being constant across a plane, $(x,y,z) = (x,y,H)$.

It is assumed that $c = 0$ at time $t = 0^-$, a total mass Q (kg m^{-2}) is released at height $z = H$ and $c \to 0$ as $z \to \pm\infty$.

The concentration $c(z,t)$ can be determined by applying Fourier and Laplace transformations, and is given by

$$c(z,t) = \frac{Q}{2\sqrt{\pi D_z t}} e^{-\frac{(z-H+St)^2}{4D_z t}}\,.$$

The deposit f (2.12) on the "ground" $(z = 0)$ is

$$\begin{aligned} f &= \int_0^\infty \left(Sc(0,t) + D_z \frac{\partial c(0,t)}{\partial z} \right) dt \\ &= Q\,. \end{aligned}$$

The result $f = Q$ verifies that the total mass released falls through the surface $z = 0$.

(See Appendix A.6 for the working of the three-dimensional model, the same technique is used for the one-dimensional model.)

2.3.2 Two-dimensional model

In this section, we assume there is no horizontal wind speed in the y-direction, i.e. $V = 0$. In this case, the three-dimensional model reduces to a two-dimensional model.

$$\frac{\partial c}{\partial t} + U\frac{\partial c}{\partial x} - S\frac{\partial c}{\partial z} - D_h\frac{\partial^2 c}{\partial x^2} - D_z\frac{\partial^2 c}{\partial z^2} = Q\delta(x - X_0)\delta(z - H)\delta(t)\,.$$

In this model, the release source is located at the point $(x, y) = (X_0, H)$. In three-dimensions the release corresponds to a line at $(x, y, z) = (X_0, y, H)$.

Similarly, it is assumed that $c = 0$ at time $t = 0^-$ and $c \to 0$ as $x \to \pm\infty$ or $z \to \pm\infty$ with a total mass Q (kg/m) released at $x = X_0$ and $z = H$.

By applying Fourier and Laplace transformations we obtain,

$$c(x, z, t) = \frac{Q}{4\pi t\sqrt{D_h D_z}} e^{-\frac{(x - X_0 - Ut)^2}{4D_h t} - \frac{(z - H + St)^2}{4D_z t}}\,.$$

Using MATLAB, the corresponding deposit on the "ground" $(z = 0)$, is found to be

$$\begin{aligned} f(x) &= \int_0^\infty \left(Sc + D_z \frac{\partial c}{\partial z} \right)_{z=0} dt \\ &= \int_0^\infty \frac{Q}{8\pi\sqrt{D_h D_z}} \left(\frac{H}{t^2} + \frac{S}{t} \right) e^{\left[-\frac{(x - X_0 - Ut)^2}{4D_h t} - \frac{(-H + St)^2}{4D_z t} \right]} dt \\ &= \int_0^\infty \frac{Q}{8\pi\sqrt{D_h D_z}} e^{\frac{1}{2}\left(\frac{xU}{D_h} + \frac{HS}{D_z}\right) - 2\alpha\beta} \left(\frac{H}{t^2} + \frac{S}{t} \right) e^{-\frac{(\beta t - \alpha)^2}{t}} dt \end{aligned}$$

$$= \frac{Q}{8\pi\sqrt{D_h D_z}} e^{\frac{1}{2}\left(\frac{(x - X_0)U}{D_h} + \frac{HS}{D_z}\right) - 2\alpha\beta} \left[\frac{2H\beta}{\alpha} e^{2\alpha\beta} K_1(2\alpha\beta) + 2Se^{2\alpha\beta} K_0(2\alpha\beta) \right]$$

$$= \frac{Q}{4\pi\sqrt{D_h D_z}} e^{\frac{1}{2}\left(\frac{(x - X_0)U}{D_h} + \frac{HS}{D_z}\right)} \left[SK_0(2\alpha\beta) + \frac{H\alpha}{\beta} K_1(2\alpha\beta) \right]$$

where K_0 and K_1 are modified Bessel functions [44] of the second kind of order zero and one, respectively, and

$$\alpha = \sqrt{\frac{1}{4}\left[\frac{(x-X_0)^2}{D_h} + \frac{H^2}{D_z}\right]} \text{ and } \beta = \sqrt{\frac{1}{4}\left[\frac{U^2}{D_h} + \frac{S^2}{D_z}\right]}.$$

2.3.3 Three-dimensional model

For a three-dimensional whole space atmosphere, the three-dimensional advection-dispersion equation (2.11) is used.

$$\begin{aligned}&\frac{\partial c}{\partial t} + U\frac{\partial c}{\partial x} + V\frac{\partial c}{\partial y} - S\frac{\partial c}{\partial z} - D_h\frac{\partial^2 c}{\partial x^2} - D_h\frac{\partial^2 c}{\partial y^2} - D_z\frac{\partial^2 c}{\partial z^2}\\ &= Q\delta(x-X_0)\delta(y-Y_0)\delta(z-H)\delta(t)\,.\end{aligned}$$

With the initial and boundary conditions: $c = 0$ at time $t = 0^-$ and $c \to 0$ as $x \to \pm\infty$, $y \to \pm\infty$ or $z \to \pm\infty$. Now, the unit of Q are in kg (the source is a point) and is released at $x = X_0$, $y = Y_0$ and $z = H$.

By applying Fourier and Laplace transformations, the concentration at point (x, y, z) after time t is found to be

$$c(x,y,z,t) = \frac{Q}{8D_h\sqrt{\pi^3 D_z t^3}} e^{-\frac{(x-X_0-Ut)^2}{4D_h t} - \frac{(y-Y_0-Vt)^2}{4D_h t} - \frac{(z-H+St)^2}{4D_z t}}. \tag{2.13}$$

Again, the downward flux of ashfall is used to determine the deposit on the "ground". The downward flux of the ashfall at $z = 0$ is $Sc(x, y, 0, t) + D_z\dfrac{\partial c(x, y, 0, t)}{\partial z}$. Integrating the downward flux with respect to time, $0 \le t < \infty$, the deposit $f(x, y)$ on the "ground" $(z = 0)$ in the three-dimensional atmosphere will be a function of x and y.

$$f(x,y) = \frac{Q}{32\pi D_h\sqrt{D_z}}\, e^{\frac{1}{2}\left(\frac{(x-X_0)U}{D_h} + \frac{(y-Y_0)V}{D_h} + \frac{HS}{D_z}\right) - 2\alpha\beta}\left[\frac{(2\alpha\beta+1)H + 2\alpha^2 S}{\alpha^3}\right] \tag{2.14}$$

where $\alpha = \sqrt{\frac{1}{4}\left[\frac{(x-X_0)^2}{D_h} + \frac{(y-Y_0)^2}{D_h} + \frac{H^2}{D_z}\right]}$ and $\beta = \sqrt{\frac{1}{4}\left[\frac{U^2}{D_h} + \frac{V^2}{D_h} + \frac{S^2}{D_z}\right]}$.

(See Appendix A.4 for the working of the solution 2.14)

We plotted equation (2.14) using the data in Table 1.1 but instead of taking $D_z = 0$, we used $D_z = 800$ and $D_z = 1$. We can see that the contour of deposition in Figure

2.4 has a elongated spread but not in Figure 2.6. With $D_z \neq 0$, the ashfall will tend to spread with respect to the wind direction, in this case, the x-direction as there is no wind in the y-direction ($V = 0$). We will discuss the limit as $D_z \to 0$ in Chapter 4.

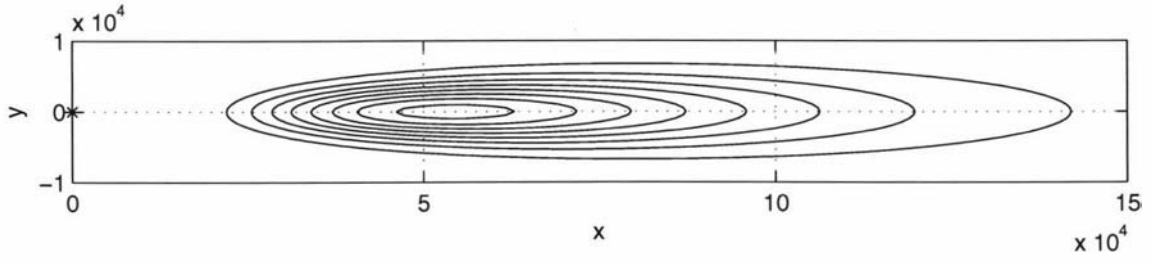

Figure 2.4: Contour of deposition at instantaneous release in three-dimensional uniform whole space with $D_z = 800$. The innermost contour has the highest deposit whilst the outermost has the lowest deposit.

2.4 Case B: Instantaneous Release in Half Space

In this section, we discuss the three-dimensional model with a half space atmosphere and an instantaneous release. We build up towards a three-dimensional model, beginning with an one-dimensional atmosphere. The same advection-dispersion equation (2.11) is used in the modelling of the half space:

$$\begin{aligned}&\frac{\partial c}{\partial t} + U\frac{\partial c}{\partial x} + V\frac{\partial c}{\partial y} - S\frac{\partial c}{\partial z} - D_h\frac{\partial^2 c}{\partial x^2} - D_h\frac{\partial^2 c}{\partial y^2} - D_z\frac{\partial^2 c}{\partial z^2}\\ &= Q\delta(x - X_0)\delta(y - Y_0)\delta(z - H)\delta(t)\,.\end{aligned}$$

There is a difference in the boundary conditions for the half space atmosphere, because the range of z in half-space is $0 \leq z < \infty$.

Initial condition: $c = 0$ at $t = 0^-$.

Boundary conditions: $z = 0$ is assumed to be the ground. As no material can penetrate the ground, there is zero downward dispersive flux at $z = 0$. Hence $D_z\dfrac{\partial c}{\partial z} = 0$ at $z = 0$. So either $D_z = 0$ or $\dfrac{\partial c}{\partial z} = 0$, but since $D_z \neq 0$ we take $\dfrac{\partial c}{\partial z} = 0$ at $z = 0$. The same as the whole space model, we also take $c \to 0$ as $x \to \pm\infty$, $y \to \pm\infty$ or $z \to \infty$.

The ash particle size considered in this thesis is very tiny (less than 2 mm), so the settling speed is small too. Even if the particle bounces up when it hits the ground,

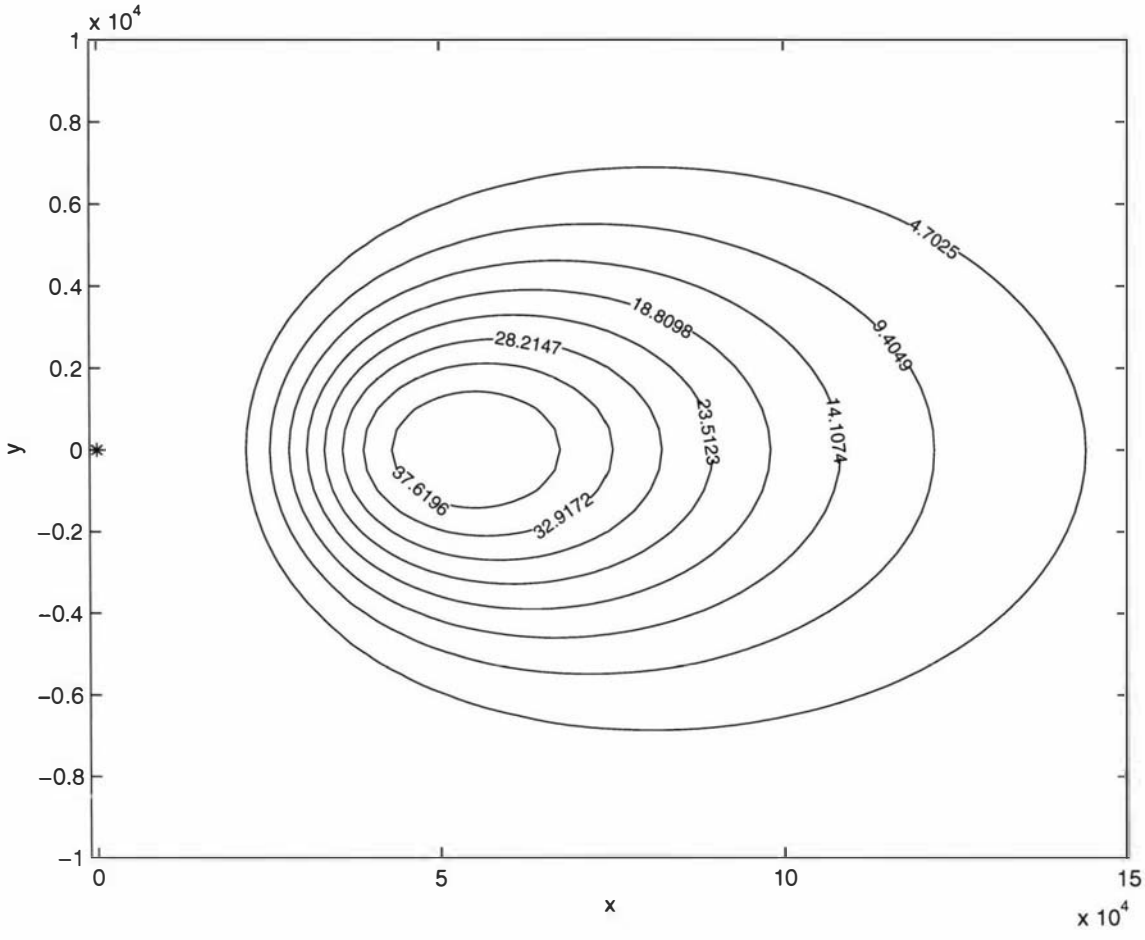

Figure 2.5: This is a scaled version of Figure 2.4 in order to label the values f (kg/m^2) for each contour lines. We show only this example in this thesis to explain the contour lines. The contour plot is the top view of a three-dimensional plot. This figure shows eight contour lines of deposition f (kg/m^2), each contour line defines a different value of f (kg/m^2). From the figure, we see that the inner contour lines have larger values of f than the outer contour lines. This illustrates (the inner contour line is close to) the centre of the deposit which is more dense than the outer part of deposit, as the farther it spreads the thinner the deposition, so the values of f are smaller towards the outer parts. The deposit close to the centre is thicker so f is larger. The innermost contour has the highest deposit whilst the outermost has the lowest deposit.

the bouncing force is insignificant due to the small settling speed, so that the bouncing distance from the ground is small. Hence it will settle onto the ground very quickly.

2.4.1 One-dimensional model

As in the whole space, in this one-dimensional atmosphere, c is a function of z and t. The one-dimensional advection-dispersion equation is

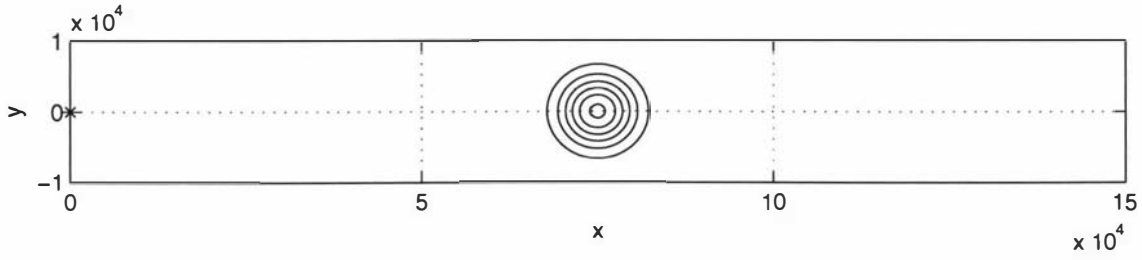

Figure 2.6: Contour of deposition at instantaneous release in three-dimensional uniform whole space with $D_z = 1$. The innermost contour has the highest deposit whilst the outermost has the lowest deposit.

$$\frac{\partial c}{\partial t} - S\frac{\partial c}{\partial z} - D_z\frac{\partial^2 c}{\partial z^2} = Q\delta(z-H)\delta(t)\,.$$

Through applying a Green's function, we obtain

$$\begin{aligned} c(z,t) \;=\; & Q\frac{e^{-\frac{S^2}{4D_z}t}}{\sqrt{4\pi D_z t}}\left\{e^{-\frac{S}{2D_z}(z-H)}\left[e^{-\frac{(z-H)^2}{4D_z t}} + e^{-\frac{(z+H)^2}{4D_z t}}\right] - 2e^{\frac{SH}{2D_z}-\frac{H^2}{4D_z t}}\right. \\ & \left. + \frac{S}{D_z}\int_0^z e^{-\frac{S(\xi-H)}{2D_z}-\frac{(\xi+H)^2}{4D_z t}}\,d\xi\right\} \\ & - \frac{Q}{4\sqrt{\pi D_z}}\int_0^t\left[\left(\frac{SH}{D_z}+2\right)\frac{1}{\tau^{3/2}} - \frac{H^2}{D_z}\frac{1}{\tau^{5/2}}\right]e^{-\frac{(-H+S\tau)^2}{4D_z\tau}}\,d\tau\,. \end{aligned}$$

The derivation of this one-dimensional model's concentration $c(z,t)$ is given in more detail in Appendix A.2.1.

Integrating the downward flux with respect to time, $0 \le t < \infty$, to determine the deposit f, on the ground we obtain

$$f \;=\; \int_0^\infty\left\{-\frac{SQ}{4\sqrt{\pi D_z}}\int_0^t\left[\left(\frac{SH}{D_z}+2\right)\frac{1}{\tau^{3/2}} - \frac{H^2}{D_z}\frac{1}{\tau^{5/2}}\right]e^{-\frac{(-H+S\tau)^2}{4D_z\tau}}\,d\tau\right\}dt.$$

The function f involves two integrals which we are not able to solve analytically.

2.4.2 Two-dimensional model

The same as in the two-dimensional whole-space modelling, the concentration $c(x,z,t)$ is a function of x, z and t, hence the advection-dispersion equation is

$$\frac{\partial c}{\partial t} + U\frac{\partial c}{\partial x} - S\frac{\partial c}{\partial z} - D_h\frac{\partial^2 c}{\partial x^2} - D_z\frac{\partial^2 c}{\partial z^2} = Q\delta(x - X_0)\delta(z - H)\delta(t)\,.$$

Again, it is not possible to completely solve the two-dimensional model analytically. The technique for solving the two-dimensional model is formulated based on the one-dimensional model. The concentration is

$$\begin{aligned} c(x,z,t) \;=\; & \frac{Q}{4\pi t\sqrt{D_h D_z}} e^{-\frac{(x-X_0-Ut)^2}{4D_h t} - \frac{S^2 t}{4D_z}} \left\{ e^{\frac{-S(z-H)}{2D_z}} \left[e^{\frac{-(z-H)^2}{4D_z t}} + e^{\frac{-(z+H)^2}{4D_z t}} \right] \right. \\ & \left. -2e^{\frac{SH}{2D_z} - \frac{H^2}{4D_z t}} + \frac{S}{D_z}\int_0^z e^{-\frac{S(\xi-H)}{2D_z} - \frac{(\xi+H)^2}{4D_z t}} d\xi \right\} - \frac{Q}{8\pi\sqrt{D_h D_z t}} \times \\ & \times e^{-\frac{(x-X-Ut)^2}{4D_h t}} \int_0^t \left[\left(\frac{SH}{D_z} + 2 \right) \frac{1}{\tau^{\frac{3}{2}}} - \frac{H^2}{D_z \tau^{\frac{5}{2}}} \right] e^{-\frac{(-H+S\tau)^2}{4D_z \tau}} d\tau\,. \end{aligned}$$

(See Appendix A.2.2.)

Integrating the downward flux with respect to time, $0 \leq t < \infty$, to determine the deposit, $f(x)$, on the ground we obtain

$$f(x) = \int_0^\infty \left\{ -\frac{SQ}{8\pi\sqrt{D_h D_z t}} e^{-\frac{(x-X-Ut)^2}{4D_h t}} \int_0^t \left[\left(\frac{SH}{D_z} + 2 \right) \frac{1}{\tau^{\frac{3}{2}}} - \frac{H^2}{D_z \tau^{\frac{5}{2}}} \right] e^{-\frac{(-H+S\tau)^2}{4D_z \tau}} d\tau \right\} dt.$$

2.4.3 Three-dimensional model

Similarly, the three-dimensional model for modelling the half-space atmosphere is

$$\begin{aligned} & \frac{\partial c}{\partial t} + U\frac{\partial c}{\partial x} + V\frac{\partial c}{\partial y} - S\frac{\partial c}{\partial z} - D_h\frac{\partial^2 c}{\partial x^2} - D_h\frac{\partial^2 c}{\partial y^2} - D_z\frac{\partial^2 c}{\partial z^2} \\ & = Q\delta(x - X_0)\delta(y - Y_0)\delta(z - H)\delta(t)\,. \end{aligned}$$

Using the same techniques as for the two-dimensional model (see Appendices A.2.2 and A.2.3), the concentration is given by

$$
\begin{aligned}
& c(x,y,z,t) \\
&= \frac{Q}{8D_h\sqrt{\pi^3 D_z t^3}} e^{-\frac{(x-X_0-Ut)^2}{4D_h t}-\frac{(y-Y_0-Vt)^2}{4D_h t}-\frac{S^2 t}{4D_z}} \left\{ e^{\frac{-S(z-H)}{2D_z}} \left[e^{\frac{-(z-H)^2}{4D_z t}} + e^{\frac{-(z+H)^2}{4D_z t}} \right] \right. \\
&\quad \left. -2e^{\frac{SH}{2D_z}-\frac{H^2}{4D_z t}} + \frac{S}{D_z}\int_0^z e^{-\frac{S(\xi-H)}{2D_z}-\frac{(\xi+H)^2}{4D_z t}} d\xi \right\} \\
&\quad - \frac{Q}{16D_h t\sqrt{\pi^3 D_z}}\, e^{-\frac{(x-X_0-Ut)^2}{4D_h t}-\frac{(y-Y_0-Vt)^2}{4D_h t}} \int_0^t \left[\left(\frac{SH}{D_z} + 2 \right) \frac{1}{\tau^{\frac{3}{2}}} - \frac{H^2}{D_z \tau^{\frac{5}{2}}} \right] e^{-\frac{(-H+S\tau)^2}{4D_z \tau}} d\tau \,.
\end{aligned}
$$

Integrating the downward flux with respect to time, $0 \leq t < \infty$, to determine the deposit $f(x,y)$, on the ground we obtain

$$
\begin{aligned}
f(x,y) \;=\; & \int_0^\infty \left\{ -\frac{SQ}{16D_h t\sqrt{\pi^3 D_z}} e^{-\frac{(x-X_0-Ut)^2}{4D_h t}-\frac{(y-Y_0-Vt)^2}{4D_h t}} \times \right. \\
& \left. \times \int_0^t \left[\left(\frac{SH}{D_z} + 2 \right) \frac{1}{\tau^{\frac{3}{2}}} - \frac{H^2}{D_z \tau^{\frac{5}{2}}} \right] e^{-\frac{(-H+S\tau)^2}{4D_z \tau}} d\tau \right\} dt. \qquad (2.15)
\end{aligned}
$$

We cannot solve Equation (2.15) analytically. Numerical solutions displayed in Figures 2.7 and 2.8 show that the half space model gives very close results to those of the whole space model (Figures 2.4 and 2.6).

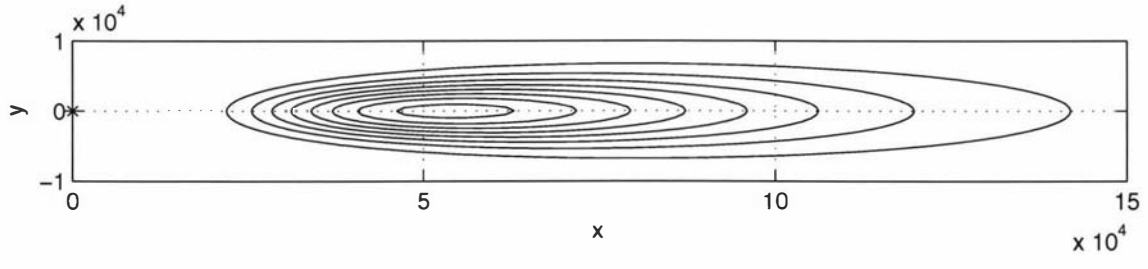

Figure 2.7: Contour of deposition at instantaneous release in three-dimensional uniform half-space with $D_z = 800$. The innermost contour has the highest deposit whilst the outermost has the lowest deposit.

2.5 Case C: Continuous Release in Whole Space

This section presents the steady-state calculation of concentration when the ashfall is released continuously from a point source. Under steady-state conditions, the term $\frac{\partial c}{\partial t}$ is zero. The advection-dispersion equation (2.11) becomes

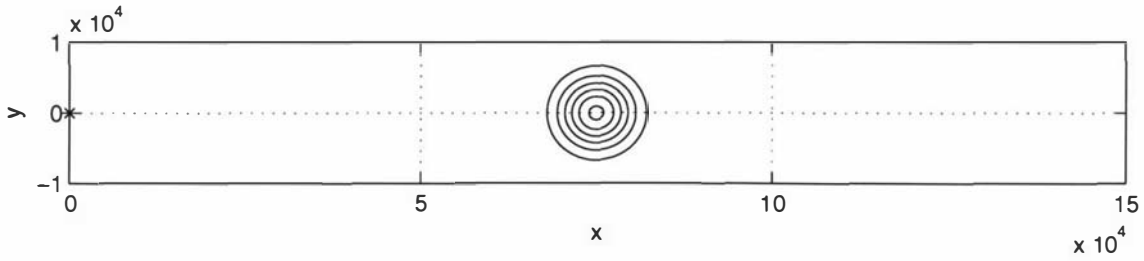

Figure 2.8: Contour of deposition at instantaneous release in three-dimensional uniform half-space with $D_z = 1$. The innermost contour has the highest deposit whilst the outermost has the lowest deposit.

$$\begin{aligned} & U\frac{\partial c}{\partial x} + V\frac{\partial c}{\partial y} - S\frac{\partial c}{\partial z} - D_h\frac{\partial^2 c}{\partial x^2} - D_h\frac{\partial^2 c}{\partial y^2} - D_z\frac{\partial^2 c}{\partial z^2} \\ &= q\delta(x - X_0)\delta(y - Y_0)\delta(z - H)\,. \end{aligned} \tag{2.16}$$

The term $Q\delta(t)$ in (2.11) has been replaced by q which is the rate of mass release.

For release point $(0, 0, H)$, Equation (2.16) becomes

$$U\frac{\partial c}{\partial x} + V\frac{\partial c}{\partial y} - S\frac{\partial c}{\partial z} - D_h\frac{\partial^2 c}{\partial x^2} - D_h\frac{\partial^2 c}{\partial y^2} - D_z\frac{\partial^2 c}{\partial z^2} = q\delta(x)\delta(y)\delta(z - H)\,. \tag{2.17}$$

2.5.1 One-dimensional model

A one-dimensional model is obtained by assuming that there is no horizontal wind, so that the ash only moves in the z-direction. The one-dimensional advection-dispersion equation at steady state reduces to

$$-S\frac{dc}{dz} - D_z\frac{d^2 c}{dz^2} = q\delta(z - H)\,.$$

We take $c \to 0$ as $z \to \infty$, c is bounded as $z \to -\infty$ and c is continuous at $z = H$.

Solving this second order differential equation, we obtain

$$c(z) = \frac{q}{S} + \frac{q}{S}\left(e^{-\frac{S(z-H)}{D_z}} - 1\right)\mathcal{H}(z - H)$$

where $\mathcal{H}$ is the Heaviside function.

This means that if $z < H$ then

$$c(z) = \frac{q}{S}$$

and if $z > H$

$$c(z) = \frac{q}{S} e^{-\frac{S(z-H)}{D_z}} .$$

2.5.2 Two-dimensional model

We construct a two-dimensional model by assuming that there is no horizontal wind in the y-direction. The material is moving only in the x and z-directions. Hence the two-dimensional advection-dispersion equation reduces to

$$U\frac{\partial c}{\partial x} - S\frac{\partial c}{\partial z} - D_h\frac{\partial^2 c}{\partial x^2} - D_z\frac{\partial^2 c}{\partial z^2} = q\delta(x - X_0)\delta(z - H) .$$

This can be solved in terms of a Bessel function [8] (see Appendix A.3.1) with boundary conditions: $c \to 0$ as $x \to \pm\infty$ or $z \to +\infty$, and c is bounded when $z \to -\infty$.

For a release point (X_0, H),

$$c(x,z) = \frac{q}{2\pi\sqrt{D_h D_z}} e^{\frac{U(x-X_0)}{2D_h} - \frac{S(z-H)}{2D_z}} K_0\left[\frac{1}{2}\sqrt{\left(\frac{U^2}{D_h} + \frac{S^2}{D_z}\right)\left(\frac{(x-X_0)^2}{D_h} + \frac{(z-H)^2}{D_z}\right)}\right] .$$

For a release point $(0, H)$,

$$c(x,z) = \frac{q}{2\pi\sqrt{D_h D_z}} e^{\frac{Ux}{2D_h} - \frac{S(z-H)}{2D_z}} K_0\left[\frac{1}{2}\sqrt{\left(\frac{U^2}{D_h} + \frac{S^2}{D_z}\right)\left(\frac{x^2}{D_h} + \frac{(z-H)^2}{D_z}\right)}\right] .$$

K_0 is a modified Bessel function of the second kind of order zero [44].

2.5.3 Three-dimensional model

The three-dimensional model is derived using the Equation (2.16):

$$U\frac{\partial c}{\partial x} + V\frac{\partial c}{\partial y} - S\frac{\partial c}{\partial z} - D_h\frac{\partial^2 c}{\partial x^2} - D_h\frac{\partial^2 c}{\partial y^2} - D_z\frac{\partial^2 c}{\partial z^2} = q\delta(x - X_0)\delta(y - Y_0)\delta(z - H) .$$

The solution of $c(x, y, z)$ can be found by using the solution to the Helmholtz equation [48] (see Appendix A.3.2) with boundary conditions: $c \to 0$ as $x \to \pm\infty$, $y \to \pm\infty$ or $z \to +\infty$, and c is bounded when $z \to -\infty$.

For release point at (X_0, Y_0, H),

$$c(x,y,z) = \frac{q}{4\pi r D_h \sqrt{D_z}} e^{\frac{U(x-X_0)}{2D_h} + \frac{V(y-Y_0)}{2D_h} - \frac{S(z-H)}{2D_z} - kr}$$

where $k^2 = \dfrac{U^2}{4D_h} + \dfrac{V^2}{4D_h} + \dfrac{S^2}{4D_z}$ and $r = \sqrt{\dfrac{(x-X_0)^2}{D_h} + \dfrac{(y-Y_0)^2}{D_h} + \dfrac{(z-H)^2}{D_z}}$.

For a release point $(0, 0, H)$,

$$c(x,y,z) = \frac{q}{4\pi r D_h \sqrt{D_z}} e^{\frac{Ux}{2D_h} + \frac{Vy}{2D_h} - \frac{S(z-H)}{2D_z} - kr}$$

where $k^2 = \dfrac{U^2}{4D_h} + \dfrac{V^2}{4D_h} + \dfrac{S^2}{4D_z}$ and $r = \sqrt{\dfrac{x^2}{D_h} + \dfrac{y^2}{D_h} + \dfrac{(z-H)^2}{D_z}}$.

We tested the three-dimensional model using the data in Table 1.1 with $D_z = 800$ and $D_z = 1$. We see that the concentration contour in Figure 2.9 has a elongated spread compared to Figure 2.10. With $D_z = 800$, the ashfall spreads with respect to the wind direction, in this case, the x-direction as there is no wind in the y-direction ($V = 0$).

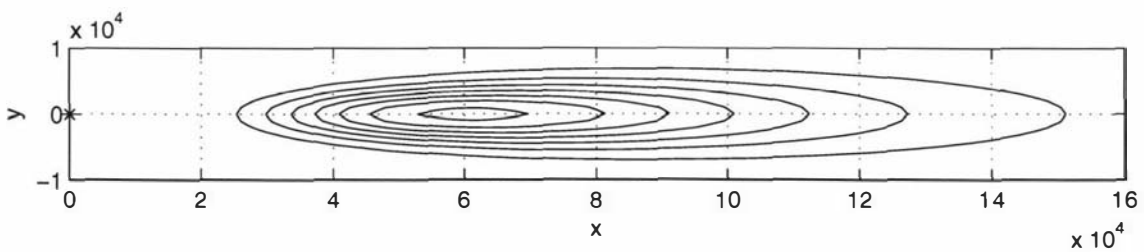

Figure 2.9: Contour of concentration at continuous release in three-dimensional uniform whole space with $D_z = 800$. The innermost contour has the highest concentration whilst the outermost has the lowest concentration.

2.6 Case D: Continuous Release in Half Space

The same boundary conditions as Case B are applied. The surface $z = 0$ is assumed to be solid ground, no material can penetrate through the ground so there is zero downward dispersive flux at the ground, hence $D_z \dfrac{\partial c}{\partial z} = 0$ at $z = 0$. So either $D_z = 0$ or $\dfrac{\partial c}{\partial z} = 0$, but since we take $D_z \neq 0$ then $\dfrac{\partial c}{\partial z} = 0$ at $z = 0$. We also take $c \to 0$ as $x \to \pm\infty$, $y \to \pm\infty$ or $z \to \infty$.

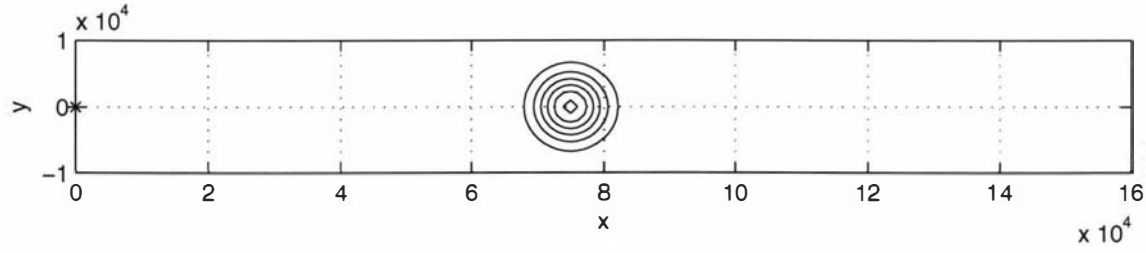

Figure 2.10: Contour of concentration at continuous release in three-dimensional uniform whole space with $D_z = 1$. The innermost contour has the highest concentration whilst the outermost has the lowest concentration.

However, we are able to solve only the one-dimensional model analytically. The two- and three-dimensional models are solved numerically and are presented in Chapter 3.

2.6.1 One-dimensional model

We again construct a one-dimensional model by assuming that there is no horizontal wind. The material is only moving in the z-direction to the ground ($z = 0$). Hence the one-dimensional advection-dispersion equation at steady state is

$$-S\frac{\partial c}{\partial z} - D_z\frac{\partial^2 c}{\partial z^2} = q\delta(z - H)\,.$$

Using the conditions $c \to 0$ as $z \to \infty$ and $\dfrac{\partial c}{\partial z} = 0$ on $z = 0$, we integrate the equation with respect to z,

$$\begin{aligned}\int_0^\infty \left(-S\frac{dc}{dz} - D_z\frac{d^2c}{dz^2}\right) dz &= \int_0^\infty q\delta(z - H)\, dz \\ \left[-Sc - D_z\frac{dc}{dz}\right]_0^\infty &= q \\ c(0) &= \frac{q}{S}\,.\end{aligned}$$

The result is same as the one-dimensional model in the whole space for $z < H$ (Section 2.5.1).

2.7 Summary

The half-space modelling is more realistic than the whole space modelling because it takes into account that on the ground there is zero downward flux. In the whole space model, the total downward flux is $Sc + D_z \frac{\partial c}{\partial z}$, whereas the downward flux in the half space model it is Sc because $\frac{\partial c}{\partial z} = 0$ at $z = 0$.

The results shown in this chapter allow for $D_z \neq 0$. As we highlighted in Chapter 1, because most volocanologists assume $D_z = 0$, we will show results for $D_z = 0$ in the following chapters in the thesis. In order to provide computed examples using the formulas already calculated, very small values of D_z are used to provide a close approximation to the case $D_z = 0$. The results shown in Figure 2.6 (whole space deposit) and in Figure 2.8 (half space deposit) are almost identical. We will assume that the results for $D_z = 1$ are close to those for $D_z = 0$ in the following chapters in the thesis.

As indicated in Chapter 1, the process of ashfall in the atmosphere is more complicated than the simple model considered in this chapter as the wind profile, dispersion coefficients and settling speed can vary with position and time. In Chapter 3, we structure the atmosphere into horizontal layers providing a more realistic transport model than a uniform atmosphere and allowing a more accurate description of the physical behaviour during ashfall.

Chapter 3

LAYERED ATMOSPHERE MODELS

non-uniform pattern may be complicated
but it is the reality

What is a layered atmosphere model?

The analysis in Chapter 2 described ashfall in a uniform atmosphere. However, in general the wind and turbulence profiles vary with elevation. Also the settling speed of particles may change during their flight because of agglomeration, etc. Because of these effects, a more realistic model allows the wind speed and direction, the dispersion tensor and the profile settling speeds to vary with height. Atmospheric conditions may also change with time, of course, but in this thesis, that aspect is not considered.

It is important to include height-varying atmospheric flow as this aids volcanologists in understanding the distribution of ashfall, patterns of deposits on the ground and the area affected or covered by these deposits. In general once elevation-dependent wind speed and velocity, dispersion and settling speed functions are included in the mass conservation equation, it becomes intractable to obtain analytical solutions. However, one method where some progress can be made is to use piecewise-constant functions which reflect average values in separate layers. Then, the equation is linear within each layer, and the solutions are matched with suitable boundary conditions at the layer interfaces.

3.1 Modelling

The atmosphere is modelled as a horizontally-layered half-space ($-\infty < x, y < \infty$, $0 \leq z < \infty$) with where each layer interface corresponds to a change in atmospheric

conditions such as wind speed, wind direction or dominant turbulent length scale. The two types of model presented in this chapter are for instantaneous point releases and continuous point releases at constant rate.

- For the modelling of an instantaneous release, the concentration in the layered atmosphere during the process of ashfall is used to calculate the deposit on the ground.
- For the modelling of a continuous release in a steady state, the model to calculate concentration of ashfall in the layered atmosphere is obtained numerically. In the continuous release the source is measured in kg/s. The deposit is calculated per unit time and its distribution on the ground will be similar to the distribution of the deposit in the case of instantaneous release.

The models in this chapter are developed using the same advection-dispersion equation as Chapter 2. As mentioned, most volcanologists assume that the vertical dispersion, D_z is negligible because it is very small at the height of 500 metres or higher [7] [25]. With the assumption of $D_z = 0$, the models for instantaneous release can be solved analytically. The models for steady state continuous release still have to be solved numerically.

Figure 3.1 is a schematic diagram showing how a layered atmosphere is structured. The numbering of layers is from top to bottom in ascending order. The interfaces between layers are also numbered from top to bottom in ascending order. For n layers, there will be $n-1$ interfaces and the interface height is represented by Z. For example, at interface j, beneath layer j and above layer $j+1$, the interface height is Z_j. If there are n layers, then the ground is $z = Z_n = 0$.

3.2 Advection-Dispersion Equation

3.2.1 A point source instantaneous release

Since $D_z = 0$ is assumed, the advection-dispersion equation (2.11) becomes

$$\frac{\partial c}{\partial t} + U\frac{\partial c}{\partial x} + V\frac{\partial c}{\partial y} - S\frac{\partial c}{\partial z} - D_h\frac{\partial^2 c}{\partial x^2} - D_h\frac{\partial^2 c}{\partial y^2} = Q\delta(x - X_0)\delta(y - Y_0)\delta(z - H)\delta(t)\,.$$

We have assumed U, V, S and D_h to be constant within each layer, with values U_j, V_j, S_j and D_{hj} in the jth layer. The advection-dispersion equation is now re-written as

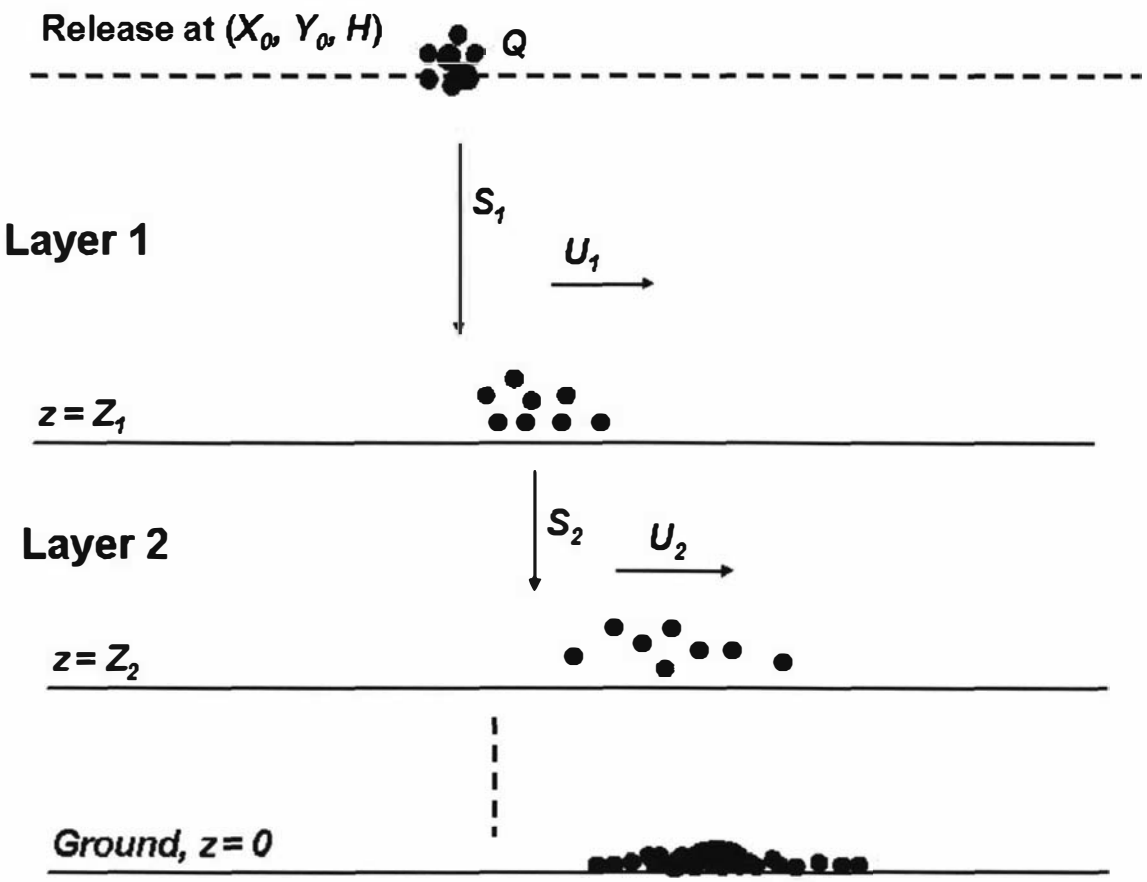

Figure 3.1: A schematic of a layered atmosphere.

$$\begin{aligned} & \frac{\partial c}{\partial t} + U_j \frac{\partial c}{\partial x} + V_j \frac{\partial c}{\partial y} - S_j \frac{\partial c}{\partial z} - D_{hj} \frac{\partial^2 c}{\partial x^2} - D_{hj} \frac{\partial^2 c_j}{\partial y^2} \\ = \; & Q\delta(x - X_0)\delta(y - Y_0)\delta(z - H)\delta(t) \end{aligned} \tag{3.1}$$

for $Z_j < z < Z_{j-1}$.

When $D_z = 0$, the downward flux $Sc + D_z \dfrac{\partial c}{\partial z}$ becomes Sc. In this case, the downward flux in a layered atmosphere, say in the nth layer, will be $S_n c$. We assume that all of the source material lands on the ground eventually and the downward flux is continuous through each interface. Therefore if S is continuous (i.e. $S_1 = S_2$, $S_2 = S_3$ etc.) then c is continuous. We have the following conditions:

Initial condition: $c(x, y, z, t) = 0$ when $t = 0$ except at $(x, y, z) = (X_0, Y_0, H)$.

Boundary conditions: the same as the Case B, the half space atmosphere in Chapter 2, $c(x, y, z, t) = 0$ when $x \to \pm\infty$, $y \to \pm\infty$ or $z \to +\infty$, and $D_z \dfrac{\partial c}{\partial z} = 0$ on the ground $z = Z_n = 0$ where n is the last layer of the atmosphere. However, since we

take $D_z = 0$ in this modelling, the condition $D_z \dfrac{\partial c}{\partial z} = 0$ on ground $z = Z_n = 0$ is automatically satisfied.

The deposit model is therefore formulated as $\left(\int_0^\infty S_n c(x, y, 0, t)\ dt \right)$ where S_n is the settling speed in the last or bottom layer of the atmosphere.

3.2.2 A point source continuous release in steady state

The steady state advection-dispersion equation (2.16) is

$$\begin{aligned} & U_j \frac{\partial c}{\partial x} + V_j \frac{\partial c}{\partial y} - S_j \frac{\partial c}{\partial z} - D_{hj} \frac{\partial^2 c}{\partial x^2} - D_{hj} \frac{\partial^2 c_j}{\partial y^2} - D_{zj} \frac{\partial^2 c_j}{\partial z^2} \\ = \ & q\delta(x - X_0)\delta(y - Y_0)\delta(z - H) \end{aligned} \tag{3.2}$$

in the jth layer.

It is also assumed that the downward flux $\left(S_j c + D_{zj} \dfrac{\partial c}{\partial z} \right)$ is continuous through each interface. However, we are only able to solve this model numerically. We wrote a code for Equation (3.2) which assumed $D_z > 0$. So we investigate the limit $D_z \to 0$.

The boundary conditions are: the same as the Case D, the half space atmosphere in Chapter 2, $c(x, y, z) = 0$ when $x \to \pm\infty$, $y \to \pm\infty$ or $z \to +\infty$ and $D_z \dfrac{\partial c}{\partial z} = 0$ at $z = Z_n = 0$ (where n is the last layer of the atmosphere). Since $D_z \dfrac{\partial c}{\partial z} = 0$, either $D_z = 0$ or $\dfrac{\partial c}{\partial z} = 0$, but since we take $D_z \neq 0$ then $\dfrac{\partial c}{\partial z} = 0$ at $z = 0$.

3.3 Instantaneous Release

This section describes the development of the models for a point source instantaneous release in one-, two- and three-dimensional layered atmospheres.

3.3.1 The one-dimensional model

As in the uniform atmosphere model, there is no horizontal variation, only vertical variation in the one-dimensional model. We construct the model by assuming that there is no horizontal wind. The material is only moving in the z-direction towards the ground ($z = Z_n = 0$). Equation (3.1) reduces to

$$\frac{\partial c}{\partial t} - S_j \frac{\partial c}{\partial z} = Q\delta(z - H)\delta(t)$$

for $Z_j < z < Z_{j-1}$ (Z_j is the interface height between the jth and $(j+1)$th layers). We assume the release is in layer 1 (the top layer), at $z = H$, and Q is in units of $\mathrm{kg/m^2}$.

For one-dimensional modelling, a new layer is only required for a change in the settling speed S. We obtain the solution c (concentration) in layer 1 by using Fourier and Laplace transformations and from layer 1 we model the concentration of the subsequent layers.

The concentration in layer 1, $j = 1$, for $0 \leq t \leq t_1 = \frac{(H - Z_1)}{S_1}$ (or $Z_1 = H - S_1 t_1$) is

$$c(z,t) = Q\delta(z - (H - S_1 t)) .$$

The corresponding concentration in layer 2 for $t_1 < t < t_2$:

$$c(z,t) \;=\; Q\delta(z - (Z_1 - S_2(t - t_1))) .$$

We deduce that for layer j, the contribution of concentration to the layer j is:

$$c(z,t) = Q\delta(z - Z)$$

where $Z = H - S_1 t_1 - S_2(t_2 - t_1) - \ldots - S_j(t - t_{j-1})$, $t_{j-1} < t < t_j$. Note that $Z_j < Z < Z_{j-1}$.

Then for an atmosphere with n layers, we compute the deposit f on the ground ($z = Z_n = 0$) using the properties of δ functions.

$$\begin{aligned} f &= \int_0^\infty S_n c(0,t)\, dt \\ &= \int_0^\infty S_n Q\delta(0 - Z)\, dt \\ &= \int_0^\infty S_n Q \frac{1}{S_n}\delta(t - \frac{Z_{n-1}}{S_n})\, dt . \\ &= Q . \end{aligned}$$

3.3.2 Two-dimensional model

We construct a two-dimensional model by assuming that there is no horizontal wind in the y-direction. The material is only moving in the x- and the z-directions. For two-dimensional modelling, Equation (3.1) is reduced to

$$\frac{\partial c}{\partial t} + U_j \frac{\partial c}{\partial x} - S_j \frac{\partial c}{\partial z} - D_{hj} \frac{\partial^2 c}{\partial x^2} = Q\delta(x - X_0)\delta(z - H)\delta(t)$$

where $Z_j < z < Z_{j-1}$ (Z_j is the interface height between the jth and $(j+1)$th layers). We assume the release is in layer 1 (the top layer), at $x = X_0$ and $z = H$, and Q is in units of kg/m.

For two-dimensional modelling, a new layer is required for any change in wind velocity U, settling speed S or dispersion D_h.

The concentration c is solved using Fourier and Laplace transformations.

In layer 1, $j = 1$, for $0 \leq t \leq t_1 = \frac{(H - Z_1)}{S_1}$,

$$c(x, z, t) = \frac{Q}{2\sqrt{\pi D_{h1} t}} e^{-\frac{(x - X_0 - U_1 t)^2}{4D_{x1} t}} \delta(z - (H - S_1 t)) .$$

At time $t = t_1$,

$$c(x, z, t_1) = \frac{Q}{2\sqrt{\pi D_{h1} t_1}} e^{-\frac{(x - X_0 - U_1 t_1)^2}{4D_{h1} t_1}} \delta(z - Z_1)$$

where $Z_1 = H - S_1 t_1$.

When the initial release is at point (X_0, H), all of the mass is concentrated at time $t = t_1$ in a sheet at height $z = Z_1$.

Dividing the sheet into small source elements, then the mass concentration at point (ξ, Z_1) on the interface is now

$$q_1(\xi) = c(\xi, Z_1, t) = \frac{Q}{2\sqrt{\pi D_{h1} t_1}} e^{-\frac{(\xi - X_0 - U_1 t_1)^2}{4D_{h1} t_1}} .$$

We take a small source element $dQ_1 = q_1(\xi)\, d\xi$ on $z = Z_1$; the corresponding concentration in layer 2 for $t_1 < t < t_2$ is

$$\begin{aligned} dc(x, z, t; \xi) &= \frac{dQ_1}{2\sqrt{\pi D_{h2}(t - t_1)}} e^{-\frac{(x - \xi - U_2(t - t_1))^2}{4D_{h2}(t - t_1)}} \delta(z - (Z_1 - S_2(t - t_1))) \\ &= \frac{1}{2\sqrt{\pi D_{h2}(t - t_1)}} e^{-\frac{(x - \xi - U_2(t - t_1))^2}{4D_{h2}(t - t_1)}} \frac{Q}{2\sqrt{\pi D_{h1} t_1}} e^{-\frac{(\xi - X_0 - U_1 t_1)^2}{4D_{h1} t_1}} \\ &\quad \times \delta(z - (Z_1 - S_2(t - t_1)))\, d\xi . \end{aligned}$$

The total mass concentration for $t_1 \leq t \leq t_2$ is obtained by integrating over all such

source elements ξ

$$\begin{aligned} c(x,z,t) &= \int_{\xi} dc(x,z,t;\xi) \\ &= \int_{-\infty}^{\infty} \frac{Q}{2\sqrt{\pi D_{h1} t_1}} e^{-\frac{(\xi - X_0 - U_1 t_1)^2}{4 D_{h1} t_1}} \frac{1}{2\sqrt{\pi D_{h2}(t-t_1)}} e^{-\frac{(x-\xi-U_2(t-t_1))^2}{4 D_{h2}(t-t_1)}} \\ &\quad \times \delta(z - (Z_1 - S_2(t-t_1))) \, d\xi \,. \end{aligned}$$

Taking

$$\xi_1 = X_0 + U_1 t_1 \quad \xi_2 = x - U_2(t-t_1)$$

$$a = \frac{1}{4 D_{h1} t_1} \qquad b = \frac{1}{4 D_{h2}(t-t_1)}$$

$$\xi_3 = \frac{a\xi_1 + b\xi_2}{a+b} \quad \xi_4 = \frac{ab(\xi_1 - \xi_2)^2}{a+b} \,,$$

we obtain

$$\begin{aligned} c(x,z,t) &= \int_{-\infty}^{\infty} \frac{Q}{2\sqrt{\pi D_{h1} t_1} 2\sqrt{\pi D_{h2}(t-t_1)}} e^{-\left[(a+b)(\xi-\xi_3)^2 + \xi_4\right]} \\ &\quad \times \delta(z - (Z_1 - S_2(t-t_1))) \, d\xi \end{aligned}$$

and taking

$$p_1^2 = (a+b)(\xi - \xi_3)^2 \quad \text{so} \quad d\xi = \frac{dp_1}{\sqrt{a+b}} \,,$$

we obtain

$$\begin{aligned} c(x,z,t) &= \int_{-\infty}^{\infty} \frac{Q}{4\pi\sqrt{t_1(t-t_1) D_{h1} D_{h2}}} e^{-\left[p_1^2 + \xi_4\right]} \frac{dp_1}{\sqrt{a+b}} \delta(z - (Z_1 - S_2(t-t_1))) \\ &= \frac{Q}{4\pi\sqrt{t_1(t-t_1) D_{h1} D_{h2}}} e^{-\xi_4} \frac{\sqrt{\pi}}{\sqrt{(a+b)}} \delta(z - (Z_1 - S_2(t-t_1))) \\ &= \frac{Q}{2\sqrt{\pi(D_{h1} t_1 + D_{h2}(t-t_1))}} e^{-\left[\frac{(x-(X_0 + U_1 t_1 + U_2(t-t_1)))^2}{4(D_{h1} t_1 + D_{h2}(t-t_1))}\right]} \delta(z - (Z_1 - S_2(t-t_1))) \\ &= \frac{Q}{2\sqrt{\pi A_j}} e^{-\frac{(x-X)^2}{4A_j}} \delta(z - Z) \end{aligned}$$

where $A_j = D_{h1} t_1 + D_{h2}(t-t_1)$, $X = X_0 + U_1 t_1 + U_2(t-t_1)$, $Z = Z_1 - S_2(t-t_1)$, $Z_2 < z < Z_1$ and $t_1 < t < t_2$.

We deduce that for layer j, the concentration is:

$$c(x,z,t) = \frac{Q}{2\sqrt{\pi A_j}} e^{-\frac{(x-X)^2}{4A_j}} \delta(z - Z)$$

where

$$
\begin{aligned}
t_j &= t_{j-1} + \frac{Z_{j-1} - Z_j}{S_j} \text{ for } j \geq 2 \text{ and } t_1 = \frac{H - Z_1}{S_1} \\
A_j &= D_{h1}t_1 + D_{h2}(t_2 - t_1) + D_{h3}(t_3 - t_2) + ... + D_{hj}(t - t_{j-1}) \\
X &= X_0 + U_1 t_1 + U_2(t_2 - t_1) + ... + U_j(t - t_{j-1}) \\
Z &= H - S_1 t_1 - S_2(t_2 - t_1) - ... - S_j(t - t_{j-1}) \\
&\text{for } t_{j-1} < t < t_j \text{ and } Z_j < z < Z_{j-1}\,.
\end{aligned}
$$

Then for an atmosphere of n layers, we compute the deposit $f(x)$ on the ground ($z = Z_n = 0$) using the properties of δ functions.

$$
\begin{aligned}
f(x) &= \int_0^\infty S_n c(x, 0, t)\ dt \\
&= \int_0^\infty \frac{S_n Q}{2\sqrt{\pi A_n}} e^{-\frac{(x-X)^2}{4A_n}} \frac{1}{S_n} \delta(t - \frac{Z_{n-1}}{S_n})\ dt \\
&= \frac{Q}{2\sqrt{\pi A_f}} e^{-\frac{(x-X_f)^2}{4A_f}}
\end{aligned}
$$

where

$$
\begin{aligned}
A_f &= D_{h1}t_1 + D_{h2}(t_2 - t_1) + D_{h3}(t_3 - t_2) + ... + D_{hn}(t_n - t_{n-1}) \\
X_f &= X_0 + U_1 t_1 + U_2(t_2 - t_1) + ... + U_n(t_n - t_{n-1})
\end{aligned}
$$

and t_n is the time when the particles land on the ground.

Figures 3.2 illustrates the distribution of ashfall in a two-dimensional layered atmosphere.

3.3.3 Three-dimensional model

We consider both horizontal and vertical variations in the three-dimensional model. Therefore the advection-dispersion equation (3.1) is used

$$
\frac{\partial c}{\partial t} + U_j \frac{\partial c}{\partial x} + V_j \frac{\partial c}{\partial z} - S_j \frac{\partial c}{\partial z} - D_{hj} \frac{\partial^2 c}{\partial x^2} - D_{hj} \frac{\partial^2 c}{\partial y^2} = Q\delta(x - X_0)\delta(y - Y_0)\delta(z - H)\delta(t)
$$

where $Z_j < z < Z_{j-1}$ (Z_j is the interface height between the jth and $(j+1)$th layers). We assume the release is in layer 1 (the top layer), at $x = X_0$, $y = Y_0$ and $z = H$, and Q is in unit of kg.

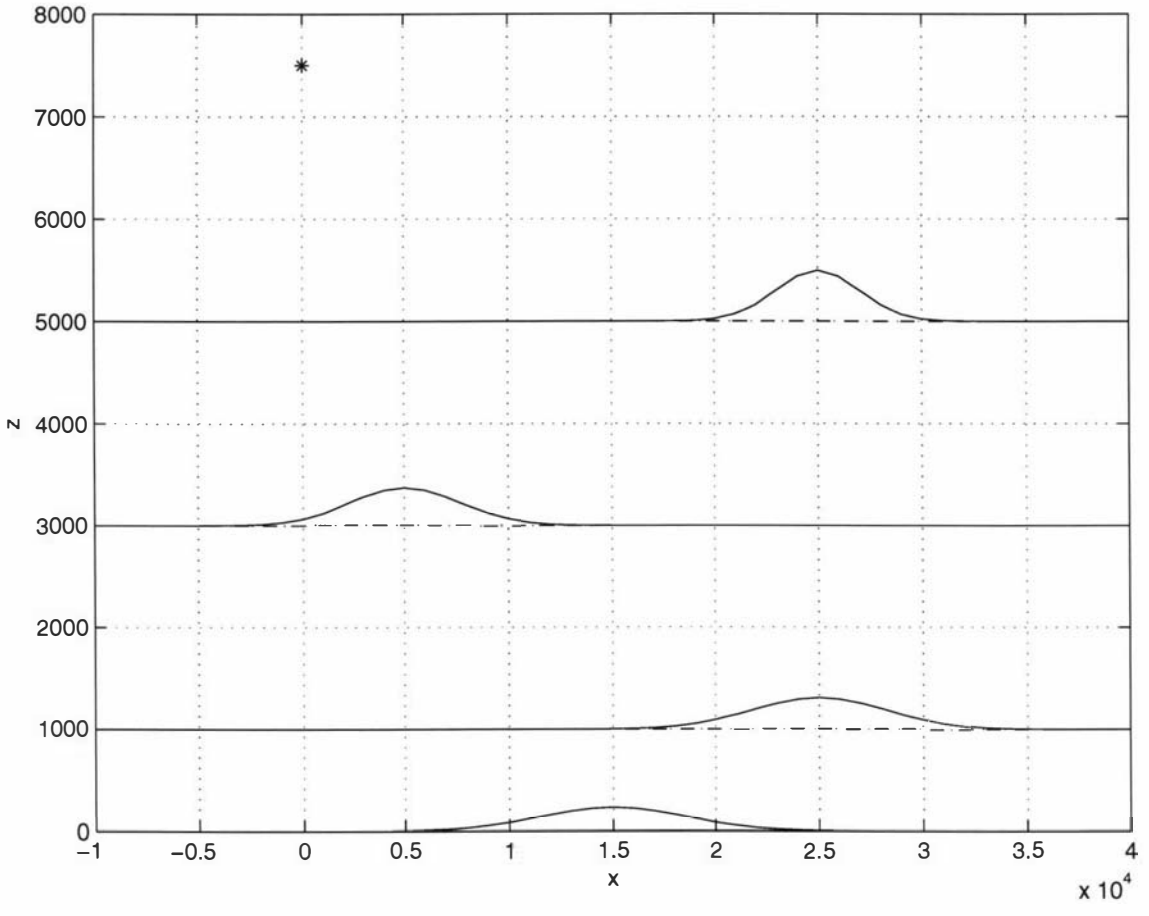

Figure 3.2: Distribution of ashfall for instantaneous release in two-dimensional layered atmosphere. The graph also illustrates the thickness of deposits in three boundary layers at three interfaces, the ash falls with respect to the wind direction and the spread of the distribution is wider towards the ground. (* indicates the release point $(X_0, H) = (0, 7500)$. Data used for the plot are from Table 1.2.)

For three-dimensional modelling, a new layer is required for any change in wind velocity U, V, settling speed S or dispersion D_h.

The concentration c is solved using Fourier and Laplace transformations.

In layer 1, $j = 1$, for $0 \leq t \leq t_1 = \frac{(H-Z_1)}{S_1}$,

$$c(x,y,z,t) = \frac{Q}{4\pi D_{h1} t_1} e^{-\frac{(x-X_0-U_1 t_1)^2}{4D_{h1}t_1} - \frac{(y-Y_0-V_1 t_1)^2}{4D_{h1}t_1}} \delta(z-(H-S_1 t)).$$

At time $t = t_1$,

$$c(x,y,z,t_1) = \frac{Q}{4\pi D_{h1} t_1} e^{-\frac{(x-X_0-U_1 t_1)^2}{4D_{h1}t_1} - \frac{(y-Y_0-V_1 t_1)^2}{4D_{h1}t_1}} \delta(z-Z_1)$$

where $Z_1 = H - S_1 t_1$.

At this time, all of the mass is concentrated in a sheet at height $z = Z_1$.

As in the two-dimensional model, we divide the sheet into small source elements, then the mass concentration at point (ξ, η, Z_1) on the interface is now

$$q_1(\xi,\eta) = c(\xi,\eta,Z_1,t_1) = \frac{Q}{4\pi D_{h1} t_1} e^{-\frac{(\xi - X_0 - U_1 t_1)^2}{4D_{h1}t_1} - \frac{(\eta - Y_0 - V_1 t_1)^2}{4D_{h1}t_1}}.$$

We take a small source element $dQ_1 = q_1(\xi,\eta)d\xi\ d\eta$ on $z = Z_1$, the corresponding concentration in layer 2 for $t_1 < t < t_2$ is

$$\begin{aligned} dc(x,y,z,t;\xi,\eta) &= \frac{dQ_1}{4\pi D_{h2}(t-t_1)} e^{-\frac{(x-\xi-U_2(t-t_1))^2}{4D_{h2}(t-t_1)} - \frac{(y-\eta-V_2(t-t_1))^2}{4D_{h2}(t-t_1)}} \delta(z-(Z_1 - S_2(t-t_1))) \\ &= \frac{1}{4\pi D_{h2}(t-t_1)} e^{-\frac{(x-\xi-U_2(t-t_1))^2}{4D_{h2}(t-t_1)} - \frac{(y-\eta-V_2(t-t_1))^2}{4D_{h2}(t-t_1)}} \\ &\quad \times \frac{Q}{4\pi D_{h1} t_1} e^{-\frac{(\xi-(X_0+U_1t_1))^2}{4D_{h1}t_1} - \frac{(\eta-(Y_0+V_1t_1))^2}{4D_{h1}t_1}} \\ &\quad \times \delta(z-(Z_1 - S_2(t-t_1)))\ d\xi\ d\eta. \end{aligned}$$

The total mass concentration for $t_1 < t < t_2$ is obtained by integrating over all such elements

$$\begin{aligned} c(x,y,z,t) &= \int_{-\infty}^{\infty}\int_{-\infty}^{\infty} \frac{Q}{4\pi D_{h1} t_1} e^{-\frac{(\xi-(X_0+U_1t_1))^2}{4D_{h1}t_1} - \frac{(\eta-(Y_0+V_1t_1))^2}{4D_{h1}t_1}} \times \\ &\quad \times \frac{1}{4\pi D_{h2}(t-t_1)} e^{-\frac{(x-\xi-U_2(t-t_1))^2}{4D_{h2}(t-t_1)} - \frac{(y-\eta-V_2(t-t_1))^2}{4D_{h2}(t-t_1)}} \\ &\quad \times \delta(z-(Z_1 - S_2(t-t_1)))\ d\xi\ d\eta. \end{aligned}$$

Taking

$$\xi_1 = X_0 + U_1 t_1 \quad \xi_2 = x - U_2(t-t_1)$$

$$a = \frac{1}{4D_{h1}t_1} \qquad b = \frac{1}{4D_{h2}(t-t_1)}$$

$$\xi_3 = \frac{a\xi_1 + b\xi_2}{a+b} \quad \xi_4 = \frac{ab(\xi_1-\xi_2)^2}{a+b}$$

$$\eta_1 = Y_0 + V_1 t_1 \quad \eta_2 = y - V_2(t-t_1)$$

$$\eta_3 = \frac{a\eta_1 + b\eta_2}{a+b} \quad \eta_4 = \frac{ab(\eta_1-\eta_2)^2}{a+b},$$

we obtain

$$\begin{aligned} c(x,y,z,t) &= \int_{-\infty}^{\infty}\int_{-\infty}^{\infty} \frac{Q}{4\pi D_{h1} t_1 4\pi D_{h2}(t-t_1)} e^{-\left[(a+b)(\xi-\xi_3)^2 + \xi_4 + (a+b)(\eta-\eta_3)^2 + \eta_4\right]} \times \\ &\quad \times \delta(z-(Z_1 - S_2(t-t_1)))\ d\xi\ d\eta \end{aligned}$$

and taking

$$p_1^2 = (a+b)(\xi - \xi_3)^2 \quad d\xi = \frac{dp_1}{\sqrt{a+b}}$$

$$p_2^2 = (a+b)(\eta - \eta_3)^2 \quad d\eta = \frac{dp_2}{\sqrt{a+b}},$$

we obtain

$$\begin{aligned} c(x,y,z,t) &= \int_{-\infty}^{\infty} \frac{dp_1}{\sqrt{a+b}} \int_{-\infty}^{\infty} \frac{dp_2}{\sqrt{a+b}} \frac{Q}{16\pi D_{h1} t_1 \pi D_{h2}(t-t_1)} \\ &\quad \times e^{-\left[p_1^2+\xi_4+p_2^2+\eta_4\right]} \delta(z-(Z_1 - S_2(t-t_1))) \\ &= \frac{Q}{16\pi D_{h1} t_1 \pi D_{h2}(t-t_1)} e^{-[\xi_4+\eta_4]} \frac{\pi}{(a+b)} \delta(z-(Z_1 - S_2(t-t_1))). \end{aligned}$$

Hence

$$c(x,y,z,t) = \frac{Q\delta(z-(Z_1 - S_2(t-t_1)))}{4\pi(D_{h1}t_1 + D_{h2}(t-t_1))} e^{-\left[\frac{(x-(X_0+U_1t_1+U_2(t-t_1)))^2}{4(D_{h1}t_1+D_{h2}(t-t_1))} + \frac{(y-(Y_0+V_1t_1+V_2(t-t_1)))^2}{4(D_{h1}t_1+D_{h2}(t-t_1))}\right]}.$$

Taking $A_2 = D_{h1}t_1 + D_{h2}(t-t_1)$, $X = X_0 + U_1t_1 + U_2(t-t_1)$, $Y = Y_0 + V_1t_1 + V_2(t-t_1)$ and $Z = Z_1 - S_2(t-t_1)$ where $Z_2 < z < Z_1$ and $t_1 < t < t_2$, then

$$c(x,y,z,t) = \frac{Q}{4\pi A_2} e^{-\left[\frac{(x-X)^2}{4A_2} + \frac{(y-Y)^2}{4A_2}\right]} \delta(z-Z).$$

We deduce that for the layer j, the concentration is:

$$c(x,y,z,t) = \frac{Q}{4\pi A_j} e^{-\left[\frac{(x-X)^2}{4A_j} + \frac{(y-Y)^2}{4A_j}\right]} \delta(z-Z) \tag{3.3}$$

where

$$\begin{aligned} t_j &= t_{j-1} + \frac{Z_{j-1} - Z_j}{S_j} \text{ for } j \geq 2 \text{ and } t_1 = \frac{H - Z_1}{S_1} \\ A_j &= D_{h1}t_1 + D_{h2}(t_2 - t_1) + D_{h3}(t_3 - t_2) + ... + D_{hj}(t - t_{j-1}) \\ X &= X_0 + U_1t_1 + U_2(t_2 - t_1) + ... + U_j(t - t_{j-1}) \\ Y &= Y_0 + V_1t_1 + V_2(t_2 - t_1) + ... + V_j(t - t_{j-1}) \\ Z &= H - S_1t_1 - S_2(t_2 - t_1) - ... - S_j(t - t_{j-1}) \\ \text{for} &\quad t_{j-1} < t < t_j \text{ and } Z_j < z < Z_{j-1}. \end{aligned}$$

From equation (3.3), for an atmosphere with n layers, we compute the deposit f on the ground ($z = Z_n = 0$) using the properties of δ functions.

$$
\begin{aligned}
f(x,y) &= \int_0^\infty S_n c(x,y,0,t)\ dt \\
&= \int_0^\infty \frac{S_n Q}{4\pi A_j} e^{-\left[\frac{(x-X)^2}{4A_j}+\frac{(y-Y)^2}{4A_j}\right]} \delta(0-Z)\ dt \\
&= \int_0^\infty \frac{S_n Q}{4\pi A_j} e^{-\left[\frac{(x-X)^2}{4A_j}+\frac{(y-Y)^2}{4A_j}\right]} \frac{1}{S_n} \delta(t-\frac{Z_{n-1}}{S_n})\ dt \\
&= \frac{Q}{4\pi A_f} e^{-\left[\frac{(x-X_f)^2}{4A_f}+\frac{(y-Y_f)^2}{4A_f}\right]}
\end{aligned}
\tag{3.4}
$$

where

$$
\begin{aligned}
A_f &= D_{h1}t_1 + D_{h2}(t_2-t_1) + D_{h3}(t_3-t_2) + ... + D_{hn}(t_n - t_{j-1}) \\
X_f &= X_0 + U_1 t_1 + U_2(t_2-t_1) + ... + U_n(t_n - t_{n-1}) \\
Y_f &= Y_0 + V_1 t_1 + V_2(t_2-t_1) + ... + V_n(t_n - t_{n-1})
\end{aligned}
$$

and t_n is the time when the particles land on the ground.

Figures 3.3, 3.4, 3.5, 3.6 and 3.7 show the distribution of ashfall in a three-dimensional layered atmosphere. Figures 3.4, 3.5, 3.6 and 3.7 are the top views of each boundary layer and they show that the spread is wider toward the ground and consequently the deposit is thinner towards the ground. These illustrate the farther the distance between the release point and the ground, the wider the spread of deposit; the travelling time is longer and therefore there is more time to spread.

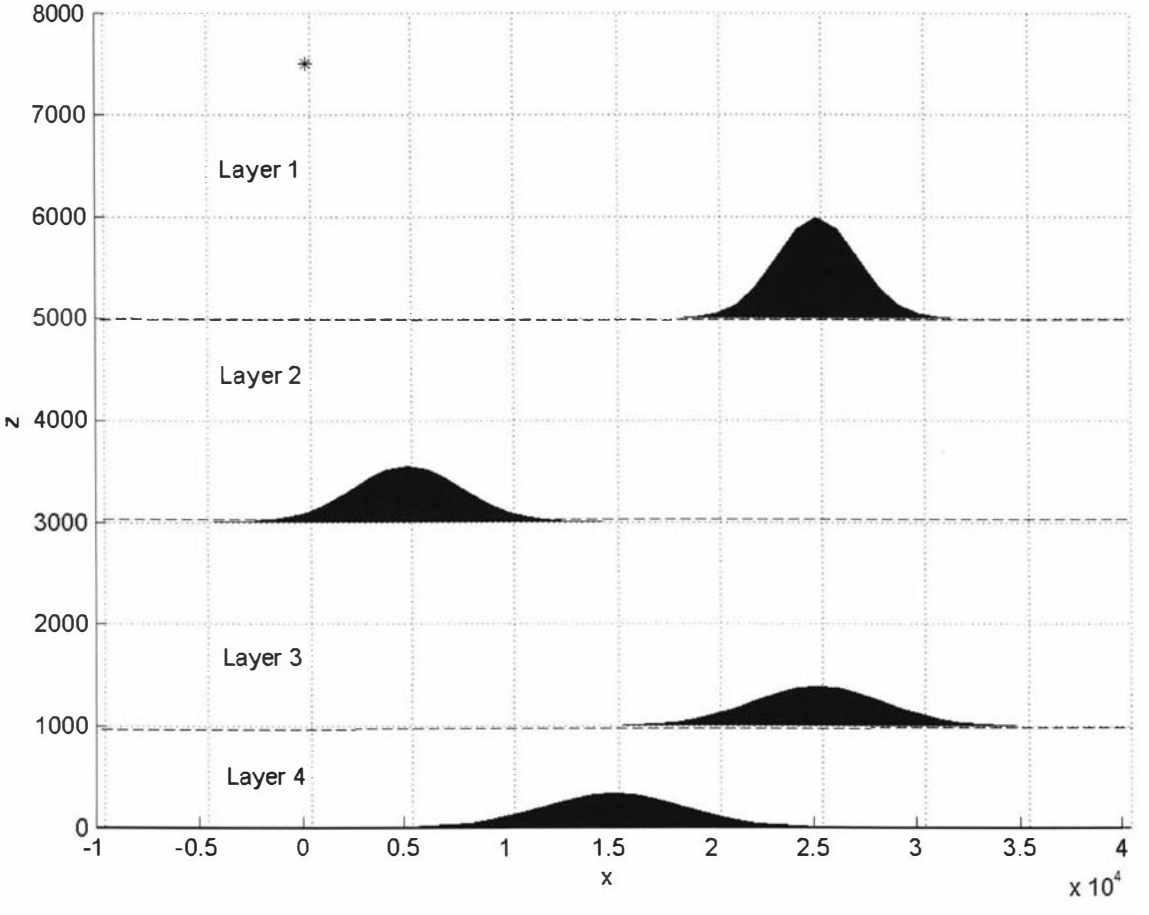

Figure 3.3: Distribution of ashfall for instantaneous release in three-dimensional layered atmosphere. The graph also illustrates the thickness of deposits in three boundary layers at three interfaces, the ash falls with respect to the wind direction and the spread of the distribution is wider towards the ground. (* indicates the release point $(X_0, Y_0, H) = (0, 0, 7500)$. Data used for the plots are from Table 1.2.)

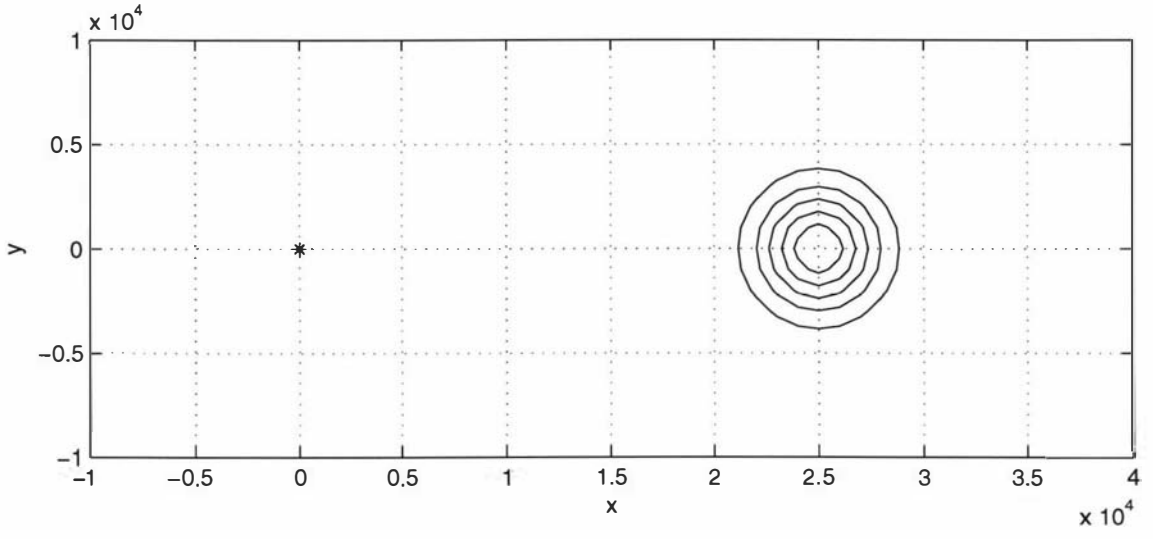

Figure 3.4: Layer one of Figure 3.3. (* indicates the release point $(X_0, Y_0, H) = (0, 0, 7500)$. The innermost contour has the highest deposit whilst the outermost has the lowest deposit.)

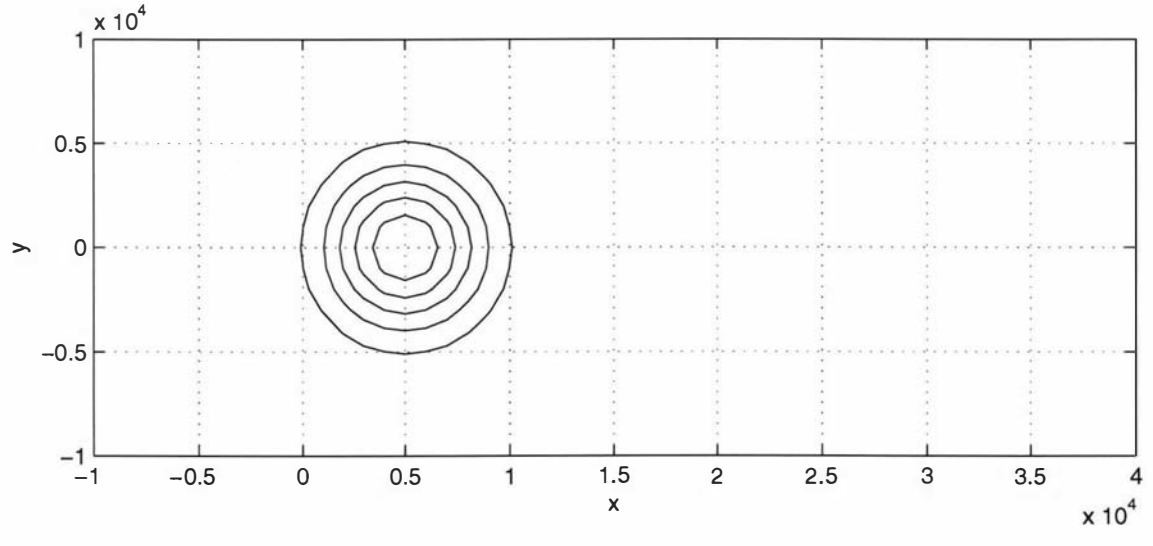

Figure 3.5: Layer two of Figure 3.3. The innermost contour has the highest deposit whilst the outermost has the lowest deposit.

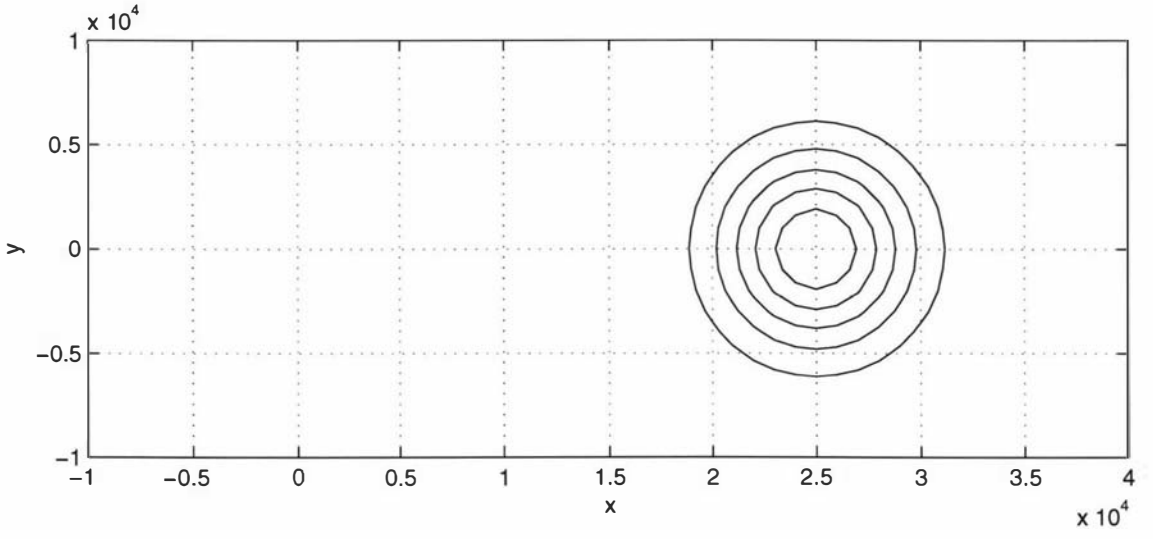

Figure 3.6: Layer three of Figure 3.3. The innermost contour has the highest deposit whilst the outermost has the lowest deposit.

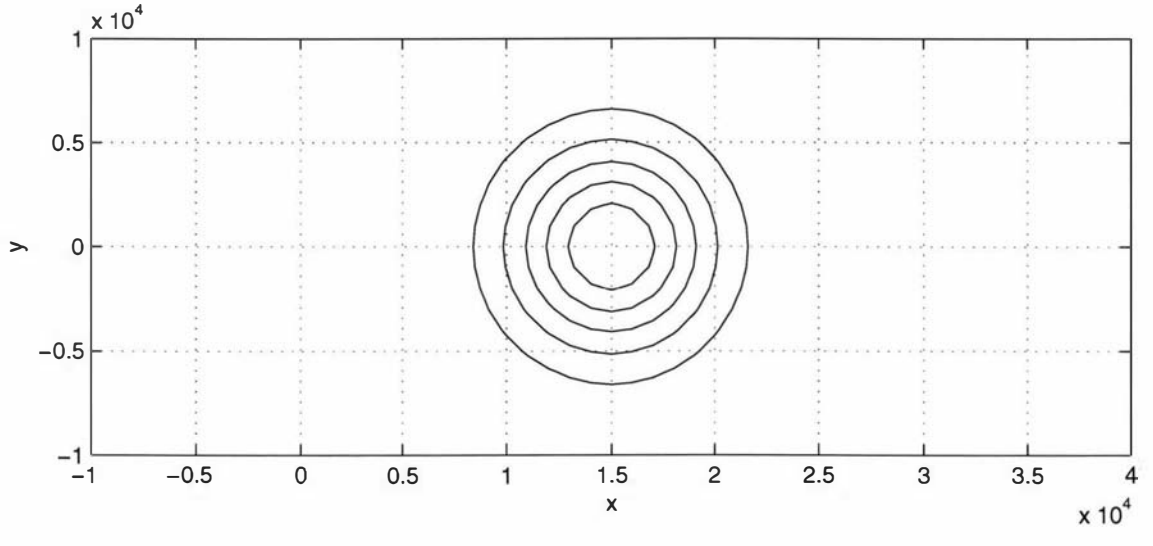

Figure 3.7: Layer four of Figure 3.3. The innermost contour has the highest deposit whilst the outermost has the lowest deposit.

3.4 A Continuous Release in Steady State

We now consider a source which is assumed to release continuously. Three models are presented in this section. The one-dimensional model is developed analytically using simple integration but the two- and three-dimensional models are solved numerically using a Finite Difference method.

3.4.1 One-dimensional model

As in the uniform atmosphere model, there is no horizontal wind, only vertical variation in the one-dimensional model. The material is only moving in the z-direction towards the ground ($z = Z_n = 0$). Equation (3.2) reduces to

$$-S_j \frac{dc}{dz} = D_{zj} \frac{d^2c}{dz^2} + q\delta(z - H)$$

where $Z_j < z < Z_{j-1}$ (Z_j is the interface height between the jth and $(j+1)$th layers). We assume the release is in layer 1 (the top layer), at $z = H$, and q is in units of $(\mathrm{kg/m^2})/\mathrm{s}$. A new layer is required for a change in settling speed S.

In layer 1, $j = 1$, the source releases at point $z = H$ and the flux down from $z = H$ to $z = Z_1$ is:

$$-S_1 \frac{dc}{dz} = D_{z1} \frac{d^2c}{dz^2} + q\delta(z - H)\,.$$

Integrating the equation,

$$\int_z^\infty \left(-S_1 \frac{dc}{dz}\right) dz = \int_z^\infty \left(D_{z1} \frac{d^2c}{dz^2} + q\delta(z - H)\right) dz$$

So

$$S_1 c + D_{z1} \frac{dc}{dz} = q$$

and we obtain

$$q - S_1 c = e^{\frac{-S_1 z}{D_{z1}} - S_1 B_1}, \text{ where } B_1 \text{ is a constant, } q - S_1 c > 0\,.$$

Hence

$$c = \frac{q}{S_1} + A_1 e^{\frac{-S_1 z}{D_{z1}}}, \text{ where } A_1 = \frac{1}{S_1} e^{-S_1 B_1}\,.$$

We evaluate the constant A_1 later.

In layer 2 ($Z_2 < z < Z_1$), we split the integral into two to obtain

$$\int_z^{Z_1} \left(S_2 \frac{dc}{dz} + D_{z2} \frac{d^2c}{dz^2} \right) \, dz + \int_{Z_1}^{\infty} \left(S_1 \frac{dc}{dz} + D_{z1} \frac{d^2c}{dz^2} \right) \, dz = \int_z^{\infty} -q\delta(z - H) \, dz \, .$$

So

$$\left[S_1 c + D_{z1} \frac{dc}{dz} \right]_{Z_1}^{\infty} + \left[S_2 c + D_{z2} \frac{dc}{dz} \right]_z^{Z_1} = -q$$

and we obtain

$$0 - \left(S_1 c + D_{z1} \frac{dc}{dz} \right)_{Z_1} + \left(S_2 c + D_{z2} \frac{dc}{dz} \right)_{Z_1} - \left(S_2 c + D_{z2} \frac{dc}{dz} \right)_z = -q \, .$$

At the interface $z = Z_1$,

$$\left(S_1 c + D_{z1} \frac{dc}{dz} \right)_{Z_1} = \left(S_2 c + D_{z2} \frac{dc}{dz} \right)_{Z_1} \, .$$

Hence, we obtain

$$\left(S_2 c + D_{z2} \frac{dc}{dz} \right)_z = q \tag{3.5}$$

and

$$\begin{aligned} c &= \frac{q}{S_2} - \frac{1}{S_2} e^{\frac{-S_2 z}{D_{z2}} - S_2 B_2}, \text{ where } B_2 \text{ is a constant} \\ &= \frac{q}{S_2} + A_2 e^{\frac{-S_2 z}{D_{z2}}}, \text{ where } A_2 \text{ is a constant} \, . \end{aligned}$$

Applying the technique used in layer 2 to layer 3, ($Z_3 < z < Z_2$) we obtain

$$c = \frac{q}{S_3} + A_3 e^{\frac{-S_3 z}{D_{z3}}}, \text{ where } A_3 \text{ is a constant} \, .$$

Similarly, the concentration in layer 4 ($Z_4 < z < Z_3$) is

$$c = \frac{q}{S_4} + A_4 e^{\frac{-S_4 z}{D_{z4}}}, \text{ where } A_4 \text{ is a constant} \, .$$

The concentration in layer j ($Z_j < z < Z_{j-1}$) is

$$c = \frac{q}{S_j} + A_j e^{\frac{-S_j z}{D_j}}, \text{ where } A_j \text{ is a constant} \, .$$

Collecting these together we have

$$\begin{aligned}
c &= A_0 e^{\frac{-S_1 z}{D_{z1}}} && \text{for } z > H \\
c &= \frac{q}{S_1} + A_1 e^{\frac{-S_1 z}{D_{z1}}} && \text{for } Z_1 < z < H \\
c &= \frac{q}{S_2} + A_2 e^{\frac{-S_2 z}{D_{z2}}} && \text{for } Z_2 < z < Z_1 \\
c &= \frac{q}{S_3} + A_3 e^{\frac{-S_3 z}{D_{z3}}} && \text{for } Z_3 < z < Z_2 \\
c &= \frac{q}{S_4} + A_4 e^{\frac{-S_4 z}{D_{z4}}} && \text{for } Z_4 < z < Z_3 \\
c &= \frac{q}{S_j} + A_j e^{\frac{-S_j z}{D_{zj}}} && \text{for } Z_j < z < Z_{j-1}\,.
\end{aligned}$$

Recall that we use the boundary condition $c(z \to -\infty)$ is a constant. Therefore $\lim_{j \to n} A_j = 0$ where n is the last layer, $z = Z_n = 0$ (the ground) and

$$\lim_{j \to n} c = \frac{q}{S_n}\,.$$

In the half space atmosphere, the boundary condition is $\dfrac{\partial c}{\partial z} = 0$ at $z = Z_n = 0$ (the ground), so if $z = Z_2 = 0$ is the ground, then Equation (3.5) becomes

$$\left(S_2 c + D_{z2}\frac{dc}{dz}\right)_0 = q\,,$$

and

$$(S_2 c)_0 = q\,,$$

so

$$c = \frac{q}{S_2}\,.$$

Hence, in the half space atmosphere, the concentration at $z = Z_n = 0$ is

$$c = \frac{q}{S_n}\,.$$

The concentration c in the last layer for both whole ($z = Z_j \to -\infty$) and half space ($z = Z_n = 0$) atmosphere is the same.

Since the downward flux is assumed continuous, we solve for $A_0, A_1, A_2, A_3, A_4, ..., A_j$ by matching the concentration c through each interface.

At $z = H$,

$$\begin{aligned} A_0 e^{\frac{-S_1 H}{D_{z1}}} &= \frac{q}{S_1} + A_1 e^{\frac{-S_1 H}{D_{z1}}} \\ A_0 &= \left(A_1 e^{\frac{-S_1 H}{D_{z1}}} + \frac{q}{S_1} \right) e^{\frac{S_1 H}{D_{z1}}} . \end{aligned}$$

At $z = Z_1$,

$$\begin{aligned} \frac{q}{S_1} + A_1 e^{\frac{-S_1 Z_1}{D_{z1}}} &= \frac{q}{S_2} + A_2 e^{\frac{-S_2 Z_1}{D_{z2}}} \\ A_1 &= \left(A_2 e^{\frac{-S_2 Z_1}{D_{z2}}} + \frac{q}{S_2} - \frac{q}{S_1} \right) e^{\frac{S_1 Z_1}{D_{z1}}} . \end{aligned}$$

At $z = Z_2$

$$\begin{aligned} \frac{q}{S_2} + A_2 e^{\frac{-S_2 Z_2}{D_{z2}}} &= \frac{q}{S_3} + A_3 e^{\frac{-S_3 Z_2}{D_{z3}}} \\ A_2 &= \left(A_3 e^{\frac{-S_3 Z_2}{D_{z3}}} + \frac{q}{S_3} - \frac{q}{S_2} \right) e^{\frac{S_2 Z_2}{D_{z2}}} . \end{aligned}$$

At $z = Z_3$

$$\begin{aligned} \frac{q}{S_3} + A_3 e^{\frac{-S_3 Z_3}{D_{z3}}} &= \frac{q}{S_4} + A_4 e^{\frac{-S_4 Z_3}{D_{z4}}} \\ A_3 &= \left(A_4 e^{\frac{-S_4 Z_3}{D_{z4}}} + \frac{q}{S_4} - \frac{q}{S_3} \right) e^{\frac{S_3 Z_3}{D_{z3}}} . \end{aligned}$$

We deduce

$$A_{j-1} = \left(A_j e^{\frac{-S_j Z_{j-1}}{D_{zj}}} + \frac{q}{S_j} - \frac{q}{S_{j-1}} \right) e^{\frac{S_{j-1} Z_{j-1}}{D_{zj-1}}} .$$

Here, we will demonstrate the solution procedure to find A_j in a four layered atmosphere, i.e. the fourth layer is the last layer of the atmosphere. As we have found the concentration in the last layer is the release rate with respect to the settling speed in the layer, so the concentration in the fourth layer is

$$c = \frac{q}{S_4} .$$

We obtain

$$A_3 = \left(\frac{q}{S_4} - \frac{q}{S_3} \right) e^{\frac{S_3 Z_3}{D_{z3}}}$$

$$A_2 = \left(\left(\frac{q}{S_4} - \frac{q}{S_3} \right) e^{\frac{S_3 Z_3}{D_{z3}}} e^{\frac{-S_3 Z_2}{D_{z3}}} + \frac{q}{S_3} - \frac{q}{S_2} \right) e^{\frac{S_2 Z_2}{D_{z2}}}$$

$$A_1 = \left(\left(\left(\frac{q}{S_4} - \frac{q}{S_3}\right) e^{\frac{S_3 Z_3}{D_{z3}}} e^{\frac{-S_3 Z_2}{D_{z3}}} + \frac{q}{S_3} - \frac{q}{S_2}\right) e^{\frac{S_2 Z_2}{D_{z2}}} e^{\frac{-S_2 Z_1}{D_{z2}}} + \frac{q}{S_2} - \frac{q}{S_1}\right) e^{\frac{S_1 Z_1}{D_{z1}}}$$

and

$$A_0 = \left\{\left[\left(\left(\frac{q}{S_4} - \frac{q}{S_3}\right) e^{\frac{S_3 Z_3}{D_{z3}}} e^{\frac{-S_3 Z_2}{D_{z3}}} + \frac{q}{S_3} - \frac{q}{S_2}\right) e^{\frac{S_2 Z_2}{D_{z2}}} e^{\frac{-S_2 Z_1}{D_{z2}}} + \frac{q}{S_2} - \frac{q}{S_1}\right] e^{\frac{S_1 Z_1}{D_{z1}}} e^{\frac{-S_1 H}{D_{z1}}} + \frac{q}{S_1}\right\} e^{\frac{S_1 H}{D_{z1}}}.$$

In jth layer, we generalise this and write

$$c = \frac{q}{S_j} + \left(A_{j-1} e^{\frac{-S_{j-1} Z_{j-1}}{D_{zj-1}}} - \frac{q}{S_j} + \frac{q}{S_{j-1}}\right) e^{\frac{-S_j Z_{j-1}}{D_{zj}}} e^{\frac{-S_j z}{D_{zj}}}$$

where

$$A_{j-1} = \left(A_j e^{\frac{-S_j Z_{j-1}}{D_{zj}}} + \frac{q}{S_j} - \frac{q}{S_{j-1}}\right) e^{\frac{S_{j-1} Z_{j-1}}{D_{zj-1}}}$$

and $A_j = 0$ for the last layer of the atmosphere.

Figure 3.8 shows the concentration c in a layered atmosphere during the process of ashfall. There is no wind component in the model. In order to demonstrate changes in the process of ashfall, coalescence is considered to change the settling speed. The settling speeds are chosen to be $S_1 = 1$, $S_2 = 1.5$, $S_3 = 2$, $S_4 = 4$ (m/s) in layers 1, 2, 3 and 4, respectively. These values are chosen is to reflect the case of agglomeration, where particles may join and be held together by water droplets while falling in the atmosphere; they therefore become heavier and so have larger settling speed as they descend. The model shows how the flux is constant with elevation, the concentration of ash decreases through the lower layers. Here, we cannot use $D_z = 0$ as we used in the previous section (instantaneous release in layered atmosphere) because of computing difficulty as previously, so we take $D_z = 0.1$, which in practice is close to zero, and take the release rate to be $q = 1$ (kg/m^2)/s.

3.4.2 Two-dimensional model

We consider horizontal variation in the x-direction and vertical variation. We construct a two-dimensional model by assuming that there is no horizontal wind in the y-direction. The material is only moving in the x and z-directions. For two-dimensional modelling, Equation (3.2) reduces to

$$U_j \frac{\partial c}{\partial x} - S_j \frac{\partial c}{\partial z} - D_{hj} \frac{\partial^2 c}{\partial x^2} - D_{zj} \frac{\partial^2 c}{\partial z^2} = q\delta(x - X_0)\delta(z - H)$$

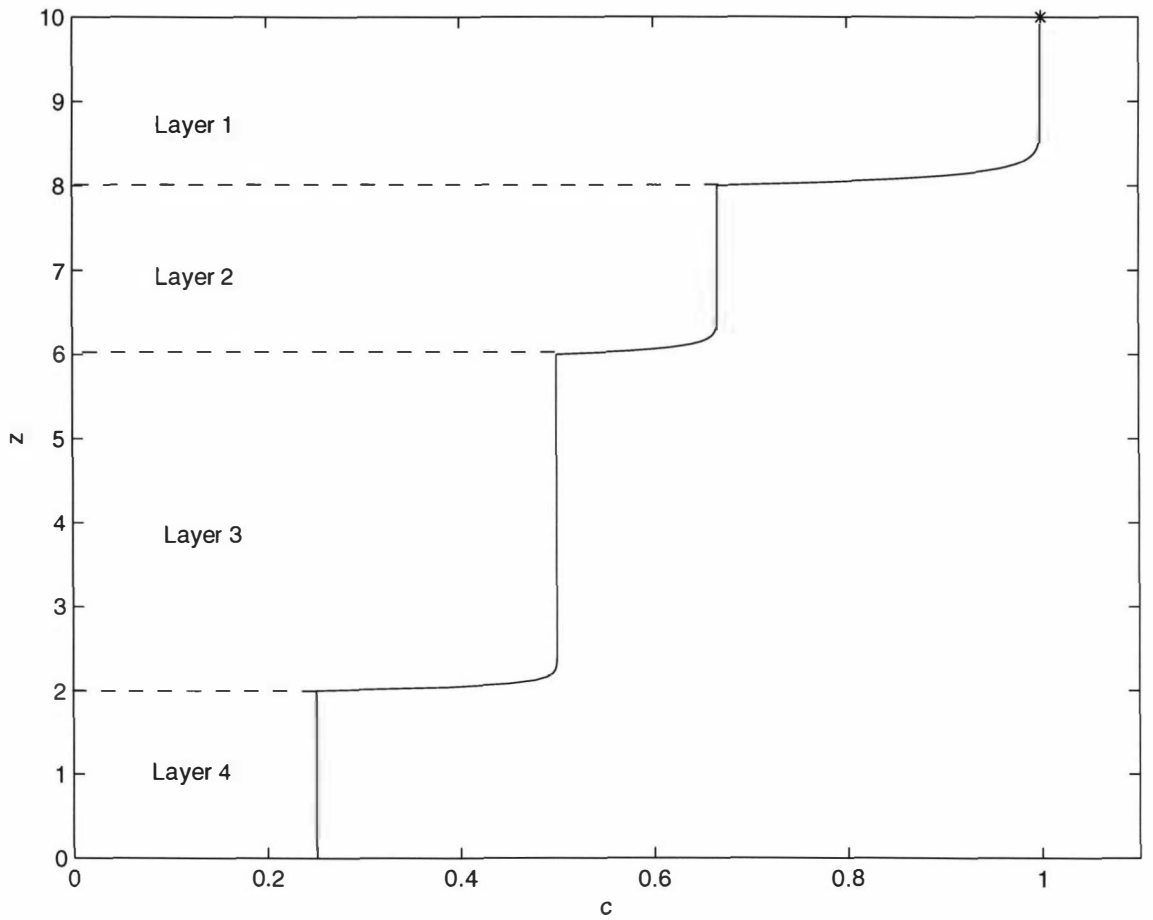

Figure 3.8: Atmospheric concentration for a continuous release in a steady state in a one-dimensional layered atmosphere. It shows that the concentration is lower towards the ground due to increase in settling speed from layer to layer. (* indicates the release point $H = 10$.)

where $Z_j < z < Z_{j-1}$ (Z_j is the interface height between the jth and $(j+1)$th layers). We assume the release is in layer 1 (the top layer), at $x = X_0$ and $z = H$, and q is in units of (kg/m)/s. A new layer is required for a change in wind velocity U or settling speed S.

We were unable to solve the two-dimensional model analytically, a Finite Difference method is employed using MATLAB [14]. Same as the one-dimensional model, we take $D_z = 0.1$.

The following discretisations were used for the derivative operators in the model:

- central difference with error of second order $O(h^2)$ - this is used for computing the flow within layers in the atmosphere.

$$
\begin{aligned}
f'(a) &= \frac{f(a+h)-f(a-h)}{2h} - \frac{h^2}{3!}f'''(a) + \ldots \\
&= \frac{f(a+h)-f(a-h)}{2h} + O(h^2)\,. \qquad (3.6)
\end{aligned}
$$

$$
\begin{aligned}
f''(a) &= \frac{f(a+h)-2f(a)+f(a-h)}{h^2} - \frac{h^2}{12}f''''(a) + \ldots \\
&= \frac{f(a+h)-2f(a)+f(a-h)}{h^2} + O(h^2)\,. \qquad (3.7)
\end{aligned}
$$

The derivative operators (3.6) and (3.7) are used for calculating the flow inside the region $l_a < x, y < l_b$ and $0 < z < l_c$ where l_a, l_b and l_c are to be large enough to capture the dynamic. This is because we consider both directions of flow within these boundary.

$$
f'(a) = \frac{-3f(a)+4f(a+h)-f(a+2h)}{2h} + O(h^2)\,. \qquad (3.8)
$$

The derivative operator (3.8) is used for calculating the concentration on the boundary where $z = 0$. This is because we restrict all released particles to land on the ground eventually and not go through beyond $z = 0$.

In the two- and three-dimensional modelling, we take i to represent the x direction, j for y and k for z. To avoid confusion, n is used to number the layers instead of j which we used in the previous sections.

The advection-dispersion equation in the two-dimensional modelling is discretised as:

$$
\begin{aligned}
c(x,z) &= c_{i,k} \\
U\frac{\partial c}{\partial x} &\approx U\frac{c_{i+1,k}-c_{i-1,k}}{2\Delta x} \\
-S\frac{\partial c}{\partial z} &\approx -S\frac{c_{i,k+1}-c_{i,k-1}}{2\Delta z} \\
D_h\frac{\partial^2 c}{\partial x^2} &\approx D_h\frac{c_{i-1,k}-2c_{i,k}+c_{i+1,k}}{\Delta x^2} \\
D_z\frac{\partial^2 c}{\partial z^2} &\approx D_z\frac{c_{i,k-1}-2c_{i,k}+c_{i,k+1}}{\Delta z^2} \\
q\delta(x-X_0)\delta(z-H) &= \frac{q}{\Delta x \Delta z}\delta_{i,i_0}\delta_{k,k_0}
\end{aligned}
$$

where Δx and Δz are the step-sizes for x and z, respectively. At the release point (X_0, H), we take $\delta_{i,i_0}\delta_{k,k_0} = 1$; otherwise $\delta_{i,i_0}\delta_{k,k_0} = 0$. ($X_0$ is represented by i_0 and H is represented by k_0.)

Hence, the advection-dispersion equation is expressed as

$$U\frac{c_{i+1,k}-c_{i-1,k}}{2\Delta x}-S\frac{c_{i,k+1}-c_{i,k-1}}{2\Delta z}$$
$$=D_h\frac{c_{i-1,k}-2c_{i,k}+c_{i+1,k}}{\Delta x^2}+D_z\frac{c_{i,k-1}-2c_{i,k}+c_{i,k+1}}{\Delta z^2}+\frac{q}{\Delta x\Delta z}\delta_{i,i_0}\delta_{k,k_0}\,.$$

Rearranging this gives

$$\begin{aligned}c_{i,k} &= \left(U\frac{-c_{i+1,k}+c_{i-1,k}}{2\Delta x}+S\frac{c_{i,k+1}-c_{i,k-1}}{2\Delta z}+D_h\frac{c_{i-1,k}+c_{i+1,k}}{\Delta x^2}\right.\\ &\quad \left.+D_z\frac{c_{i,k-1}+c_{i,k+1}}{\Delta z^2}+\frac{q}{\Delta x\Delta z}\delta_{i,i_0}\delta_{k,k_0}\right)\left(\frac{\Delta x^2\Delta z^2}{2D_h\Delta z^2+2D_z\Delta x^2}\right)\,.\end{aligned}$$

For the boundary condition $\dfrac{\partial c}{\partial z}=0$ on $z=0$,

$$\begin{aligned}\frac{\partial c(x,0)}{\partial z} &\approx \frac{-3c(x,0)+4c(x,0+h)-c(x,0+2h)}{2h}\\ 0 &\approx \frac{-3c(x,0)+4c(x,0+h)-c(x,0+2h)}{2h}\end{aligned}$$

and so

$$c(x,0)\approx\frac{4c(x,0+h)-c(x,0+2h)}{3}\,.$$

Hence

$$c_{i,1}=\frac{4c_{i,2}-c_{i,3}}{3}\,,$$

where $k=1$ corresponds to the value on $z=0$.

By matching the flux on the interface between the nth and $(n+1)$th layers, we obtain

$$\begin{aligned}S_nc_n+D_{zn}\frac{\partial c_n}{\partial z} &= S_{n+1}c_n+D_{zn+1}\frac{\partial c_{n+1}}{\partial z}\\ S_nc_n+D_{zn}\left(\frac{-3c_n+4c_{n+1}-c_{n+2}}{2\Delta z}\right) &= S_{n+1}c_n+D_{zn+1}\left(\frac{3c_n-4c_{n-1}+c_{n-2}}{2\Delta z}\right)\\ c_n &= \frac{D_{zn+1}(-4c_{n-1}+c_{n-2})-D_{zn}(4c_{n+1}-c_{n+2})}{2\Delta z(S_n-S_{n+1})-3(D_{zn}+D_{zn+1})}\,,\end{aligned}$$

where c_n represents $c_{i,k}$ on nth layer.

Figure 3.9 illustrates the concentration in a two-dimensional layered atmosphere during the ashfall. As in the one-dimensional model, we use $D_z=0.1$ m^2/s and $q=1$ (kg/m)/s. For the wind speed in the x-direction U, we take $U_1=10$, $U_2=-10$, $U_3=10$ and $U_4=-10$ m/s for layer 1, layer 2, layer 3 and layer 4, respectively. We take the dispersion in the x-direction as $D_{h1}=D_{h2}=D_{h3}=D_{h4}=800$ m^2/s for all layers. The release point is situated at $(X_0,H)=(0,1500)$.

The model is programmed to use step sizes (Δx and Δz) in an iterative procedure. The iterative process will repeat until the value of the flow in the bottom layer is

unchanged. As we set the atmosphere into four layers, the ground flow in the last layer is $S_4 \int_{-\infty}^{\infty} c \, dx$. Also, in order to obtain convergence of the ground flow, we compute the concentration c by under relaxation. We ran the program with various ranges and mesh sizes. It is found that provided the x-range is large enough and the mesh size small enough, all of the main features of the boundary conditions and the solution detail are satisfied. Figure 3.9 is computed using a x-range from -40000 to 40000 and the z-range from 0 to 2000. The mesh is divided into 1000 grid points horizontally and vertically ($\Delta x = 80000/1000 = 80$ and $\Delta z = 2000/1000 = 2$).

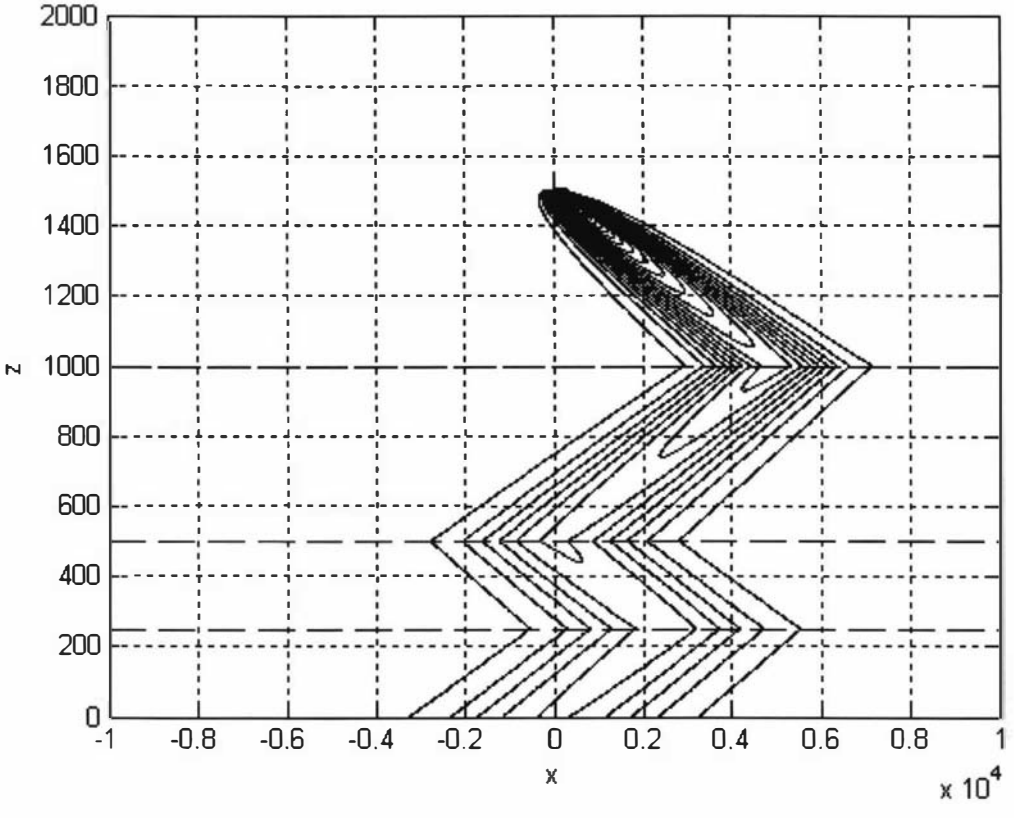

Figure 3.9: Concentration for a continuous release in a steady state in a two-dimensional layered atmosphere. It shows that the ash falls with respect to the wind direction and that the spread of the distribution is wider nearer the ground. The contour shows concentration per unit length is smaller when it is towards the ground. The release point is $(X_0, H) = (0, 1500)$. The innermost contour has the highest concentration whilst the outermost has the lowest concentration.

3.4.3 Three-dimensional model

We consider both horizontal and vertical variations in the three-dimensional model. For three-dimensional modelling, Equation (3.2) is used

$$U_j\frac{\partial c}{\partial x}+V_j\frac{\partial c}{\partial z}-S_j\frac{\partial c}{\partial z}-D_{hj}\frac{\partial^2 c}{\partial x^2}-D_{hj}\frac{\partial^2 c}{\partial y^2}-D_{zj}\frac{\partial^2 c}{\partial z^2}=q\delta(x-X_0)\delta(y-Y_0)\delta(z-H)$$

where $Z_j < z < Z_{j-1}$ (Z_j is the interface height between the jth and $(j+1)$th layers). We assume the release is in layer 1 (the top layer), at $x = X_0$, $y = Y_0$ and $z = H$, and q is in units of kg/s. A new layer is required for a change in wind velocity U or V, settling speed S, or dispersion D_h.

The terms in the advection-dispersion equation are discretised as follows:

$$\begin{aligned}
c(x,y,z) &= c_{i,j,k}\\
U\frac{\partial c}{\partial x} &\approx U\frac{c_{i+1,j,k}-c_{i-1,j,k}}{2\Delta x}\\
V\frac{\partial c}{\partial y} &\approx V\frac{c_{i,j+1,k}-c_{i,j-1,k}}{\Delta y}\\
-S\frac{\partial c}{\partial z} &\approx -S\frac{c_{i,j,k+1}-c_{i,j,k-1}}{2\Delta z}\\
D_h\frac{\partial^2 c}{\partial x^2} &\approx D_h\frac{c_{i-1,j,k}-2c_{i,j,k}+c_{i+1,j,k}}{\Delta x^2}\\
D_h\frac{\partial^2 c}{\partial y^2} &\approx D_h\frac{c_{i,j-1,k}-2c_{i,j,k}+c_{i,j+1,k}}{\Delta y^2}\\
D_z\frac{\partial^2 c}{\partial z^2} &\approx D_z\frac{c_{i,j,k-1}-2c_{i,j,k}+c_{i,j,k+1}}{\Delta z^2}\\
q\delta(x-X_0)\delta(y-Y_0)\delta(z-H) &= \frac{q}{\Delta x\Delta y\Delta z}\delta_{i,i_0}\delta_{j,j_0}\delta_{k,k_0}
\end{aligned}$$

where Δx, Δy and Δz are step-sizes for x, y and z, respectively. At the release point (X_0, Y_0, H), we take $\delta_{i,i_0}\delta_{j,j_0}\delta_{k,k_0} = 1$; otherwise $\delta_{i,i_0}\delta_{j,j_0}\delta_{k,k_0} = 0$. ($X_0$ is represented by i_0, Y_0 is represented by j_0 and H is represented by k_0.)

The advection-dispersion equation becomes

$$\begin{aligned}
&U\frac{c_{i+1,j,k}-c_{i-1,j,k}}{2\Delta x}+V\frac{c_{i,j+1,k}-c_{i,j-1,k}}{2\Delta y}-S\frac{c_{i,j,k+1}-c_{i,j,k-1}}{2\Delta z}\\
&=D_h\frac{c_{i-1,j,k}-2c_{i,j,k}+c_{i+1,j,k}}{\Delta x^2}+D_h\frac{c_{i,j-1,k}-2c_{i,j,k}+c_{i,j+1,k}}{\Delta y^2}\\
&\quad+D_z\frac{c_{i,j,k-1}-2c_{i,j,k}+c_{i,j,k+1}}{\Delta z^2}+\frac{q}{\Delta x\Delta y\Delta z}\delta_{i,i_0}\delta_{j,j_0}\delta_{k,k_0}.
\end{aligned}$$

Rearranging this equation, we obtain

$$c_{i,j,k} = \left(U\frac{-c_{i+1,j,k}+c_{i-1,j,k}}{2\Delta x}+V\frac{-c_{i,j+1,k}+c_{i,j-1,k}}{2\Delta y}+S\frac{c_{i,j,k+1}-c_{i,j,k-1}}{2\Delta z}\right.$$
$$+D_h\frac{c_{i-1,j,k}+c_{i+1,j,k}}{\Delta x^2}+D_h\frac{c_{i,j-1,k}+c_{i,j+1,k}}{\Delta y^2}+D_z\frac{c_{i,j,k-1}+c_{i,j,k+1}}{\Delta z^2}$$
$$\left.+\frac{q}{\Delta x\Delta y\Delta z}\delta_{i,i_0}\delta_{j,j_0}\delta_{k,k_0}\right)\left(\frac{\Delta x^2\Delta y^2\Delta z^2}{2D_h\Delta y^2\Delta z^2+2D_h\Delta x^2\Delta z^2+2D_z\Delta x^2\Delta y^2}\right).$$

As in the two-dimensional model, the boundary condition $\dfrac{\partial c}{\partial z}=0$ on $z=0$ is written

$$0 = \frac{-3c(x,y,0)+4c(x,y,0+h)-c(x,y,0+2h)}{2h}.$$

So

$$c(x,y,0) = \frac{4c(x,y,0+h)-c(x,y,0+2h)}{3}.$$

Hence

$$c_{i,j,1}=\frac{4c_{i,j,2}-c_{i,j,3}}{3},$$

where $k=1$ corresponds to the value on $z=0$.

By matching the flux on the interface between the nth and $(n+1)$th layers, we obtain

$$S_nc_n+D_{zn}\frac{\partial c_n}{\partial z} = S_{n+1}c_n+D_{zn+1}\frac{\partial c_{n+1}}{\partial z}$$
$$S_nc_n+D_{zn}\left(\frac{-3c_n+4c_{n+1}-c_{n+2}}{2\Delta z}\right) = S_{n+1}c_n+D_{zn+1}\left(\frac{3c_n-4c_{n-1}+c_{n-2}}{2\Delta z}\right)$$
$$c_n = \frac{D_{zn+1}(-4c_{n-1}+c_{n-2})-D_{zn}(4c_{n+1}-c_{n+2})}{2\Delta z(S_n-S_{n+1})-3(D_{zn}+D_{zn+1})},$$

where c_n represents $c_{i,j,k}$ on nth layer.

Figure 3.10 illustrates the concentration in a three-dimensional layered atmosphere during the ashfall. As in the two-dimensional model, we take $D_z=0.1$ m^2/s and $q=1$ (kg/m)/s. For the wind speed in the x-direction, U, we take $U_1=10$, $U_2=-10$, $U_3=10$ and $U_4=-10$ m/s. The wind speed in the y-direction $V_1=V_2=V_3=V_4=0$ m/s for layer 1, layer 2, layer 3 and layer 4, respectively. We take the dispersion in the x- and y-directions as $D_{h1}=D_{h2}=D_{h3}=D_{h4}=800$ m^2/s for all layers. The release point is situated at $(X_0,Y_0,H)=(0,0,400)$.

The model is programmed with respect to step sizes (Δx, Δy and Δz) in an iterative procedure. The iterative procedure runs until the ground flow in the last layer which is $S_4\displaystyle\int_{-\infty}^{\infty}\int_{-\infty}^{\infty}c\,dx\,dy$ has converged. Also, in order to obtain convergence of the

ground flow, we compute the concentration c by under relaxation. We have run the program with various ranges and mesh sizes. It is found that we are able to converge if the x and y ranges are sufficiently large and the mesh size is sufficiently small. Figure 3.10 is computed using the x and y ranges from -24000 to 24000 and the z-range from 0 to 500, and the mesh is divided into 120 grid points horizontally and vertically ($\Delta x = \Delta y = 48000/120 = 400$ and $\Delta z = 500/120 = 4.1667$).

Figure 3.10 shows the concentration for a continuous release in a three-dimensional layered atmosphere. Figures 3.11, 3.12, 3.13 and 3.14 are top views of the contours at each interface. We observe the effect of dispersion from the distribution of the ashfall. The spread of ashfall is wider toward the ground and the thickness of the deposit is thinner towards the ground. The contours shown in Figures 3.10, 3.11, 3.12, 3.13 and 3.14 are not as smooth as in the two-dimensional simulation because the mesh size used in the two-dimensional model was finer.

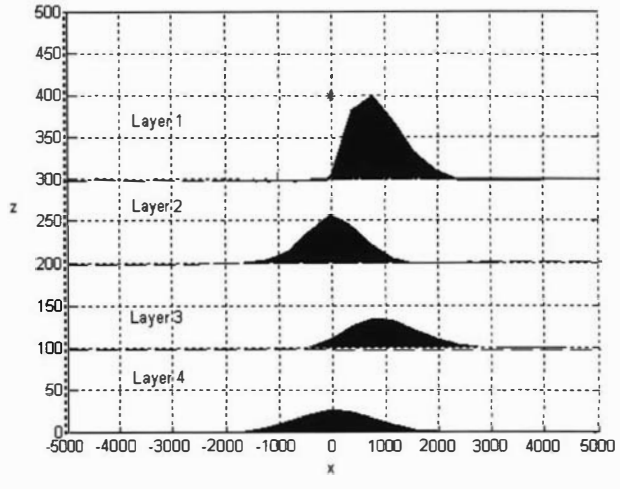

Figure 3.10: Concentrations at the interface for a continuous release in steady state in a three-dimensional layered atmosphere. It shows that the ash falls with respect to the wind direction and the spread of the distribution is wider towards the ground. (* indicates the release point $(X_0, Y_0, H) = (0, 0, 400)$.)

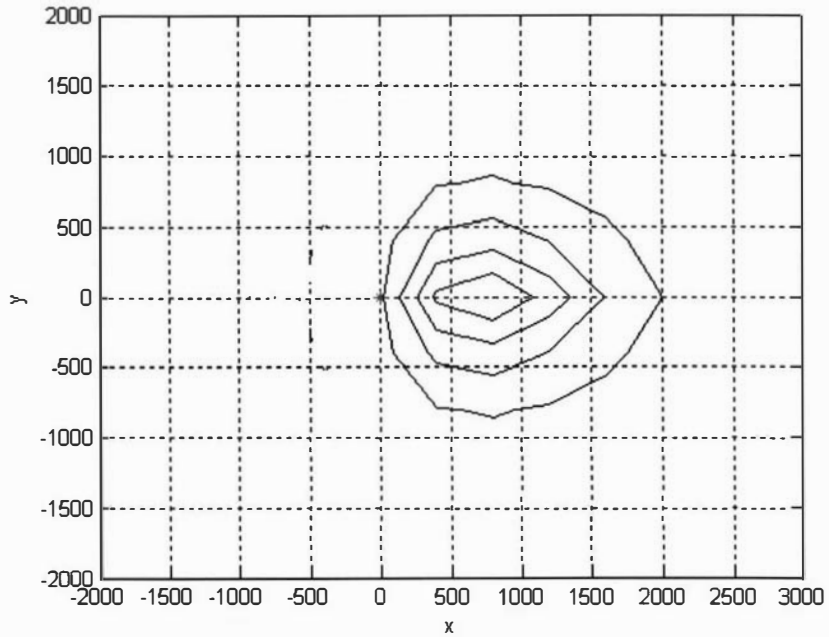

Figure 3.11: Interface one of Figure 3.10. (* indicates the release point $(X_0, Y_0, H) = (0, 0, 400)$.) The innermost contour has the highest concentration whilst the outermost has the lowest concentration.

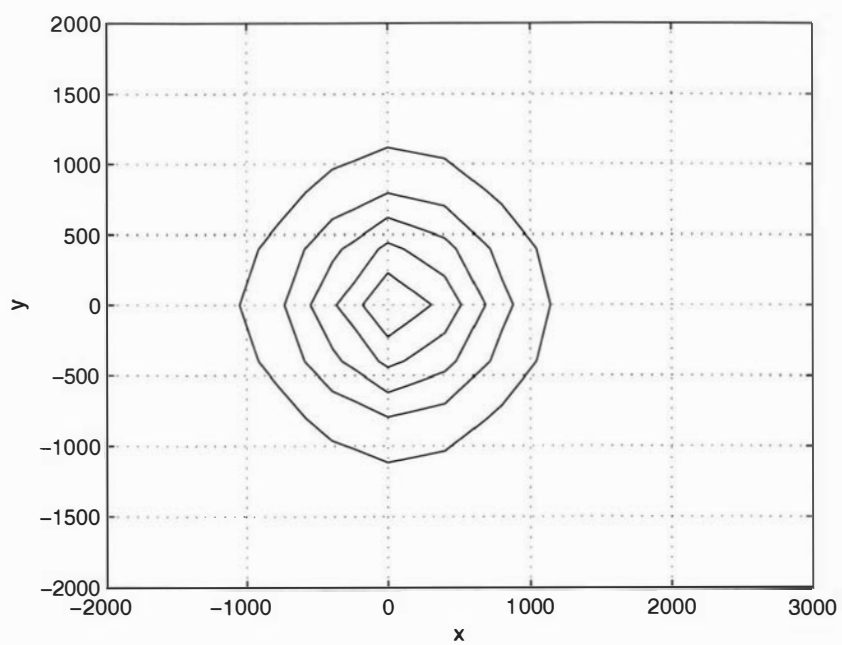

Figure 3.12: Interface two of Figure 3.10. The innermost contour has the highest concentration whilst the outermost has the lowest concentration.

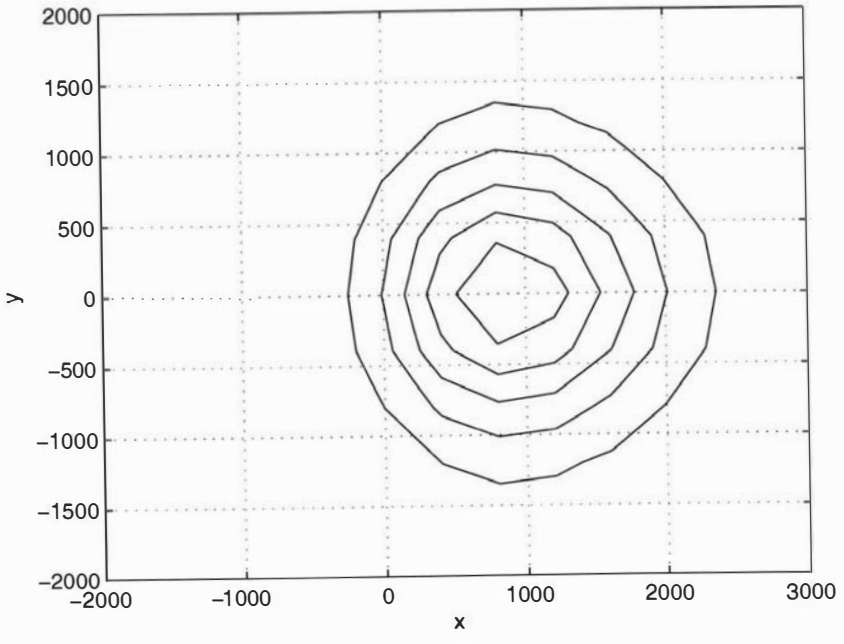

Figure 3.13: Interface three of Figure 3.10. The innermost contour has the highest concentration whilst the outermost has the lowest concentration.

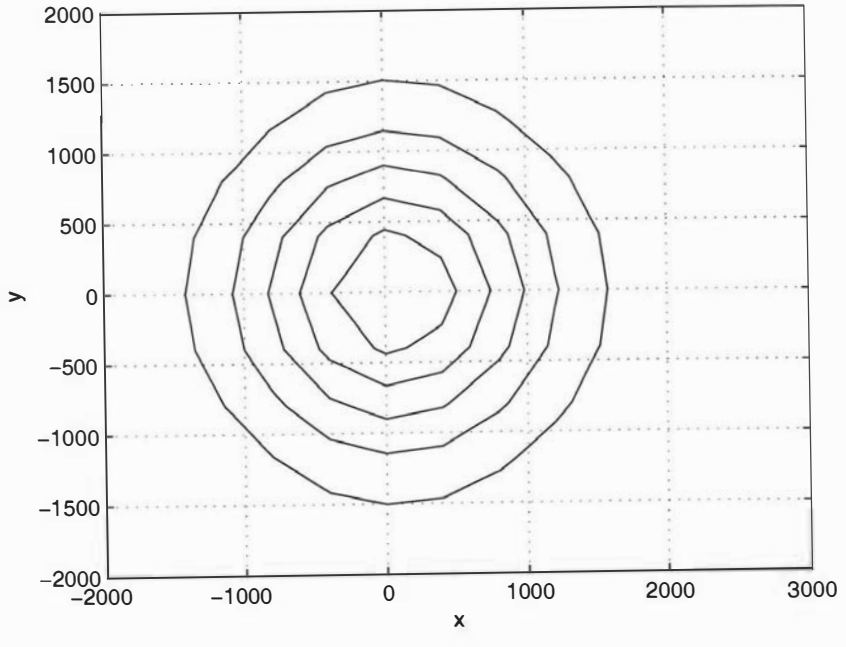

Figure 3.14: Ground level of Figure 3.10. The innermost contour has the highest concentration whilst the outermost has the lowest concentration. The accumulation rate on the ground (in $\mathrm{kg/m^2/s}$) is given by S_4 times the value of c.

3.5 Summary

In this chapter, we have presented analytical solutions for modelling an instantaneous point release in a one-, two- and three-dimensional layered atmosphere based on the condition of $D_z = 0$ and a continuous point release in a one-dimensional layered atmosphere with $D_z = 0.1$.

We are unable to solve the steady state continuous release in two- and three-dimensional layered atmosphere analytically, so they are solved numerically. In order to achieve convergence, under relaxation is used in computing the solutions with large x and y ranges, and a small mesh grid. The advantage of analytical solutions is that they allow the effect of parameter variation to be explored more readily. The graphs produced by both the analytical and numerical solutions show the expected distribution pattern of ashfall. They illustrate that the spread is wider if the release point is higher, as the dispersion time is longer.

Most volcanologists assume that $D_z = 0$, so in the next chapter we investigate the case $D_z = 0$ in more detail on both whole and half space models. In particular, we give more examples of deposits with $D_z = 0$ for the case of instantaneous release. We also use the data from Tables 1.1 and 1.2 to compute the deposits and illustrate them graphically.

Chapter 4

ANALYSIS OF DEPOSITS

cosmetics may not represent the personality

Why analyse deposits?

Suzuki [49] noted that the patterns of deposition vary between eruptions even though the total mass released might be the same. The causes of the variation could be due to differences in release height, eruption column height, wind speed and direction. Therefore it is important to analyse the contours of deposition on the ground in order to obtain information about the atmospheric conditions and release parameters during eruption. This information will help volcanologists and geologists to make hazard maps for future eruptions. The patterns of deposition will help to give approximate values for data such as the release height, eruption column height, wind speed and direction and eruption duration [11] [46]. For example, according to the report of Hurst [25], the release height and the rate of eruption can be estimated by the spread of the ashfall.

In addition to analysis of deposit patterns this chapter also demonstrates how the thickness of the deposit and the 'centre' of the deposit can be determined. We investigate patterns of deposition in whole and half-spaces for both $D_z \neq 0$ and $D_z = 0$. As mentioned at the end of the previous chapter most volcanologists assume that $D_z = 0$ because they find that D_z is very small at the height of 500 metres and above [7] [25].

4.1 Thickness of the Deposit

Here we will only consider very small particles which reach their settling speed in a short time and distance. In general the size of particles deposited decreases with increasing distance from the eruption. As mentioned in Chapter 2 the size of the particles affects the settling speed. Small particles have low settling speeds so they

have more time to travel before they reach the ground. Thus they travel further. The location of the deposition also reflects the strength of the eruption. A stronger eruption propels the particles higher and carries the particles farther than a weak eruption.

The thickness of the deposit can be determined from the deposition density function $f(x, y)$ (defined in Chapters 2 and 3). This can be written

$$f(x, y) = \rho_r(1 - \phi)h(x, y)$$

where ρ_r is the density of individual particles, ϕ is the porosity of the deposit and $h(x, y)$ is the thickness of the deposit. Here, we consider many mass classes of particles, and ϕ is usually very small, because the deposit is composed of many particle sizes. Therefore, we take

$$h(x, y) = \frac{f(x, y)}{\rho_r}.$$

4.2 Centre of the Deposit

The 'centre' of the deposit is defined as the point where the deposit $f(x, y)$ is a maximum. It can be determined from the turning point of $f(x, y)$ (2.14) due to release from the point (X_0, Y_0, H).

$$f(x, y) = \frac{Q}{32\pi D_h\sqrt{D_z}}\, e^{\left[\frac{1}{2}\left(\frac{(x-X_0)U}{D_h}+\frac{(y-Y_0)V}{D_h}+\frac{HS}{D_z}\right)-2\alpha\beta\right]}\left[\frac{(2\alpha\beta+1)H+2\alpha^2 S}{\alpha^3}\right]$$

where $\alpha = \sqrt{\frac{1}{4}\left[\frac{(x-X_0)^2}{D_h}+\frac{(y-Y_0)^2}{D_h}+\frac{H^2}{D_z}\right]}$ and $\beta = \sqrt{\frac{1}{4}\left[\frac{U^2}{D_h}+\frac{V^2}{D_h}+\frac{S^2}{D_z}\right]}$.

It may be deduced from Equation (2.14) that the coordinates of the critical point, x_c and y_c satisfy $y_c U = x_c V$, This means that the centre of the deposit lies on the line through the origin with gradient $\frac{V}{U}$, i.e. downwind of the release point. The point (x_c, y_c) where the deposit is maximum is found numerically.

4.3 Deposition from an Instantaneous Point Source Release in a Uniform Whole Space

In this section two cases are considered, one is where vertical dispersion is significant $(D_z \neq 0)$ and the other is when vertical dispersion is negligible $(D_z = 0)$.

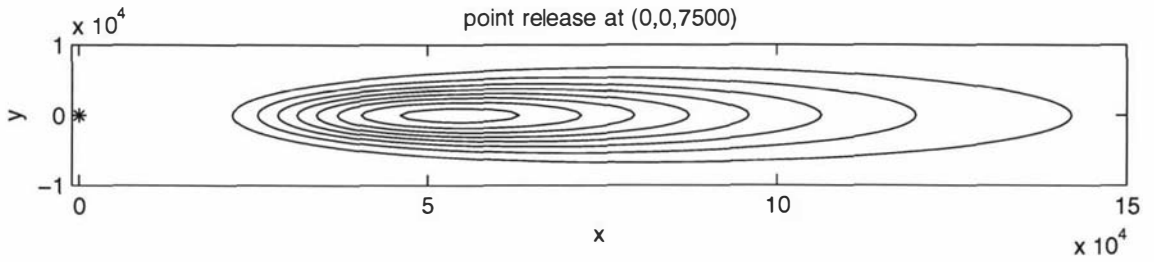

Figure 4.1: Deposition contours for instantaneous release in a uniform whole space with $D_z = 800$. The innermost contour has the highest deposit whilst the outermost has the lowest deposit.

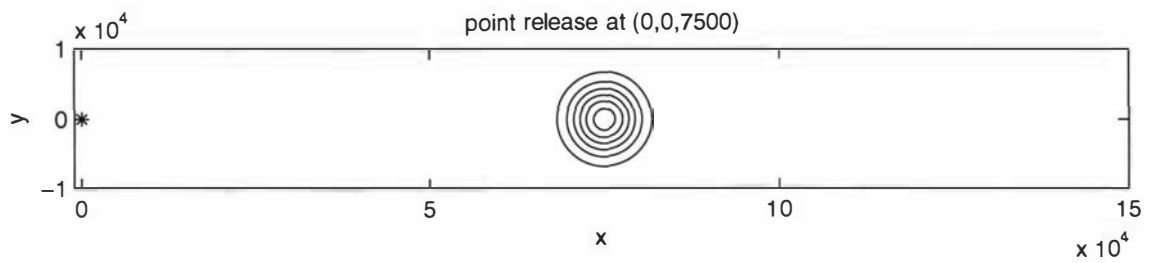

Figure 4.2: Deposition contours for instantaneous release in a uniform whole space with $D_z = 0.01$. The innermost contour has the highest deposit whilst the outermost has the lowest deposit.

4.3.1 The case $D_z \neq 0$

Equation (2.14) is used to calculate the deposit from a point source with instantaneous release in a uniform whole space. Using the data from Table 1.1 we have

$$f(x,y) = \frac{Q}{32\pi D_h \sqrt{D_z}}\, e^{\left[\frac{1}{2}\left(\frac{(x-X_0)U}{D_h}+\frac{(y-Y_0)V}{D_h}+\frac{HS}{D_z}\right)-2\alpha\beta\right]} \left[\frac{(2\alpha\beta+1)H+2\alpha^2 S}{\alpha^3}\right]$$

where $\alpha = \sqrt{\frac{1}{4}\left[\frac{(x-X_0)^2}{D_h}+\frac{(y-Y_0)^2}{D_h}+\frac{H^2}{D_z}\right]}$ and $\beta = \sqrt{\frac{1}{4}\left[\frac{U^2}{D_h}+\frac{V^2}{D_h}+\frac{S^2}{D_z}\right]}$

in the two cases where $D_z = 800$ and 0.01 m^2/s.

The contours of deposition in Figure 4.1 have a more elongated profile whereas in Figure 4.2 they are more rounded. This is because the higher vertical dispersion when $D_z = 800$ disperses the ash with respect to the wind direction.

Interestingly, the contour in Figure 4.2 looks very similar to the contour in Figure 2.6 which had $D_z = 1$. This shows that vertical dispersion has little effect between the

values $D_z = 0.01$ and $D_z = 1$.

The profile of the spread in Figure 4.1 also reflects that x_c is directly proportional to the wind speed U in the x-direction and y_c is directly proportional to the wind speed V in the y-direction (Section 4.2). Since the data we used were $U = 10$m/s but $V = 0$ m/s (no wind in the y-direction), the ashfall only disperses in the x-direction and not in the y-direction.

4.3.2 The case $D_z = 0$

When $D_z = 0$ the concentration is given by (2.13) which becomes

$$c(x, y, z, t) = \frac{Q}{4\pi D_h t} e^{-\frac{(x-(X_0+Ut))^2}{4D_h t} - \frac{(y-(Y_0+Vt))^2}{4D_h t}} \delta(z - (H - St)) .$$

The ash density on the ground ($z = 0$) at the point (x, y) is given by

$$\begin{aligned} f(x,y) &= \int_0^\infty Sc(x, y, 0, t)\, dt \\ &= S \int_0^\infty \frac{Q}{4\pi D_h t} e^{-\frac{(x-(X_0+Ut))^2}{4D_h t} - \frac{(y-(Y_0+Vt))^2}{4D_h t}} \delta(St - H)\, dt \\ &= \frac{SQ}{4\pi D_h H} e^{-\frac{(x-(X_0+U\frac{H}{S}))^2}{4D_h \frac{H}{S}} - \frac{(y-(Y_0+V\frac{H}{S}))^2}{4D_h \frac{H}{S}}} . \end{aligned} \tag{4.1}$$

Alternatively, if deposit(2.14) is used, we may take the limit as D_z tends towards zero to obtain

$$f(x, y) = \frac{SQ}{4\pi D_h H} e^{-\frac{(x-(X_0+U\frac{H}{S}))^2}{4D_h \frac{H}{S}} - \frac{(y-(Y_0+V\frac{H}{S}))^2}{4D_h \frac{H}{S}}} .$$

Using the data from Table 1.1, the deposition contours in Figure 4.3 are very close to the case in Figure 4.2 where $D_z = 0.01$. This verifies the solution of the deposit (4.1) with $D_z = 0$.

The point (x_c, y_c) where the deposit is maximum in this case is $(X_0 + U\frac{H}{S}, Y_0 + V\frac{H}{S})$.

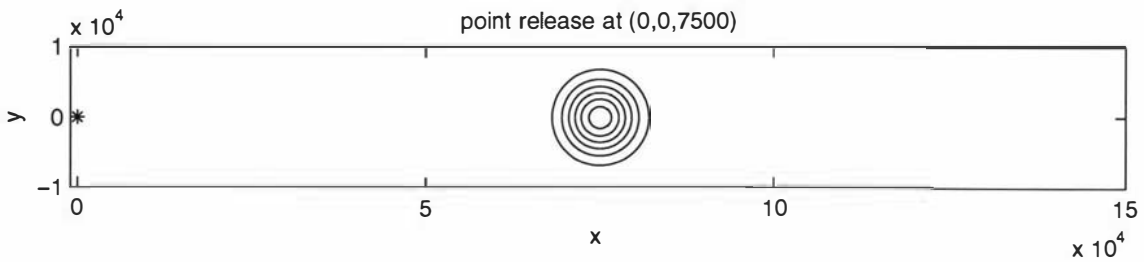

Figure 4.3: Deposition contours for instantaneous release in a uniform whole space with $D_z = 0$. The innermost contour has the highest deposit whilst the outermost has the lowest deposit.

4.4 Deposit from an Instantaneous Point Source with Release in a Uniform Half-Space

In this section, we consider two cases, one in which vertical dispersion is significant ($D_z \neq 0$) and one in which vertical dispersion is negligible ($D_z = 0$).

4.4.1 The case $D_z \neq 0$

The deposit (2.15) is used to calculate the deposition from a point source with an instantaneous release in a uniform half-space. Using the data from Table 1.1, we consider the deposit:

$$f(x,y) = \int_0^\infty \left\{ -\frac{SQ}{16D_h t\sqrt{\pi^3 D_z}} e^{-\frac{(x-X_0-Ut)^2}{4D_h t} - \frac{(y-Y_0-Vt)^2}{4D_h t}} \times \right.$$
$$\left. \times \int_0^t \left[\left(\frac{SH}{D_z} + 2 \right) \frac{1}{\tau^{\frac{3}{2}}} - \frac{H^2}{D_z \tau^{\frac{5}{2}}} \right] e^{-\frac{(-H+S\tau)^2}{4D_z \tau}} d\tau \right\} dt$$

with $D_z = 800$ and $D_z = 0.01$ m^2/s.

The half-space deposit (2.15) is not solvable analytically and numerical methods are used. Nevertheless, we see that the results, shown in Figures 4.4 and 4.5, using the half-space deposit closely resemble the results from the whole space deposit (2.14).

Interestingly, the contour in Figure 4.5 resembles Figure 2.8 in which $D_z = 1$. This shows that the vertical dispersion has little effect between the values of $D_z = 0.01$ and $D_z = 1$. The profile of the spread in Figure 4.4 also reflects that the location of x_c is directly proportional to the wind speed U in the x-direction and the location of y_c is directly proportional to the wind speed V in the y-direction (Section 4.2). Since the data we used were $U = 10$m/s but $V = 0$ m/s (no wind in the y-direction), the ashfall moves forwards in the x-direction and not in the y-direction.

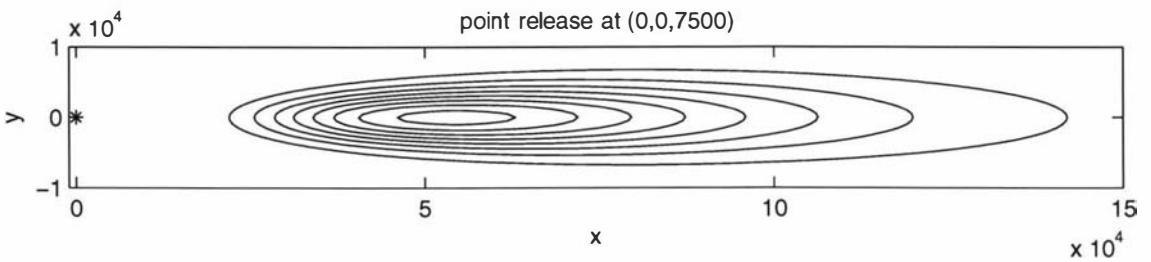

Figure 4.4: Deposition contours for instantaneous release in a uniform half-space with $D_z = 800$. The innermost contour has the highest deposit whilst the outermost has the lowest deposit.

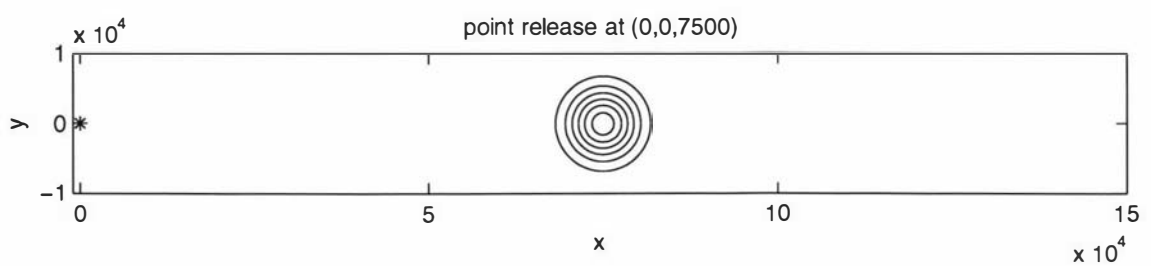

Figure 4.5: Deposition contours for instantaneous release in a uniform half-space with $D_z = 0.01$. The innermost contour has the highest deposit whilst the outermost has the lowest deposit.

4.4.2 The case $D_z = 0$

When $D_z = 0$, Equation (2.15) is used to calculate the deposit from a point source with instantaneous release in a uniform half-space (see Appendix A.5 for the working). We obtain

$$f(x,y) = \frac{SQ}{4\pi D_h H} e^{-\frac{(x-(X_0+U\frac{H}{S}))^2}{4D_h\frac{H}{S}} - \frac{(y-(Y_0+V\frac{H}{S}))^2}{4D_h\frac{H}{S}}}$$

which is the expression as for the whole space deposit (4.1) with $D_z = 0$. This shows that the deposits are identical in a whole space and a half-space models when $D_z = 0$.

The vertical flux at $z = 0$ for the whole space is

$$\text{vertical flux} = \left(Sc + D_z\frac{\partial c}{\partial z}\right)_{z=0},$$

and the vertical flux at $z = 0$ for half space is

$$\text{vertical flux} = (Sc)_{z=0}$$

because we assume $D_z\frac{\partial c}{\partial z} = 0$ at $z = 0$ in the half space and if $D_z \neq 0$ then $\frac{\partial c}{\partial z} = 0$.

If we take $D_z = 0$, which most volcanologists do, then the vertical flux at $z = 0$ is

$$\text{vertical flux} = (Sc)_{z=0}.$$

The vertical flux is the same for both whole and half space when $D_z = 0$.

4.5 Deposition from Two Point Sources with Instantaneous Release in a Half-Space and $D_z = 0$

Although our figures have shown that the observed contours of deposition with $D_z = 0$ resembles concentric circles, in practice, the contours of deposition are not circular. To obtain different deposition contours, we use two point sources instead of the single point source considered in previous chapters and sections. This analysis investigates possible causes for the shape of a deposit on the ground. The formula (3.4) describing the deposit after fall through a layered atmosphere is used in this analysis.

$$f(x,y) = \frac{Q}{4\pi A_f} e^{-\left[\frac{(x-X_f)^2}{4A_f} + \frac{(y-Y_f)^2}{4A_f}\right]}$$

Table 4.1: Experiment 1 - different release heights.

Source	Parameter	Layer 1	Layer 2	Layer 3
a	U	10	10	10
	V	0	0	0
	S	1	1	1
	D_h	800	800	800
b	U	10	10	10
	V	0	0	0
	S	1	1	1
	D_h	800	800	800

where

$$\begin{aligned} H_n &= H - S_1 t_1 - S_2(t_2 - t_1) - ... - S_n(t_n - t_{n-1}) \\ A_f &= D_{h1} t_1 + D_{h2}(t_2 - t_1) + D_{h3}(t_3 - t_2) + ... + D_{hn}(t_n - t_{j-1}) \\ X_f &= X_0 + U_1 t_1 + U_2(t_2 - t_1) + ... + U_n(t_n - t_{n-1}) \\ Y_f &= Y_0 + V_1 t_1 + V_2(t_2 - t_1) + ... + V_n(t_n - t_{n-1}) \end{aligned}$$

and t_n is the time when the particles land on the ground.

Note that under the substitution $U_1 = U_2 = ... = U_j$, $V_1 = V_2 = ... = V_j$, $S_1 = S_2 = ... = S_j$, $D_{h1} = D_{h2} = ... = D_{hj}$, the atmosphere is uniform and the deposit becomes

$$f(x,y) = \frac{SQ}{4\pi D_h H} e^{-\frac{(x - X_0 - U\frac{H}{S})^2}{4D_h \frac{H}{S}} - \frac{(y - Y_0 - V\frac{H}{S})^2}{4D_h \frac{H}{S}}}$$

which is the deposit formula (4.1) of the uniform atmosphere.

The data from Table 1.2 may alter in each experiment in this section. The two point sources are denoted source-a and source-b where the release point of source-a is $(X_0, Y_0, H) = (0, 0, 7000)$ and the release point of source-b is $(X_0, Y_0, H) = (0, 0, 5000)$. The atmosphere for the two point sources is divided into three layers: the first interface is at a height of 3000 metres from the ground and the second interface is at 1000 metres from the ground. The two point sources release ash at different values of time.

4.5.1 Experiment 1 - different release heights

The data for Experiment 1 shown are consistent with a uniform half-space atmosphere as all the parameters are constant throughout all layers: wind speeds $U = 10$ m/s,

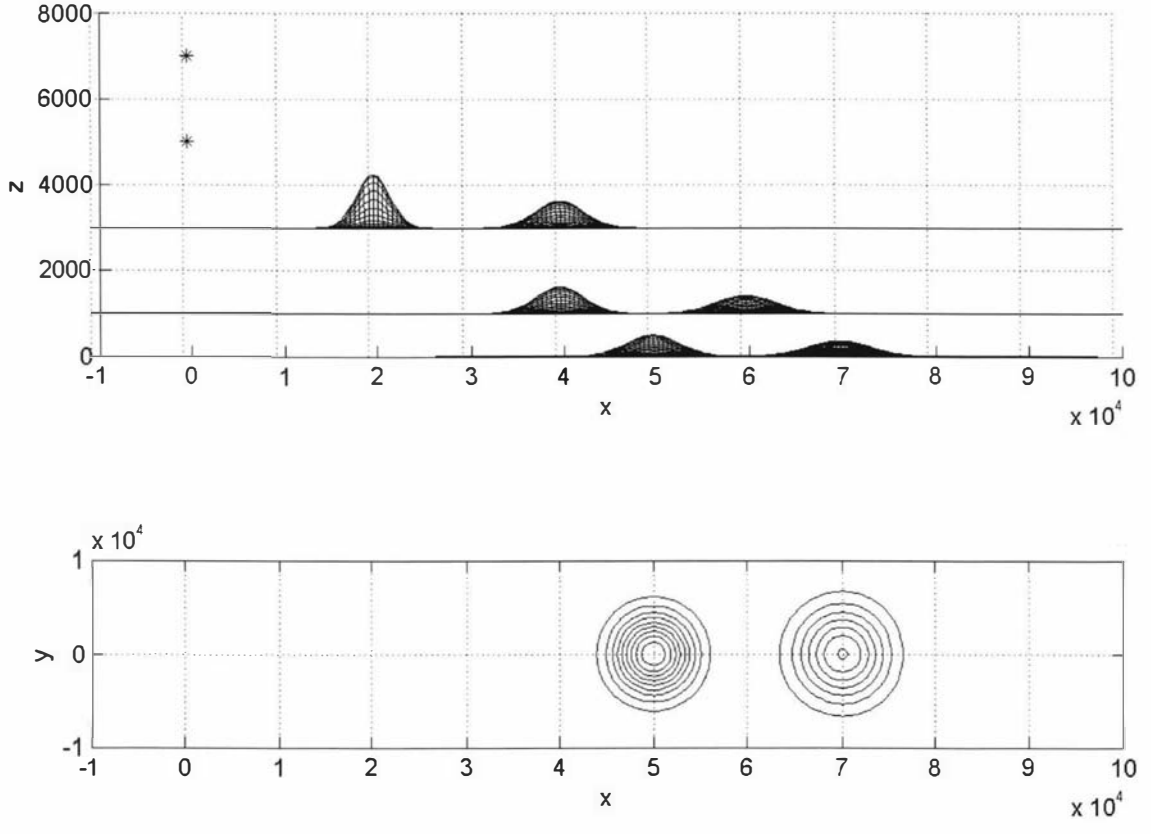

Figure 4.6: Experiment 1 - Distribution of ashfall from different release heights. The innermost contour has the highest deposit whilst the outermost has the lowest deposit. Release point for source-a is at $(0, 0, 7000)$ and source-b is at $(0, 0, 5000)$. Parameter values given in Table 4.1.

Table 4.2: Experiment 2 - larger dispersion.

Source	Parameter	Layer 1	Layer 2	Layer 3
a	U	10	10	10
	V	0	0	0
	S	1	1	1
	D_h	4000	4000	4000
b	U	10	10	10
	V	0	0	0
	S	1	1	1
	D_h	4000	4000	4000

$V = 0$ m/s, settling speed $S = 1$ m/s, and horizontal dispersion $D_h = 800$ m^2/s. The purpose of Experiment 1 is to observe the deposition from two sources at different release heights in a uniform atmosphere.

The bottom graph for Figure 4.6 of Experiment 1 shows that the ash from the two point sources landed apart, because they were released at different heights. Source-b landed closer to the release point, $(X_0, Y_0) = (0, 0)$ because the release height is lower than source-a and so the particulates had a shorter time to disperse. On the other hand, the release height for source-a was higher so these particles had a longer time to spread. Consequently, the ashfall from source-a (on the right in the top graph of Figure 4.6) landed farther from $(X_0, Y_0) = (0, 0)$ than that from source-b and the resulting deposit also spread wider than that from source-b.

4.5.2 Experiment 2 - larger dispersion

Based on Experiment 1, we consider two sources, using the same data, but with a larger horizontal dispersion, $D_h = 4000$ m^2/s throughout ashfall in Experiment 2. The purpose of this experiment is to observe the shape of the deposit contour on the ground. We again assume a uniform atmosphere.

The bottom graph of Figure 4.7 from Experiment 2 shows that the deposits from the two sources overlap. We see that dispersion has an impact on the ashfall: even though the two sources are released at different heights they can land close to each other if the dispersion rate is high enough. From the top graph of Figure 4.7, we see that the spread of the ashfall is wider than in Experiment 1 because dispersion is larger. Again we see that the deposit from source-a is thinner than that from source-b and wider than that from source-b as it is released from a higher point and so had a longer time to fall and therefore more time to spread.

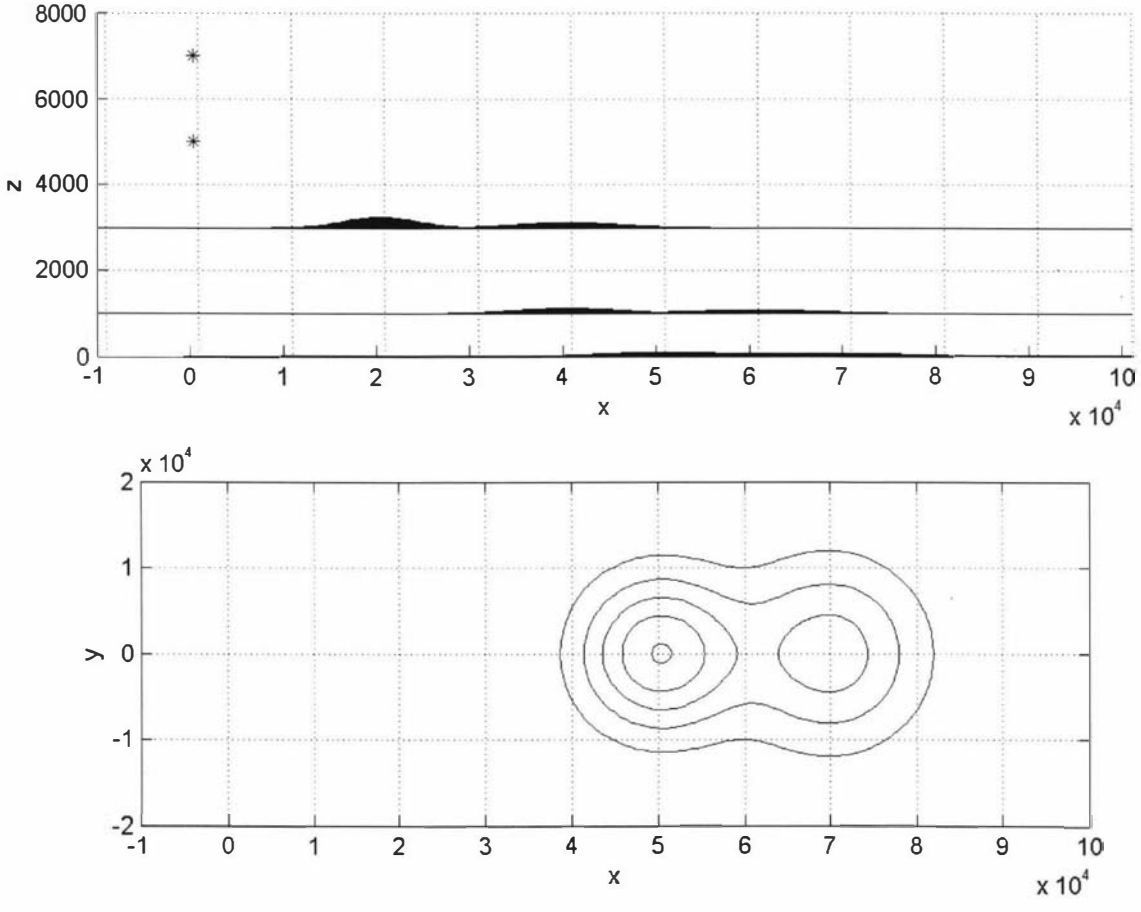

Figure 4.7: Experiment 2 - Distribution of ashfall with larger dispersion. The innermost contour has the highest deposit whilst the outermost has the lowest deposit. Release point for source-a is at $(0, 0, 7000)$ and source-b is at $(0, 0, 5000)$. Parameter values given in Table 4.2.

Table 4.3: Experiment 3 - change in wind speeds.

Source	Parameter	Layer 1	Layer 2	Layer 3
a	U	10	5	10
	V	0	0	0
	S	1	1	1
	D_h	800	800	800
b	U	10	10	10
	V	0	0	0
	S	1	1	1
	D_h	800	800	800

4.5.3 Experiment 3 - change in wind speeds

This time we change the wind speed in the x-direction to $U = 5$ in layer 2 of the atmosphere for source-a, the remainder of the data remain as the Experiment 1. Hence source-a is released in layered atmosphere but source-b is released into a uniform atmosphere. Recall that the sources are released at different times.

The bottom graph of Figure 4.8 from Experiment 3 shows that the deposits from the two sources overlap each other. The deposit is elongated as the wind speed was changed to 5 m/s in the x-direction for source-a in layer two of the atmosphere and then changed back to a wind speed of 10 m/s in layer one. This demonstrates that a change of wind speed and direction during the fall will affect the resulting deposition. From the top graph of Figure 4.8, we see that the spread of the ashfall is moving towards the left when the wind speed reduces.

4.5.4 Experiment 4 - different settling speeds

We use the same data as in Experiment 3 except that the settling speed of source-b is changed to 1.5 m/s, i.e. the particles in source-b are now larger in size than those in source-a. Therefore they fall faster than those of source-a.

The bottom graph of Figure 4.9 from experiment 4 shows that the deposits from the two sources are separated. This is due to their different settling speeds. Source-b has a higher settling speed so deposits from it reach the ground faster than deposits from source-a. Furthermore, source-b is released at a lower height than source-a. This is because larger particles usually do not rise as high from an eruption as smaller ones. Note that the settling speed formula (2.8) implies that settling speed is dependent on the size of the particle (with larger particles having a higher settling speed). We observe that the source with lower settling speed spreads wider than one with higher settling speed. Particles with lower settling speed have more time to disperse, so

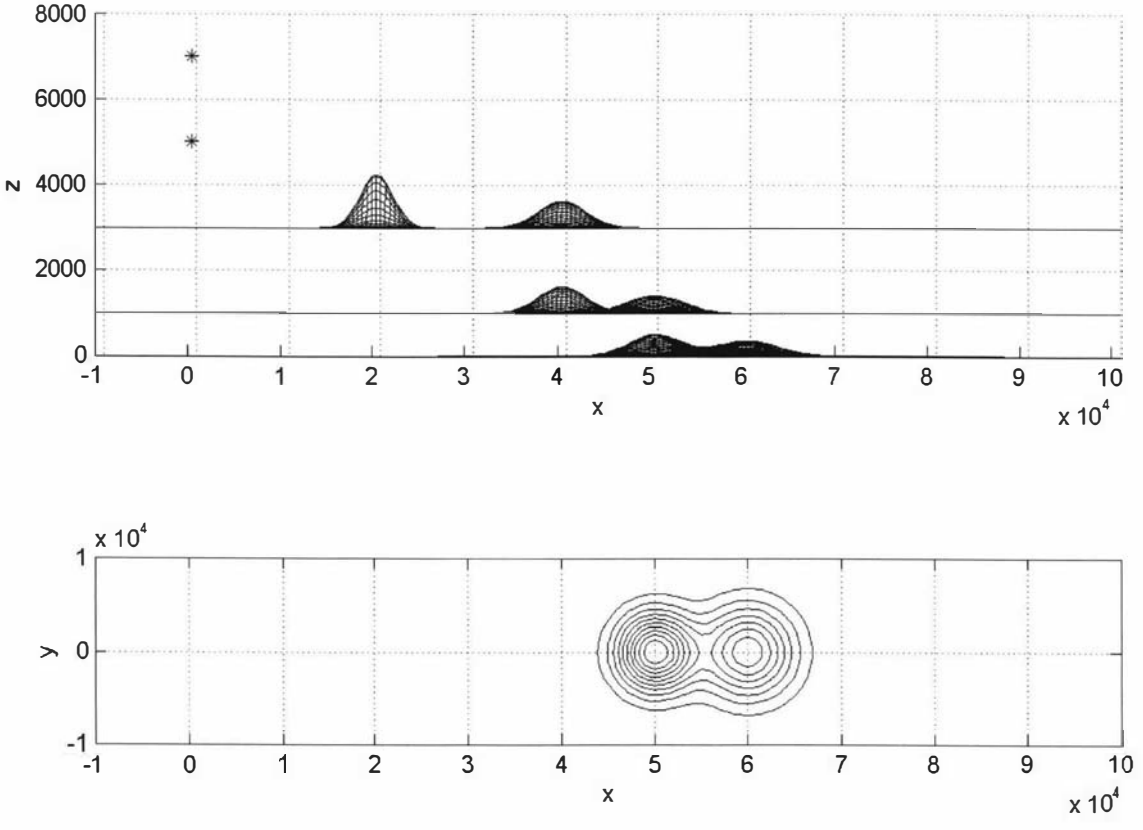

Figure 4.8: Experiment 3 - Distribution of ashfall for change in wind speeds. The innermost contour has the highest deposit whilst the outermost has the lowest deposit. Release point for source-a is at $(0, 0, 7000)$ and source-b is at $(0, 0, 5000)$. Parameter values given in Table 4.3.

Table 4.4: Experiment 4 - different settling speeds.

Source	Parameter	Layer 1	Layer 2	Layer 3
a	U	10	5	10
	V	0	0	0
	S	1	1	1
	D_h	800	800	800
b	U	10	10	10
	V	0	0	0
	S	1.5	1.5	1.5
	D_h	800	800	800

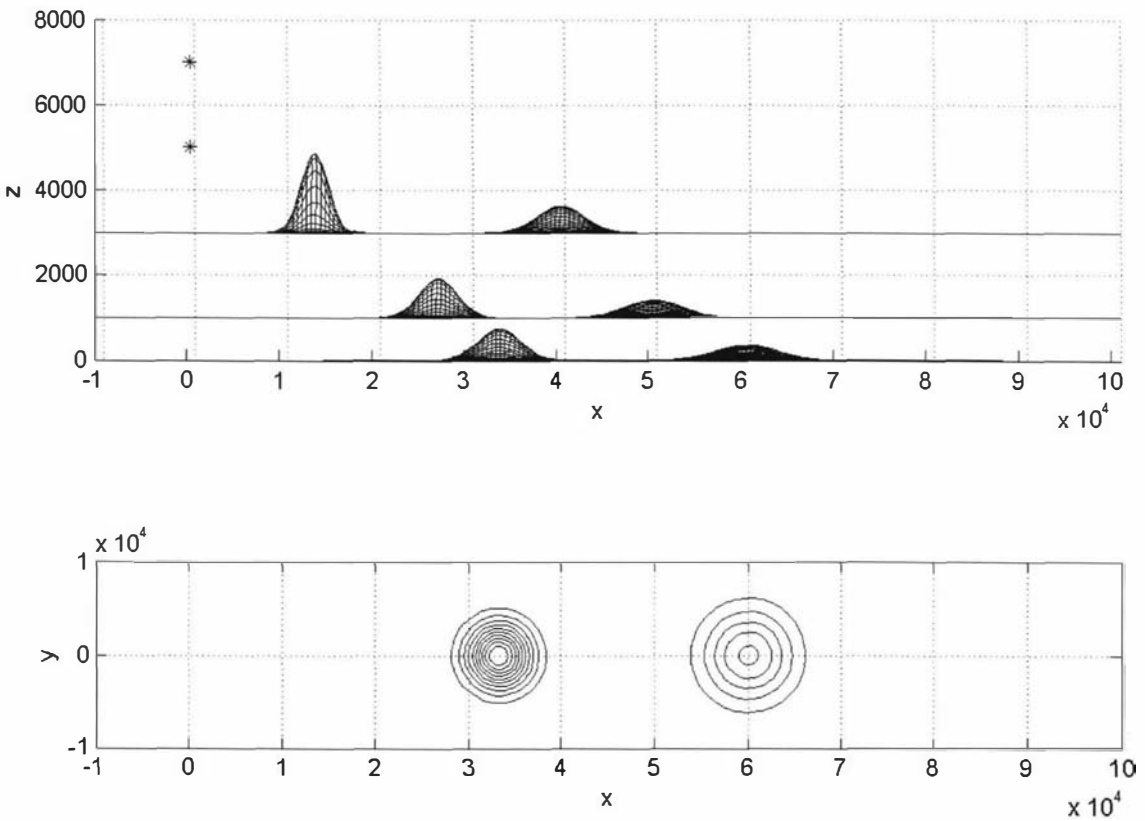

Figure 4.9: Experiment 4 - Distribution of ashfall with different settling speeds. The innermost contour has the highest deposit whilst the outermost has the lowest deposit. Release point for source-a is at $(0, 0, 7000)$ and source-b is at $(0, 0, 5000)$. Parameter values given in Table 4.4.

Table 4.5: Experiment 5 - different settling speeds with change in wind speed and direction.

Source	Parameter	Layer 1	Layer 2	Layer 3
a	U	10	-5	10
	V	0	0	0
	S	1	1	1
	D_h	800	800	800
b	U	10	10	10
	V	0	0	0
	S	1.5	1.5	1.5
	D_h	800	800	800

the spread of the ash is wider. Particles with higher settling speed have less time to disperse and hence the spread of the deposit on the ground is smaller.

4.5.5 Experiment 5 - different settling speeds with change in wind speed and direction

Using the same data as in Experiment 4 except that wind direction in the x-axis is changed to $U = -5$ m/s in layer 2 for source-a in Experiment 5.

Figure 4.10 shows that the deposits for the two sources overlap each other. We observe that if the change in wind speed or direction is great enough during ashfall, it affects the distribution of the deposit even though the size of the source particles are different. Hence, changes in the physical conditions in the atmosphere exert strong influence on the movement of particles. Again, particles with lower settling speed have more time to disperse so the spread of the ash is wider and particles with higher settling speed have less time to disperse and hence the spread of the deposit on the ground is smaller.

4.6 Deposit for Sources of Different Shapes in a uniform atmosphere with $D_z = 0$

In this section we experiment with sources of different shapes and observe the shape of the resulting deposit. We also investigate the effect of release height upon dispersion. The atmosphere used in this analysis is based on the uniform model with $D_z = 0$ (Equation (4.1)).

$$f(x,y) = \frac{SQ}{4\pi D_h H} e^{-\frac{(x-X_0-U\frac{H}{S})^2}{4D_h\frac{H}{S}} - \frac{(y-Y_0-V\frac{H}{S})^2}{4D_h\frac{H}{S}}}.$$

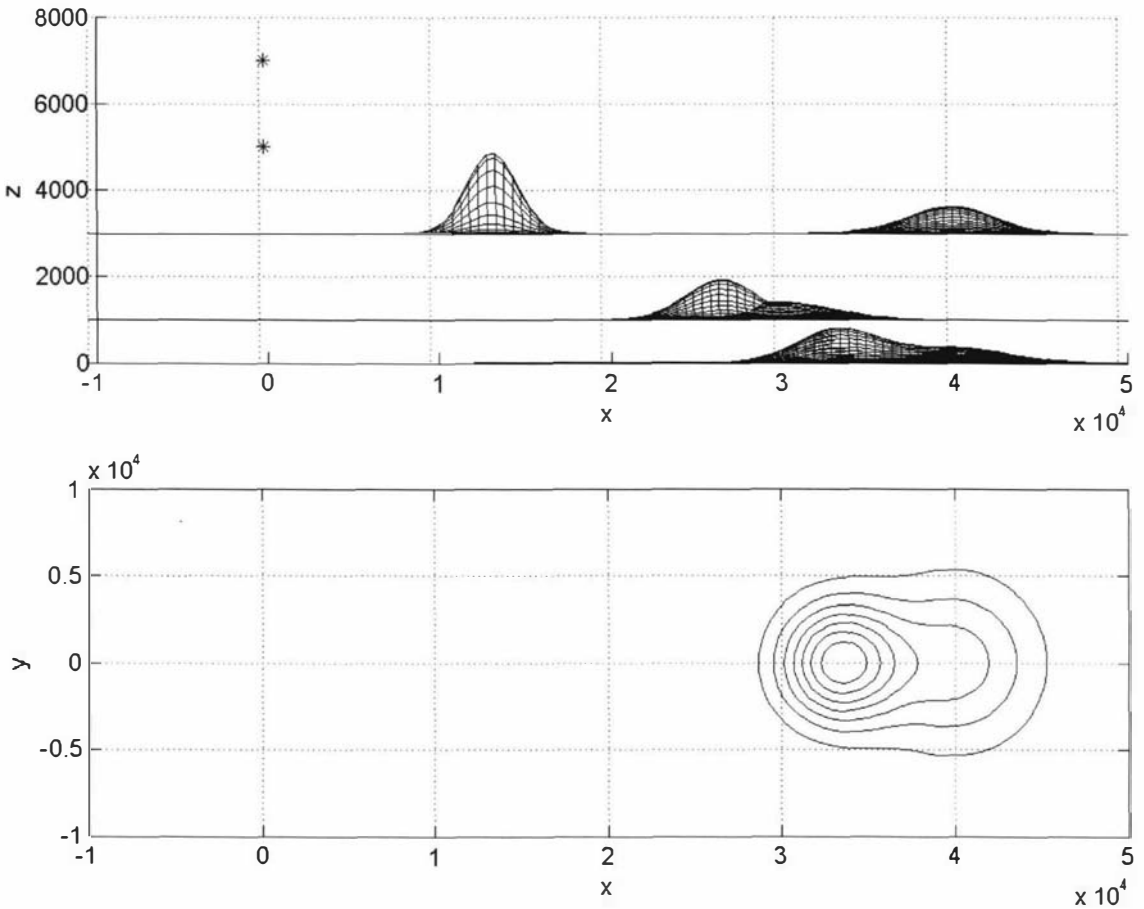

Figure 4.10: Experiment 5 - Distribution of ashfall with different settling speeds and a change in wind speeds. The innermost contour has the highest deposit whilst the outermost has the lowest deposit. Release point for source-a is at $(0, 0, 7000)$ and source-b is at $(0, 0, 5000)$. Parameter values given in Table 4.5.

The purpose of this analysis is to compare the results obtained using different source shapes with the results obtained using the point source. For example, in order to obtain a formula for a horizontal source, we allow X_0 to vary and replace it by X for a horizontal line source. We have to reformulate the model for each shape of source, for example, for a horizontal line source releases in the direction of x, we write the deposit as

$$f(x,y;X) = \frac{SQ}{4\pi D_h H} e^{-\frac{(x-X-U\frac{H}{S})^2}{4D_h\frac{H}{S}} - \frac{(y-Y_0-V\frac{H}{S})^2}{4D_h\frac{H}{S}}}.$$

The work in this section is motivated by Prof. Chuck Connor of the Department of Geology at the University of South Florida. At the conference [28] I gave a presentation on deposition of ashfall from a point source. Following this presentation, Prof. Chuck Connor suggested that it would be useful to investigate the deposit from a circular source. We followed this suggestion and also investigated the deposition from other shapes of sources. The shapes of source we consider are: a horizontal line segment, a vertical line segment, a rectangle and a circle. The data from Table 1.1 is used for this analysis. In the following subsections we calculate the deposit from different shapes of source. The ash deposition from each shape of source is presented graphically.

4.6.1 Release from a horizontal line

We consider a horizontal line source parallel to the x-axis on the interval $(X_1 \leq x \leq X_2)$ with mass $\frac{Q}{(X_2-X_1)}$ kg per metre length released at $t = 0$. By integrating the deposit from each small segment dX of the line source, namely $[Q/(X_2 - X_1)]dX$, we get

$$\begin{aligned} f(x,y) &= \frac{1}{X_2-X_1}\int_{X_1}^{X_2} \frac{SQ}{4\pi D_h H}\, e^{-\frac{(x-X-U\frac{H}{S})^2}{4D_h\frac{H}{S}} - \frac{(y-Y_0-V\frac{H}{S})^2}{4D_h\frac{H}{S}}} dX \\ &= \frac{Q}{4\sqrt{\pi D_h\frac{H}{S}}(X_1-X_2)} e^{-\frac{(y-Y_0-V\frac{H}{S})^2}{4D_h\frac{H}{S}}} \\ &\quad \times \left\{ \operatorname{erf}\left(\frac{(x-X_2-U\frac{H}{S})}{2\sqrt{D_h\frac{H}{S}}} \right) - \operatorname{erf}\left(\frac{(x-X_1-U\frac{H}{S})}{2\sqrt{D_h\frac{H}{S}}} \right) \right\}. \end{aligned}$$

For a horizontal line source parallel to the y-axis on the interval $(Y_1 \leq y \leq Y_2)$, the

deposit is given by:

$$f(x,y) = \frac{Q}{4\sqrt{\pi D_h \frac{H}{S}}(Y_1 - Y_2)} e^{-\frac{(x - X_0 - U\frac{H}{S})^2}{4D_h\frac{H}{S}}} \times \left\{ \text{erf}\left(\frac{(y - Y_2 - V\frac{H}{S})}{2\sqrt{D_h\frac{H}{S}}} \right) - \text{erf}\left(\frac{(y - Y_1 - V\frac{H}{S})}{2\sqrt{D_h\frac{H}{S}}} \right) \right\}.$$

We consider two different lengths of horizontal line parallel to the x-axis and y-axis; 1500 m and 10000 m. We see from figures 4.11 and 4.12 that the deposit from the shorter horizontal line source is similar to the ash deposit from a point source. If the release height of the longer horizontal line is very large, the deposit appears no different from the deposit due to a point source.

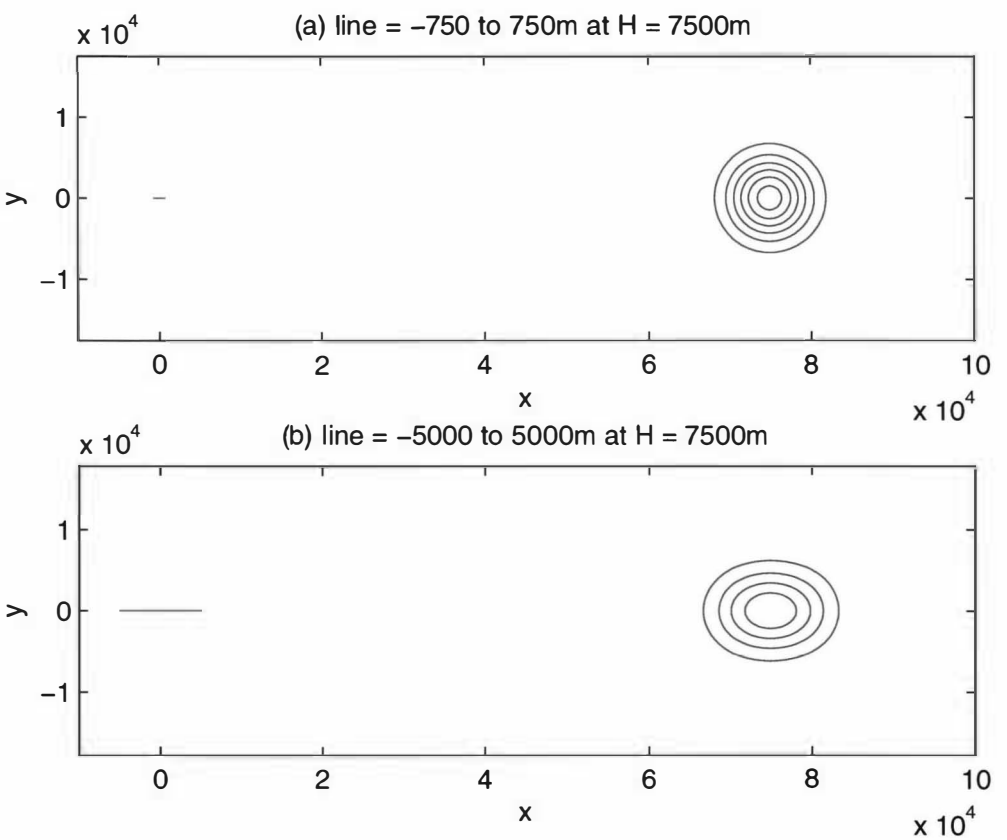

Figure 4.11: Contour of deposition from horizontal line source parallel to x-axis. The innermost contour has the highest deposit whilst the outermost has the lowest deposit.

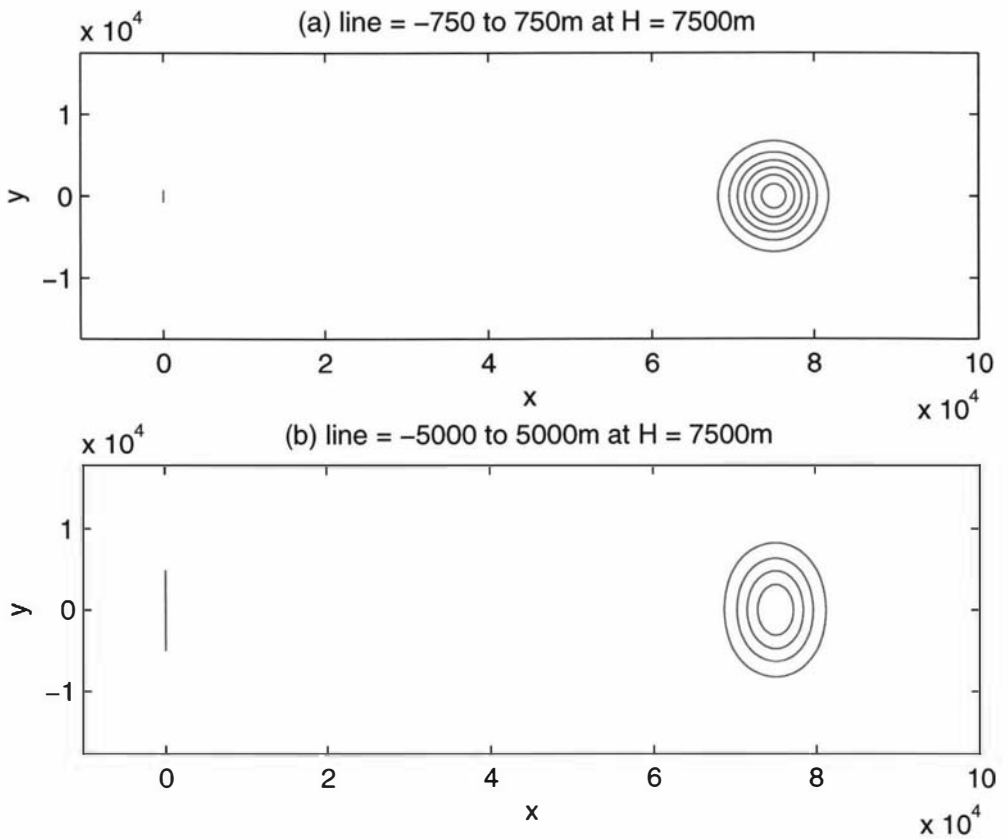

Figure 4.12: Contour of deposition from horizontal line source parallel to y-axis. The innermost contour has the highest deposit whilst the outermost has the lowest deposit.

4.6.2 Release from a vertical line

The vertical line source is worth investigating because eruptions sometime eject ash into a column [54]. We consider a vertical line source parallel to the z-axis along the interval $(H_1 \leq H \leq H_2)$. The deposit due to the vertical source is given by:

$$\begin{aligned} f(x,y) &= \frac{1}{H_2 - H_1} \int_{H_1}^{H_2} f(x,y;H)dH \\ &= \frac{1}{H_2 - H_1} \int_{H_1}^{H_2} \frac{SQ}{4\pi D_h H} e^{-\frac{(x-X_0-U\frac{H}{S})^2}{4D_h\frac{H}{S}} - \frac{(y-Y_0-V\frac{H}{S})^2}{4D_h\frac{H}{S}}} dH\,. \end{aligned}$$

We also consider two lengths of vertical line, 100 m and 2000 m. From Figure 4.13(a) we see that the deposit from the shorter vertical line source is similar to the deposit from a point source. Figure 4.13(b) shows an elongated distribution from the longer vertical line.

Figure 4.14 is a vertical line source with a length 6000 m from 2500 to 8500 m, the

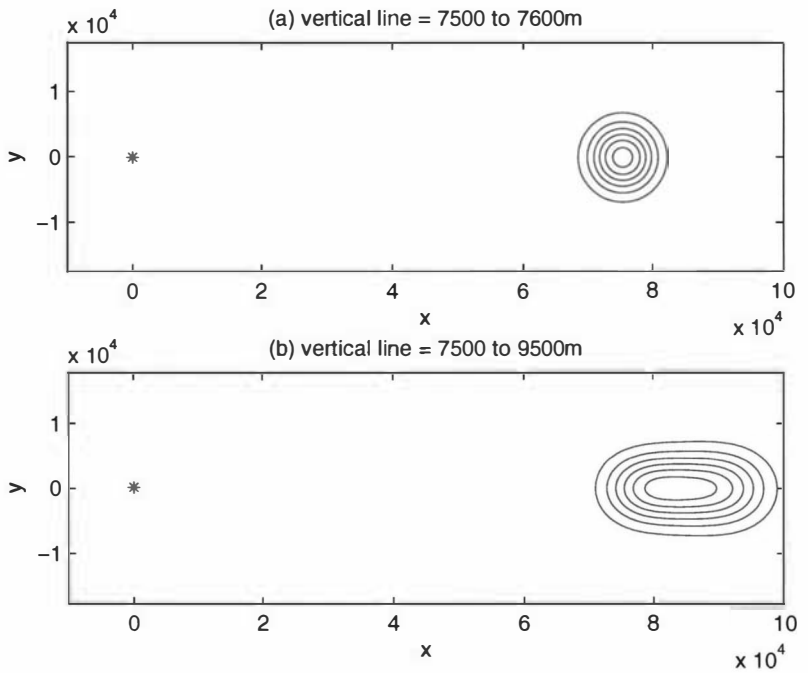

Figure 4.13: Contour of deposition from a vertical line segment source above origin. (* indicates the release point at $(X_0, Y_0) = (0, 0)$ from the top view.) The innermost contour has the highest deposit whilst the outermost has the lowest deposit.

Table 4.6: Data of the two vertical line sources in Figure 4.16.

Parameter	X_0	Y_0	length of vertical line	Q	U	V	S	D_h	D_z
Line 1	0	0	7500 to 9500	2.5×10^{10}	10	0	1	800	0
Line 2	0	0	7500 to 8500	2.5×10^{10}	10	0	1.05	800	0

contour is a "fan" shape deposit, the right-hand-side of the contour is wider than the left. The deposit on the left comes from ash released at the lower portion of the vertical line source and the deposit on the right is from ash released in the upper portion of the vertical line source. The higher the release (the upper portion) the wider the spread as there is more time to spread farther. The lower the release (the lower portion) the smaller the spread as there is less time to spread farther.

Figure 4.13(b) shows some similarities to the contours of deposition produced from the Taupo eruption (see 4.15), though the contours produced from the Taupo eruption are not as even as those in figure 4.13(b). This leads us to speculate that a vertical line source may be a good model for the ejection of ash into the atmosphere following an eruption. We continue the study of vertical line sources by considering two overlapping (simultaneous) vertical line sources with different settling speeds representing two different sizes of particles.

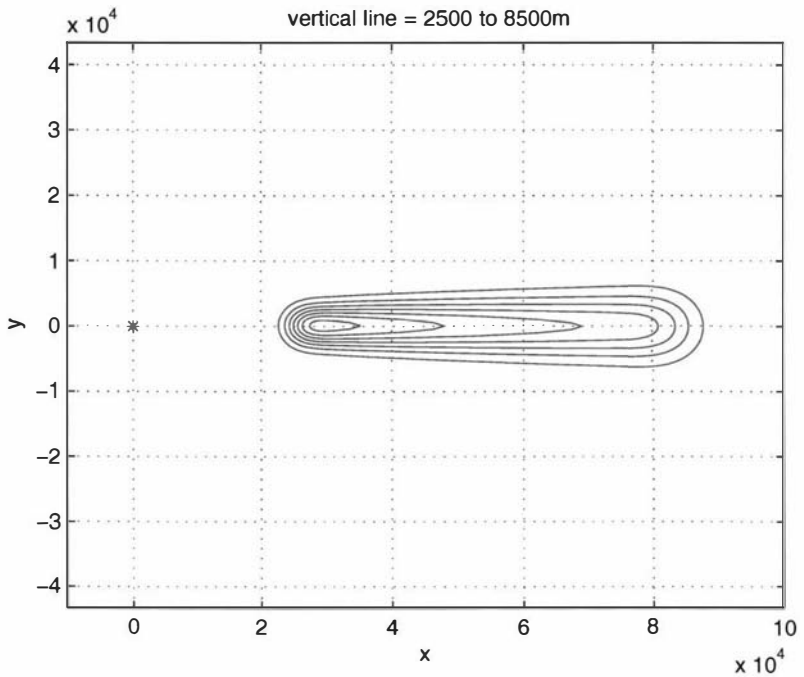

Figure 4.14: Contour of deposition for a longer vertical line source. The innermost contour has the highest deposit whilst the outermost has the lowest deposit.

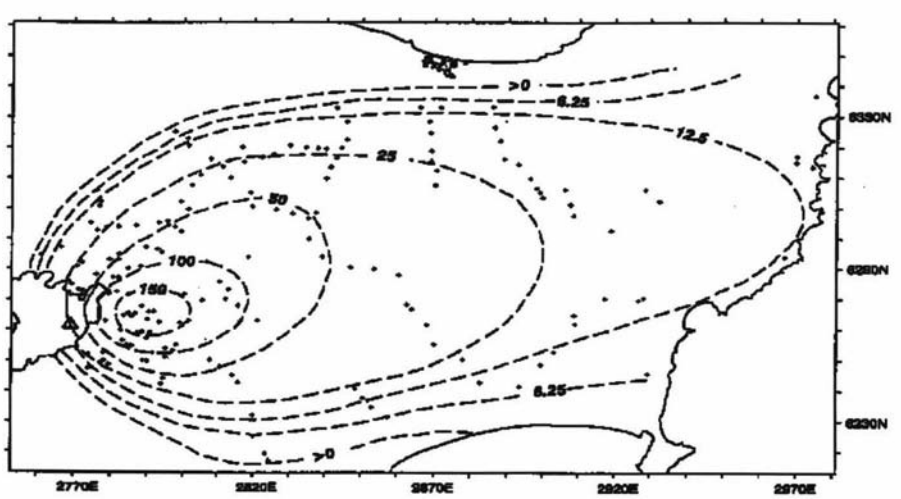

Figure 4.15: Contour of deposition from the Taupo eruption [53].

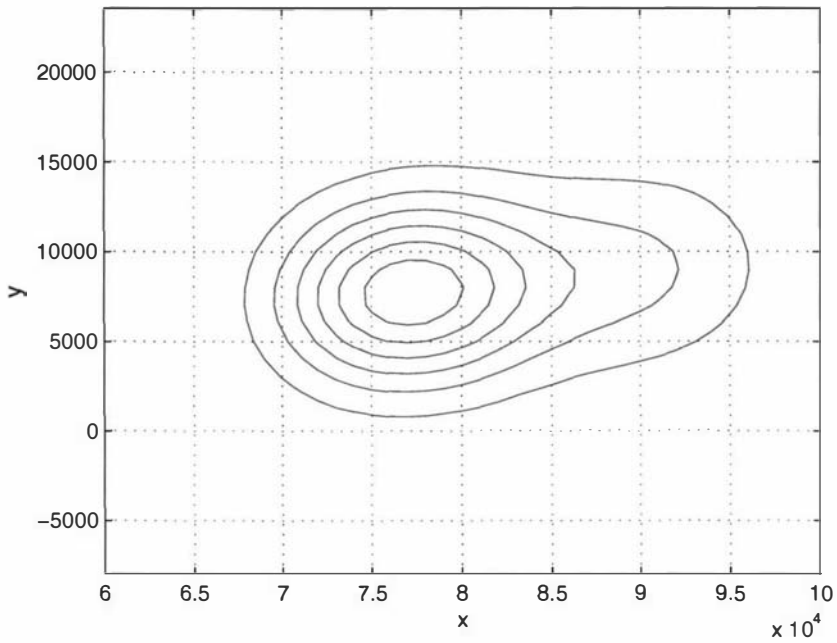

Figure 4.16: Contour of deposition from two overlapping vertical line sources. The innermost contour has the highest deposit whilst the outermost has the lowest deposit (Table 4.6.)

Qualitatively, it appears that the deposit from two vertical line sources as shown in figure 4.16 gives an elongated distribution similar to figure 4.15. It could be that different sizes of particles released along the same column explain the observed elongated distribution.

4.6.3 Release from a rectangle

We assume a rectangular plane source with sides given by the intervals $(X_1 \leq x \leq X_2)$ and $(Y_1 \leq y \leq Y_2)$. The deposition from the source is given by:

$$\begin{aligned} f(x,y) &= \frac{1}{(X_2-X_1)(Y_2-Y_1)} \int_{Y_1}^{Y_2} \int_{X_1}^{X_2} f(x,y;X,Y)dX\ dY \\ &= \frac{1}{(X_2-X_1)(Y_2-Y_1)} \int_{Y_1}^{Y_2} \int_{X_1}^{X_2} \frac{SQ}{4\pi D_h H} e^{-\frac{(x-X-U\frac{H}{S})^2}{4D_h\frac{H}{S}} - \frac{(y-Y-V\frac{H}{S})^2}{4D_h\frac{H}{S}}} dX\ dY \\ &= \frac{Q}{4(X_1-X_2)(Y_1-Y_2)} \left\{ \operatorname{erf}\left(\frac{(x-X_2-U\frac{H}{S})}{2\sqrt{D_h\frac{H}{S}}} \right) - \operatorname{erf}\left(\frac{(x-X_1-U\frac{H}{S})}{2\sqrt{D_h\frac{H}{S}}} \right) \right\} \\ &\quad \times \left\{ \operatorname{erf}\left(\frac{(y-Y_2-V\frac{H}{S})}{2\sqrt{D_h\frac{H}{S}}} \right) - \operatorname{erf}\left(\frac{(y-Y_1-V\frac{H}{S})}{2\sqrt{D_h\frac{H}{S}}} \right) \right\}. \end{aligned}$$

We consider two sizes of rectangles (in fact squares) of dimensions 1500 m $\times$ 1500 m and 15000 m $\times$ 15000 m. We see from figures 4.17(a) and 4.17(b) that the deposit due to the smaller rectangular source is similar to the deposit due to a point source. Considering the previous results, it seems that the shape of source is unimportant if it is relatively small. If the release height of the larger rectangular source is very large the resulting deposit appears no different from the deposit due to a point source.

4.6.4 Release from a circle

In this section we consider a circular source. The circular source is worth investigating because eruptions sometime generate a circular cloud [54]. We consider a circular source of radius R and centre (X_0, Y_0). The model, in polar form, used to calculate the deposition from this source is:

$$\begin{aligned} f(x,y) &= \frac{1}{\pi R^2} \int_{r=0}^{R} \int_{0}^{2\pi} f(x,y;r,\theta) r\,dr\,d\theta \\ &= \frac{SQ}{4D_h\pi^2R^2H} \int_{r=0}^{R} \int_{0}^{2\pi} e^{-\frac{(x-X_0-r\cos\theta-U\frac{H}{S})^2}{4D_h\frac{H}{S}}} e^{-\frac{(y-Y_0-r\sin\theta-V\frac{H}{S})^2}{4D_h\frac{H}{S}}} r\,dr\,d\theta\,. \end{aligned}$$

We consider two circles: one of radius 750 m and one of radius 7500 m. From figures 4.18(a) and 4.18(b) we see, once again, that the deposition of ash from the smaller source is similar to the deposit from a point source. The deposit forms a circle because the horizontal dispersion is isotropic, however, the size of deposit from the smaller circular source is similar to that from the point source. If the release height of the larger circular source is very large the resulting deposit is no different from the deposit due to a point source.

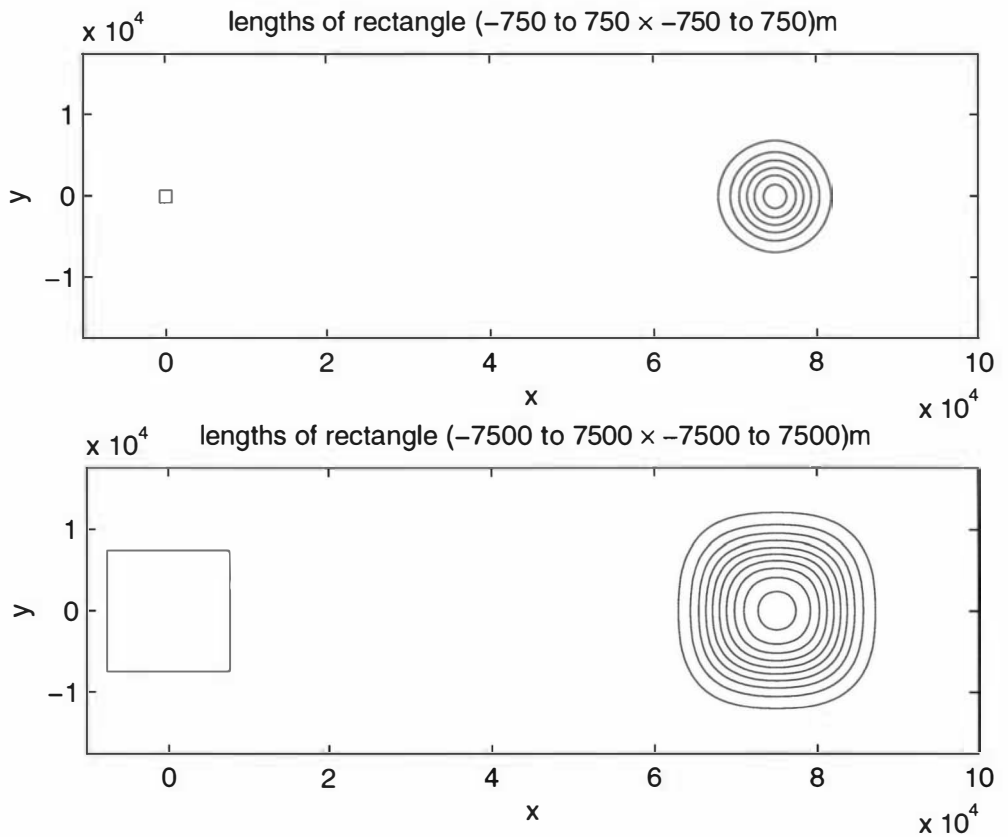

Figure 4.17: Contour of deposition from a rectangular source. The release height for both rectangular sources is at 7500 m. The innermost contour has the highest deposit whilst the outermost has the lowest deposit.

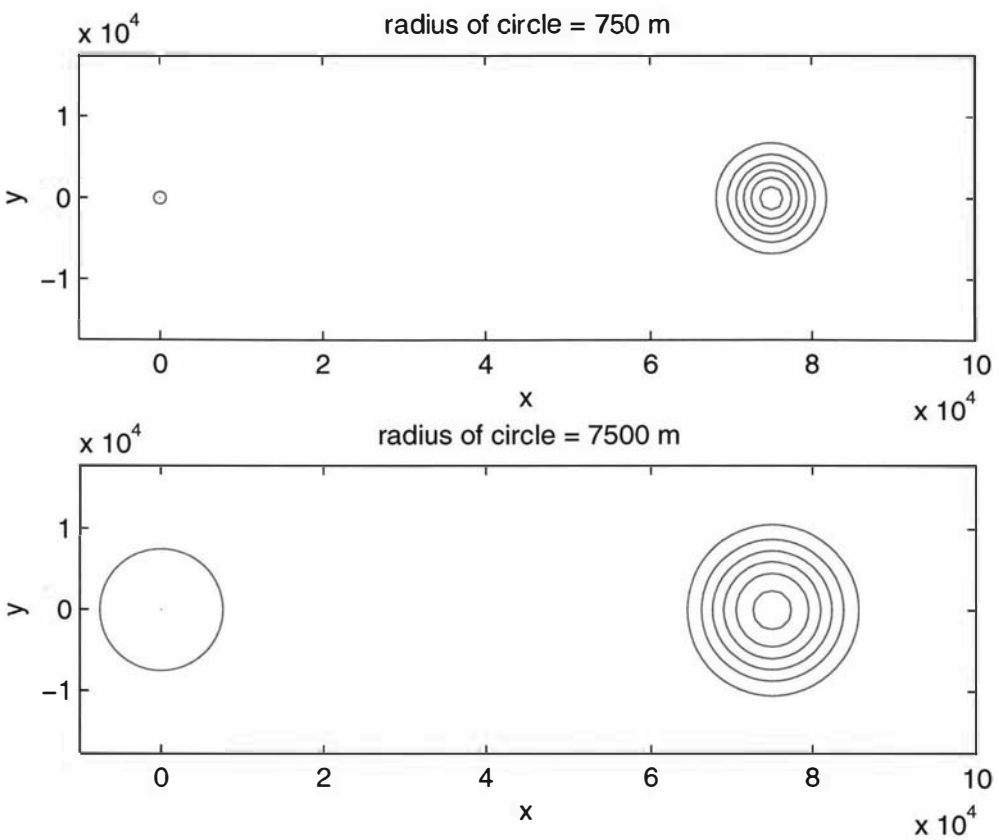

Figure 4.18: Contour of deposition from a circular source. The release height for both circular sources is at 7500 m. The innermost contour has the highest deposit whilst the outermost has the lowest deposit.

4.7 Summary

In this chapter we have shown that the half-space and whole space deposits are the same when there is no vertical dispersion ($D_z = 0$). Though we are unable to solve the half-space deposit analytically when the vertical dispersion is positive ($D_z > 0$), our numerical results show that it is very similar to the whole space deposit. Hence, the whole space model can be used as the half space model.

From the results of the analyses using a point source, we conclude that the distribution of ashfall is controlled by the wind speed, wind direction, dispersion, release height and the settling speed. Our analyses show that particles with lower settling speed have more time to disperse and therefore travel farther; hence the spread of the ashfall is wider and the deposit on the ground is thinner.

Experiments with different shapes of source found that the resulting deposits are the same as the deposit from a point source at the same release height if the deposit source is small. If the release height is reasonably high , the contour deposition is very similar to the point source releases at the same height. The result of a larger source at a greater release height is similar to the point source at the same release height.

Chapter 5

ANALYSIS OF PARAMETERS

result presents the fact
analysis proves the fact

5.1 Analyses

Why analyse the parameters?

The purpose of this chapter is to develop an improved understanding of the impact of the parameters in the advection-dispersion equation and to investigate the sensitivity of results to variation in these parameters. For this analysis, we use the layered model with no vertical dispersion and instantaneous release from a single point, given by Equation (3.1). The mass distribution in kg/m^2 on the ground (the bottom of the nth layer) is given by, formula (3.4):

$$f(x,y) = \frac{Q}{4\pi A_f} e^{-\left[\frac{(x-X_f)^2}{4A_f} + \frac{(y-Y_f)^2}{4A_f}\right]} \tag{5.1}$$

where

$$\begin{aligned} A_f &= D_{h1}t_1 + D_{h2}(t_2 - t_1) + D_{h3}(t_3 - t_2) + ... + D_{hn}(t_n - t_{n-1}) \\ X_f &= X_0 + U_1 t_1 + U_2(t_2 - t_1) + ... + U_n(t_n - t_{n-1}) \\ Y_f &= Y_0 + V_1 t_1 + V_2(t_2 - t_1) + ... + V_n(t_n - t_{n-1}) \end{aligned}$$

and t_n is the time when the particles land on the ground.

We will investigate the effect of the parameters in both the uniform atmosphere and the layered atmosphere models. We take the uniform atmosphere as the base case.

We vary the parameters in the layered atmosphere model and compare it with the uniform atmosphere model. For simplicity we consider only two layers for the layered atmosphere (see Figure 5.1).

Several parameters are assumed to be the same for the two models (uniform atmosphere and layered atmosphere):

- the release point is fixed at $(0, 0, H)$;

- the vertical dispersion is zero, $D_z = 0$;

- the wind speed V in the y-direction is zero ($V = 0$), i.e. the wind is only in the x-direction;

- the horizontal dispersion (D_h) is isotropic;

- $D_{hj} = L_j U_j$ where L_j is the turbulence length-scale;

where $j = 1, 2$.

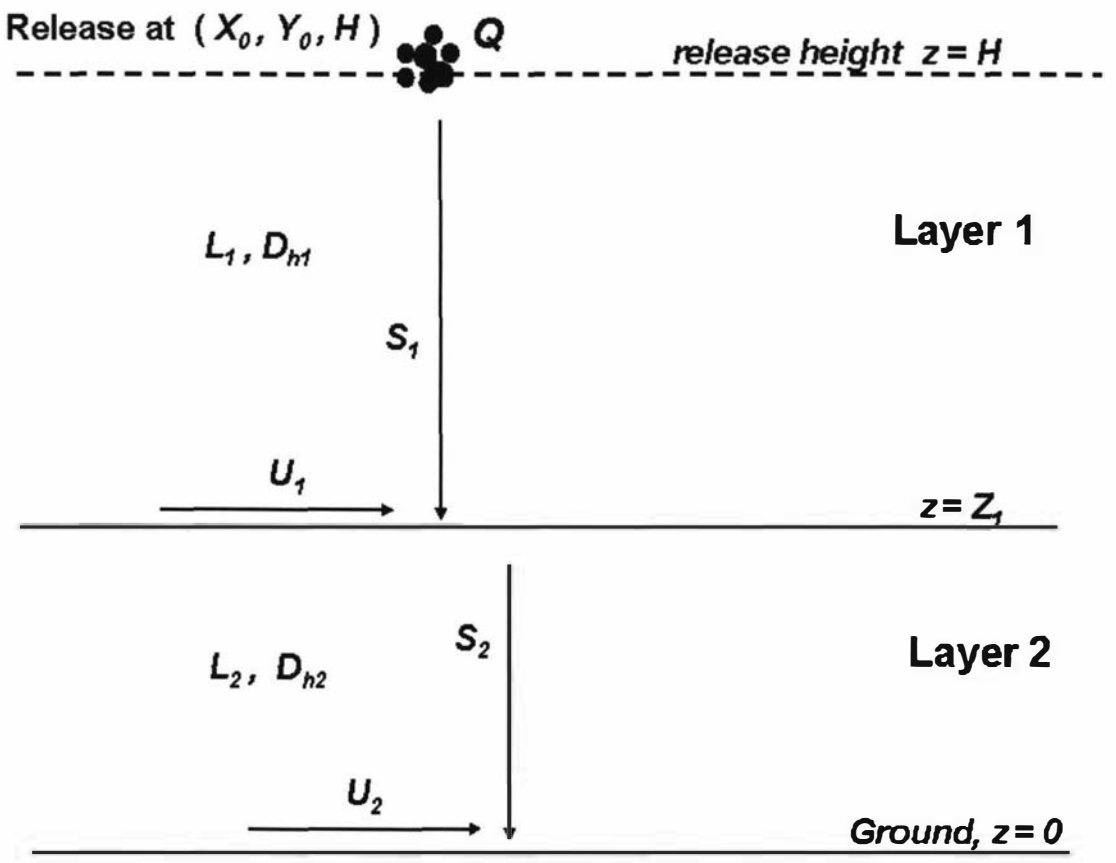

Figure 5.1: A schematic illustration of a two-layered atmosphere.

5.1.1 Uniform atmosphere

Based on the layered model (3.4), the deposit for the uniform atmosphere is

$$f(x,y) = \frac{S_1 Q}{4\pi D_{h1} H} e^{-\frac{(x-U_1\frac{H}{S_1})^2}{4D_{h1}\frac{H}{S_1}}} . \tag{5.2}$$

$f(x,y)$ is of the form of two-dimensional normal distribution.

Based on the normal distribution model, the quantity $2D_{h1}\frac{H}{S_1}$ in the exponent can be variance. The standard deviation is therefore identified as the

$$\sigma = \sqrt{2D_{h1}\frac{H}{S_1}} .$$

The standard deviation [31] describes the spread of ashfall due to dispersion. The dispersion is caused by turbulence, the "mixing" movement of air in the atmosphere. The measure of the spread of ash is therefore σ.

At the point $(x,y) = (x_{max}, y_{max})$ on the ground where f attains its maximum value f_{max}, we have $x = x_{max} = U_1\frac{H}{S_1}$ and $y = y_{max} = 0$. We use x_{max} to study the distance travelled by the ash.

From (5.2) the maximum deposit in a uniform atmosphere is

$$f_{max} = \frac{S_1 Q}{4\pi D_{h1} H} .$$

The three quantities we study for the uniform atmosphere are:

$$x_{max} = U_1\frac{H}{S_1} \tag{5.3}$$

$$f_{max} = \frac{S_1 Q}{4\pi D_{h1} H} \tag{5.4}$$

$$\sigma = \sqrt{2D_{h1}\frac{H}{S_1}} . \tag{5.5}$$

Using Equation (5.5), we may write Equation (5.4) as

$$\begin{aligned} f_{max} &= \frac{Q}{2\pi\left(\sqrt{2D_{h1}\frac{H}{S_1}}\right)^2} \\ &= \frac{Q}{2\pi\sigma^2} . \end{aligned} \tag{5.6}$$

5.1.2 Two-layered atmosphere

Based on the layered formula (5.1) with the same assumptions as above, the deposit in a two-layered atmosphere is given by

$$f(x,y) = \frac{Q}{4\pi A_f} e^{-\left[\frac{(x-X_f)^2}{4A_f} + \frac{y^2}{4A_f}\right]} \tag{5.7}$$

where

$$\begin{aligned} A_f &= D_{h1}t_1 + D_{h2}(t_2 - t_1) \\ X_f &= U_1 t_1 + U_2(t_2 - t_1) \\ t_1 &= \frac{H - Z_1}{S_1}, \quad t_2 = \frac{Z_1}{S_2}. \end{aligned}$$

The three quantities for the two-layered atmosphere are:

$$x_{max} = U_1 \frac{H - Z_1}{S_1} + U_2 \frac{Z_1}{S_2} \tag{5.8}$$

$$f_{max} = \frac{Q}{4\pi \left(D_{h1} \frac{H - Z_1}{S_1} + D_{h2} \frac{Z_1}{S_2} \right)} \tag{5.9}$$

$$\sigma = \sqrt{2 \left(D_{h1} \frac{H - Z_1}{S_1} + D_{h2} \frac{Z_1}{S_2} \right)}. \tag{5.10}$$

As was the case for the uniform atmosphere, we can write Equation (5.9) as

$$f_{max} = \frac{Q}{2\pi\sigma^2}. \tag{5.11}$$

We set up the analyses of Equations (5.3) to (5.5) and (5.9) to (5.11) as follows:

x-coordinate at f_{max}:

$$x_{max\ ratio} = \frac{x_{max}(\text{two} - \text{layered})}{x_{max}(\text{uniform})}$$

maximum thickness:

$$f_{max\ ratio} = \frac{f_{max}(\text{two} - \text{layered})}{f_{max}(\text{uniform})}$$

standard deviation:

$$\sigma_{ratio} = \frac{\sigma(\text{two} - \text{layered})}{\sigma(\text{uniform})}.$$

We obtain

$$x_{max\ ratio} = 1 - \frac{Z_1}{H}\left(1 - \frac{S_1}{S_2}\frac{U_2}{U_1}\right) \tag{5.12}$$

$$f_{max\ ratio} = \frac{1}{1 - \frac{Z_1}{H}\left(1 - \frac{L_2}{L_1}\frac{S_1}{S_2}\frac{U_2}{U_1}\right)} \tag{5.13}$$

$$\sigma_{ratio} = \sqrt{1 - \frac{Z_1}{H}\left(1 - \frac{L_2}{L_1}\frac{S_1}{S_2}\frac{U_2}{U_1}\right)}. \tag{5.14}$$

We study how the ratios $x_{max\ ratio}$, $f_{max\ ratio}$ and σ_{ratio} vary with respect to $\frac{L_2}{L_1}$, $\frac{U_2}{U_1}$ and $\frac{S_1}{S_2}\left(= 1/\frac{S_2}{S_1}\right)$ for the cases where $\frac{Z_1}{H}$ has the values 0, 0.25, 0.5, 0.75 and 1; and also we study variation of quantities ($x_{max\ ratio}$, $f_{max\ ratio}$ and σ_{ratio}) with respect to $\frac{Z_1}{H}$, for the cases where $\frac{L_2}{L_1}$, $\frac{U_2}{U_1}$ and $\frac{S_1}{S_2}\left(= 1/\frac{S_2}{S_1}\right)$ all have values of 0.5, 1 and 1.5.

$\frac{Z_1}{H} = 0$ i.e. $Z_1 = 0$, therefore the atmosphere is completely dominated by layer 1.

$\frac{Z_1}{H} = 0.25$ i.e. layer 1 is larger than layer 2, i.e. the vertical height of layer 1 is longer than layer 2.

$\frac{Z_1}{H} = 0.5$ i.e. layer 1 is same size as layer 2, i.e. layer 1 and layer 2 have the same length in the vertical height.

$\frac{Z_1}{H} = 0.75$ i.e. layer 1 is smaller than layer 2, i.e. the vertical height of layer 1 is shorter than layer 2.

$\frac{Z_1}{H} = 1$ i.e. $Z_1 = H$, therefore the atmosphere is completely dominated by layer 2.

$\frac{L_2}{L_1} = 0.5$ i.e. the turbulence length-scale in layer 1 is larger than in layer 2, $L_1 > L_2$.

$\frac{L_2}{L_1} = 1$ i.e. the turbulence length-scale in layer 1 is same as in layer 2, $L_1 = L_2$.

$\frac{L_2}{L_1} = 1.5$ i.e. the turbulence length-scale in layer 1 is smaller than in layer 2, $L_1 < L_2$.

$\frac{U_2}{U_1} = 0.5$ i.e. the wind speed in layer 1 is larger than in layer 2, $U_1 > U_2$.

$\frac{U_2}{U_1} = 1$ i.e. the wind speed in layer 1 is same as in layer 2, $U_1 = U_2$.

$\frac{U_2}{U_1} = 1.5$ i.e. the wind speed in layer 1 is smaller than in layer 2, $U_1 < U_2$.

$\frac{S_1}{S_2} = 0.5$ i.e. the settling speed in layer 1 is smaller than in layer 2, $S_1 < S_2$.

$\frac{S_1}{S_2} = 1$ i.e. the settling speed in layer 1 is same as in layer 2, $S_1 = S_2$.

$\frac{S_1}{S_2} = 1.5$ i.e. the settling speed in layer 1 is larger than in layer 2, $S_1 > S_2$.

The analyses are illustrated in the following sections.

In our analyses, we write $L_r = \frac{L_2}{L_1}$, $U_r = \frac{U_2}{U_1}$, $S_r = \frac{S_1}{S_2}\left(= 1/\frac{S_2}{S_1}\right)$ and $Z_r = \frac{Z_1}{H}$ and obtain

$$x_{max\ ratio} = 1 - Z_r\left(1 - S_r U_r\right) \tag{5.15}$$

$$f_{max\ ratio} = \frac{1}{1 - Z_r\left(1 - L_r S_r U_r\right)} \tag{5.16}$$

$$\sigma_{ratio} = \sqrt{1 - Z_r\left(1 - L_r S_r U_r\right)}\,. \tag{5.17}$$

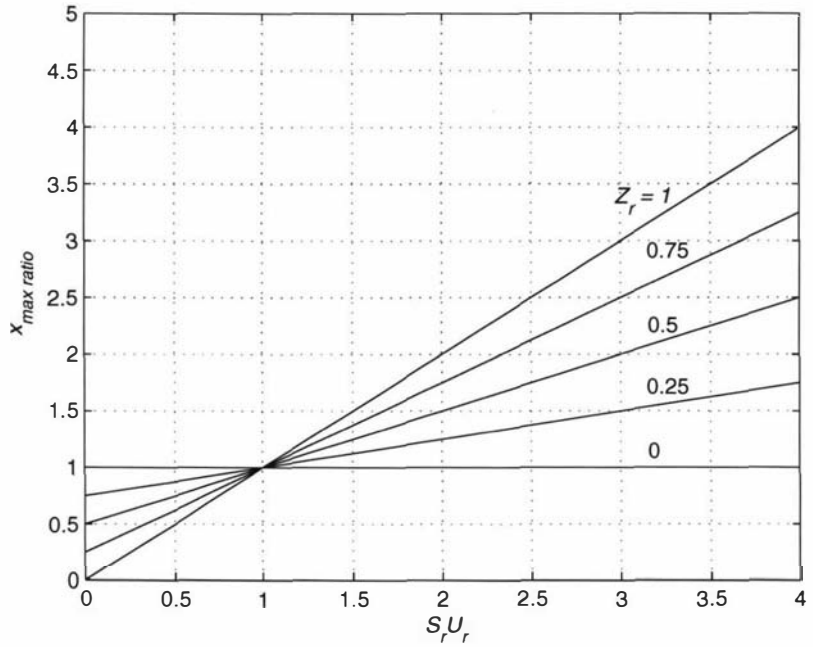

Figure 5.2: $x_{max\ ratio}$ versus S_rU_r for various values of Z_r.

5.1.3 $x_{max\ ratio}$ versus S_rU_r for Z_r=0, 0.25, 0.5, 0.75 and 1

In this analysis we investigate the impact of the parameters on $x_{max\ ratio}$ for Z_r=0, 0.25, 0.5, 0.75 and 1. From Equation (5.15),

$$x_{max\ ratio} = 1 - Z_r\left(1 - S_rU_r\right),$$

we have

$$\frac{dx_{max\ ratio}}{dZ_r} = S_rU_r - 1 \begin{cases} < 0 & \text{if } S_rU_r < 1 \\ = 0 & \text{if } S_rU_r = 1 \\ > 0 & \text{if } S_rU_r > 1 \end{cases}.$$

Figure 5.2 shows that $x_{max\ ratio}$ increases when $S_rU_r = \dfrac{S_1}{S_2}\dfrac{U_2}{U_1}$ increases. When the lower layer wind speed is high and/or the settling speed there is small, then S_rU_r is large and $x_{max\ ratio}$ increases for all values of Z_r. As the value of Z_r increases, layer 2 occupies increasingly more space than layer 1, so the particles have more movement in layer 2. When $Z_r = 0$, $x_{max\ ratio} = 1$, because the atmosphere is dominated by layer one and there is no flow in layer 2. The critical point at $S_rU_r = 1$ happens when $\dfrac{S_2}{S_1} = \dfrac{U_2}{U_1}$.

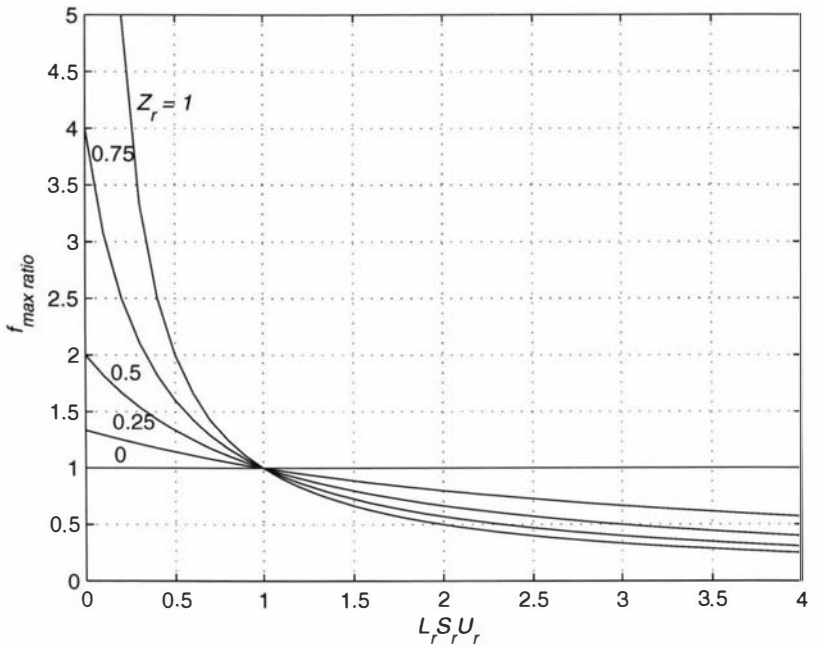

Figure 5.3: $f_{max\ ratio}$ versus $L_rS_rU_r$ for various values of Z_r.

5.1.4 $f_{max\ ratio}$ versus $L_rS_rU_r$ for Z_r=0, 0.25, 0.5, 0.75 and 1

This analysis investigates the impact of the parameters on $f_{max\ ratio}$ when Z_r=0, 0.25, 0.5, 0.75 and 1. From Equation (5.16),

$$f_{max\ ratio} = \frac{1}{1 - Z_r\left(1 - L_rS_rU_r\right)},$$

we have

$$\frac{df_{max\ ratio}}{dZ_r} = \frac{1 - L_rS_rU_r}{\left[1 - Z_r\left(1 - L_rS_rU_r\right)\right]^2} \begin{cases} < 0 & \text{if } L_rS_rU_r > 1 \\ = 0 & \text{if } L_rS_rU_r = 1 \\ > 0 & \text{if } L_rS_rU_r < 1 \end{cases}.$$

Figure 5.3 shows that $f_{max\ ratio}$ is a decreasing function of $L_rS_rU_r$. When the wind speed is large, the turbulence is large and this disperses the particle farther; when the settling speed is small, the particle's size is small too and so the particles have more time to travel. As the value of Z_r increases layer 2 occupies increasingly more space than layer 1, so the particles have more movement in layer 2, hence $f_{max\ ratio}$ increases. When $Z_r = 0$, $f_{max\ ratio} = 1$, because the atmosphere is dominated by layer one and there is no flow in layer 2. The critical point at $L_rS_rU_r = 1$ gives $\frac{df_{max\ ratio}}{dZ_r} = 0$, $f_{max\ ratio} = 1$, which happens when $\frac{S_2}{S_1} = \frac{L_2U_2}{L2U_1} = \frac{D_{h2}}{D_{h1}}$.

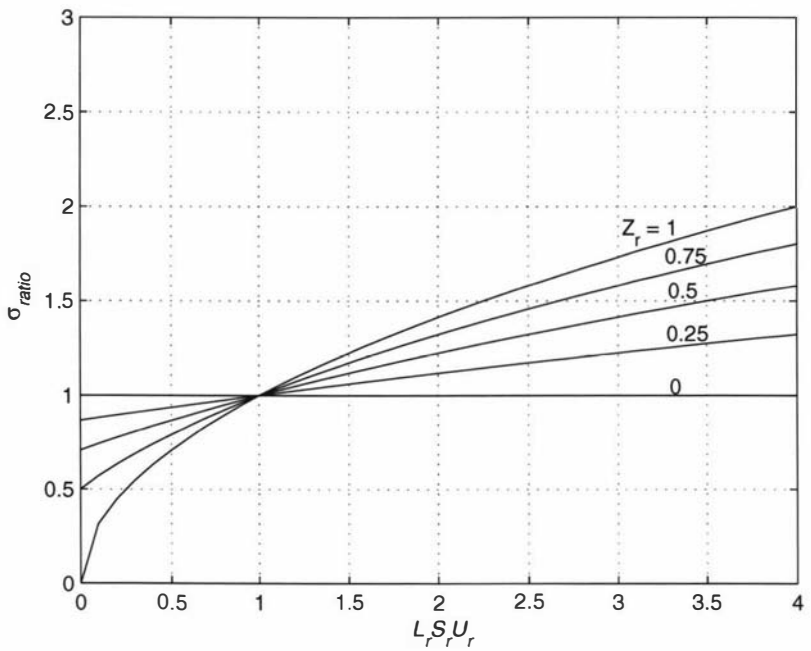

Figure 5.4: σ_{ratio} versus $L_rS_rU_r$ for various values of Z_r.

5.1.5 σ_{ratio} versus $L_rS_rU_r$ for Z_r=0, 0.25, 0.5, 0.75 and 1

This analysis investigates the impact of the parameters on σ_{ratio} when Z_r=0, 0.25, 0.5, 0.75 and 1. From Equation (5.17),

$$\sigma_{ratio} = \sqrt{1 - Z_r\left(1 - L_rS_rU_r\right)},$$

we have

$$\frac{d\sigma_{ratio}}{dZ_r} = \frac{L_rS_rU_r - 1}{2\sqrt{\left[1 - Z_r\left(1 - L_rS_rU_r\right)\right]}} \begin{cases} > 0 & \text{if } L_rS_rU_r > 1 \\ = 0 & \text{if } L_rS_rU_r = 1 \\ < 0 & \text{if } L_rS_rU_r < 1 \end{cases}.$$

Figure 5.4 shows that σ_{ratio} is an increasing function of $L_rS_rU_r$. When the wind speed is large, the turbulence is large and so the spread is wide; when settling speed is small, the particle's size is small too and so the particles have more time to travel. The value of Z_r increases when layer 2 is occupying more space than layer 1, so the particles have more movement in layer 2. When $Z_r = 0$, $\sigma_{ratio} = 1$, because the atmosphere is dominated by layer one and there is no flow in layer 2. The critical point at $L_rS_rU_r = 1$ gives $\frac{d\sigma_{ratio}}{dZ_r} = 0$, $f_{max\ ratio} = 1$, which happens when $\frac{S_2}{S_1} = \frac{L_2U_2}{L2U_1} = \frac{D_{h2}}{D_{h1}}$.

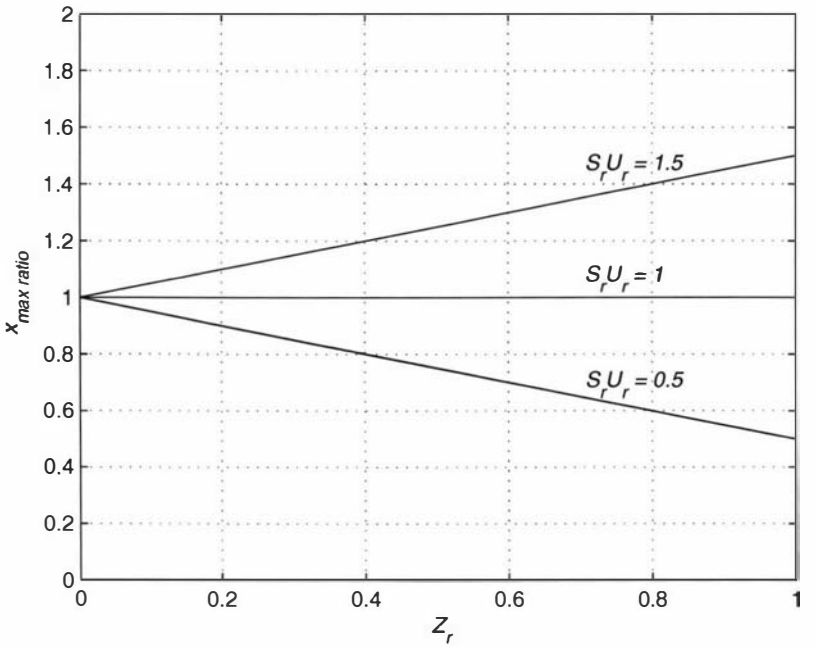

Figure 5.5: $x_{max\ ratio}$ versus Z_r for various values of S_rU_r.

5.1.6 $x_{max\ ratio}$ versus Z_r for S_rU_r=0.5, 1 and 1.5

This analysis investigates the impact of the parameters on $x_{max\ ratio}$ for S_rU_r=0.5, 1 and 1.5 using Equation (5.15):

$$x_{max\ ratio} = 1 - Z_r\,(1 - S_rU_r)\ .$$

Figure 5.5 and Equation (5.15) show that $x_{max\ ratio}$ is an increasing function of Z_r if $S_rU_r > 1$ because the wind speed is larger and settling speed is smaller in layer 2, therefore particles have more time to travel farther. $x_{max\ ratio}$ is uniform when Z_r increases for $S_rU_r = 1$, this happens when $\frac{S_2}{S_1} = \frac{U_2}{U_1}$. $x_{max\ ratio}$ is a decreasing function of Z_r when $0 < S_rU_r < 1$. This is due to the wind speed being smaller and settling speed being larger in layer 2, therefore particles have less time to travel farther.

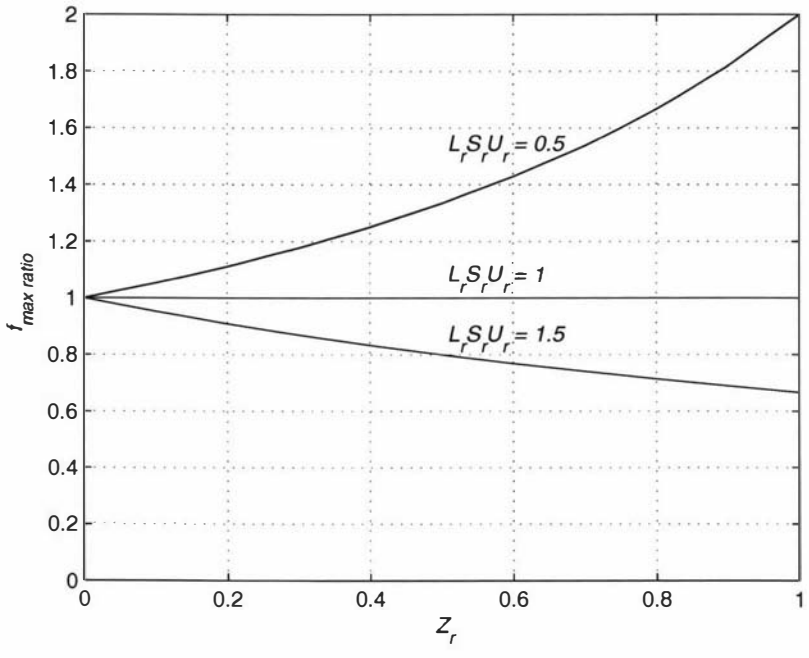

Figure 5.6: $f_{max\ ratio}$ versus Z_r for various values of $L_rS_rU_r$.

5.1.7 $f_{max\ ratio}$ versus Z_r for $L_rS_rU_r$=0.5, 1 and 1.5

This analysis investigates the impact of the parameters on $f_{max\ ratio}$ for $L_rS_rU_r$=0.5, 1 and 1.5. using Equation (5.16):

$$f_{max\ ratio} = \frac{1}{1 - Z_r\left(1 - L_rS_rU_r\right)}.$$

$f_{max\ ratio}$ is an increasing function of Z_r if $0 < L_rS_rU_r < 1$, because the wind speed and turbulence length-scale are smaller and settling speed is larger in layer 2, therefore particles have less time to travel and so the dispersion is small and the spread is smaller. $f_{max\ ratio}$ is a constant function of Z_r when $L_rS_rU_r = 1$, this happens when $\frac{S_2}{S_1} = \frac{L_2U_2}{L_2U_1} = \frac{D_{h2}}{D_{h1}}$. $f_{max\ ratio}$ is a decreasing function of Z_r when $L_rS_rU_r > 1$, this is due to the wind speed and turbulence length-scale are larger and settling speed is smaller in layer 2, therefore particles have more time to travel and so the dispersion is large and spread wider.

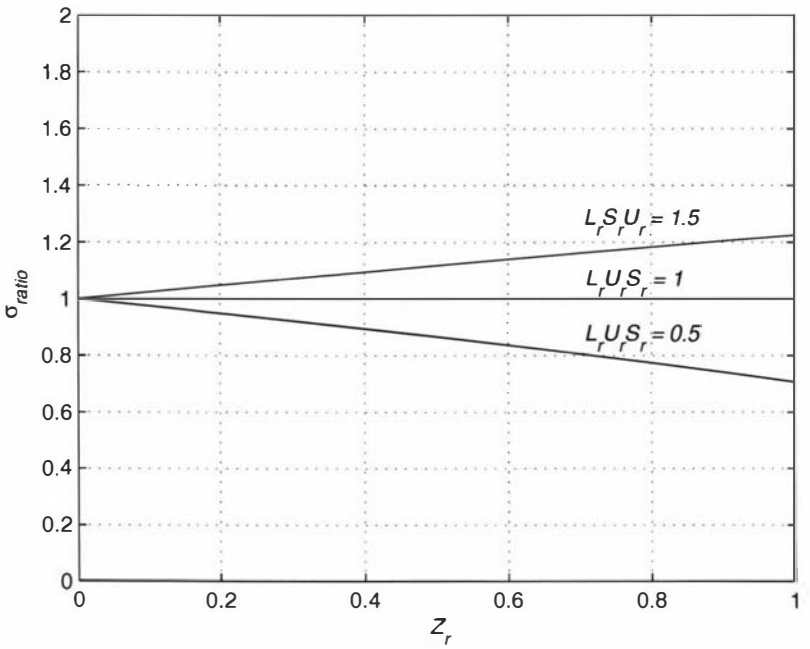

Figure 5.7: σ_{ratio} versus Z_r for various values of $L_rS_rU_r$.

5.1.8 σ_{ratio} versus Z_r for $L_rS_rU_r$=0.5, 1 and 1.5

This analysis investigates the impact of the parameters on σ_{ratio} for $L_rS_rU_r$=0.5, 1 and 1.5 using Equation (5.17):

$$\sigma_{ratio} = \sqrt{1 - Z_r\left(1 - L_rS_rU_r\right)}.$$

σ_{ratio} is an increasing function of Z_r when $L_rS_rU_r > 1$. The wind speed and turbulence length-scale are larger and settling speed is smaller in layer 2, therefore particles have more time to travel and so the dispersion is large and spread wider. σ_{ratio} is a constant function of Z_r when $L_rS_rU_r = 1$, this again happens when $\frac{S_2}{S_1} = \frac{L_2U_2}{L_2U_1} = \frac{D_{h2}}{D_{h1}}$. σ_{ratio} is a decreasing function of Z_r when $0 < L_rS_rU_r < 1$, this is due to the wind speed and turbulence length-scale are smaller and settling speed is larger in layer 2, therefore particles travel have less time to travel and so the dispersion is small and the spread is smaller.

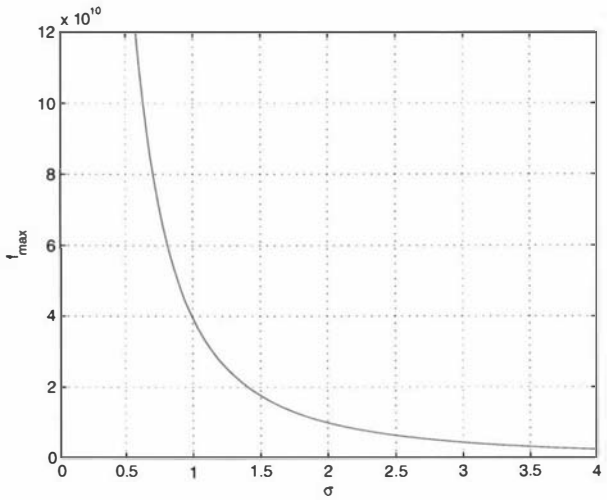

Figure 5.8: f_{max} versus σ.

5.1.9 Deposition versus standard deviation

Equation (5.6) shows the relationship between f_{max} and σ,

$$f_{max} = \frac{Q}{2\pi\sigma^2}$$

for both the uniform and layered atmospheres and also from Equations (5.13) and (5.14), we have

$$f_{max\ ratio} = \frac{1}{\sigma_{ratio}^2}.$$

Figure 5.8 illustrates that the greater the standard deviation of the spread of particles, the thinner the deposit and Figure 5.9 illustrates that the larger the $f_{max\ ratio}$, the smaller the σ_{ratio}.

5.2 Summary

From the equations for f_{max}, σ and x_{max}, only the equation of x_{max} does not contain L, this illustrates the particle is affected by the settling speed of particle, wind speed and its direction. The analyses shows that parameters have more impact in the larger layer. The results also show that particles with higher settling speed fall faster,

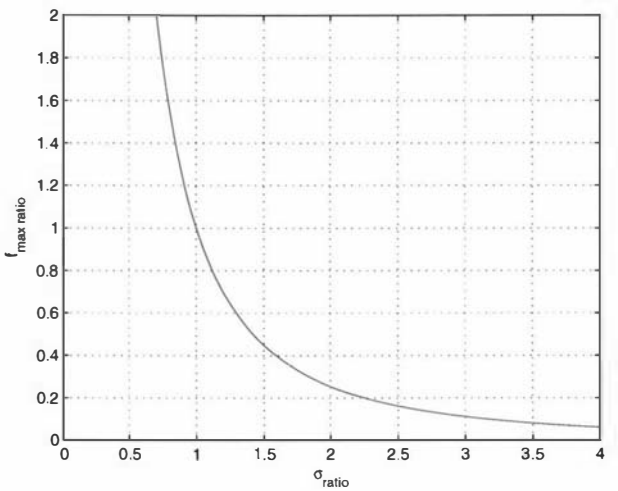

Figure 5.9: $f_{max\ ratio}$ versus σ_{ratio}.

therefore having a shorter time to spread and a thicker deposit (and vice versa). The greater the wind speed, the farther away the particle lands and the spread is wider and hence the deposit is thinner.

We showed that the standard deviation is large with large wind speed, large turbulence length-scale or small settling speed; the deposit is thinner with large wind speed, large turbulence length-scale or small settling speed; the value of x_{max} (i.e. the point where the deposit is maximum) is large (therefore farther from the release point in the x-coordinate) with large wind speed, large turbulence length-scale or small settling speed.

From the results of $x_{max\ ratio}$, $f_{max\ ratio}$ and σ_{ratio}, we see that $x_{max\ ratio}$ and σ_{ratio} give similar results. This is because the larger the value for x_{max} the wider the spread. The results of $f_{max\ ratio}$ are opposite to those of $x_{max\ ratio}$ and σ_{ratio}, because the deposit is thinner because of the wider spread.

Chapter 6

PARAMETER ESTIMATION

go inside the box
turn it inside out

6.1 Introduction

In Chapters 2 and 3 we considered the forward modelling of volcanic ashfall. To do this we needed to know appropriate parameter values. In this chapter, we discuss a method for estimating parameters of volcanic ashfall from data.

The initial aim of this thesis was inverse modelling of ashfall. It would be a great help to volcanologists if information about a volcanic eruption could be extracted from the deposit on the ground [12]. Volcanologists could use the information in forecasting the future risk if a similar scale of volcanic eruption occurs.

Due to lack of data, we switched to forward modelling instead of inverse modelling. Nevertheless, in this chapter we present our attempts at estimating parameters associated with volcanic ashfall. As described in the previous chapters, the distribution patterns of ashfall deposits on the ground are affected by the wind speed, wind direction, particle settling speed, the atmospheric dispersion and the height of release. In Chapters 2 and 3, we showed that the atmospheric concentration of ashfall and the consequent deposit could be determined from these parameters. It is not easy to determine these parameters from the measured output (concentration or deposit).

6.2 Analogy

There was only one published work on inverse modelling of volcanic ashfall found during the study. The work was presented at the International Association of Volcanology

and Chemistry of the Earth's Interior conference in November 2004 in Chile [28], and was implemented by Laura Connor [15] [16] [17] of the Department of Geology at University of South Florida. This approach required intensive computing techniques, it was executed on multiple processors and implemented using a combination of the downhill simplex method and assessing the goodness of fit.

The information which needs to be extracted from the volcanic ashfall pattern includes the dispersion in the horizontal (D_h) and vertical (D_z) directions, the wind speeds (U, V) in (x, y) directions, the settling speed S, the release point (X_0, Y_0) and the release height H. There are eight unknown parameters ($D_h, D_z, U, V, S, X_0, Y_0$ and H) and therefore eight equations are required. We created eight moments for the eight equations. The following subsections show how these moment equations are created and solved using a numerical method, and some alternatives for simplifying the moment equations.

We tried using a variety of numerical methods to determine the parameters. This chapter will report on only one numerical method, which we found to be the best. MATLAB [14] was the tool used for this work. Another advantage of using MATLAB is that it has "ready-made" subroutines for some numerical methods, hence it saves time in writing the codes manually.

6.2.1 Uniform whole space model

We first formulate eight moment equations based on the uniform whole space deposit (2.14):

$$f(x,y) = \frac{Q}{32\pi D_h \sqrt{D_z}}\, e^{\frac{1}{2}\left(\frac{(x-X_0)U}{D_h}+\frac{(y-Y_0)V}{D_h}+\frac{HS}{D_z}\right)-2\alpha\beta}\left[\frac{(2\alpha\beta+1)H+2\alpha^2 S}{\alpha^3}\right]$$

where $\alpha = \sqrt{\frac{1}{4}\left[\frac{(x-X_0)^2}{D_h}+\frac{(y-Y_0)^2}{D_h}+\frac{H^2}{D_z}\right]}$ and $\beta = \sqrt{\frac{1}{4}\left[\frac{U^2}{D_h}+\frac{V^2}{D_h}+\frac{S^2}{D_z}\right]}$.

The moment equations are formulated with respect to the x and y coordinates of the deposit (2.14):

$$x^a y^b - \text{moment} = M_{x^a y^b} = \int_{-\infty}^{\infty} x^a\, dx \int_{-\infty}^{\infty} y^b\, dy\, f(x,y)$$

where a and b are positive integers.

The mass source Q can be calculated from the zeroth moment:

$$x^0y^0 - \text{moment} = M_{x^0y^0} = \int_{-\infty}^{\infty}\int_{-\infty}^{\infty} f(x,y)\,dx\,dy = Q\,.$$

The eight moments are:

$$x - \text{moment} = M_x = \int_{-\infty}^{\infty}\int_{-\infty}^{\infty} xf(x,y)\,dx\,dy$$

$$y - \text{moment} = M_y = \int_{-\infty}^{\infty}\int_{-\infty}^{\infty} yf(x,y)\,dx\,dy$$

$$x^2 - \text{moment} = M_{x^2} = \int_{-\infty}^{\infty}\int_{-\infty}^{\infty} x^2f(x,y)\,dx\,dy$$

$$y^2 - \text{moment} = M_{y^2} = \int_{-\infty}^{\infty}\int_{-\infty}^{\infty} y^2f(x,y)\,dx\,dy$$

$$xy - \text{moment} = M_{xy} = \int_{-\infty}^{\infty}\int_{-\infty}^{\infty} xyf(x,y)\,dx\,dy$$

$$x^3 - \text{moment} = M_{x^3} = \int_{-\infty}^{\infty}\int_{-\infty}^{\infty} x^3f(x,y)\,dx\,dy$$

$$y^3 - \text{moment} = M_{y^3} = \int_{-\infty}^{\infty}\int_{-\infty}^{\infty} y^3f(x,y)\,dx\,dy$$

$$x^2y - \text{moment} = M_{x^2y} = \int_{-\infty}^{\infty}\int_{-\infty}^{\infty} x^2yf(x,y)\,dx\,dy$$

or alternatively

$$xy^2 - \text{moment} = M_{xy^2} = \int_{-\infty}^{\infty}\int_{-\infty}^{\infty} xy^2f(x,y)\,dx\,dy\,.$$

Using Equation (2.14), it is possible to find explicit expressions for these moments. Some examples of the calculated procedure are given in the Appendix A.7. The eight moments are:

$$M_x = Q\left[X_0 + U\left(\frac{H}{S} + \frac{D_z}{S^2}\right)\right] \tag{6.1}$$

$$M_y = Q\left[Y_0 + V\left(\frac{H}{S} + \frac{D_z}{S^2}\right)\right] \tag{6.2}$$

$$M_{x^2} = Q\left[X_0^2 + 2(X_0U + D_h)\left(\frac{H}{S} + \frac{D_z}{S^2}\right) + U^2\left(\frac{H^2}{S^2} + \frac{4HD_z}{S^3} + \frac{6D_z^2}{S^4}\right)\right] \tag{6.3}$$

$$M_{y^2} = Q\left[Y_0^2 + 2(Y_0V + D_h)\left(\frac{H}{S} + \frac{D_z}{S^2}\right) + V^2\left(\frac{H^2}{S^2} + \frac{4HD_z}{S^3} + \frac{6D_z^2}{S^4}\right)\right] \tag{6.4}$$

$$M_{xy} = Q\left[X_0Y_0 + (VX_0 + UY_0)\left(\frac{H}{S} + \frac{D_z}{S^2}\right) + UV\left(\frac{H^2}{S^2} + \frac{4HD_z}{S^3} + \frac{6D_z^2}{S^4}\right)\right] \tag{6.5}$$

$$M_{x^3} = Q\left[X_0^3 + 3(X_0^2U + 2X_0D_h)\left(\frac{H}{S} + \frac{D_z}{S^2}\right) + 3(X_0U^2 + 2UD_h)\left(\frac{H^2}{S^2} + \frac{4HD_z}{S^3} + \frac{6D_z^2}{S^4}\right) + U^3\left(\frac{H^3}{S^3} + \frac{9H^2D_z}{S^4} + \frac{36HD_z^2}{S^5} + \frac{60D_z^3}{S^6}\right)\right] \tag{6.6}$$

$$M_{y^3} = Q\left[Y_0^3 + 3(Y_0^2V + 2YD_h)\left(\frac{H}{S} + \frac{D_z}{S^2}\right) + 3(Y_0V^2 + 2VD_h)\left(\frac{H^2}{S^2} + \frac{4HD_z}{S^3} + \frac{6D_z^2}{S^4}\right) + V^3\left(\frac{H^3}{S^3} + \frac{9H^2D_z}{S^4} + \frac{36HD_z^2}{S^5} + \frac{60D_z^3}{S^6}\right)\right] \tag{6.7}$$

$$M_{x^2y} = Q\left[X_0^2Y_0 + (X_0^2V + 2X_0Y_0U + 2Y_0D_h)\left(\frac{H}{S} + \frac{D_z}{S^2}\right)\right.$$
$$+(2X_0UV + Y_0U^2 + 2VD_h)\left(\frac{H^2}{S^2} + \frac{4HD_z}{S^3} + \frac{6D_z^2}{S^4}\right)$$
$$\left.+U^2V\left(\frac{H^3}{S^3} + \frac{9H^2D_z}{S^4} + \frac{36HD_z^2}{S^5} + \frac{60D_z^3}{S^6}\right)\right] \tag{6.8}$$

or alternatively

$$M_{xy^2} = Q\left[X_0Y_0^2 + (Y_0^2U + 2X_0Y_0V + 2X_0D_h)(\frac{H}{S} + \frac{D_z}{S^2})\right.$$
$$+(2Y_0UV + X_0V^2 + 2UD_h)(\frac{H^2}{S^2} + \frac{4HD_z}{S^3} + \frac{6D_z^2}{S^4})$$
$$\left.+(UV^2)(\frac{H^3}{S^3} + \frac{9H^2D_z}{S^4} + \frac{36HD_z^2}{S^5} + \frac{60D_z^3}{S^6})\right]. \tag{6.9}$$

(See Appendix A.7.1 for the working of a moment solution.)

The eight moment equations show an interesting sequential pattern. Unfortunately, the moment Equations (6.1) to (6.8) are nonlinear and it is not possible to determine the parameters analytically. Some numerical methods have been tried to solve the eight equations. Methods such as Broyden's, Newton's and Steepest Descent methods [20] [33] require a first guess for each parameter. However, none of these methods gave accurate results if the guess was not close to the actual solution. Zheng *et al.* [56] state that guessing a solution is not practical and is also time consuming; they suggest that a practical way to tackle this kind of problem is to restrict the likely range of the solution for each parameter.

We used Newton's method to solve the moment equations with the suggestion given by Zheng *et al.* using the 'fsolve' command in MATLAB. It is found that this is a better approach than the other methods we experimented with.

We substitute the data from Table 1.1 into the moment equations to obtain the eight moments and then tried using the values of the eight moments to find the eight parameters.

We input the likely ranges of solutions for all parameters in the program instead of guessing the solutions. The program goes through the input ranges and picks up the solutions for the system. From Table 6.1, for example, the input range, 0:10:20 means the start point starts from 0 to 20 with interval of 10; 0:10 means the range is from 0 to 10 with interval of 1. Hence from Table 6.1, there are 8^3 permutations for starting point in Input range 1 and 8^2 permutations for Input range 2. Table 6.1 shows that the program found two sets of solutions from Input range 1 but one set from Input range 2. Thus if the range is too wide, we may obtain more than one solution. But,

Table 6.1: Results by Newton's method.

Parameter	actual solution	Input range 1	Result 1		Input range 2	Result 2
X_0	0	0:1:2	0	0	0:1	0
Y_0	0	0:1:2	0	0	0:1	0
H	7500	0:7500:150000	7500	7500	0:7500	7500
U	10	0:10:20	10	20	0:10	10
V	0	0:1:2	0	0	0:1	0
S	1	0:1:2	1	2	0:1	1
D_h	800	0:800:1600	800	1600	0:800	800
D_z	0	0:1:2	0	0	0:1	0

if the range is not close to the actual solution, we obtain no solution; if the range is small and close to the actual solution, we obtain the desired solution. This shows a problem: that if we have no idea about the actual solutions and the program gives more than one set of solution, we do not know which solution to pick. Also, if the input range is wide, the program running time is long too.

Interestingly, we also see that there is a common ratio in the two sets of U, S and D_h from result 1. The U, S and D_h in the second column are twice as large as the first column ones. This is because D_h is directly proportional to U ($D_h = U\,L$) and so if the wind is two times higher, the dispersion will be two times higher as well. When the particle's settling speed is double, the value of U needs also to be double in order to land on the same point. So if any of U, S and D_h increases, the others will increase proportionally in order to obtain the same output.

6.2.2 Uniform half space model

We formulate moment equations using the uniform half space deposit (2.15):

$$\begin{aligned} f(x,y) &= \int_0^\infty \left\{ -\frac{SQ}{16D_h t\sqrt{\pi^3 D_z}} e^{-\frac{(x-X_0-Ut)^2}{4D_h t} - \frac{(y-Y_0-Vt)^2}{4D_h t}} \right. \\ &\quad \left. \times \int_0^t \left[\left(\frac{SH}{D_z} + 2 \right) \frac{1}{\tau^{\frac{3}{2}}} - \frac{H^2}{D_z \tau^{\frac{5}{2}}} \right] e^{-\frac{(-H+S\tau)^2}{4D_z \tau}} d\tau \right\} dt. \end{aligned}$$

As in the uniform whole space model, the mass source Q can be calculated from the zeroth moment:

$$x^0y^0 - \text{moment} = M_{x^0y^0} = \int_{-\infty}^{\infty}\int_{-\infty}^{\infty} f(x,y)\,dx\,dy = Q\,.$$

Here are five of the moment equations:

$$M_x = Q\left[X_0 + U\left(\frac{H}{S} + \frac{D_z}{S^2}\right)\right] \tag{6.10}$$

$$M_y = Q\left[Y_0 + V\left(\frac{H}{S} + \frac{D_z}{S^2}\right)\right] \tag{6.11}$$

$$M_{x^2} = Q\left[X_0^2 + 2(X_0U + D_h)\left(\frac{H}{S} + \frac{D_z}{S^2}\right) + U^2\left(\frac{H^2}{S^2} + \frac{4HD_z}{S^3} + \frac{4D_z^2}{S^4}\right)\right] \tag{6.12}$$

$$M_{y^2} = Q\left[Y_0^2 + 2(Y_0V + D_h)\left(\frac{H}{S} + \frac{D_z}{S^2}\right) + V^2\left(\frac{H^2}{S^2} + \frac{4HD_z}{S^3} + \frac{4D_z^2}{S^4}\right)\right] \tag{6.13}$$

$$M_{xy} = Q\left[X_0Y_0 + (X_0V + Y_0U)\left(\frac{H}{S} + \frac{D_z}{S^2}\right) + UV\left(\frac{H^2}{S^2} + \frac{4HD_z}{S^3} + \frac{4D_z^2}{S^4}\right)\right]. \tag{6.14}$$

(See Appendix A.7.1 for the working of a moment solution.)

Again, we face the same difficulty as the uniform whole space moments. It appears that Equations (6.1) and (6.2) of the uniform whole space model are same as Equations (6.10) and (6.11). It is also found that for $D_z = 0$, the moment equations for both uniform whole and half space models are the same.

6.2.3 Simplification 1

In order to simplify the moment equations (the uniform whole space model), we group some of the terms of the moments into a single variable.

$$M_x = Q\left[X_0 + UA\right] \tag{6.15}$$

$$M_y = Q\left[Y_0 + VA\right] \tag{6.16}$$

$$M_{x^2} = Q\left[X_0^2 + 2(X_0U + D_h)A + U^2B\right] \tag{6.17}$$

$$M_{y^2} = Q\left[Y_0^2 + 2(Y_0V + D_h)A + V^2B\right] \tag{6.18}$$

$$M_{xy} = Q\left[X_0Y_0 + (VX_0 + UY_0)A + UVB\right] \tag{6.19}$$

$$M_{x^3} = Q\left[X_0^3 + 3(X_0^2U + 2X_0D_h)A + 3(X_0U^2 + 2UD_h)B + U^3C\right] \tag{6.20}$$

$$M_{y^3} = Q\left[Y_0^3 + 3(Y_0^2V + 2YD_h)A + 3(Y_0V^2 + 2VD_h)B + V^3C\right] \tag{6.21}$$

$$\begin{aligned} M_{x^2y} = Q\big[&X_0^2Y_0 + (X_0^2V + 2X_0Y_0U + 2Y_0D_h)A \\ &+(2X_0UV + Y_0U^2 + 2VD_h)B + U^2VC\big] \end{aligned} \tag{6.22}$$

where $A = \frac{H}{S} + \frac{D_z}{S^2}$, $B = \frac{H^2}{S^2} + \frac{4HD_z}{S^3} + \frac{6D_z^2}{S^4}$ and $C = \frac{H^3}{S^3} + \frac{9H^2D_z}{S^4} + \frac{36HD_z^2}{S^5} + \frac{60D_z^3}{S^6}$.

However, we are not able to solve for the parameters explicitly. With the numerical method, again, the initial guess is needed to be close to the actual solutions in order to obtain the desired solutions.

6.2.4 Simplification 2

We further simplify the moment equations (the uniform whole space model) and write the parameters X_0, Y_0, H and D_h in term of U, V, S and D_z explicitly. The parameters X_0, Y_0, H and D_h are obtained from the x, y, x^2 and xy moment equations with $Q = 1$.

$$X_0 = M_x - U\left(\frac{H}{S} + \frac{D_z}{S^2}\right)$$

$$Y_0 = M_y - V\left(\frac{H}{S} + \frac{D_z}{S^2}\right)$$

$$H = \frac{S^3 M_{xy}}{2D_z UV} - \frac{S^3 M_x M_y}{2D_z UV} - \frac{5D_z}{2S}$$

$$D_h = \frac{M_{x^2} - X_0^2 - U^2\left(\frac{H^2}{S^2} + \frac{4HD_z}{S^3} + \frac{6D_z^2}{S^4}\right)}{2\left(\frac{H}{S} + \frac{D_z}{S^2}\right)} - X_0 U$$

or

$$D_h = \frac{M_{y^2} - Y_0^2 - V^2\left(\frac{H^2}{S^2} + \frac{4HD_z}{S^3} + \frac{6D_z^2}{S^4}\right)}{2\left(\frac{H}{S} + \frac{D_z}{S^2}\right)} - Y_0 V\,.$$

We then substitute the four parameters into the other four moment equations. This reduces the number of moment equations to four. However, we are unable to solve explicitly for the other four parameters and we encounter the same difficulty with the numerical method; the initial guess still needs to be close to the actual solution to obtain the desired solution.

6.3 Discussion

We tried finding the parameter values with the "ready-made" subroutines based on some well-known numerical methods provided by MATLAB. The attempts were unsuccessful. My supervisor, Robert said, "It is like pouring a basket of ash onto the ground and picking it up by hand." It is hard to collect all the ash on the ground, very likely we will collect less than we threw. We may collect more, which mean we may include some other tiny particles on the ground together with the ash. In order to retrieve the whole basket of ash on the ground we will need substantial time.

The desired solutions can be obtained provided that the initial guess is close to the actual solutions. The suggestion from Zheng *et al.* [56] is helpful, but it takes

substantial computing time if the system has many parameters or the range set for each parameter is wide.

It appears that the system we created using moments is ill-posed and it is difficult to solve. The inverse modelling of volcanic ashfall requires further investigation. The work done by Laura Connor [16] is sophisticated and used intensive computing techniques. Hence, further investigations may require substantial work and time. Unfortunately, we are unable to attempt this within the given time frame of the study.

A plan for future work is to investigate and develop a model to solve the eight parameters $D_h, D_z, U, V, S, X_0, Y_0$ and H. More importantly, real data from ashfall deposit depths and particle size distributions are needed to check the work.

Chapter 7

DISCUSSION AND CONCLUSIONS

all journeys will come to their destinations
but do not give them a full stop
share the experiences and pass them on
we came to the world empty-handed
we will leave the world empty-handed too

This aim of this thesis was to develop analytical models for modelling volcanic ashfall. We showed that, subject to some assumptions, it is possible to develop useful analytical models of ashfall. We presented such analytical models and used them to calculate the concentration of volcanic ashfall in the atmosphere and deposition of ash on the ground.

The basic assumption which we used in our models was that the atmosphere could be viewed either as being uniform or consisting of a few horizontal layers. The reason for dividing the atmosphere into horizontal layers is to present a more realistic transport model for the atmosphere; as the physical conditions, such as wind speed and dispersion rate, are not constant throughout.

7.1 Summary

In summary, we considered the following basic models:

- instantaneous release in whole space uniform atmosphere;

- instantaneous release in half-space uniform atmosphere;

- continuous release in whole space uniform atmosphere;

- continuous release in half-space uniform atmosphere;

- instantaneous release in half-space layered atmosphere;

- continuous release in half-space layered atmosphere.

The atmosphere modelled as a half-space ($0 \leq z < \infty$) is more realistic than that as a whole space ($-\infty < z < \infty$), the half-space model takes into account the zero dispersive flux on the ground when $z = 0$ (in the half-space model the ground is defined as $z = 0$). Nevertheless, the results from the whole space model, which can be derived exactly, are very close to those of the half-space model with instantaneous release in uniform atmosphere, for which we can only find an approximate analytical solution.

Except for the continuous release model at steady state in a layered atmosphere and the instantaneous release model in a non-steady state in a uniform half-space atmosphere, all models were developed analytically. The advection-dispersion equation has been used by many volcanologists to model volcanic ashfall, however, most existing models such as those of Ashfall [25] and Hazmap [7] were solved numerically. In particular, in the modelling of instantaneous release in a layered atmosphere, we have shown that our model can be written in an explicit form with the same assumptions as the Ashfall and Hazmap models.

7.2 Analyses

Having developed our models we performed a number of simulations. The motivation was to investigate the possible cause of different deposit contours. The experiments we performed were:

- deposition from different shapes of source with instantaneous release in a uniform atmosphere (this was suggested by Prof. Chuck Connor of the Department of Geology at the University of South Florida);

- deposition from more than one point source with instantaneous release in layered atmosphere;

- understanding the impact of the parameters in the advection-dispersion equation.

7.3 Conclusions

In conclusion, we observed that the results from both the half-space and whole space models were very close even though the whole space does not give zero dispersive flux on the ground. In addition, the resulting ash deposits are also very close regardless of the shape of the release source if the release height is large or the release sources

are small. This suggests that inverse modelling will be very difficult.

The model with instantaneous release and no vertical dispersion in a layered atmosphere captures the changes in physical properties of the atmosphere during ashfall and demonstrates patterns of ashfall and deposit explicitly and efficiently compared with existing models, i.e. Ashfall [25] and Hazmap [7].

Compared to the existing models mentioned in Chapter 1, our models are highly simplified, but they capture the essential physics of volcanic eruptions. Our models can take into account: increases in settling speed during ashfall, which ASHFALL [26] was not able to; changes in wind pattern, which Connor *et al.* [15] do not consider; and expected changes in dispersion, which HAZMAP [7] does not consider.

In the experiments illustrated in Chapter 4 we investigate the effects of different ash release geometries on the resulting deposits. Compared to the deposit pattern for a point source release the only significant change is produced from either a tall vertical column or a horizontal release geometry which is close to the ground compared to its lateral dimension. If the release height is large compared to the lateral extent of the release, then the deposit pattern is very close to that of a point source released at the same height. Ashfall deposit variation is only caused by very large lateral spread of the release shape closer to the ground.

The analysis of Chapter 5 shows that in a two layered atmosphere, the parameters in the larger layer have a bigger effect on the deposition than those in the smaller layer.

7.4 Consideration for Publication as Papers

There are three chapters in this thesis which we are considering for publication as papers after the completion of my PhD. They are the uniform atmosphere models (Chapter 2), layered atmosphere models (Chapter 3) and the analysis of deposits (Chapter 4).

In Chapter 2, we give an introduction of the advection-dispersion equation and how it can be used to describe transport of particles by wind and scattering by dispersion. We use it to develop simple models and give analytical solutions. The simple models show that they are able to describe uniform or homogeneous atmosphere explicitly.

The layered atmosphere models are important as the models are more realistic as they take into consideration that the wind and turbulence profiles may vary with elevation. In particular, the model for an instantaneous release in the three-dimensional atmosphere has analytical solutions. The advantage of analytical solutions is that they allow the effect of parameter variation to be explored more readily.

The analysis of deposits was motivated by Prof. Chuck Connor (see acknowledgment) at the conference [28] in Chile. He was interested in the deposits produced by different source shapes and asked if this could be investigated. This investigation led us to

want to find out the cause of different contours of deposition on the ground. This investigation will help to obtain information about the atmospheric conditions and release parameters during eruption. This information will help volcanologists and geologists to make hazard maps for future eruptions. The patterns of deposition will help to give approximate values for data such as the release height, eruption column height, wind speed and direction and eruption duration.

During the course of this study, we also published a refereed conference paper [39].

7.5 Future Work

The model for ashfall with instantaneous release in a layered atmosphere can be further extended to consider non-isotropic horizontal dispersions ($D_x \neq D_y$). Another area to investigate is the vertical dispersion D_z as here we assumed D_z was zero for modelling instantaneous release in a layered atmosphere. Also, variation in particle size distributions would be useful.

Last, but not least, future research may consider the interesting problem of inverse modelling. Due to time constraints, we were unable to carry on a deep investigation of inverse modelling of ashfall. It is an area which needs to be addressed as it would help volcanologists reconstruct information about volcanic eruptions. However, inverse modelling of volcanic ashfall is difficult and requires sophisticated computational tools. To date inverse modelling has only been investigated by Laura Connor of the Department of Geology at the University of South Florida [16].

Bibliography

[1] P. Armienti, G. Macedonio and M. Pareschi. *A numerical model for simulation of tephra transport and deposition: application to May 18, 1980 Mount St. Helens eruption.* Journal of Geophysical Research (B6) **93** (1988), 6463–6476.

[2] J. Atmadja and A. C. Bagtzoglou. *State of the art report on mathematical methods for groundwater pollution source identification.* Environmental Forensics **2** (2001) 205–214.

[3] P. G. Baines and R. S. J. Sparks. *Dynamics of giant volcanic ash clouds from supervolcanic eruptions.* Geophysical Research Letters **32** (2005) L24808.

[4] S. Barsotti, A. Neri and J. Scire. *Assessing volcanic ash hazard by using the Calpuff system.* Retrieved 14 October 2005, from http://www.ofcm.gov/ICVAAS/presentations/s3-03barsotti.ppt.

[5] C. Bonadonna, G. G. J. Ernst and R. S. J. Sparks. *Thickness variations and volume estimates of tephra fall deposits: the importance of particle Reynolds number.* Journal of Volcanology and Geothermal Research **81** (1998) 173–187.

[6] C. Bonadonna, G. C. Mayberry, E. S. Calder, R. S. J. Sparks, C. Choux, P. Jackson, A. M. Lejeune, S. C. Loughlin, G. E. Norton, W. I. Rose, G. Ryan and S. R. Young. *Tephra fallout in the eruption of Soufriere Hills Volcano, Montserrat.* The Eruption of Soufriere Hill Volcano, Montserrat, from 1995 to 1999 (T. H. Druitt and B. P. Kokelaar, eds). The Geological Society of London: London, 2002, 483–516.

[7] C. Bonadonna, G. Macedonio and R. S. J. Sparks. *Numerical modelling of tephra fallout associated with dome collapses and Vulcanian explosions: application to hazard assessment on Montserrat.* The Eruption of Soufriere Hill Volcano, Montserrat, from 1995 to 1999 (T. H. Druitt and B. P. Kokelaar, eds). The Geological Society of London: London, 2002, 517–537.

[8] F. Bowman. Introduction to Bessel Functions. Dover Publications: New York, 1958.

[9] P. Briole and J. Le Mouel. *Space Volcano Observatory Report from Institut de Physique du Globe de Paris, 1 December 1998.* Retrieved 14 October 2005, from http://pcsgen4.ipgp.jussieu.fr/pb/pro_esa99_svo9.pdf

[10] Ewen Cameron, Bruce Hayward and Graeme Murdoch, A Field Guide to Auckland, Godwit Publishing Ltd, Auckland, 1997.

[11] S. Carey and R. S. J. Sparks. *Quantitative model of the fallout and dispersal of tephra from volcanic eruption columns.* Bulletin of Volcanology **48** (1986) 109–125.

[12] S. N. Carey. *Modelling of tephra fallout from explosive eruption.* Monitoring and Mitigation of Volcano Hazards (R. Scarpa and R. I. Tilling, eds). Springer: Berlin, 1996, 429–461.

[13] T. J. Casadevall. *The 1989-1990 eruption of Redoubt Volcano, Alaska: impacts on aircraft operations.* Journal of Volcanology and Geothermal Research **62** (1994) 301–316.

[14] S. C. Chapra. Applied Numerical Methods with MATLAB for Engineering and Scientists. McGraw-Hill Higher Education: Boston, 2005.

[15] C. B. Connor, B. E. Hill, B. Winfrey, N. M. Franklin, and P. C. La Femina. *Estimation of volcanic hazards from tephra fallout.* Natural Hazards Review (1) **2** (2001) 33–42.

[16] L. Connor and C. B. Connor. *Inversion is the key to dispersion: understanding eruption dynamics by inverting tephra fallout.* Retrieved 14 October 2005, from http://www.cas.usf.edu/~cconnor/vg@usf/tephra_files/Connor-Inversion.pdf.

[17] C. B. Connor and L. Connor. *Tephra dispersion modelling in parallel, an open-source computer code for probabilistic volcanic hazard assessment.* Retrieved 14 October 2005, from http://www.cas.usf.edu/~cconnor/parallel/tephra/tephra.html.

[18] G. J. Cox. Fountains of Fire : The Story of Auckland's Volcanoes. HarperCollins: Auckland, 2000.

[19] S. Cronin. *Under the volcanoes.* Retrieved 14 October 2005, from http://masseynews.massey.ac.nz/2004/research-mag/pdf/Research-Vulcanology.pdf.

[20] R. L. Burden and J. D. Faires. Numerical Analysis. Dover Publications: New York, 2001.

[21] J. Fierstein and M. Nathenson. *Another look at the calculation of fallout tephra volume.* Bulletin of Volcanology **54** (1989) 156–167.

[22] L. Glaze and S. Self. *Ashfall dispersal from the 16 September 1986, eruption of Lascar, Chile, calculated by a turbulent diffusion model.* Geophysical Research Letters **18** (1991) 1237–1240.

[23] B. E. Hill, C. B. Connor, M. S. Jarzemba, P. C. La Femina, M. Navarro, and W. Strauch. *1995 eruptions of Cerro Negro volcano, Nicaragua, and risk assessment for future eruptions.* Geological Society of America Bulletin (10) **100** (1998) 1231–1241.

[24] R. E. Holasek, A. W. Woods and S. Self. *Experiments on gas-ash separation processes in volcanic umbrella plumes.* Journal of Volcanology and Geothermal Research **70** (1996) 169–181.

[25] A. W. Hurst. *ASHFALL - a computer program for estimating volcanic ash fallout. Report and user guide.* Institute of Geological & Nuclear Sciences Science Report 94/23, 1994.

[26] A. W. Hurst and R. Turner. *Performance of the program ASHFALL for forecasting ashfall during the 1995 and 1996 eruptions of Ruapehu volcano.* Journal of Volcanology and Geothermal Research **76** (1997) 163–171.

[27] A. W. Hurst and R. Turner. *Performance of the program ASHFALL for forecasting ashfall during the 1995 and 1996 eruptions of Ruapehu volcano.* New Zealand Journal of Geology and Geophysics **42** (1999) 615–622.

[28] International Association of Volcanology and Chemistry of the Earths Interior 2004 (IAVCEI) General Assembly meeting, 14-19 Nov 2004, Pucon, Chile.

[29] J. Kevorkian. Partial Differential Equations. Wadsworth & Brooks/Cole: California, 1990.

[30] T. Koyaguchi. *Volume estimation of tephra-fall deposits from the June 15, 1991, eruption of Mount Pinatubo by theoretical and geological methods.* Fire and Mud: Eruptions and Lahars of Mount Pinatubo, Philippines (C. G. Newhall and R. S. Punongbayan, eds), University of Wash. Press: Seattle, 1996, 583–600.

[31] E. Kreyszig. Introductory Mathematical Statistics. John Wiley & Sons: New York, 1970.

[32] G. Laske. *Why are volcanoes different?.* Retrieved 16 March 2006, from http://quakeinfo.ucsd.edu/~ gabi/erth15/Lecture10.html.

[33] G. Lindfield and J. Penny. Numerical Methods Using MATLAB. Ellis Horwood: New York, 1995.

[34] J. D. Logan. Applied Partial Differential Equations. Springer: New York, 1998.

[35] G. Macedonio, M. T. Pareschi and R. Santacroce. *A numerical simulation of plinian fall phase of 79 A.D. eruption of Vesuvius.* Journal of Volcanology and Geothermal Research (B12) **93** (1988) 14817–14827.

[36] G. Macedonio, M. T. Pareschi and R. Santacroce. *Renewal of explosive activity at Vesuvius: model for the expected tephra fallout.* Journal of Volcanology and Geothermal Research **40** (1990) 327–342.

[37] A. G. Mackie, Boundary Value Problems. Oliver & Boyd Ltd: London, 1965.

[38] R. McKibbin. *Discovering the source of current-borne particles from their deposition pattern.* International Symposium of the Kanazawa University 21st-century COE Program - Environmental Monitoring and Prediction of Long- and Short-Term Dynamics of Pan-Japan Sea Area: Construction of Monitoring Network and Assessment of Human Effects. Kanazawa University, Japan (2003) 191-196.

[39] R. McKibbin, L. L. Lim, T.A. Smith and W.L. Sweatman. *A model for dispersal of eruption ejecta.* Proceedings of the World Geothermal Conference 2005, Antalya, Turkey, 24-29 April 2005 (R. D. Horne and E. Okandan, eds). International Geothermal Association (2005) ISBN 975-98332-0-4 (CD).

[40] P. M. Morse and H. Feshbach. Methods of Theoretical Physics, Part 1. McGraw-Hall: New York, 1953.

[41] P. M. Morse and H. Feshbach. Methods of Theoretical Physics, Part 2. McGraw-Hall: New York, 1953.

[42] New Zealand Official Yearbook 2000.

[43] R. H. Perry, D. W. Green and J. O. Maloney. Perry's Chemical Engineers' Handbook. McGraw-Hill: New York, 1997.

[44] L. Rade and B. Westergren. Mathematics Handbook for Science and Engineering. Springer: London, 1999.

[45] T. Simkin and L. Siebert. Volcanoes of the World. Geoscience Press: Arizona, 1994.

[46] R. S. J. Sparks, M. I. Bursik, S. N. Carey, J. S. Gilbert, L. S. Glaze, H. Sigurdsson and A. W. Woods. Volcanic Plumes, Wiley: New York, 1997.

[47] R. S. J. Sparks. *Forecasting volcanic eruptions.* Earth and Planetary Science Letters **210** (2003) 1–15.

[48] G. Stephenson. Partial Differential Equations for Scientists and Engineers. Imperial College Press: London, 1996.

[49] T. Suzuki. *A theoretical model for dispersion of Tephra.* Arc Volcanism: Physics and Tectonics (D. Shimozuru and I. Yokoyama, eds). Terra Scientific Publishing: Tokyo, 1983, 95–113.

[50] W. L. Sweatman and P. C. Chatwin. *Dosages from instantaneous releases of dense gases in wind tunnels and into a neutrally stable atmosphere.* Boundary-Layer Meteorology **77** (1996) 211–231.

[51] R. I. Tilling, L. Topinka and D. Swanson. Eruptions of Mount St. Helens: Past, Present, and Future, U.S. Government Printing Office, Washington, D.C., 1990.

[52] R. Turner and T. Hurst. *Factors influencing volcanic ash dispersal from the 1995 and 1996 eruptions of Mount Ruapehu, New Zealand.* Journal of Applied Meteorology **40** (2001) 56–69.

[53] G. P. L. Walker G. P. L. *The Taupo Pumice: Product of the most powerful known ultraplinian eruption?* Journal of Volcanology and Geothermal Research **8** (1980) 69–94.

[54] Kathie Watson. *Types of volcanic eruptions.* Retrieved 31 October 2005, from http://pubs.usgs.gov/gip/volc/eruptions.html.

[55] E. W. Weisstein. *Helmholtz equation.* Retrieved 14 October 2005, from http://scienceworld.wolfram.com/physics/HelmholtzEquation.html.

[56] C. Zheng and G. D. Bennett. Applied Contaminant Transport Modelling. Wiley-Interscience: New York, 2002.

[57] C. Zoppou and J. H. Knight. *Analytical solution of a spatially variable coefficient advection diffusion equation in up to three dimensions.* Applied Mathematical Modelling **23** (1999) 667–685.

Appendix A

SOME WORKINGS

recording the history is not to live in the past
reading the history is to understand the difference
acknowledging the history is a token of sensitiveness

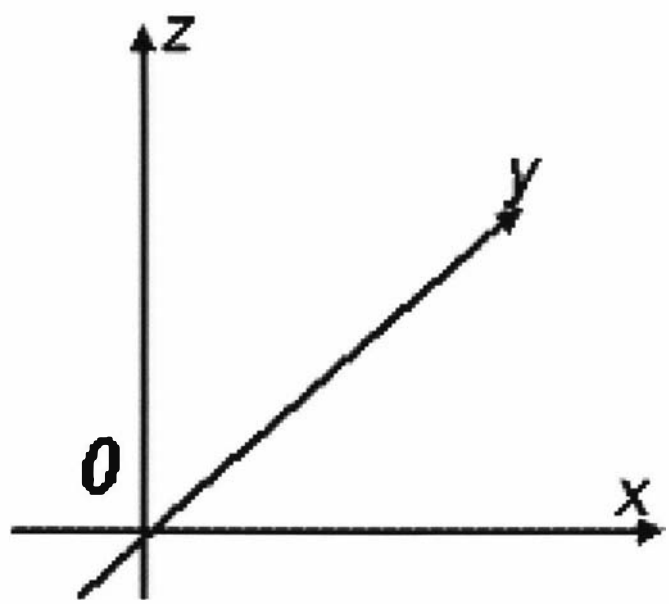

Figure A.1: Three dimensional space

A.1 Concentration for Instantaneous Release in Uniform Whole Space

A.1.1 Three-dimensional model (Section 2.3.3)

The governing equation is

$$\frac{\partial c}{\partial t} + U\frac{\partial c}{\partial x} + V\frac{\partial c}{\partial y} - S\frac{\partial c}{\partial z} - D_h\frac{\partial^2 c}{\partial x^2} - D_h\frac{\partial^2 c}{\partial y^2} - D_z\frac{\partial^2 c}{\partial z^2}$$
$$= Q\delta(t)\delta(x - X_0)\delta(y - Y_0)\delta(z - H)$$

with initial condition: $c = 0$ when $t = 0$ for $(x, y, z) \neq (X_0, Y_0, H)$ and boundary conditions: $c \to 0$ as $x \to \pm\infty$, $y \to \pm\infty$ or $z \to \pm\infty$.

By applying successive Fourier and Laplace transforms, we obtain

$\mathfrak{L}_t$: $c(x, y, z, t) \to \overline{c}(x, y, z, s)$

$$s\overline{c} - Q\delta(x - X_0)\delta(y - Y_0)\delta(z - H) + U\frac{\partial \overline{c}}{\partial x} + V\frac{\partial \overline{c}}{\partial y} - S\frac{\partial \overline{c}}{\partial z} = D_h\frac{\partial^2 \overline{c}}{\partial x^2} + D_h\frac{\partial^2 \overline{c}}{\partial y^2} + D_z\frac{\partial^2 \overline{c}}{\partial z^2}$$

$\mathfrak{F}_x$: $\overline{c}(x, y, z, s) \to \widehat{\overline{c}}(w, y, z, s)$

$$s\widehat{\overline{c}} - Qe^{-iXw}\delta(y - Y_0)\delta(z - H) + iwU\widehat{\overline{c}} + V\frac{\partial \widehat{\overline{c}}}{\partial y} - S\frac{\partial \widehat{\overline{c}}}{\partial z} = -w^2 D_h\widehat{\overline{c}} + D_h\frac{\partial^2 \widehat{\overline{c}}}{\partial y^2} + D_z\frac{\partial^2 \widehat{\overline{c}}}{\partial z^2}$$

$\mathfrak{F}_y$: $\widehat{\overline{c}}(w, y, z, s) \to \tilde{\widehat{\overline{c}}}(w, p, z, s)$

$$s\tilde{\widehat{\overline{c}}} - Qe^{-iXw-iYp}\delta(z - H) + iwU\tilde{\widehat{\overline{c}}} + ipV\tilde{\widehat{\overline{c}}} - S\frac{\partial \tilde{\widehat{\overline{c}}}}{\partial z} = -w^2 D_h\widehat{\overline{c}} - p^2 D_h\tilde{\widehat{\overline{c}}} + D_z\frac{\partial^2 \tilde{\widehat{\overline{c}}}}{\partial z^2}$$

$\mathfrak{F}_z$: $\tilde{\widehat{\overline{c}}}(w, p, z, s) \to \overset{\vee}{\tilde{\widehat{\overline{c}}}}(w, p, q, s)$

$$s\overset{\vee}{\tilde{\widehat{\overline{c}}}} - Qe^{-iXw-iYp-iHq} + iwU\overset{\vee}{\tilde{\widehat{\overline{c}}}} + ipV\overset{\vee}{\tilde{\widehat{\overline{c}}}} - iqS\overset{\vee}{\tilde{\widehat{\overline{c}}}} = -w^2 D_h\widehat{\overline{c}} - p^2 D_h\tilde{\widehat{\overline{c}}} - q^2 D_z\overset{\vee}{\tilde{\widehat{\overline{c}}}}.$$

Rearranging the quadruple transform we obtain

$$\overset{\vee}{\tilde{\widehat{\overline{c}}}}(w, p, q, s) = \frac{Qe^{-iXw-iYp-iHq}}{s + iwU + ipV - iqS + w^2 D_h + p^2 D_h + q^2 D_z}.$$

Inversion gives:

$$\mathfrak{L}_t^{-1}: \overset{\vee}{\tilde{\widehat{\overline{c}}}}(w, p, q, t) = Qe^{-iXw-iYp-iHq}e^{-(iwU+ipV-iqS+w^2 D_h+p^2 D_h+q^2 D_z)t}$$

$$\mathfrak{F}_x^{-1}: \overset{\vee}{\tilde{c}}(x, p, q, t) = \frac{Qe^{-iYp-iHq}}{2\sqrt{\pi D_h t}}e^{-\frac{(x-(X_0+Ut))^2}{4D_h t}}e^{-(ipV-iqS+p^2 D_h+q^2 D_z)t}$$

$$\mathfrak{F}_y^{-1}\colon \overset{\vee}{c}(x,y,q,t) = \frac{Qe^{-iHq}}{4D_h\sqrt{\pi^2 t^2}} e^{-\frac{(x-(X_0+Ut))^2}{4D_h t} - \frac{(y-(Y_0+Vt))^2}{4D_h t}} e^{iqSt - q^2 D_z t}$$

$$\mathfrak{F}_z^{-1}\colon c(x,y,z,t) = \frac{Q}{8D_h\sqrt{\pi^3 D_z t^3}} e^{-\frac{(x-(X_0+Ut))^2}{4D_h t} - \frac{(y-(Y_0+Vt))^2}{4D_h t} - \frac{(z-(H-St))^2}{4D_z t}}.$$

Thus

$$c(x,y,z,t) = \frac{Q}{8D_h\sqrt{\pi^3 D_z t^3}} e^{-\frac{(x-(X_0+Ut))^2}{4D_h t} - \frac{(y-(Y_0+Vt))^2}{4D_h t} - \frac{(z-(H-St))^2}{4D_z t}}.$$

A.2 Concentration for Instantaneous Release in Uniform Half-Space

A.2.1 One-dimensional model (Section 2.4.1)

In this section, we outline how to obtain the solution $c(z,t)$ for the governing equation

$$\frac{\partial c}{\partial t} - S\frac{\partial c}{\partial z} - D_z\frac{\partial^2 c}{\partial z^2} = Q\delta(z-H)\delta(t) \tag{A.1}$$

with initial condition: $c(z,0^-) = 0$ and boundary conditions: $c(\infty,t) = 0$ and $\dfrac{\partial c(0,t)}{\partial z} = 0$.

We first do some preparatory calculations that will be useful later. We start the solution procedure by following [34] and writing

$$c(z,t) = U(z,t)\; e^{-\frac{S}{2D_z}z - \frac{S^2}{4D_z}t}\,. \tag{A.2}$$

Substituting this into Equation (A.1), we obtain

$$\frac{\partial U}{\partial t} - D_z\frac{\partial^2 U}{\partial z^2} = p(z,t) \tag{A.3}$$

where

$$\begin{aligned} p(z,t) &= e^{\frac{S}{2D_z}z + \frac{S^2}{4D_z}t} Q\delta(z-H)\delta(t) \\ &= e^{\frac{S}{2D_z}H} Q\delta(z-H)\delta(t)\,. \end{aligned} \tag{A.4}$$

(Note, we have substituted $z = H$ and $t = 0$.)

We now write

$$V = \frac{\partial U}{\partial z} - \frac{S}{2D_z}U \tag{A.5}$$

and apply the operator $\left(\dfrac{\partial}{\partial t} - D_z\dfrac{\partial^2}{\partial z^2}\right)$ to (A.5) to obtain

$$\begin{aligned} \frac{\partial V}{\partial t} - D_z\frac{\partial^2 V}{\partial z^2} &= \frac{\partial}{\partial z}\left(\frac{\partial U}{\partial t} - D_z\frac{\partial^2 U}{\partial z^2}\right) - \frac{S}{2D_z}\left(\frac{\partial U}{\partial t} - D_z\frac{\partial^2 U}{\partial z^2}\right) \\ &= \frac{\partial p}{\partial z} - \frac{S}{2D_z}p\,. \end{aligned} \tag{A.6}$$

Writing

$$q = \frac{\partial p}{\partial z} - \frac{S}{2D_z} p\,, \tag{A.7}$$

we solve (A.5) for U using the technique of integrating factor to obtain

$$e^{-\frac{S}{2D_z}z}\, U = \int_0^z e^{-\frac{S}{2D_z}\xi} V(\xi, t)\, d\xi + \Phi(t)\,. \tag{A.8}$$

Substituting $z = 0$ gives

$$U(0,t) = \Phi(t)\,.$$

Differentiating (A.8) with respect to t gives

$$e^{-\frac{S}{2D_z}z}\, \frac{\partial U}{\partial t} = \int_0^z e^{-\frac{S}{2D_z}\xi} \frac{\partial V}{\partial t}(\xi, t)\, d\xi + \dot{\Phi}\,(t) \tag{A.9}$$

and differentiating (A.5) with respect to z gives

$$\frac{\partial^2 U}{\partial z^2} - \frac{S}{2D_z}\frac{\partial U}{\partial z} = \frac{\partial V}{\partial z}\,.$$

With the substitution of $z = 0$, (A.9) becomes

$$\frac{\partial U}{\partial t}(0,t) = \dot{\Phi}\,(t)\,. \tag{A.10}$$

Then

$$\frac{\partial^2 U}{\partial z^2}(0,t) = \frac{S}{2D_z}\frac{\partial U}{\partial z}(0,t) + \frac{\partial V}{\partial z}(0,t)\,.$$

Now, with the substitution of $z = 0$ in (A.3), we obtain

$$\begin{aligned} p(0,t) &= \frac{\partial U}{\partial t}(0,t) - D_z \frac{\partial^2 U}{\partial z^2}(0,t) \\ &= \dot{\Phi}\,(t) - D_z \left[\frac{S}{2D_z}\frac{\partial U}{\partial z}(0,t) + \frac{\partial V}{\partial z}(0,t)\right] \\ &= \dot{\Phi}\,(t) - \frac{S}{2}\frac{\partial U}{\partial z}(0,t) - D_z \frac{\partial V}{\partial z}(0,t)\,. \end{aligned} \tag{A.11}$$

Then (A.8) becomes

$$U(0,t) = \Phi(t)$$

and with conditions: $V(z,0) = 0$, $V(0,t) = 0$ and $V(\infty,t) = 0$, (A.5) becomes

$$U(0,t) = \frac{2D_z}{S}\frac{\partial U}{\partial z}(0,t)\,.$$

Hence

$$\frac{\partial U}{\partial z}(0,t) = \frac{S}{2D_z}\Phi(t)$$

and (A.11) becomes

$$p(0,t) = \dot{\Phi}\ (t) - \frac{S^2}{4D_z}\Phi(t) - D_z\frac{\partial V}{\partial z}(0,t)\,.$$

At $t \neq 0$,

$$\dot{\Phi}\ (t) - \frac{S^2}{4D_z}\Phi(t) = D_z\frac{\partial V}{\partial z}(0,t)$$

so

$$\frac{d}{dt}\left[e^{-\frac{S^2}{4D_z}t}\Phi(t)\right] = D_z\frac{\partial V}{\partial z}(0,t)e^{-\frac{S^2}{4D_z}t}$$

and

$$e^{-\frac{S^2}{4D_z}t}\Phi(t) = \int_0^t D_z\frac{\partial V}{\partial z}(0,\tau)e^{-\frac{S^2}{4D_z}\tau}\ d\tau\,. \tag{A.12}$$

At $z = 0$, the downward flux is given by $Sc(0,t) = S\ e^{-\frac{S^2}{4D_z}t}U(0,t)$

Therefore, the total flux is $= S\int_0^\infty e^{-\frac{S^2}{4D_z}t}U(0,t)dt$

$$= S\int_0^\infty e^{-\frac{S^2}{4D_z}t}\Phi(t)dt$$

$$= S\int_0^\infty dt\int_0^t D_z\ e^{-\frac{S^2}{4D_z}\tau}\frac{\partial V}{\partial z}(0,\tau)\ d\tau \quad \text{(by (A.12))}\,.$$

From (A.6), we write $\dfrac{\partial V}{\partial t} - D_z\dfrac{\partial^2 V}{\partial z^2} = \dfrac{\partial p}{\partial z} - \dfrac{S}{2D_z}p = q$

and scale $x = \dfrac{z}{D_z} \rightarrow xD_z = z$ and $\tau = \dfrac{t}{D_z} \rightarrow \tau D_z = t$ and write $V(z,t) = \tilde{V}(x,\tau)$, hence

$$\frac{\partial \tilde{V}}{\partial x} - \frac{\partial^2 \tilde{V}}{\partial x^2} = D_z\tilde{q}(x,\tau)\,. \tag{A.13}$$

Referring to [29], we have

$$\tilde{V}(x,\tau) = \int_0^\tau d\theta\int_0^\infty \tilde{q}(\tau,\theta)\ G_1(x,\xi,\tau-\theta)\ d\xi \tag{A.14}$$

where

$$G_1(x,\xi,\tau-\theta) = \frac{1}{\sqrt{4\pi(\tau-\theta)}}\left(e^{-\frac{(x-\xi)^2}{4(\tau-\theta)}} - e^{-\frac{(x+\xi)^2}{4(\tau-\theta)}}\right)\,. \tag{A.15}$$

Since $q(z,t) = \dfrac{\partial p}{\partial z}(z,t) - \dfrac{S}{2D_z}p(z,t)$ (from (A.7)), then

$$\tilde{q}(x,\tau) = \frac{\partial \tilde{p}}{\partial x}(x,\tau) - \frac{S}{2}\tilde{p}(x,\tau)$$

and (A.14) becomes

$$\begin{aligned}\tilde{V}(x,\tau) &= \int_0^\tau d\theta \int_0^\infty \left[\tilde{p_x}(x,\tau) - \frac{S}{2}\tilde{p}(x,\tau)\right] G_1(x,\xi,\tau-\theta)\, d\xi \\ &= \int_0^\tau d\theta \left\{ [\tilde{p}(\xi,\theta)G_1]_0^\infty - \int_0^\infty \tilde{p}(\xi,\theta)\left[\frac{S}{2}G_1 + \frac{\partial G_1}{\partial \xi}\right] d\xi \right\} \\ &= \int_0^\tau d\theta \left\{ (0) - \int_0^\infty \tilde{p}(\xi,\theta)\left[\frac{S}{2}G_1 + \frac{\partial G_1}{\partial \xi}\right] d\xi \right\} \qquad \text{(A.16)}\end{aligned}$$

where $\dfrac{\partial G_1}{\partial \xi} = \dfrac{1}{\sqrt{4\pi(\tau-\theta)}}\left[\dfrac{x-\xi}{2(\tau-\theta)}\, e^{-\frac{(x-\xi)^2}{4(\tau-\theta)}} + \dfrac{x+\xi}{2(\tau-\theta)}\, e^{-\frac{(x+\xi)^2}{4(\tau-\theta)}}\right]$

and $\tilde{p}(0,t) = \tilde{p}(\infty,t) = 0$.

Scaling (A.4), gives $p(x,\tau) = \dfrac{Q}{D_z^{\frac{1}{2}}} e^{\frac{S}{2D_z}H}\delta(x - \dfrac{H}{D_z})\delta(\tau)$.

Hence (A.16) becomes

$$\begin{aligned}\tilde{V}(x,\tau) &= -\int_0^\tau d\theta \int_0^\infty \tilde{p}(\xi,\theta)\left[\frac{S}{2}G_1 + \frac{\partial G_1}{\partial \xi}\right] d\xi \\ &= -\int_0^\tau d\theta \int_0^\infty \frac{Q}{D_z^2} e^{\frac{S}{2D_z}H}\delta(\xi - \frac{H}{D_z})\delta(\theta)\left[\frac{S}{2}G_1 + \frac{\partial G_1}{\partial \xi}\right] d\xi \\ &= -\frac{Q}{D_z^2} e^{\frac{SH}{2D_z}} \int_0^\tau \int_0^\infty \delta(\xi - \frac{H}{D_z})\delta(\theta) \;\times \\ &\quad \times \left\{ \frac{S}{2}G_1 + \frac{1}{\sqrt{4\pi(\tau-\theta)}}\left[\frac{x-\xi}{2(\tau-\theta)}\, e^{-\frac{(x-\xi)^2}{4(\tau-\theta)}} + \frac{x+\xi}{2(\tau-\theta)}\, e^{-\frac{(x+\xi)^2}{4(\tau-\theta)}}\right]\right\} d\xi d\theta\,.\end{aligned}$$

When $\xi = \dfrac{H}{D_z}, \theta = 0$ (for (A.15)), we obtain

$$G_1(x, \frac{H}{D_z}, \tau) = \frac{1}{\sqrt{4\pi\tau}}(e^{-\frac{(x-\frac{H}{D_z})^2}{4\tau}} - e^{-\frac{(x+\frac{H}{D_z})^2}{4\tau}})\,.$$

So,

$$\begin{aligned}\tilde{V}(x,\tau) &= -\frac{Q}{D_z^2} e^{\frac{SH}{2D_z}} \left\{ \frac{S}{2}G_1(x,\frac{H}{D_z},\tau) \right. \\ &\quad \left. + \frac{1}{\sqrt{4\pi\tau}}\left[\frac{x-\frac{H}{D_z}}{2\tau}\, e^{-\frac{(x-\frac{H}{D_z})^2}{4\tau}} + \frac{x+\frac{H}{D_z}}{2\tau}\, e^{-\frac{(x+\frac{H}{D_z})^2}{4\tau}}\right]\right\} \\ &= -\frac{Q}{D_z^2} e^{\frac{SH}{2D_z}} \left\{ \frac{S}{2}\frac{1}{\sqrt{4\pi\tau}}(e^{-\frac{(x-\frac{H}{D_z})^2}{4\tau}} - e^{-\frac{(x+\frac{H}{D_z})^2}{4\tau}}) \right. \\ &\quad \left. + \frac{1}{\sqrt{4\pi\tau}}\left[\frac{x-\frac{H}{D_z}}{2\tau}\, e^{-\frac{(x-\frac{H}{D_z})^2}{4\tau}} + \frac{x+\frac{H}{D_z}}{2\tau}\, e^{-\frac{(x+\frac{H}{D_z})^2}{4\tau}}\right]\right\}.\end{aligned}$$

Substituting $x = \dfrac{z}{D_z}$ and $\tau = \dfrac{t}{D_z}$ gives

$$\begin{aligned} V(z,t) &= -\frac{Q}{D_z^2} e^{\frac{SH}{2D_z}} \left\{ \frac{S}{2} \frac{\sqrt{D_z}}{\sqrt{4\pi t}} (e^{-\frac{(z-H)^2}{4D_z t}} - e^{-\frac{(z+H)^2}{4D_z t}}) \right. \\ &\quad \left. + \frac{\sqrt{D_z}}{\sqrt{4\pi t}} \left[\frac{z-H}{2t}\ e^{-\frac{(z-H)^2}{4D_z t}} + \frac{z+H}{2t}\ e^{-\frac{(z+H)^2}{4D_z t}} \right] \right\} \\ &= -\frac{Q}{D_z} e^{\frac{SH}{2D_z}} \left\{ \frac{S}{2} \frac{1}{\sqrt{4\pi D_z t}} (e^{-\frac{(z-H)^2}{4D_z t}} - e^{-\frac{(z+H)^2}{4D_z t}}) \right. \\ &\quad \left. + \frac{1}{\sqrt{4\pi D_z t}} \left[\frac{z-H}{2t}\ e^{-\frac{(z-H)^2}{4D_z t}} + \frac{z+H}{2t}\ e^{-\frac{(z+H)^2}{4D_z t}} \right] \right\}. \end{aligned}$$

Then

$$\begin{aligned} V(\xi,t) &= -\frac{Q}{D_z} e^{\frac{SH}{2D_z}} \left\{ \frac{S}{2} \frac{1}{\sqrt{4\pi D_z t}} \left(e^{-\frac{(\xi-H)^2}{4D_z t}} - e^{-\frac{(\xi+H)^2}{4D_z t}} \right) \right. \\ &\quad \left. + \frac{1}{\sqrt{4\pi D_z t}} \left[\frac{\xi-H}{2t}\ e^{-\frac{(\xi-H)^2}{4D_z t}} + \frac{\xi+H}{2t}\ e^{-\frac{(\xi+H)^2}{4D_z t}} \right] \right\} \\ &= \frac{-Q e^{\frac{SH}{2D_z}}}{\sqrt{4\pi D_z t}} \left\{ \left[\frac{S}{2D_z} + \frac{\xi-H}{2D_z t} \right] e^{-\frac{(\xi-H)^2}{4D_z t}} + \left[-\frac{S}{2D_z} + \frac{\xi+H}{2D_z t} \right] e^{-\frac{(\xi+H)^2}{4D_z t}} \right\} \end{aligned}$$

and

$$\begin{aligned} \frac{\partial V}{\partial z}(z,t) &= -\frac{Q}{D_z} e^{\frac{SH}{2D_z}} \left\{ \frac{S}{2\sqrt{4\pi D_z t}} \left(\frac{-2(z-H)}{4D_z t} e^{-\frac{(z-H)^2}{4D_z t}} - \frac{2(z+H)}{4D_z t} e^{-\frac{(z+H)^2}{4D_z t}} \right) \right. \\ &\quad + \frac{1}{\sqrt{4\pi D_z t}} \left[\left(\frac{z-H}{2t} \right) \left(\frac{-2(z-H)}{4D_z t} \right) e^{-\frac{(z-H)^2}{4D_z t}} \right. \\ &\quad \left. \left. + \left(\frac{z+H}{2t} \right) \left(\frac{-2(z+H)}{4D_z t} \right) e^{-\frac{(z+H)^2}{4D_z t}} + \frac{1}{2t} e^{-\frac{(z-H)^2}{4D_z t}} + \frac{1}{2t} e^{-\frac{(z+H)^2}{4D_z t}} \right] \right\}. \end{aligned}$$

So

$$\frac{\partial V}{\partial z}(0,\tau) = \left(-\frac{Q}{D_z} e^{\frac{SH}{2D_z}} \right) \frac{1}{\sqrt{4\pi D_z \tau}} \left(\frac{SH}{2D_z \tau} + \frac{1}{\tau} - \frac{H^2}{2D_z \tau^2} \right) e^{-\frac{H^2}{4D_z \tau}}.$$

Hence (A.2) becomes

$$c(z,t) = e^{-\frac{S}{2D_z} z - \frac{S^2}{4D_z} t}\ U(z,t) = e^{-\frac{S^2}{4D_z} t} \left(\int_0^z e^{-\frac{S\xi}{2D_z}} V(\xi,t) d\xi + \Phi(t) \right).$$

By (A.12), we obtain

$$\begin{aligned} c(z,t) &= e^{-\frac{S^2}{4D_z}t}\int_0^z e^{-\frac{S\xi}{2D_z}}V(\xi,t)d\xi + \int_0^t D_z e^{-\frac{S^2}{4D_z}\tau}\frac{\partial V}{\partial z}(0,\tau)d\tau \\ &= e^{-\frac{S^2}{4D_z}t}\int_0^z -\frac{Q}{D_z}e^{-\frac{S(\xi-H)}{2D_z}}\frac{1}{\sqrt{4\pi D_z t}}\left\{\left[\frac{S}{2}+\frac{\xi-H}{2t}\right]e^{-\frac{(\xi-H)^2}{4D_z t}}\right. \\ &\quad \left.+\left[-\frac{S}{2}+\frac{\xi+H}{2t}\right]e^{-\frac{(\xi+H)^2}{4D_z t}}\right\}d\xi + \int_0^t D_z e^{-\frac{S^2\tau}{4D_z}}\left(-\frac{Q}{D_z}e^{\frac{SH}{2D_z}}\right) \\ &\quad \times\frac{1}{\sqrt{4\pi D_z\tau}}\left(\frac{SH}{2D_z\tau}+\frac{1}{\tau}-\frac{H^2}{2D_z\tau^2}\right)e^{-\frac{H^2}{4D_z\tau}}d\tau\,. \end{aligned}$$

Integrating by parts gives

$$\begin{aligned} c(z,t) &= \frac{Q}{\sqrt{4\pi D_z t}}e^{-\frac{S^2}{4D_z}t}\left\{e^{-\frac{S}{2D_z}(z-H)}\left[e^{-\frac{(z-H)^2}{4D_z t}}+e^{-\frac{(z+H)^2}{4D_z t}}\right]\right. \\ &\quad \left.-2e^{\frac{SH}{2D_z}-\frac{H^2}{4D_z t}}+\frac{S}{D_z}\int_0^z e^{-\frac{S(\xi-H)}{2D_z}-\frac{(\xi+H)^2}{4D_z t}}d\xi\right\} \\ &\quad -\frac{Q}{4\sqrt{\pi D_z}}\int_0^t\left[\left(\frac{SH}{D_z}+2\right)\frac{1}{\tau^{3/2}}-\frac{H^2}{D_z}\frac{1}{\tau^{5/2}}\right]e^{-\frac{(-H+S\tau)^2}{4D_z\tau}}d\tau\,. \quad \text{(A.17)} \end{aligned}$$

A.2.2 Two- and three-dimensional models (Section 2.4.2 and 2.4.3)

The two-dimensional model for the half-space is developed from the one-dimensional model (A.17). The governing equation for the two-dimensional model is:

$$\frac{\partial c}{\partial t}+U\frac{\partial c}{\partial x}-S\frac{\partial c}{\partial z}-D_h\frac{\partial^2 c}{\partial x^2}-D_z\frac{\partial^2 c}{\partial z^2} = Q\delta(x-X_0)\delta(z-H)\delta(t)\,. \quad \text{(A.18)}$$

The solution to Equation (A.18) is

$$c(x,z,t) = f(x,t)g(z,t)$$

where $f(x,t) = \dfrac{Q}{2\sqrt{\pi D_h t}}e^{-\frac{(x-X_0-Ut)^2}{4D_h t}}$ with conditions $f(x,0)=0$ and $f(\pm\infty,t)=0$, and $g(z,t)$ is the solution of the one-dimensional model (Section A.2.1) with $Q=1$, i.e.

$$\frac{\partial g}{\partial t}-S\frac{\partial g}{\partial z}-D_z\frac{\partial^2 g}{\partial z^2} = \delta(z-H)\delta(t)\,.$$

Using the solution (A.17) from the one-dimensional model (A.1), we obtain

$$\begin{aligned} c(x,z,t) &= \frac{Q}{4\pi t\sqrt{D_h D_z}} e^{-\frac{(x-X_0-Ut)^2}{4D_h t}-\frac{S^2 t}{4D_z}} \left\{ e^{\frac{-S(z-H)}{2D_z}} \left[e^{\frac{-(z-H)^2}{4D_z t}} + e^{\frac{-(z+H)^2}{4D_z t}} \right] \right. \\ &\quad \left. -2e^{\frac{SH}{2D_z}-\frac{H^2}{4D_z t}} + \frac{S}{D_z}\int_0^z e^{-\frac{S(\xi-H)}{2D_z}-\frac{(\xi+H)^2}{4D_z t}} d\xi \right\} - \frac{Q}{8\pi\sqrt{D_h D_z t}} \\ &\quad \times e^{-\frac{(x-X_0-Ut)^2}{4D_h t}} \int_0^t \left[\left(\frac{SH}{D_z} + 2 \right) \frac{1}{\tau^{\frac{3}{2}}} - \frac{H^2}{D_z \tau^{\frac{5}{2}}} \right] e^{-\frac{(-H+S\tau)^2}{4D_z \tau}} d\tau \,. \end{aligned}$$

• The three-dimensional model for the half-space is also developed from the one-dimensional model (A.1). The governing equation for the three-dimensional model is:

$$\begin{aligned} &\frac{\partial c}{\partial t} + U\frac{\partial c}{\partial x} + V\frac{\partial c}{\partial y} - S\frac{\partial c}{\partial z} - D_h\frac{\partial^2 c}{\partial x^2} - D_h\frac{\partial^2 c}{\partial y^2} - D_z\frac{\partial^2 c}{\partial z^2} \\ &= Q\delta(x-X_0)\delta(y-Y_0)\delta(z-H)\delta(t)\,. \end{aligned} \tag{A.19}$$

The solution to Equation (A.19) is

$$c(x,y,z,t) = f(x,y,t)g(z,t)$$

where $f(x,y,t) = \dfrac{Q}{4\pi D_h t} e^{-\frac{(x-X_0-Ut)^2}{4D_h t}-\frac{(y-Y_0-Vt)^2}{4D_h t}}$ with conditions $f(x,y,0) = 0$, $f(x,\pm\infty,t) = 0$ and $f(\pm\infty,y,t) = 0$, and $g(z,t)$ is the solution of the one-dimensional model (Section A.2.1) with $Q = 1$, i.e.

$$\frac{\partial g}{\partial t} - S\frac{\partial g}{\partial z} - D_z\frac{\partial^2 g}{\partial z^2} = \delta(z-H)\delta(t)\,.$$

The solution $c(x,y,z,t)$ for the three-dimensional model for the half-space is:

$$\begin{aligned} c(x,y,z,t) &= \frac{Q}{8D_h\sqrt{\pi^3 D_z t^3}} e^{-\frac{(x-X_0-Ut)^2}{4D_h t}-\frac{(y-Y_0-Vt)^2}{4D_h t}-\frac{S^2 t}{4D_z}} \\ &\quad \times \left\{ e^{\frac{-S(z-H)}{2D_z}} \left[e^{\frac{-(z-H)^2}{4D_z t}} + e^{\frac{-(z+H)^2}{4D_z t}} \right] - 2e^{\frac{SH}{2D_z}-\frac{H^2}{4D_z t}} \right. \\ &\quad \left. + \frac{S}{D_z}\int_0^z e^{-\frac{S(\xi-H)}{2D_z}-\frac{(\xi+H)^2}{4D_z t}} d\xi \right\} - \frac{Q}{16D_h t\sqrt{\pi^3 D_z}} \\ &\quad \times e^{-\frac{(x-X_0-Ut)^2}{4D_h t}-\frac{(y-Y_0-Vt)^2}{4D_h t}} \\ &\quad \times \int_0^t \left[\left(\frac{SH}{D_z} + 2 \right) \frac{1}{\tau^{\frac{3}{2}}} - \frac{H^2}{D_z \tau^{\frac{5}{2}}} \right] e^{-\frac{(-H+S\tau)^2}{4D_z \tau}} d\tau \,. \end{aligned}$$

We will show the detailed working for the verification of the three-dimensional solution in the next section. The same technique can be used to verify the two-dimensional model.

A.2.3 Verification of the three-dimensional model

We wish to verify that

$$c(x, y, z, t) = f(x, y, t)g(z, t)$$

which is

$$c(x, y, z, t) = \frac{Q}{4\pi D_h t}\, e^{-\frac{(x-X_0-Ut)^2}{4D_h t} - \frac{(y-Y_0-Vt)^2}{4D_h t}} g(z, t)$$

is the solution of the governing equation

$$\frac{\partial c}{\partial t} + U\frac{\partial c}{\partial x} + V\frac{\partial c}{\partial y} - S\frac{\partial c}{\partial z} - D_h\frac{\partial^2 c}{\partial x^2} - D_h\frac{\partial^2 c}{\partial y^2} - D_z\frac{\partial^2 c}{\partial z^2} = Q\delta(x-X_0)\delta(y-Y_0)\delta(z-H)\delta(t)$$

for

$$\frac{\partial g}{\partial t} - S\frac{\partial g}{\partial z} - D_z\frac{\partial^2 g}{\partial z^2} = \delta(z-H)\delta(t)\,. \tag{A.20}$$

Straightforward calculation shows that

$$\begin{aligned}
\frac{\partial c}{\partial t} &= \frac{-Q}{4\pi D_h t^2}\, e^{-\frac{(x-X_0-Ut)^2}{4D_h t} - \frac{(y-Y_0-Vt)^2}{4D_h t}} g(z,t) \\
&\quad + \frac{Q}{4\pi D_h t}\, e^{-\frac{(x-X_0-Ut)^2}{4D_h t} - \frac{(y-Y_0-Vt)^2}{4D_h t}} g(z,t) \left[\frac{(x-X_0-Ut)^2}{4D_h t^2}\right. \\
&\quad \left. + \frac{(y-Y_0-Vt)^2}{4D_h t^2} + \frac{U(x-X_0-Ut)}{2D_h t} + \frac{V(y-Y_0-Vt)}{2D_h t}\right] \\
&\quad + \frac{Q}{4\pi D_h t}\, e^{-\frac{(x-X_0-Ut)^2}{4D_h t} - \frac{(y-Y_0-Vt)^2}{4D_h t}} \frac{\partial g}{\partial t} \\
U\frac{\partial c}{\partial x} &= \frac{-Q}{4\pi D_h t}\, e^{-\frac{(x-X_0-Ut)^2}{4D_h t} - \frac{(y-Y_0-Vt)^2}{4D_h t}} g(z,t)\frac{U(x-X_0-Ut)}{2D_h t} \\
V\frac{\partial c}{\partial y} &= \frac{-Q}{4\pi D_h t}\, e^{-\frac{(x-X_0-Ut)^2}{4D_h t} - \frac{(y-Y_0-Vt)^2}{4D_h t}} g(z,t)\frac{V(y-Y_0-Vt)}{2D_h t} \\
S\frac{\partial c}{\partial z} &= \frac{Q}{4\pi D_h t}\, e^{-\frac{(x-X_0-Ut)^2}{4D_h t} - \frac{(y-Y_0-Vt)^2}{4D_h t}} S\frac{\partial g}{\partial z}
\end{aligned}$$

$$
\begin{aligned}
D_h\frac{\partial^2 c}{\partial x^2} &= \frac{-Q}{4\pi D_h t}\, e^{-\frac{(x-X_0-Ut)^2}{4D_h t}-\frac{(y-Y_0-Vt)^2}{4D_h t}} g(z,t)\frac{1}{2t} \\
&\quad + \frac{Q}{4\pi D_h t}\, e^{-\frac{(x-X_0-Ut)^2}{4D_h t}-\frac{(y-Y_0-Vt)^2}{4D_h t}} g(z,t)\frac{(x-X_0-Ut)^2}{4D_h t^2} \\
D_h\frac{\partial^2 c}{\partial y^2} &= \frac{-Q}{4\pi D_h t}\, e^{-\frac{(x-X_0-Ut)^2}{4D_h t}-\frac{(y-Y_0-Vt)^2}{4D_h t}} g(z,t)\frac{1}{2t} \\
&\quad + \frac{Q}{4\pi D_h t}\, e^{-\frac{(x-X_0-Ut)^2}{4D_h t}-\frac{(y-Y_0-Vt)^2}{4D_h t}} g(z,t)\frac{(y-Y_0-Vt)^2}{4D_h t^2} \\
D_z\frac{\partial^2 c}{\partial z^2} &= \frac{Q}{4\pi D_h t}\, e^{-\frac{(x-X_0-Ut)^2}{4D_h t}-\frac{(y-Y_0-Vt)^2}{4D_h t}} D_z\frac{\partial^2 g}{\partial z^2}\,.
\end{aligned}
$$

We substitute the above into the governing equation gives

$$
\frac{Q}{4\pi D_h t} e^{-\frac{(x-X_0-Ut)^2}{4D_h t}-\frac{(y-Y_0-Vt)^2}{4D_h t}} \left\{ \frac{\partial g}{\partial t} - S\frac{\partial g}{\partial z} - D_z\frac{\partial^2 g}{\partial z^2} \right\} = Q\delta(x-X_0)\delta(y-Y_0)\delta(z-H)\delta(t)\,.
$$

Integrating with respect to x and y we obtain

$$
\begin{aligned}
&\int_{-\infty}^{\infty}\int_{-\infty}^{\infty} \left\{ \frac{Q}{4\pi D_h t} e^{-\frac{(x-X_0-Ut)^2}{4D_h t}-\frac{(y-Y_0-Vt)^2}{4D_h t}} \left[\frac{\partial g}{\partial t} - S\frac{\partial g}{\partial z} - D_z\frac{\partial^2 g}{\partial z^2} \right] \right\} dxdy \\
&\qquad = \int_{-\infty}^{\infty}\int_{-\infty}^{\infty} \{Q\delta(x-X_0)\delta(y-Y_0)\delta(z-H)\delta(t)\}\, dxdy \\
&\qquad\qquad \Rightarrow \quad \frac{\partial g}{\partial t} - S\frac{\partial g}{\partial z} - D_z\frac{\partial^2 g}{\partial z^2} = \delta(z-H)\delta(t)\,.
\end{aligned}
$$

A.3 Steady State Concentration for a Constant Release in a Uniform Whole Space

A.3.1 Two-dimensional model (Section 2.5.2)

The governing equation is

$$U\frac{\partial c}{\partial x} - S\frac{\partial c}{\partial z} - D_h\frac{\partial^2 c}{\partial x^2} - D_z\frac{\partial^2 c}{\partial z^2} = q\delta(x - X_0)\delta(z - H)$$

with boundary conditions: $c \to 0$ as $x \to \pm\infty$ or $z \to +\infty$, and c is bounded when $z \to -\infty$.

Without loss of generality, we take $X_0 = 0$ and write $X = \frac{x}{\sqrt{D_h}}$ and $Z = \frac{z}{\sqrt{D_z}}$ for $C(X, Z) = c(x, z)$ to give

$$C_{XX} + C_{ZZ} - \frac{U}{\sqrt{D_h}}C_X + \frac{S}{\sqrt{D_z}}C_Z = -\frac{q}{\sqrt{D_h D_z}}\delta(X)\delta(Z - \frac{H}{\sqrt{D_z}}). \qquad \text{(A.21)}$$

Writing $C(X, Z) = e^{\frac{UX}{2\sqrt{D_h}} - \frac{SZ}{2\sqrt{D_z}}}\phi(X, Z)$, then (A.21) becomes

$$e^{\frac{UX}{2\sqrt{D_h}} - \frac{SZ}{2\sqrt{D_z}}}\left[\phi_{XX} + \phi_{ZZ} - \left(\frac{U^2}{4D_h} + \frac{S^2}{4D_z}\right)\phi\right] = -\frac{q}{\sqrt{D_h D_z}}\delta(X)\delta(Z - \frac{H}{\sqrt{D_z}}).$$

So

$$\phi_{XX} + \phi_{ZZ} - \left(\frac{U^2}{4D_h} + \frac{S^2}{4D_z}\right)\phi = -\frac{q}{\sqrt{D_h D_z}}e^{\frac{SH}{2D_z}}\delta(X)\delta(Z - \frac{H}{\sqrt{D_z}})$$

and

$$\nabla^2\phi - k^2\phi = -\frac{q}{\sqrt{D_h D_z}}e^{\frac{SH}{2D_z}}\delta(X)\delta(Z - \frac{H}{\sqrt{D_z}}) \qquad \text{(A.22)}$$

where $\nabla^2 = \frac{\partial}{\partial X^2} + \frac{\partial}{\partial Z^2}$ and $k^2 = \frac{U^2}{4D_h} + \frac{S^2}{4D_z}$.

We convert Equation (A.22) into polar form to obtain

$$\phi_{rr} + \frac{1}{r}\phi_r + \frac{1}{r^2}\phi_{\theta\theta} - k^2\phi = -\frac{q}{\sqrt{D_h D_z}}e^{\frac{SH}{2D_z}}\delta(X)\delta(Z - \frac{H}{\sqrt{D_z}}) \qquad \text{(A.23)}$$

where $r = \sqrt{X^2 + (Z - \frac{H}{\sqrt{D_z}})^2}$.

We assume that ϕ is isotropic and is independent of rotation of angle ϑ in θ where ϑ is arbitrary for $\theta \to \theta + \vartheta$. Therefore $\phi(r, \theta) = \phi(r, \theta + \vartheta) \equiv \phi(r)$.

From [8, page 43], we see that the equation $\phi_{rr} + \frac{1}{r}\phi_r - k^2\phi = 0$ has the general solution $\phi = AI_0(kr) + BK_0(kr)$ where I_0 is a modified Bessel function of the first kind of order zero and K_0 is a modified Bessel function of the second kind of order zero.

From [8, figure 12 on page 42], $\lim_{z\to\infty} I_0(z) = \infty$ and $\lim_{z\to\infty} K_0(z) = 0$. In order for ϕ to be bounded as $kr \to \infty$, then $A = 0$. Therefore we obtain $\phi = BK_0(kr)$.

Integrating both sides of (A.23) with respect to a circular region A with centre $(X, Z) = (0, \frac{H}{\sqrt{D_z}})$ with radius r_{A}, we obtain

$$\begin{aligned}\iint_{\mathrm{A}} \left(\phi_{rr} + \frac{1}{r}\phi_r - k^2\phi\right)\, d\mathrm{A} &= -\iint \frac{q}{\sqrt{D_h D_z}} e^{\frac{SH}{2D_z}} \delta(X)\delta(Z - \frac{H}{\sqrt{D_z}})\, dX\, dZ \\ &= -\frac{q}{\sqrt{D_h D_z}} e^{\frac{SH}{2D_z}}\,.\end{aligned}$$

Since the function $\phi(r)$ must satisfy $\phi_{rr} + \frac{1}{r}\phi_r - k^2\phi = 0$ away from $r = 0$, and $I_0(kr)$ does not possesses the necessary singularity at $r = 0$, we require $\phi(r)$ must behave asymptotically like the Green's function for the Laplacian operator near $r = 0$ [37].

With reference to [37], for $A_\epsilon = \{(X, Z) : r_{\boldsymbol{A}} < \epsilon\}$, we take

$$\begin{aligned}&\lim_{\epsilon\to 0^+} \left[\iint_{\mathrm{A}\setminus\mathrm{A}_\epsilon} \left(\phi_{rr} + \frac{1}{r}\phi_r - k^2\phi\right)\, d\mathrm{A} + \iint_{\mathrm{A}_\epsilon} \left(\phi_{rr} + \frac{1}{r}\phi_r - k^2\phi\right)\, d\mathrm{A}\right] \\ &= -\frac{q}{\sqrt{D_h D_z}} e^{\frac{SH}{2D_z}}\,,\end{aligned}$$

so we obtain

$$\lim_{\epsilon\to 0^+} \left[0 + \iint_{\mathrm{A}_\epsilon} \left(\phi_{rr} + \frac{1}{r}\phi_r - k^2\phi\right)\, d\mathrm{A}\right] = -\frac{q}{\sqrt{D_h D_z}} e^{\frac{SH}{2D_z}}\,,$$

and

$$\lim_{\epsilon\to 0^+} \left[\iint_{\mathrm{A}_\epsilon} \frac{1}{r}\left(r\phi_r + \phi_r\right)\, d\mathrm{A} - k^2 \iint_{\mathrm{A}_\epsilon} \phi\, d\mathrm{A}\right] = -\frac{q}{\sqrt{D_h D_z}} e^{\frac{SH}{2D_z}}\,.$$

So

$$\lim_{\epsilon\to 0^+} \left[\iint_{\mathrm{A}_\epsilon} \frac{1}{r}\left(r\phi_r\right)_r\, d\mathrm{A} - k^2 \iint_{\mathrm{A}_\epsilon} \phi\, d\mathrm{A}\right] = -\frac{q}{\sqrt{D_h D_z}} e^{\frac{SH}{2D_z}}\,.$$

Now $d\mathrm{A} = 2\pi r dr$ gives

$$\lim_{\epsilon \to 0^+} \left[\int_0^{r_\mathrm{A}} \frac{1}{r} (r\phi_r)_r \; 2\pi r dr - k^2 \iint_{\mathrm{A}_\epsilon} \phi \; d\mathrm{A} \right] = -\frac{q}{\sqrt{D_h D_z}} e^{\frac{SH}{2D_z}} .$$

For $r = r_\mathrm{A}$, we obtain

$$2\pi r \phi_r - \lim_{\epsilon \to 0^+} \left[k^2 \iint_{\mathrm{A}_\epsilon} \phi \; d\mathrm{A} \right] = -\frac{q}{\sqrt{D_h D_z}} e^{\frac{SH}{2D_z}} .$$

Thus

$$2\pi k r B K_0'(kr) - \lim_{\epsilon \to 0^+} \left[k^2 \iint_{\mathrm{A}_\epsilon} \phi \; d\mathrm{A} \right] = -\frac{q}{\sqrt{D_h D_z}} e^{\frac{SH}{2D_z}} .$$

Since $K_0'(kr) \approx -\dfrac{1}{kr}$ for $r \to 0$, and $\phi \approx \ln r \Rightarrow \displaystyle\iint_{\mathrm{A}_\epsilon} \phi \; d\mathrm{A} \to 0$ as $\epsilon \to 0^+$,

this gives

$$-2\pi B = -\frac{q}{\sqrt{D_h D_z}} e^{\frac{SH}{2D_z}} .$$

$$B = \frac{q}{2\pi \sqrt{D_h D_z}} e^{\frac{SH}{2D_z}} .$$

Therefore

$$C(X, Z) = e^{\frac{UX}{2\sqrt{D_h}} - \frac{S}{2\sqrt{D_z}} \left(Z - \frac{H}{\sqrt{D_z}} \right)} \frac{q}{2\pi \sqrt{D_h D_z}} K_0(kr) .$$

Hence,

$$c(x, z) = \frac{q}{2\pi \sqrt{D_h D_z}} e^{\frac{U_x}{2D_h} - \frac{S(z-H)}{2D_z}} K_0 \left[\frac{1}{2} \sqrt{\left(\frac{U^2}{D_h} + \frac{S^2}{D_z} \right) \left(\frac{x^2}{D_h} + \frac{(z-H)^2}{D_z} \right)} \right] .$$

In a more general case, the release point is situated at the point $(x, z) = (X_0, H)$. The governing equation is now

$$U \frac{\partial c}{\partial x} - S \frac{\partial c}{\partial z} - D_h \frac{\partial^2 c}{\partial x^2} - D_z \frac{\partial^2 c}{\partial z^2} = q \delta(x - X_0) \delta(z - H) .$$

Note, if we translate the x-axis by defining a new variable $x^* = x - X_0$ so that release point becomes $(x^*, z) = (0, H)$, we obtain equation

$$U \frac{\partial c}{\partial x^*} - S \frac{\partial c}{\partial z} - D_h \frac{\partial^2 c}{\partial x^{*2}} - D_z \frac{\partial^2 c}{\partial z^2} = q \delta(x^*) \delta(z - H) .$$

This is the same equation we solved earlier, with x replaced by x^*. It follows that the solution for the more general case is obtained by simply replacing x by $x - X_0$ in the previous solution. Thus we obtain

$$c(x,z) = \frac{q}{2\pi\sqrt{D_h D_z}} e^{\frac{U(x-X_0)}{2D_h} - \frac{S(z-H)}{2D_z}} K_0 \left[\frac{1}{2} \sqrt{\left(\frac{U^2}{D_h} + \frac{S^2}{D_z} \right) \left(\frac{(x-X_0)^2}{D_h} + \frac{(z-H)^2}{D_z} \right)} \right] .$$

For more information about the solution see [8], [37], [40], [41] and [48].

A.3.2 Three-dimensional model (Section 2.5.3)

The governing equation is

$$U\frac{\partial c}{\partial x}+V\frac{\partial c}{\partial y}-S\frac{\partial c}{\partial z}-D_h\frac{\partial^2 c}{\partial x^2}-D_h\frac{\partial^2 c}{\partial y^2}-D_z\frac{\partial^2 c}{\partial z^2}=q\delta(x-X_0)\delta(y-Y_0)\delta(z-H)$$

with boundary conditions: $c \to 0$ as $x \to \pm\infty$, $y \to \pm\infty$ or $z \to +\infty$, and c is bounded when $z \to -\infty$.

Without loss of generalisation, we take $X_0 = 0$, $Y_0 = 0$ and write $X = \frac{x}{\sqrt{D_h}}$, $Y = \frac{y}{\sqrt{D_h}}$ and $Z = \frac{z}{\sqrt{D_z}}$ for $C(X,Y,Z) = c(x,y,z)$ to give

$$\begin{aligned} &C_{XX}+C_{YY}+C_{ZZ}-\frac{U}{\sqrt{D_h}}C_X-\frac{V}{\sqrt{D_h}}C_Y+\frac{S}{\sqrt{D_z}}C_Z \\ &=-\frac{q}{D_h\sqrt{D_z}}\delta(X)\delta(Y)\delta(Z-\frac{H}{\sqrt{D_z}}). \end{aligned} \tag{A.24}$$

Taking $C(X,Y,Z) = e^{\frac{UX}{2\sqrt{D_h}}+\frac{VY}{2\sqrt{D_h}}-\frac{SZ}{2\sqrt{D_z}}}\phi(X,Y,Z)$, Equation (A.24) becomes

$$\begin{aligned} &e^{\frac{UX}{2\sqrt{D_h}}+\frac{VY}{2\sqrt{D_h}}-\frac{SZ}{2\sqrt{D_z}}}\left[\phi_{XX}+\phi_{YY}+\phi_{ZZ}-\left(\frac{U^2}{4D_h}+\frac{V^2}{4D_h}+\frac{S^2}{4D_z}\right)\phi\right] \\ &=-\frac{q}{D_h\sqrt{D_z}}\delta(X)\delta(Y)\delta(Z-\frac{H}{\sqrt{D_z}}). \end{aligned}$$

So

$$\phi_{XX}+\phi_{YY}+\phi_{ZZ}-\left(\frac{U^2}{4D_h}+\frac{V^2}{4D_h}+\frac{S^2}{4D_z}\right)\phi=-\frac{q}{D_h\sqrt{D_z}}e^{\frac{SH}{2D_z}}\delta(X)\delta(Y)\delta(Z-\frac{H}{\sqrt{D_z}})$$

and

$$\nabla^2\phi-k^2\phi=-\frac{q}{\sqrt{D_hD_z}}e^{\frac{SH}{2D_z}}\delta(X)\delta(Y)\delta(Z-\frac{H}{\sqrt{D_z}}) \tag{A.25}$$

where $\nabla^2 = \frac{\partial}{\partial X^2}+\frac{\partial}{\partial Y^2}+\frac{\partial}{\partial Z^2}$ and $k^2 = \frac{U^2}{4D_h}+\frac{V^2}{4D_h}+\frac{S^2}{4D_z}$.

Converting Equation (A.25) to polar form [48] we obtain

$$\begin{aligned} &\frac{1}{r^2}\left[\left(r^2\phi_r\right)_r+\frac{1}{\sin^2\theta}\phi_{\varphi\varphi}+\frac{1}{\sin\theta}\left(\sin\theta\ \phi_\theta\right)_\theta\right]-k^2\phi \\ &=-\frac{q}{D_h\sqrt{D_z}}e^{\frac{SH}{2D_z}}\delta(X)\delta(Y)\delta(Z-\frac{H}{\sqrt{D_z}}). \end{aligned}$$

As for the two-dimensional model, we also assume that ϕ is independent of rotation of angles θ and φ. For ϑ in θ where ϑ is arbitrary for $\theta \to \theta + \vartheta$ and σ in φ where σ is arbitrary for $\varphi \to \varphi + \sigma$, therefore $\phi(r, \theta, \varphi) = \phi(r)$.

By [55], the equation $\nabla^2\phi - k^2\phi = 0$ has the solution of $\phi = -A\frac{e^{-kr}}{4\pi r} - B\frac{e^{kr}}{4\pi r}$ where $k^2 = \frac{U^2}{4D_h} + \frac{V^2}{4D_h} + \frac{S^2}{4D_z}$ and $r = \sqrt{\frac{x^2}{D_h} + \frac{y^2}{D_h} + \frac{(z-H)^2}{D_z}}$.

In order for ϕ to be bounded as $r \to \infty$, then $B = 0$ as $\frac{e^{kr}}{4\pi r} \to \infty$ as $r \to \infty$, therefore $\phi = -A\frac{e^{-kr}}{4\pi r}$, and $\phi_r = Ak\frac{e^{-kr}}{4\pi r} + A\frac{e^{-kr}}{4\pi r^2}$.

Integrating both sides of (A.25) with respect to a spherical region V with centre $(X, Y, Z) = (0, 0, \frac{H}{\sqrt{D_z}})$ with radius r_{V}, we obtain

$$\begin{aligned} &\iiint_V \left(\nabla^2\phi - k^2\phi\right)\, d\mathrm{V} \\ &= -\iiint \frac{q}{D_h\sqrt{D_z}} e^{\frac{SH}{2D_z}} \delta(X)\delta(Y)\delta(Z - \frac{H}{\sqrt{D_z}})\, dX\, dY\, dZ\,. \end{aligned} \tag{A.26}$$

$\iiint_V \nabla^2\phi\, d\mathrm{V}$ can be written as

$$\iiint_V \mathrm{div}\,(\nabla\phi)\; d\mathrm{V} = \iint_{\mathrm{S}} (\nabla\phi)\cdot\, d\mathbf{S} = \iint_{\mathrm{S}} \phi_r\; d\mathrm{S} = \phi_r\; 4\pi r^2$$

for $d\mathbf{S} = d\mathrm{S}\,\hat{\mathrm{r}}$.

For the singularity at $r = 0$, we use the same approach as the two-dimensional model. For the three-dimensional model, we take $\mathrm{V}_\epsilon = \{(X, Y, Z) : r_{\mathrm{V}} < \epsilon\}$.

Using the same techniques and arguments as the two-dimensional model, we consider $r = r_{\mathrm{V}}$ and obtain

$$4\pi r^2\phi_r - \lim_{\epsilon\to 0^+}\left[k^2 \iiint_{\mathrm{V}_\epsilon} \phi\, d\mathrm{V}\right] \;=\; -\frac{q}{D_h\sqrt{D_z}} e^{\frac{SH}{2D_z}}\,.$$

Thus

$$4\pi r^2\left(Ak\frac{e^{-kr}}{4\pi r} + A\frac{e^{-kr}}{4\pi r^2}\right) - \lim_{\epsilon\to 0^+}\left[k^2 \iiint_{\mathrm{V}_\epsilon} \phi\, d\mathrm{V}\right] \;=\; -\frac{q}{D_h\sqrt{D_z}} e^{\frac{SH}{2D_z}}\,.$$

Taking $r \to 0$, we obtain

$$A = -\frac{q}{D_h\sqrt{D_z}} e^{\frac{SH}{2D_z}}\,.$$

Then

$$\phi = \frac{q}{D_h\sqrt{D_z}} e^{\frac{SH}{2D_z}} \left(\frac{e^{-kr}}{4\pi r}\right).$$

Therefore

$$C(X,Y,Z) = e^{\frac{UX}{2\sqrt{D_h}} + \frac{VY}{2\sqrt{D_h}} - \frac{SZ}{2\sqrt{D_z}}} \frac{q}{D_h\sqrt{D_z}} e^{\frac{SH}{2D_z}} \left(\frac{e^{-kr}}{4\pi r}\right).$$

Thus

$$c(x,y,z) = \frac{q}{4\pi r D_h\sqrt{D_z}} e^{\frac{Ux}{2D_h} + \frac{Vy}{2D_h} - \frac{S(z-H)}{2D_z} - kr}$$

where $k^2 = \dfrac{U^2}{4D_h} + \dfrac{V^2}{4D_h} + \dfrac{S^2}{4D_z}$ and $r = \sqrt{\dfrac{x^2}{D_h} + \dfrac{y^2}{D_h} + \dfrac{(z-H)^2}{D_z}}$.

In a more general case, the release point is situated at the point $(x, y, z) = (X_0, Y_0, H)$. The governing equation is now

$$U\frac{\partial c}{\partial x} + V\frac{\partial c}{\partial y} - S\frac{\partial c}{\partial z} - D_h\frac{\partial^2 c}{\partial x^2} - D_h\frac{\partial^2 c}{\partial y^2} - D_z\frac{\partial^2 c}{\partial z^2} = q\delta(x - X_0)\delta(y - Y_0)\delta(z - H).$$

Note, if we translate the x-axis by defining a new variable $x^* = x - X_0$ and the y-axis by defining a new variable $y^* = y - Y_0$ so that the release point becomes $(x^*, y^*, z) = (0, 0, H)$, we obtain equation

$$U\frac{\partial c}{\partial x^*} + V\frac{\partial c}{\partial y^*} - S\frac{\partial c}{\partial z} - D_h\frac{\partial^2 c}{\partial x^{*2}} - D_h\frac{\partial^2 c}{\partial y^{*2}} - D_z\frac{\partial^2 c}{\partial z^2} = q\delta(x^*)\delta(y^*)\delta(z - H).$$

This is the same equation we solved earlier, with x replaced by x^* and y replaced by y^*. It follows that the solution for the more general case is obtained by simply replacing x by $x - X_0$ and y by $y - Y_0$ in the previous solution. Thus we obtain

$$c(x,y,z) = \frac{q}{4\pi r D_h\sqrt{D_z}} e^{\frac{U(x-X_0)}{2D_h} + \frac{V(y-Y_0)}{2D_h} - \frac{S(z-H)}{2D_z} - kr}$$

where $k^2 = \dfrac{U^2}{4D_h} + \dfrac{V^2}{4D_h} + \dfrac{S^2}{4D_z}$ and $r = \sqrt{\dfrac{(x-X_0)^2}{D_h} + \dfrac{(y-Y_0)^2}{D_h} + \dfrac{(z-H)^2}{D_z}}$.

For more information about the solution see [55], [37], [40], [41] and [48].

A.4 The Deposit for Instantaneous Release in a Three-dimensional Uniform Whole Space with $D_z \neq 0$ (Section 2.3.3)

In this section we will show how the solution (2.14) is derived from the governing equation

$$\begin{aligned}&\frac{\partial c}{\partial t}+U\frac{\partial c}{\partial x}+V\frac{\partial c}{\partial y}-S\frac{\partial c}{\partial z}-D_h\frac{\partial^2 c}{\partial x^2}-D_h\frac{\partial^2 c}{\partial y^2}-D_z\frac{\partial^2 c}{\partial z^2}\\&=Q\delta(x-X_0)\delta(y-Y_0)\delta(z-H)\delta(t)\,.\end{aligned}$$

From A.1.1, we found that the concentration is

$$c(x,y,z,t) = \frac{Q}{8D_h\sqrt{\pi^3 D_z t^3}}e^{-\frac{(x-(X_0+Ut))^2}{4D_h t}-\frac{(y-(Y_0+Vt))^2}{4D_h t}-\frac{(z-(H-St))^2}{4D_z t}}\,.$$

To find the deposit as time goes to infinity, we write

$$\begin{aligned}f(x,y) &= \int_0^\infty \left(Sc(x,y,z,t)+D_z\frac{\partial c(x,y,z,t)}{\partial z}\right)\Big|_{z=0} dt\\&= \int_0^\infty \left(Sc(x,y,0,t)+D_z\frac{\partial c(x,y,0,t)}{\partial z}\right) dt\\&= \int_0^\infty \frac{Q}{16D_h\sqrt{\pi^3 D_z}}\left[\frac{H}{t^{\frac{5}{2}}}+\frac{S}{t^{\frac{3}{2}}}\right] e^{[-\frac{(x-X_0-Ut)^2}{4D_h t}-\frac{(y-Y_0-Vt)^2}{4D_h t}-\frac{(-H+St)^2}{4D_z t}]}\,dt\,.\end{aligned}$$

Rearranging the expression in the exponent,

$$\begin{aligned}&[-\frac{(x-X_0-Ut)^2}{4D_h t}-\frac{(y-Y_0-Vt)^2}{4D_h t}-\frac{(-H+St)^2}{4D_z t}]\\&= \frac{1}{2}\left(\frac{(x-X_0)U}{D_h}+\frac{(y-Y_0)V}{D_h}+\frac{HS}{D_z}\right)-\left(\frac{t^2\beta^2+\alpha^2}{t}\right)\\&= \frac{1}{2}\left(\frac{(x-X_0)U}{D_h}+\frac{(y-Y_0)V}{D_h}+\frac{HS}{D_z}\right)-2\alpha\beta-\frac{(\beta t-\alpha)^2}{t}\end{aligned}$$

where $\alpha=\sqrt{\frac{1}{4}\left[\frac{(x-X_0)^2}{D_h}+\frac{(y-Y_0)^2}{D_h}+\frac{H^2}{D_z}\right]}$ and $\beta=\sqrt{\frac{1}{4}\left[\frac{U^2}{D_h}+\frac{V^2}{D_h}+\frac{S^2}{D_z}\right]}$.

Hence

$$\begin{aligned}f(x,y) &= \int_0^\infty \frac{Q}{16D_h\sqrt{\pi^3 D_z}}[\frac{H}{t^{\frac{5}{2}}}+\frac{S}{t^{\frac{3}{2}}}]\, e^{\frac{1}{2}\left(\frac{(x-X_0)U}{D_h}+\frac{(y-Y_0)V}{D_h}+\frac{HS}{D_z}\right)-2\alpha\beta}e^{-\frac{(\beta t-\alpha)^2}{t}}\,dt\\&= \frac{Q}{16D_h\sqrt{\pi^3 D_z}}\, e^{\frac{1}{2}\left(\frac{(x-X_0)U}{D_h}+\frac{(y-Y_0)V}{D_h}+\frac{HS}{D_z}\right)-2\alpha\beta}\int_0^\infty\left(\frac{H}{t^{\frac{5}{2}}}e^{-\frac{(\beta t-\alpha)^2}{t}}+\frac{S}{t^{\frac{3}{2}}}e^{-\frac{(\beta t-\alpha)^2}{t}}\right)dt\\&= \frac{Q}{16D_h\sqrt{\pi^3 D_z}}\, e^{\frac{1}{2}\left(\frac{(x-X_0)U}{D_h}+\frac{(y-Y_0)V}{D_h}+\frac{HS}{D_z}\right)-2\alpha\beta}\left(H\sqrt{\pi}(\frac{\beta}{\alpha^2}+\frac{1}{2\alpha^3})+\frac{S\sqrt{\pi}}{\alpha}\right)\\&= \frac{Q}{32\pi D_h\sqrt{D_z}}\, e^{\frac{1}{2}\left(\frac{(x-X_0)U}{D_h}+\frac{(y-Y_0)V}{D_h}+\frac{HS}{D_z}\right)-2\alpha\beta}\left[\frac{(2\alpha\beta+1)H+2\alpha^2 S}{\alpha^3}\right]\,.\end{aligned}$$

A.5 The Deposit for Instantaneous Release in a Three-dimensional Uniform Half-Space with $D_z = 0$ (Section 4.4.2)

From Equation (2.15) and also in Section 4.4.1, we found that the total deposition (mass per unit area) with $D_z \neq 0$ is

$$f(x,y) = \int_0^\infty \left\{ -\frac{SQ}{16D_h t\sqrt{\pi^3 D_z}} e^{-\frac{(x-X_0-Ut)^2}{4D_h t} - \frac{(y-Y_0-Vt)^2}{4D_h t}} \times \right.$$
$$\left. \times \int_0^t \left[\left(\frac{SH}{D_z} + 2 \right) \frac{1}{\tau^{\frac{3}{2}}} - \frac{H^2}{D_z \tau^{\frac{5}{2}}} \right] e^{-\frac{(-H+S\tau)^2}{4D_z\tau}} d\tau \right\} \, dt \, .$$

Here, we will show how to obtain the solution in Section 4.4.2 in the limit $D_z \to 0$. We write

$$f(x,y) = \int_0^\infty \frac{SQ}{16D_h t\sqrt{\pi^3}} e^{-\frac{(x-X_0-Ut)^2}{4D_h t} - \frac{(y-Y_0-Vt)^2}{4D_h t}} I(t) \, dt$$

where $I(t) = \dfrac{-1}{\sqrt{D_z}} \displaystyle\int_0^t \left[\left(\frac{SH}{D_z} + 2 \right) \frac{1}{\tau^{\frac{3}{2}}} - \frac{H^2}{D_z \tau^{\frac{5}{2}}} \right] e^{-\frac{(-H+S\tau)^2}{4D_z\tau}} d\tau$ and take $p = \dfrac{-H+S\tau}{2\sqrt{D_z\tau}}$,

then $d\tau = \dfrac{4\sqrt{D_z}\tau^{\frac{3}{2}}}{H+S\tau} dp$.

So

$$\begin{aligned} -H + S\tau &= 2p\sqrt{D_z\tau} \\ p^2 &= \frac{H^2}{4D_z\tau} + \frac{S^2\tau}{4D_z} - \frac{HS}{2D_z} . \end{aligned}$$

Using Maple,

$$\tau = \frac{H}{S} + \frac{2D_z p^2}{S^2} \pm \frac{2p\sqrt{D_z}}{S} \sqrt{\frac{H}{S} + \frac{D_z p^2}{S^2}}$$

and we only take the positive τ,

$$\tau = \frac{H}{S} + \frac{2D_z p^2}{S^2} + \frac{2p\sqrt{D_z}}{S} \sqrt{\frac{H}{S} + \frac{D_z p^2}{S^2}} .$$

Again using Maple,

$$\frac{1}{\tau + \frac{H}{S}} = \frac{S^2}{2\left[p^2 D_z + HS + \sqrt{p^2 D_z \left(p^2 D_z + HS\right)}\right]}$$

and

$$\frac{1}{\tau^{\frac{1}{2}}} = \frac{S}{\sqrt{2p^2 D_z + HS + 2\sqrt{p^2 D_z \left(p^2 D_z + HS\right)}}} .$$

Now, expand $I(t)$ using the above expressions and taking $D_z \to 0$, we obtain

$$\begin{aligned} I(t) &= \frac{-1}{\sqrt{D_z}} \int_0^t \left[\left(\frac{SH}{D_z} + 2 \right) \frac{1}{\tau^{\frac{3}{2}}} - \frac{H^2}{D_z \tau^{\frac{5}{2}}} \right] e^{-\frac{(-H+S\tau)^2}{4D_z\tau}} d\tau \\ &\Rightarrow \frac{4\sqrt{\pi}}{S} \delta(t - \frac{H}{S}) . \end{aligned}$$

Hence,

$$\begin{aligned} f(x,y) &= \int_0^\infty \frac{SQ}{16 D_h t \sqrt{\pi^3}} e^{-\frac{(x-X_0-Ut)^2}{4D_h t} - \frac{(y-Y_0-Vt)^2}{4D_h t}} \frac{4\sqrt{\pi}}{S} \delta(t - \frac{H}{S}) \, dt \\ &= \frac{SQ}{4\pi D_h H} e^{-\frac{(x-(X_0+U\frac{H}{S}))^2}{4D_h \frac{H}{S}} - \frac{(y-(Y_0+V\frac{H}{S}))^2}{4D_h \frac{H}{S}}} . \end{aligned}$$

A.6 Total Mass Deposit for Instantaneous Release in a Three-dimensional Uniform Whole and Half Spaces

In this section we show that the total mass deposited on the ground ($z = 0$) is the same for both $D_z \neq 0$ and $D_z = 0$ in the three-dimensional uniform whole and half spaces. These results are in Sections 2.3.3 an 2.4.3. We will show that the total mass release will eventually land on the ground.

To find the total mass deposit on the ground, we write

$$\text{Total mass} = \int_{-\infty}^{\infty}\int_{-\infty}^{\infty} f(x,y)\ dx\ dy$$

where $f(x,y) = \int_0^{\infty} \left(Sc + D_z \frac{\partial c}{\partial z}\right)_{z=0} dt.$

Since the deposition solutions are the same for both whole and half spaces with $D_z = 0$, we will only show the working for $D_z \neq 0$ in the half space.

A.6.1 Whole space with $D_z \neq 0$

The concentration for the uniform whole space with $D_z \neq 0$ (Section 2.3.3) is

$$c(x,y,z,t) = \frac{Q}{8D_h\sqrt{\pi^3 D_z t^3}} e^{-\frac{(x-(X_0+Ut))^2}{4D_h t} - \frac{(y-(Y_0+Vt))^2}{4D_h t} - \frac{(z-(H-St))^2}{4D_z t}}.$$

We take the release point be $(0,0,H)$, then

$$f(x,y) = \int_0^{\infty} \frac{Q}{16D_h\sqrt{\pi^3 D_z}} \left(\frac{H}{t^{\frac{5}{2}}} + \frac{S}{t^{\frac{3}{2}}}\right) e^{[-\frac{(x-Ut)^2}{4D_h t} - \frac{(y-Vt)^2}{4D_h t} - \frac{(-H+St)^2}{4D_z t}]} dt\,.$$

Therefore, the total mass deposition on the "ground":

$$= \int_{-\infty}^{\infty}\int_{-\infty}^{\infty}\int_0^{\infty} \frac{Q}{16D_h\sqrt{\pi^3 D_z}} \left(\frac{H}{t^{\frac{5}{2}}} + \frac{S}{t^{\frac{3}{2}}}\right) e^{[-\frac{(x-Ut)^2}{4D_h t} - \frac{(y-Vt)^2}{4D_h t} - \frac{(-H+St)^2}{4D_z t}]} dt\ dx\ dy\,.$$

With the substitution of $p = \dfrac{(y-Vt)}{2\sqrt{D_h t}}$,

$$y = Vt + 2\sqrt{D_h t}p \Rightarrow \frac{dp}{dy} = \frac{1}{2\sqrt{D_h t}} \Rightarrow dy = 2\sqrt{D_h t}dp\,.$$

Hence

$$\begin{aligned}
&\int_{-\infty}^{\infty}\int_{-\infty}^{\infty} f(x,y)\,dx\,dy \\
&= \frac{Q}{16D_h\sqrt{\pi^3 D_z}}\int_0^{\infty}\int_{-\infty}^{\infty}\int_{-\infty}^{\infty}\left[\frac{H}{t^{\frac{5}{2}}}+\frac{S}{t^{\frac{3}{2}}}\right]e^{-\frac{(x-Ut)^2}{4D_h t}-p^2-\frac{(-H+St)^2}{4D_z t}}2\sqrt{D_h t}\,dp\,dx\,dt \\
&= \frac{Q}{8\pi\sqrt{D_h D_z}}\int_0^{\infty}\int_{-\infty}^{\infty}\left[\frac{H}{t^2}+\frac{S}{t}\right]e^{-\frac{(x-Ut)^2}{4D_h t}-\frac{(-H+St)^2}{4D_z t}}\,dx\,dt\,.
\end{aligned}$$

By doing the same substitution for the x term, we obtain

$$\begin{aligned}
\int_{-\infty}^{\infty}\int_{-\infty}^{\infty} f(x,y)\,dx\,dy &= \frac{Q}{8\pi\sqrt{D_h D_z}}\int_0^{\infty}\int_{-\infty}^{\infty}\left[\frac{H}{t^2}+\frac{S}{t}\right]e^{-\frac{(x-Ut)^2}{4D_h t}-\frac{(-H+St)^2}{4D_z t}}\,dx\,dt \\
&= \frac{Q}{8\pi\sqrt{D_h D_z}}\int_0^{\infty}\int_{-\infty}^{\infty}\left[\frac{H}{t^2}+\frac{S}{t}\right]e^{-p^2-\frac{(-H+St)^2}{4D_z t}}\,2\sqrt{D_h t}\,dp\,dt \\
&= \frac{Q}{4\sqrt{\pi D_z}}\int_0^{\infty}\left[\frac{H}{t^{\frac{3}{2}}}+\frac{S}{t^{\frac{1}{2}}}\right]e^{-\frac{(-H+St)^2}{4D_z t}}\,dt\,.
\end{aligned}$$

Writing $\alpha = \dfrac{H}{2\sqrt{D_z}}$ and $\beta = \dfrac{S}{2\sqrt{D_z}}$, the above expression becomes

$$\begin{aligned}
&\frac{Q}{4\sqrt{\pi D_z}}\int_0^{\infty}\left[\frac{H}{t^{\frac{3}{2}}}+\frac{S}{t^{\frac{1}{2}}}\right]e^{-\frac{(-H+St)^2}{4D_z t}}\,dt \\
&= \frac{Q}{4\sqrt{\pi D_z}}\int_0^{\infty}\left[\frac{H}{t^{\frac{3}{2}}}+\frac{S}{t^{\frac{1}{2}}}\right]e^{-\frac{(-\alpha+\beta t)^2}{t}}\,dt \\
&= \frac{Q}{4\sqrt{D_z}}\left[\frac{H2\sqrt{D_z}}{H}+\frac{S2\sqrt{D_z}}{S}\right] \\
&= Q\,.
\end{aligned}$$

A.6.2 Whole space with $D_z = 0$

The concentration for the uniform whole space with $D_z = 0$ (Section 4.3.2) is

$$c(x,y,z,t) = \frac{Q}{4\pi D_h t}e^{-\frac{(x-(X_0+Ut))^2}{4D_h t}-\frac{(y-(Y_0+Vt))^2}{4D_h t}}\delta(z-(H-St))$$

and the deposit

$$f(x,y) = \frac{SQ}{4\pi D_h H}e^{-\frac{(x-(X_0+U\frac{H}{S}))^2}{4D_h\frac{H}{S}}-\frac{(y-(Y_0+V\frac{H}{S}))^2}{4D_h\frac{H}{S}}}\,.$$

When the release point is at $(0,0,H)$, we obtain

$$f(x,y) = \frac{SQ}{4\pi D_h H}e^{-\frac{(x-U\frac{H}{S})^2}{4D_h\frac{H}{S}}-\frac{(y-V\frac{H}{S})^2}{4D_h\frac{H}{S}}}\,.$$

Therefore, the total mass deposited on the "ground":

$$= \int_{-\infty}^{\infty}\int_{-\infty}^{\infty} \frac{SQ}{4\pi D_h H} e^{-\frac{(x-U\frac{H}{S})^2}{4D_h\frac{H}{S}} - \frac{(y-V\frac{H}{S})^2}{4D_h\frac{H}{S}}}\, dx\, dy\,.$$

With the substitution of new variable p for both x and y,

$$p = \frac{y - V\frac{H}{S}}{2\sqrt{D_h\frac{H}{S}}} \qquad y = V\frac{H}{S} + 2\sqrt{D_h\frac{H}{S}}p$$

$$\frac{dp}{dy} = \frac{1}{2\sqrt{D_h\frac{H}{S}}} \qquad dy = 2\sqrt{D_h\frac{H}{S}}\, dp$$

and

$$p = \frac{x - U\frac{H}{S}}{2\sqrt{D_h\frac{H}{S}}} \qquad x = U\frac{H}{S} + 2\sqrt{D_h\frac{H}{S}}p$$

$$\frac{dp}{dx} = \frac{1}{2\sqrt{D_h\frac{H}{S}}} \qquad dx = 2\sqrt{D_h\frac{H}{S}}\, dp\,,$$

we obtain

$$\begin{aligned}
\int_{-\infty}^{\infty}\int_{-\infty}^{\infty} f(x,y)dxdy &= \int_{-\infty}^{\infty}\int_{-\infty}^{\infty} \frac{Q}{4\pi D_h\frac{H}{S}}\, e^{-\frac{(x-U\frac{H}{S})^2}{4D_h\frac{H}{S}} - p^2} dx\; 2\sqrt{D_h\frac{H}{S}}\, dp \\
&= \int_{-\infty}^{\infty} \frac{Q}{2\sqrt{\pi D_h\frac{H}{S}}}\, e^{-\frac{(x-U\frac{H}{S})^2}{4D_h\frac{H}{S}}} dx \\
&= \int_{-\infty}^{\infty} \frac{Q}{2\sqrt{\pi D_h\frac{H}{S}}}\, e^{-p^2} 2\sqrt{D_h\frac{H}{S}} dp \\
&= Q\,.
\end{aligned}$$

A.6.3 Half space with $D_z \neq 0$

The concentration for the uniform half space with $D_z \neq 0$ (Section 2.4.3) is

$$\begin{aligned}
&c(x,y,z,t) \\
&= \frac{Q}{8D_h\sqrt{\pi^3 t^3 D_z}} e^{-\frac{(x-X_0-Ut)^2}{4D_h t} - \frac{(y-Y_0-Vt)^2}{4D_h t} - \frac{S^2 t}{4D_z}} \left\{ e^{\frac{-S(z-H)}{2D_z}} \left[e^{\frac{-(z-H)^2}{4D_z t}} + e^{\frac{-(z+H)^2}{4D_z t}} \right] \right. \\
&\left. -2e^{\frac{SH}{2D_z} - \frac{H^2}{4D_z t}} + \frac{S}{D_z}\int_0^z e^{-\frac{S(\xi-H)}{2D_z} - \frac{(\xi+H)^2}{4D_z t}} d\xi \right\} \\
&- \frac{Q}{16D_h\sqrt{\pi^3 t^2 D_z}}\, e^{-\frac{(x-X_0-Ut)^2}{4D_h t} - \frac{(y-Y_0-Vt)^2}{4D_h t}} \int_0^t \left[\left(\frac{SH}{D_z} + 2 \right) \frac{1}{\tau^{\frac{3}{2}}} - \frac{H^2}{D_z \tau^{\frac{5}{2}}} \right] e^{-\frac{(-H+S\tau)^2}{4D_z\tau}} d\tau\,.
\end{aligned}$$

and the deposit is given by

$$f(x,y) = \int_0^\infty \left\{ -\frac{SQ}{16D_h\sqrt{\pi^3 t^2 D_z}} e^{-\frac{(x-X_0-Ut)^2}{4D_h t} - \frac{(y-Y_0-Vt)^2}{4D_h t}} \right.$$
$$\left. \times \int_0^t \left[\left(\frac{SH}{D_z} + 2 \right) \frac{1}{\tau^{\frac{3}{2}}} - \frac{H^2}{D_z \tau^{\frac{5}{2}}} \right] e^{-\frac{(-H+S\tau)^2}{4D_z\tau}} d\tau \right\} dt.$$

Therefore, the total mass deposition on the ground is

$$= \int_{-\infty}^\infty \int_{-\infty}^\infty f(x,y)dxdy$$
$$= \int_{-\infty}^\infty \int_{-\infty}^\infty \int_0^\infty -\frac{SQ}{16D_h\sqrt{\pi^3 t^2 D_z}} e^{-\frac{(x-X_0-Ut)^2}{4D_h t} - \frac{(y-Y_0-Vt)^2}{4D_h t}}$$
$$\times \int_0^t \left[\left(\frac{SH}{D_z} + 2 \right) \frac{1}{\tau^{\frac{3}{2}}} - \frac{H^2}{D_z \tau^{\frac{5}{2}}} \right] e^{-\frac{(-H+S\tau)^2}{4D_z\tau}} d\tau \; dt \; dx \; dy \,.$$

With the substitution of new variable p for both x and y,

$$p = \frac{y - (Y_0 + Vt)}{2\sqrt{D_h t}} \qquad y = Y_0 + Vt + 2\sqrt{D_h t}p$$
$$\frac{dp}{dy} = \frac{1}{2\sqrt{D_h t}} \qquad dy = 2\sqrt{D_h t}\; dp$$

and

$$p = \frac{x - (X_0 + Ut)}{2\sqrt{D_h t}} \qquad x = X_0 + Ut + 2\sqrt{D_h t}p$$
$$\frac{dp}{dx} = \frac{1}{2\sqrt{D_h t}} \qquad dx = 2\sqrt{D_h t}\; dp\,,$$

we obtain

$$\int_{-\infty}^\infty dx \int_0^\infty dt \int_{-\infty}^\infty -\frac{SQ}{16D_h t\sqrt{\pi^3 D_z}} e^{-\frac{(x-X_0-Ut)^2}{4D_h t} - p^2}$$
$$\times \int_0^t \left[\left(\frac{SH}{D_z} + 2 \right) \frac{1}{\tau^{\frac{3}{2}}} - \frac{H^2}{D_z \tau^{\frac{5}{2}}} \right] e^{-\frac{(-H+S\tau)^2}{4D_z\tau}} d\tau \; 2\sqrt{D_h t}\; dp$$
$$= \int_{-\infty}^\infty dx \int_0^\infty -\frac{SQ}{8\pi\sqrt{D_h D_z t}} e^{-\frac{(x-X_0-Ut)^2}{4D_t t}}$$
$$\times \int_0^t \left[\left(\frac{SH}{D_z} + 2 \right) \frac{1}{\tau^{\frac{3}{2}}} - \frac{H^2}{D_z \tau^{\frac{5}{2}}} \right] e^{-\frac{(-H+S\tau)^2}{4D_z\tau}} d\tau \; dt$$

$$
\begin{aligned}
&= \int_{-\infty}^{\infty} e^{-p^2} \int_0^{\infty} -\frac{SQ}{8\sqrt{\pi^3 t D_h D_z}} \int_0^t \left[\left(\frac{SH}{D_z} + 2 \right) \frac{1}{\tau^{\frac{3}{2}}} - \frac{H^2}{D_z \tau^{\frac{5}{2}}} \right] e^{-\frac{(-H+S\tau)^2}{4D_z\tau}} d\tau \; dt \; 2\sqrt{D_h t} dp \\
&= \int_0^{\infty} -\frac{SQ}{4\sqrt{\pi D_z}} \int_0^t \left[\left(\frac{SH}{D_z} + 2 \right) \frac{1}{\tau^{\frac{3}{2}}} - \frac{H^2}{D_z \tau^{\frac{5}{2}}} \right] e^{-\frac{(-H+S\tau)^2}{4D_z\tau}} d\tau \; dt \\
&= -\frac{SQ}{4\sqrt{\pi D_z}} \int_0^{\infty} \int_0^t \left[\left(\frac{SH}{D_z} + 2 \right) \frac{1}{\tau^{\frac{3}{2}}} - \frac{H^2}{D_z \tau^{\frac{5}{2}}} \right] e^{-\frac{(-H+S\tau)^2}{4D_z\tau}} d\tau \; dt \quad (*) \\
&= -\frac{SQ}{4\sqrt{\pi D_z}} \int_0^{\infty} \int_t^{\infty} \left[\frac{H^2}{D_z \tau^{\frac{5}{2}}} - \left(\frac{SH}{D_z} + 2 \right) \frac{1}{\tau^{\frac{3}{2}}} \right] e^{-\frac{(-H+S\tau)^2}{4D_z\tau}} d\tau \; dt . \quad (**) \\
&= Q .
\end{aligned}
$$

The working for the inner integral of (*):

$$
\begin{aligned}
&\int_0^t \left[\left(\frac{SH}{D_z} + 2 \right) \frac{1}{\tau^{\frac{3}{2}}} - \frac{H^2}{D_z \tau^{\frac{5}{2}}} \right] e^{-\frac{(-H+S\tau)^2}{4D_z\tau}} d\tau \\
= &\int_0^{\infty} \left[\left(\frac{SH}{D_z} + 2 \right) \frac{1}{\tau^{\frac{3}{2}}} - \frac{H^2}{D_z \tau^{\frac{5}{2}}} \right] e^{-\frac{(-H+S\tau)^2}{4D_z\tau}} d\tau \\
&- \int_t^{\infty} \left[\left(\frac{SH}{D_z} + 2 \right) \frac{1}{\tau^{\frac{3}{2}}} - \frac{H^2}{D_z \tau^{\frac{5}{2}}} \right] e^{-\frac{(-H+S\tau)^2}{4D_z\tau}} d\tau \\
= &\int_0^{\infty} \left[\left(\frac{SH}{D_z} + 2 \right) \frac{1}{\tau^{\frac{3}{2}}} - \frac{H^2}{D_z \tau^{\frac{5}{2}}} \right] e^{-\frac{(-H+S\tau)^2}{4D_z\tau}} d\tau \\
&+ \int_t^{\infty} \left[\frac{H^2}{D_z \tau^{\frac{5}{2}}} - \left(\frac{SH}{D_z} + 2 \right) \frac{1}{\tau^{\frac{3}{2}}} \right] e^{-\frac{(-H+S\tau)^2}{4D_z\tau}} d\tau .
\end{aligned}
$$

Writing $\alpha = \dfrac{H}{2\sqrt{D_z}}$ and $\beta = \dfrac{S}{2\sqrt{D_z}}$, we obtain

$$
\begin{aligned}
&\int_0^{\infty} \left[\left(\frac{SH}{D_z} + 2 \right) \frac{1}{\tau^{\frac{3}{2}}} - \frac{H^2}{D_z \tau^{\frac{5}{2}}} \right] e^{-\frac{-\alpha+\beta\tau}{\tau}} d\tau \\
&+ \int_t^{\infty} \left[\frac{H^2}{D_z \tau^{\frac{5}{2}}} - \left(\frac{SH}{D_z} + 2 \right) \frac{1}{\tau^{\frac{3}{2}}} \right] e^{-\frac{(-H+S\tau)^2}{4D_z\tau}} d\tau \\
= &\left[\left(\frac{SH}{D_z} + 2 \right) \frac{\sqrt{\pi}}{\alpha} - \frac{H^2}{D_z} \sqrt{\pi} \left(\frac{\beta}{\alpha^2} + \frac{1}{2\alpha^3} \right) \right] \\
&+ \int_t^{\infty} \left[\frac{H^2}{D_z \tau^{\frac{5}{2}}} - \left(\frac{SH}{D_z} + 2 \right) \frac{1}{\tau^{\frac{3}{2}}} \right] e^{-\frac{(-H+S\tau)^2}{4D_z\tau}} d\tau \\
= &\; 0 + \int_t^{\infty} \left[\frac{H^2}{D_z \tau^{\frac{5}{2}}} - \left(\frac{SH}{D_z} + 2 \right) \frac{1}{\tau^{\frac{3}{2}}} \right] e^{-\frac{(-H+S\tau)^2}{4D_z\tau}} d\tau \\
= &\int_t^{\infty} \left[\frac{H^2}{D_z \tau^{\frac{5}{2}}} - \left(\frac{SH}{D_z} + 2 \right) \frac{1}{\tau^{\frac{3}{2}}} \right] e^{-\frac{(-H+S\tau)^2}{4D_z\tau}} d\tau .
\end{aligned}
$$

Taking $\tau = t\theta$ and $d\tau = t\ d\theta$, (**) becomes

$$\begin{aligned} & -\frac{SQ}{4\sqrt{\pi D_z}} \int_0^\infty \int_1^\infty \left[\frac{H^2}{D_z (t\theta)^{\frac{5}{2}}} - \left(\frac{SH}{D_z} + 2 \right) \frac{1}{(t\theta)^{\frac{3}{2}}} \right] e^{-\frac{(-H+S(t\theta))^2}{4D_z(t\theta)}} t\ d\theta\ dt \\ = & -\frac{SQ}{4\sqrt{\pi D_z}} \int_1^\infty d\theta \int_0^\infty \left[\frac{H^2}{D_z t^{\frac{3}{2}} \theta^{\frac{5}{2}}} - \left(\frac{SH}{D_z} + 2 \right) \frac{1}{t^{\frac{1}{2}} \theta^{\frac{3}{2}}} \right] e^{-\frac{(-H+S(t\theta))^2}{4D_z(t\theta)}} dt\,. \end{aligned}$$

We take $\alpha = \dfrac{H}{2\sqrt{D_z \theta}}$ and $\beta = \dfrac{S\sqrt{\theta}}{2\sqrt{D_z}}$ to obtain

$$\begin{aligned} & -\frac{SQ}{4\sqrt{\pi D_z}} \int_1^\infty d\theta \int_0^\infty \left[\frac{H^2}{D_z t^{\frac{3}{2}} \theta^{\frac{5}{2}}} - \left(\frac{SH}{D_z} + 2 \right) \frac{1}{t^{\frac{1}{2}} \theta^{\frac{3}{2}}} \right] e^{-\frac{(-\alpha+\beta t)^2}{t}} dt \\ = & -\frac{SQ}{4\sqrt{\pi D_z}} \int_1^\infty \left[\frac{H^2}{D_z \theta^{\frac{5}{2}}} \frac{\sqrt{\pi}}{\alpha} - \left(\frac{SH}{D_z} + 2 \right) \frac{1}{\theta^{\frac{3}{2}}} \frac{\sqrt{\pi}}{\beta} \right] d\theta \\ = & -\frac{SQ}{4\sqrt{D_z}} \int_1^\infty \left[\frac{H^2}{D_z \theta^{\frac{5}{2}}} \frac{2\sqrt{D_z \theta}}{H} - \left(\frac{SH}{D_z} + 2 \right) \frac{1}{\theta^{\frac{3}{2}}} \frac{2\sqrt{D_z}}{S\sqrt{\theta}} \right] d\theta \\ = & Q \int_1^\infty \frac{1}{\theta^2}\ d\theta \\ = & Q \left[\frac{-1}{\theta} \right]_1^\infty \\ = & Q\,. \end{aligned}$$

A.7 Moment Equations

A.7.1 Uniform whole space (Section 6.2.1)

The deposit (2.14) for uniform whole space is

$$f(x,y) = \frac{Q}{32\pi D_h\sqrt{D_z}}\, e^{\frac{1}{2}\left(\frac{(x-X_0)U}{D_h}+\frac{(y-Y_0)V}{D_h}+\frac{HS}{D_z}\right)-2\alpha\beta}\left[\frac{(2\alpha\beta+1)H+2\alpha^2 S}{\alpha^3}\right]$$

where $\alpha = \sqrt{\frac{1}{4}\left[\frac{(x-X_0)^2}{D_h}+\frac{(y-Y_0)^2}{D_h}+\frac{H^2}{D_z}\right]}$ and $\beta = \sqrt{\frac{1}{4}\left[\frac{U^2}{D_h}+\frac{V^2}{D_h}+\frac{S^2}{D_z}\right]}$.

The moment equations are formulated using $f(x,y)$ with respect to x and y coordinates:

$$M_{x^a y^b} = \int_{-\infty}^{\infty} x^a\, dx \int_{-\infty}^{\infty} y^b\, dy\, f(x,y)$$

where a and b are positive integers.

Here, we will only show the working of the x-moment M_x equation with $a = 1$, the same technique can be applied to other moment equations.

- x-moment M_x

$$\begin{aligned} M_x &= \int_{-\infty}^{\infty} dx \int_{-\infty}^{\infty} dy\; x\; f(x,y) \\ &= \int_{-\infty}^{\infty} dx \int_{-\infty}^{\infty} dy \int_0^{\infty} x\frac{A}{2}\left[\frac{H}{t^{\frac{5}{2}}}+\frac{S}{t^{\frac{3}{2}}}\right] e^{-\frac{(x-(X_0+Ut))^2}{4D_h t}-\frac{(y-(Y_0+Vt))^2}{4D_h t}-\frac{(-H+St)^2}{4D_z t}} dt\,. \end{aligned}$$

Taking $p = \dfrac{(x-(X_0+Ut))}{2\sqrt{D_h t}}$ then $x = X_0 + Ut + 2\sqrt{D_h t}\; p$, $\dfrac{dp}{dx} = \dfrac{1}{2\sqrt{D_h t}}$

and $dx = 2\sqrt{D_h t}\; dp$, we obtain

$$\begin{aligned} M_x &= \frac{A}{2}\int_0^{\infty} dt \int_{-\infty}^{\infty} dy \int_{-\infty}^{\infty} (X_0+Ut+2\sqrt{D_h t}\; p)\left[\frac{H}{t^{\frac{5}{2}}}+\frac{S}{t^{\frac{3}{2}}}\right] \\ &\quad \times e^{-p^2-\frac{(y-(Y_0+Vt))^2}{4D_h t}-\frac{(-H+St)^2}{4D_z t}} 2\sqrt{D_h t}\, dp \\ &= \frac{A}{2}\int_0^{\infty} dt \int_{-\infty}^{\infty} dy \int_{-\infty}^{\infty} \left[\frac{H}{t^{\frac{5}{2}}}+\frac{S}{t^{\frac{3}{2}}}\right]\left[2X_0\sqrt{D_h t}\; e^{-p^2-\frac{(y-(Y_0+Vt))^2}{4D_h t}-\frac{(-H+St)^2}{4D_z t}}\right. \\ &\quad \left. + 2Ut\sqrt{D_h t}e^{-p^2-\frac{(y-(Y_0+Vt))^2}{4D_h t}-\frac{(-H+St)^2}{4D_z t}} + 4D_h tp\; e^{-p^2-\frac{(y-(Y_0+Vt))^2}{4D_h t}-\frac{(-H+St)^2}{4D_z t}}\right] dp \\ &= \frac{A}{2}\int_0^{\infty} dt \int_{-\infty}^{\infty} dy \left[\frac{H}{t^{\frac{5}{2}}}+\frac{S}{t^{\frac{3}{2}}}\right] 2(X_0+Ut)\sqrt{\pi D_h t}\; e^{-\frac{(y-(Y_0+Vt))^2}{4D_h t}-\frac{(-H+St)^2}{4D_z t}}\,. \end{aligned}$$

Again, we write $p = \dfrac{(y-(Y_0+Vt))}{2\sqrt{D_h t}}$ then $y = Y_0 + Vt + 2\sqrt{D_h t}\, p$

and $\dfrac{dp}{dy} = \dfrac{1}{2\sqrt{D_h t}}$ then $dy = 2\sqrt{D_h t}\, dp$, we obtain

$$\begin{aligned}
M_x &= \frac{A}{2}\int_0^\infty dt \int_{-\infty}^\infty \left[\frac{H}{t^{\frac{5}{2}}} + \frac{S}{t^{\frac{3}{2}}}\right] 2(X_0+Ut)\sqrt{\pi D_h t}\, e^{-p^2 - \frac{(-H+St)^2}{4D_z t}} 2\sqrt{D_h t}\, dp \\
&= \frac{A}{2}\int_0^\infty \left[\frac{H}{t^{\frac{5}{2}}} + \frac{S}{t^{\frac{3}{2}}}\right] 4(X_0+Ut)\pi D_h t\, e^{-\frac{(-H+St)^2}{4D_z t}} dt \\
&= 2A\int_0^\infty \left[\frac{H}{t^{\frac{3}{2}}} + \frac{S}{t^{\frac{1}{2}}}\right] (X_0+Ut) D_h \pi e^{-\frac{(-H+St)^2}{4D_z t}} dt \\
&= 2A\int_0^\infty \left[\frac{HX_0}{t^{\frac{3}{2}}} + \frac{SX_0+HX_0}{t^{\frac{1}{2}}} + SUt^{\frac{1}{2}}\right] \pi D_h e^{-\frac{(-H+St)^2}{4D_z t}} dt\,.
\end{aligned}$$

Taking $\alpha = \dfrac{H}{2\sqrt{D_z}}$ and $\beta = \dfrac{S}{2\sqrt{D_z}}$, we obtain

$$\begin{aligned}
M_x &= 2A\int_0^\infty \left[\frac{HX_0}{t^{\frac{3}{2}}} + \frac{SX_0+HX_0}{t^{\frac{1}{2}}} + SUt^{\frac{1}{2}}\right] U\pi D_h e^{-\frac{(-\alpha+\beta t)^2}{t}} dt \\
&= 2A\pi D_h \left[\frac{HX_0\sqrt{\pi}}{\alpha} + \frac{(SX_0+HU)\sqrt{\pi}}{\beta} + SU\sqrt{\pi}\left(\frac{1}{2\beta^3} + \frac{\alpha}{\beta^2}\right)\right] \\
&= 2AD_h\sqrt{\pi^3}\left[\frac{2HX_0\sqrt{D_z}}{H} + \frac{2(SX_0+HU)\sqrt{D_z}}{S} + \frac{SU8D_z\sqrt{D_z}}{2S^3} + \frac{4SUD_zH}{2S^2\sqrt{D_z}}\right] \\
&= 2AD_h\sqrt{\pi^3 D_z}\left[2X_0 + 2X_0 + \frac{2HU}{S} + \frac{4UD_z}{S^2} + \frac{2HU}{S}\right] \\
&= Q\left[X_0 + U\left(\frac{H}{S} + \frac{D_z}{S^2}\right)\right].
\end{aligned}$$

A.7.2 Uniform half space (Section 6.2.2)

Similar to the uniform whole space, the uniform half space moment equations are formulated using the deposit (2.15):

$$\begin{aligned}
f(x,y) &= \int_0^\infty \left\{ -\frac{SQ}{16D_h t\sqrt{\pi^3 D_z}} e^{-\frac{(x-X_0-Ut)^2}{4D_h t} - \frac{(y-Y_0-Vt)^2}{4D_h t}} \right. \\
&\quad \left. \times \int_0^t \left[\left(\frac{SH}{D_z} + 2\right)\frac{1}{\tau^{\frac{3}{2}}} - \frac{H^2}{D_z\tau^{\frac{5}{2}}}\right] e^{-\frac{(-H+S\tau)^2}{4D_z\tau}} d\tau \right\} dt.
\end{aligned}$$

Here, we will only show the working of x-moment M_x equation with $a = 1$, the same technique can be applied to the rest of the moment equations.

- x-moment (M_x)

$$
\begin{aligned}
M_x &= \int_{-\infty}^{\infty}\int_{-\infty}^{\infty} x f(x,y)dxdy \\
&= \int_{-\infty}^{\infty}\int_{-\infty}^{\infty}\int_{0}^{\infty} x\left[Sc + D_z\frac{\partial c}{\partial z}\right]_{z=0} dt\ dx\ dy \\
&= \int_{-\infty}^{\infty}\int_{-\infty}^{\infty}\int_{0}^{\infty} x\left[Sc\right]_{z=0} dt\ dx\ dy \\
&= \int_{-\infty}^{\infty}\int_{-\infty}^{\infty}\int_{0}^{\infty} -\frac{SQ}{16\sqrt{\pi^3 t^2 D_h D_h D_z}} x e^{-\frac{(x-X_0-Ut)^2}{4D_h t} - \frac{(y-Y_0-Vt)^2}{4D_h t}} \\
&\quad \times \int_0^t \left[\left(\frac{SH}{D_z}+2\right)\frac{1}{\tau^{\frac{3}{2}}} - \frac{H^2}{D_z\tau^{\frac{5}{2}}}\right] e^{-\frac{(-H+S\tau)^2}{4D_z\tau}} d\tau\ dt\ dx\ dy\,.
\end{aligned}
$$

$$
\begin{aligned}
\text{Taking}\quad p &= \frac{y-(Y_0+Vt)}{2\sqrt{D_h t}} \qquad & y &= Y_0 + Vt + 2\sqrt{D_h t}p \\
\frac{dp}{dy} &= \frac{1}{2\sqrt{D_h t}} & dy &= 2\sqrt{D_h t}\ dp
\end{aligned}
$$

$$
\begin{aligned}
M_x &= \int_{-\infty}^{\infty} dx \int_0^{\infty} dt \int_{-\infty}^{\infty} -\frac{SQ}{16\sqrt{\pi^3 t^2 D_h D_h D_z}} x e^{-\frac{(x-X_0-Ut)^2}{4D_h t} - p^2} \\
&\quad \int_0^t \left[\left(\frac{SH}{D_z}+2\right)\frac{1}{\tau^{\frac{3}{2}}} - \frac{H^2}{D_z\tau^{\frac{5}{2}}}\right] e^{-\frac{(-H+S\tau)^2}{4D_z\tau}} d\tau\ 2\sqrt{D_h t}\ dp \\
&= \int_{-\infty}^{\infty} dx \int_0^{\infty} -\frac{SQ}{8\sqrt{\pi^2 t D_h D_z}} x e^{-\frac{(x-X_0-Ut)^2}{4D_h t}} \times \\
&\quad \times \int_0^t \left[\left(\frac{SH}{D_z}+2\right)\frac{1}{\tau^{\frac{3}{2}}} - \frac{H^2}{D_z\tau^{\frac{5}{2}}}\right] e^{-\frac{(-H+S\tau)^2}{4D_z\tau}} d\tau\ dt\,.
\end{aligned}
$$

$$
\begin{aligned}
\text{Taking}\quad p &= \frac{x-(X_0+Ut)}{2\sqrt{D_h t}} \qquad & x &= X_0 + Ut + 2\sqrt{D_h t}p \\
\frac{dp}{dx} &= \frac{1}{2\sqrt{D_h t}} & dx &= 2\sqrt{D_h t}\ dp
\end{aligned}
$$

$$
\begin{aligned}
M_x &= \int_{-\infty}^{\infty}\int_{0}^{\infty} -\frac{SQ}{8\sqrt{\pi^3 t D_h D_z}}(X_0+Ut+2\sqrt{D_h t})e^{-p^2} \\
&\quad \times \int_0^t \left[\left(\frac{SH}{D_z}+2\right)\frac{1}{\tau^{\frac{3}{2}}} - \frac{H^2}{D_z\tau^{\frac{5}{2}}}\right] e^{-\frac{(-H+S\tau)^2}{4D_z\tau}} d\tau \; 2\sqrt{D_h t} dp \; dt \\
&= \int_0^{\infty} -\frac{SQ}{4\sqrt{\pi D_z}}(X_0+Ut)\int_0^t \left[\left(\frac{SH}{D_z}+2\right)\frac{1}{\tau^{\frac{3}{2}}} - \frac{H^2}{D_z\tau^{\frac{5}{2}}}\right] e^{-\frac{(-H+S\tau)^2}{4D_z\tau}} d\tau \; dt \\
&= -\frac{SQ}{4\sqrt{\pi D_z}}\int_0^{\infty}\int_t^{\infty}\left[\frac{H^2}{D_z\tau^{\frac{5}{2}}} - \left(\frac{SH}{D_z}+2\right)\frac{1}{\tau^{\frac{3}{2}}}\right](X_0+Ut)e^{-\frac{(-H+S\tau)^2}{4D_z\tau}} d\tau \; dt .
\end{aligned}
$$

Now taking $\tau = t\theta \qquad d\tau = t d\theta$

$$
\begin{aligned}
M_x &= -\frac{SQ}{4\sqrt{\pi D_z}}\int_0^{\infty}\int_1^{\infty}\left[\frac{H^2}{D_z(t\theta)^{\frac{5}{2}}} - \left(\frac{SH}{D_z}+2\right)\frac{1}{(t\theta)^{\frac{3}{2}}}\right](X_0+Ut)e^{-\frac{(-H+S(t\theta))^2}{4D_z(t\theta)}} t \; d\theta \; dt \\
&= -\frac{SQ}{4\sqrt{\pi D_z}}\int_1^{\infty} d\theta \int_0^{\infty}\left[\frac{H^2}{D_z t^{\frac{3}{2}}\theta^{\frac{5}{2}}} - \left(\frac{SH}{D_z}+2\right)\frac{1}{t^{\frac{1}{2}}\theta^{\frac{3}{2}}}\right](X_0+Ut)e^{-\frac{(-H+S(t\theta))^2}{4D_z(t\theta)}} dt \\
&= -\frac{SQ}{4\sqrt{\pi D_z}}\int_1^{\infty} d\theta \int_0^{\infty}\left\{X_0\left[\frac{H^2}{D_z t^{\frac{3}{2}}\theta^{\frac{5}{2}}} - \left(\frac{SH}{D_z}+2\right)\frac{1}{t^{\frac{1}{2}}\theta^{\frac{3}{2}}}\right]\right. \\
&\quad \left. +U\left[\frac{H^2}{D_z t^{\frac{1}{2}}\theta^{\frac{5}{2}}} - \left(\frac{SH}{D_z}+2\right)\frac{t^{\frac{1}{2}}}{\theta^{\frac{3}{2}}}\right]\right\} e^{-\frac{(-H+S(t\theta))^2}{4D_z(t\theta)}} dt .
\end{aligned}
$$

Substituting $\alpha = \dfrac{H}{2\sqrt{D_z\theta}} \qquad \beta = \dfrac{S\sqrt{\theta}}{2\sqrt{D_z}}$

$$
\begin{aligned}
M_x &= -\frac{SQ}{4\sqrt{\pi D_z}}\int_1^{\infty} d\theta \int_0^{\infty}\left\{X_0\left[\frac{H^2}{D_z t^{\frac{3}{2}}\theta^{\frac{5}{2}}} - \left(\frac{SH}{D_z}+2\right)\frac{1}{t^{\frac{1}{2}}\theta^{\frac{3}{2}}}\right]\right. \\
&\quad \left. +U\left[\frac{H^2}{D_z t^{\frac{1}{2}}\theta^{\frac{5}{2}}} - \left(\frac{SH}{D_z}+2\right)\frac{t^{\frac{1}{2}}}{\theta^{\frac{3}{2}}}\right]\right\} e^{\frac{-(-\alpha+\beta t)}{t}} dt \\
&= -\frac{SQ}{4\sqrt{\pi D_z}}\int_1^{\infty}\left\{X_0\left[\frac{H^2\sqrt{\pi}}{D_z\theta^{\frac{5}{2}}\alpha} - \left(\frac{SH}{D_z}+2\right)\frac{\sqrt{\pi}}{\theta^{\frac{3}{2}}\beta}\right]\right. \\
&\quad \left. +U\left[\frac{H^2\sqrt{\pi}}{D_z\theta^{\frac{5}{2}}\beta} - \left(\frac{SH}{D_z}+2\right)\frac{\sqrt{\pi}}{\theta^{\frac{3}{2}}}\left(\frac{1}{2\beta^3}+\frac{\alpha}{\beta^2}\right)\right]\right\} d\theta \\
&= -\frac{SQ}{4}\int_1^{\infty}\left[\frac{-4X_0}{S\theta^2} + \frac{-8HU}{S^2\theta^3} + \frac{-8UD_z}{S^3\theta^3}\right] d\theta \\
&= Q\left[X_0 + U\left(\frac{H}{S}+\frac{D_z}{S^2}\right)\right] .
\end{aligned}
$$